# Geology and Geochemistry of the Copper Canyon Porphyry Copper Deposit and Surrounding Area, Lander County, Nevada

GEOLOGICAL SURVEY PROFESSIONAL PAPER 798-B

# Geology and Geochemistry of the Copper Canyon Porphyry Copper Deposit and Surrounding Area, Lander County, Nevada

*By* TED G. THEODORE *and* DAVID W. BLAKE

GEOCHEMISTRY OF THE PORPHYRY COPPER ENVIRONMENT IN THE BATTLE MOUNTAIN MINING DISTRICT, NEVADA

GEOLOGICAL SURVEY PROFESSIONAL PAPER 798-B


UNITED STATES GOVERNMENT PRINTING OFFICE, WASHINGTON : 1975

UNITED STATES DEPARTMENT OF THE INTERIOR

ROGERS C. B. MORTON, *Secretary*

GEOLOGICAL SURVEY

V. E. McKelvey, *Director*

Library of Congress Catalog-card No. 74-600023

For sale by the Superintendent of Documents, U.S. Government Printing Office
Washington, D.C. 20402
Stock Number 2401-02597

# CONTENTS


| | Page |
|---|---|
| Abstract | B1 |
| Introduction | 1 |
| Acknowledgments | 3 |
| Structural and stratigraphic features of the mining district | 3 |
| Geology of the Copper Canyon area | 5 |
| Siliceous and volcanic assemblage | 5 |
| Cambrian System | 5 |
| Scott Canyon Formation | 5 |
| Transitional assemblage | 7 |
| Cambrian System | 7 |
| Harmony Formation | 7 |
| Havallah sequence | 7 |
| Pennsylvanian(?) System | 8 |
| Pumpernickel Formation | 8 |
| Overlap assemblage | 9 |
| Pennsylvanian System | 9 |
| Battle Formation | 9 |
| Pennsylvanian and Permian Systems | 10 |
| Antler Peak Limestone | 10 |
| Permian System | 10 |
| Edna Mountain Formation | 10 |
| Surficial deposits | 10 |
| Quaternary System | 10 |
| Intrusive rocks | 10 |
| Altered granodiorite of Copper Canyon | 10 |
| Geometry of the intrusive body | 10 |
| Lithology and chemistry | 10 |
| Xenoliths | 12 |
| Age of intrusive body | 12 |
| Depth of emplacement | 12 |
| Petrogenetic implications of primary biotite compositions | 13 |
| Altered granodiorite of the Wilson-Independence mine area | 15 |
| Miscellaneous intrusive rocks | 15 |
| Extrusive rocks | 15 |
| Caetano Tuff | 15 |
| Basalt flows | 15 |
| Structural geology | 15 |
| Antler orogeny deformation | 15 |
| Sonoma orogeny deformation | 16 |
| Regional considerations | 16 |
| Folding in the Pumpernickel Formation | 16 |
| Tertiary faulting | 18 |
| Origin of hematite in red beds of the Battle Formation | 20 |
| Copper Canyon porphyry copper deposit | 21 |
| Stratigraphy and structure along the 6450 bench | 22 |
| Petrology of rocks on the 6450 bench | 27 |
| Harmony Formation metashale and metasandstone | 27 |
| Battle Formation conglomerate | 31 |
| Major sulfide veins | 33 |
| Fault zones | 35 |
| Hydrothermal biotite from the 6500 bench | 35 |
| Investigations of specific sulfides from the ore body | 36 |
| Chalcopyrite etch tests | 36 |
| Pyrrhotite etch tests and annealing experiments | 36 |
| Copper Canyon porphyry copper deposit—Continued | |
| Investigations of specific sulfides—Continued | |
| Pyrrhotite etch tests—Continued | |
| Pyrrhotite types and textures | B36 |
| Experimental techniques | 38 |
| Pyrrhotite compositions | 39 |
| X-ray determination of arsenopyrite composition | 39 |
| Paragenesis of minerals in the east ore body | 39 |
| Chemistry of the ore and wallrock | 40 |
| Major-element variations | 40 |
| Composition of hydrothermal biotite | 43 |
| Distribution of economic metals in the 6450 bench | 43 |
| Copper | 43 |
| Gold | 45 |
| Silver | 45 |
| Other minor-element variations | 46 |
| Geochemistry of gold | 47 |
| Age of metallization | 47 |
| Environment of ore deposition | 48 |
| Depth of metallization | 49 |
| Temperature variation in the east ore body | 51 |
| Chemistry of the fluids | 53 |
| Transport | 53 |
| Conditions of deposition | 54 |
| Oxygen and sulfur fugacities | 54 |
| Deductions from alteration reactions | 54 |
| Summary of depositional conditions | 56 |
| Role of carbon in the Scott Canyon Formation | 57 |
| Source of copper | 57 |
| Geochemistry of the Copper Canyon Area | 58 |
| Sampling and analytical procedures | 58 |
| Frequency distributions and concentration classes | 58 |
| Distribution of elements in the Copper Canyon area | 60 |
| Copper | 60 |
| Gold | 61 |
| Silver | 62 |
| Other elements | 62 |
| Antimony | 62 |
| Arsenic | 62 |
| Barium | 63 |
| Bismuth | 63 |
| Boron | 64 |
| Cadmium | 65 |
| Chromium | 65 |
| Cobalt | 65 |
| Lead | 66 |
| Manganese | 66 |
| Mercury | 67 |
| Molybdenum | 68 |
| Nickel | 68 |
| Strontium | 69 |
| Tin | 70 |
| Vanadium | 70 |
| Zinc | 71 |
| Primary dispersed element distributions | 71 |
| Statistical evaluation of element associations | 73 |
| Selected references | 78 |
| Index | 85 |

# ILLUSTRATIONS

[Plates are in pocket]


Page

PLATE 1. Geologic map of the Copper Canyon area, Lander County, Nev.
2. Maps showing distribution patterns of copper, gold, and silver in 2,927 rock samples from the Copper Canyon area

FIGURE 1. Index map of north-central Nevada ... B2
2. Index map showing location of the Battle Mountain mining district ... 4
3. Geologic sketch map of the Antler Peak quadrangle ... 6
4. Oblique northwest aerial view of the Copper Canyon mine area ... 8
5. Photograph of primary phenocrystic biotite from altered granodiorite ... 11
6. Diagram showing relation of $Fe^{+3}-Fe^{+2}-Mg$ contents in biotites ... 13
7. Diagram showing stability curves for biotites ... 14
8–11. Photographs of Pumpernickel Formation showing—
8. Outcrop of unaltered chert beds and laminated chert ... 16
9. A worm trail in chert ... 17
10. Tightly folded beds of chert ... 17
11. Chert float with small-amplitude crenulations of bedding and penetrative lineations in chert ... 18
12. Plots showing planar and axial structural data from the upper plate of the Golconda thrust ... 19
13. Photograph showing sawed surface of unaltered sample from red bed in the lower member of the Middle Pennsylvanian Battle Formation ... 20
14. Map showing the generalized geology around the intrusive body at Copper Canyon and the location of the west and east ore bodies ... 21
15. Geologic map of the 6450 bench, east ore body ... 23
16. Contoured copper concentrations on the 6450 bench ... 24
17. Contoured gold concentrations on the 6450 bench ... 25
18. Contoured silver concentrations on the 6450 bench ... 26
19. Photograph showing panoramic view toward the north from the 6450 bench in the east ore body ... 27
20. Photograph, taken at the north end of the 6450 bench, showing a clay-rich breccia zone along a fault with about a 3-m offset ... 28
21–28. Photomicrographs showing—
21. Quartz set in partially recrystallized quartz–K-feldspar–mica matrix from metasandstones of the Harmony Formation ... 28
22. Pyrrhotite rimmed by siderite in a quartz vein in the Harmony Formation ... 30
23. Biotite and pyrrhotite in a vein ... 30
24. Quartz, chalcopyrite, chlorite, and epidote in a vein from metasandstones of the Harmony Formation ... 30
25. Massive arsenopyrite matrix replacement in a sample of metallized rock belonging to the lower member of the Middle Pennsylvanian Battle Formation ... 32
26. Textural relations of biotite in the east ore body ... 32
27. Tremolite, pyrite, possible sphene, and quartz from the Battle Formation ... 33
28. Quartz-lined open cavity filled with siderite and marcasite-pyrite ... 33
29. Photograph of a predominantly arsenopyrite-quartz vein from the 6500 bench ... 33
30. Photomicrograph of arsenopyrite veined by chalcopyrite with a trace of covellite ... 34
31. Photomicrograph of pyrite rimming earlier pyrite mottled by numerous very fine silicate inclusions ... 34
32. Photomicrograph of native gold along microfractures through chalcopyrite, and gold ore from the Copper Canyon underground mine ... 35
33. Diagram showing diffractometer traces of selected monoclinic and hexagonal pyrrhotite peaks ... 37
34. Photomicrographs of lamellar "flame" intergrowths of hexagonal and monoclinic pyrrhotite ... 38
35. Photomicrograph of bird's-eye texture of fine-grained granular marcasite-pyrite aggregates that replace pyrrhotite ... 38
36. Sketch showing paragenesis of principal hypogene ore and gangue minerals ... 41
37. Variation diagrams comparing chemically analyzed altered and unaltered rocks ... 44
38. Variation diagram of As, Mn, Mo, Ni, W, Zn, Ba, Co, and Bi concentrations along the traverse line *A–B* on the 6450 bench, east ore body ... 48
39. Histogram of radiometrically age-dated porphyry copper deposits ... 51
40. Diagrammatic summary of temperature variation in the east ore body ... 52
41. Phase diagram of the Fe-S system between 0° and 400°C ... 53
42. Diagram showing stability fields of pyrrhotite, pyrite, magnetite, and hematite ... 55
43. Diagram showing calculated stability fields for the Fe-S-O system with other aqueous species and minerals at 250°C ... 56
44. North-south idealized geochemical profiles for dispersed Ag, Bi, Ba, Ni, Pb, Zn, Mo, Sr, Cr, Au, and Co ... 72
45. Histograms showing percent frequency distributions of 31 elements in 2,927 rock samples from the Copper Canyon area ... 74
46. Sketch map showing copper:gold:silver ratios and elements strongly associated with copper, gold, and silver in 11 partitioned areas at Copper Canyon ... 75

# TABLES


| | | Page |
|---|---|---|
| TABLE 1. | Production of copper by Duval Corp. in 1967–70 from the Battle Mountain mining district | B3 |
| 2. | Chemical analyses of rocks from the Pumpernickel Formation, Copper Canyon area, Lander County, Nev | 9 |
| 3. | Compositions and structural formulas of biotites from the altered granodiorite of Copper Canyon | 11 |
| 4. | Mineralogy of rocks from the Upper Cambrian Harmony Formation on the 6450 bench | 29 |
| 5. | Mineralogy of typical veins in the Upper Cambrian Harmony Formation on the 6450 bench, Copper Canyon east ore body | 29 |
| 6. | Mineralogy of hydrothermally altered rocks belonging to the Middle Pennsylvanian Battle Formation on the 6450 bench | 31 |
| 7. | Composite mineral assemblages of fault breccia and fault gouge on the 6450 bench | 35 |
| 8. | X-ray diffraction data and composition of pyrrhotite from the east ore body, Copper Canyon porphyry copper deposit, Lander County, Nev | 40 |
| 9. | Analyses of rocks from the Battle and Harmony Formations in and near the east ore body, Copper Canyon porphyry copper deposit | 42 |
| 10. | Analyses of rock samples from the 6450 bench, Copper Canyon east ore body | 46 |
| 11. | Custom six-step spectrographic analyses of lode and placer gold samples from Copper Canyon and qualitative spectrographic analyses of gold coatings | 50 |
| 12. | Number of spectrographic results less than the lower detection limit and greater than the upper detection limit in 2,927 analyses around the Copper Canyon porphyry copper deposit | 59 |
| 13. | Spearman and product moment correlation coefficients for gold versus all other analyzed elements at Copper Canyon | 73 |
| 14. | Array of number of paired-element analyses and product moment correlation coefficients for 2,927 rock analyses at Copper Canyon | 76 |
| 15. | Element pairs other than copper, gold, and silver from areas 7, 8, 10, and 11 that have positive Spearman correlation coefficients greater than 0.5049 and that are based on at least 50 element pair concentrations | 77 |

GEOCHEMISTRY OF THE PORPHYRY COPPER ENVIRONMENT IN THE BATTLE MOUNTAIN MINING DISTRICT, NEVADA

# GEOLOGY AND GEOCHEMISTRY OF THE COPPER CANYON PORPHYRY COPPER DEPOSIT AND SURROUNDING AREA, LANDER COUNTY, NEVADA

By TED G. THEODORE and DAVID W. BLAKE[1]


## ABSTRACT

The Copper Canyon deposit, largest producer of copper in the Battle Mountain mining district, is about 19 km southwest of the town of Battle Mountain, in north-central Nevada. The district is at the north end of the Eureka–Battle Mountain mineral belt, a northwest-southeast zone of metal-mining districts. Duval Corp. has mined copper, gold, and silver from the Copper Canyon deposit by open-pit methods since 1967.

The deposit formed in chemically favorable wallrock adjacent to a small potassic-altered granodiorite intrusion. The granodiorite was emplaced under about 1,500 m of cover into a complex thrust sequence of lower and upper Paleozoic rock in late Eocene or early Oligocene time (about 38 million years ago). Emplacement is inferred to have been controlled partly by the Virgin fault, a major north-striking normal fault in this part of the district, along which movements continued after crystallization of the intrusion. Experimentally determined minimum melting curves, together with univariant breakdown curves for primary biotites from this intrusive, suggest that biotite may have crystallized at about 800°C and suggest high $P_{H_2O}$:$P_{total}$ equilibrium ratios during the crystallization.

The deposit occurs predominantly as hypogene replacement sulfides in altered rocks belonging to the Middle Pennsylvanian Battle Formation. Smaller amounts of ore occur in the Upper Cambrian Harmony Formation and in the Pennsylvanian(?) Pumpernickel Formation. Most ore was deposited in beds that originally contained hematite and calcite. The hypogene minerals include pyrite, chalcopyrite, pyrrhotite, marcasite, arsenopyrite, sphalerite, molybdenite, galena, and gold. Gold is the second most economically important metal in the deposit. The most common gangue minerals are quartz, K-feldspar, biotite, and white mica, typical of the potassium silicate alteration facies.

Early-stage sulfide deposition, beginning at temperatures of about 300°C and continuing to at least 360°C, may have occurred when metal-bearing fluids reacted with hematite-rich beds of the Battle Formation. Oxygen fugacities in the environment of ore deposition appear to have been very low during this stage. Later, during the intermediate stages, siderite- and marcasite-bearing assemblages developed as the fluide became enriched in $CO_2$ and became possibly more acidic because of the dissociation of hydrogen gas. Most gold may have been deposited very late in the metallization sequence, along with quartz that fills vugs.

Ore deposits peripheral to the intrusion at Copper Canyon are zoned successively from copper-gold-silver deposits near the center to gold-silver to lead-zinc-silver deposits in the northernmost parts of the area. Over 2,900 rocks across all three zones were analyzed for 31 elements in an area of about 16 sq km, up to about 3.2 km north of the main intrusion at Copper Canyon. The chemical data indicate many very high local concentrations of metals near the lead-zinc-silver and the gold-silver peripheral vein deposits. Also, many metals are concentrated for several hundred meters along the north-striking faults that localized many of these peripheral deposits. Mercury is probably the best pathfinder element for both the outlying vein deposits in the area and for the replacement copper ore bodies. Primary distributions of Ag, Au, Ba, Bi, Co, Cu, Hg, Mo, Ni, Pb, Sr, and Zn seem to be related geographically to the intrusion and are best reflected in rocks belonging to the Pumpernickel Formation. Rocks with more than 1,000 parts per million (ppm) copper generally occur throughout the area of the intrusion and the copper ore bodies. Much of this copper, however, is secondary. Anomalous molybdenum concentrations are fairly well restricted to the outcrop area of the intrusion at Copper Canyon.

Statistical analysis of the chemical data using Spearman rank correlation techniques indicates that Ag, Fe, As, Pb, Cu, Bi, and Hg have the strongest positive associations with gold. However, after first partitioning the entire Copper Canyon area into 11 areas and then evaluating the element associations within these 11 areas, we found that as the copper:gold and copper:silver ratios increase, the number of elements statistically strongly associated with copper, gold, and silver decreases. This relationship, however, may be largely a function of increased mobilities of metals in the oxide zone.


## INTRODUCTION

For many years the Battle Mountain mining district has been the largest producer of copper in north-central Nevada. The district lies within the Antler Peak 15-minute quadrangle in Lander and Humboldt Counties. The Copper Canyon area, in the southern part of the mining district (fig. 1), includes the Copper Canyon porphyry copper deposit, one of two bulk, low-grade copper zones that are being mined (1973) simultane-

[1]Duval Corp., Battle Mountain, Nev. 89820.

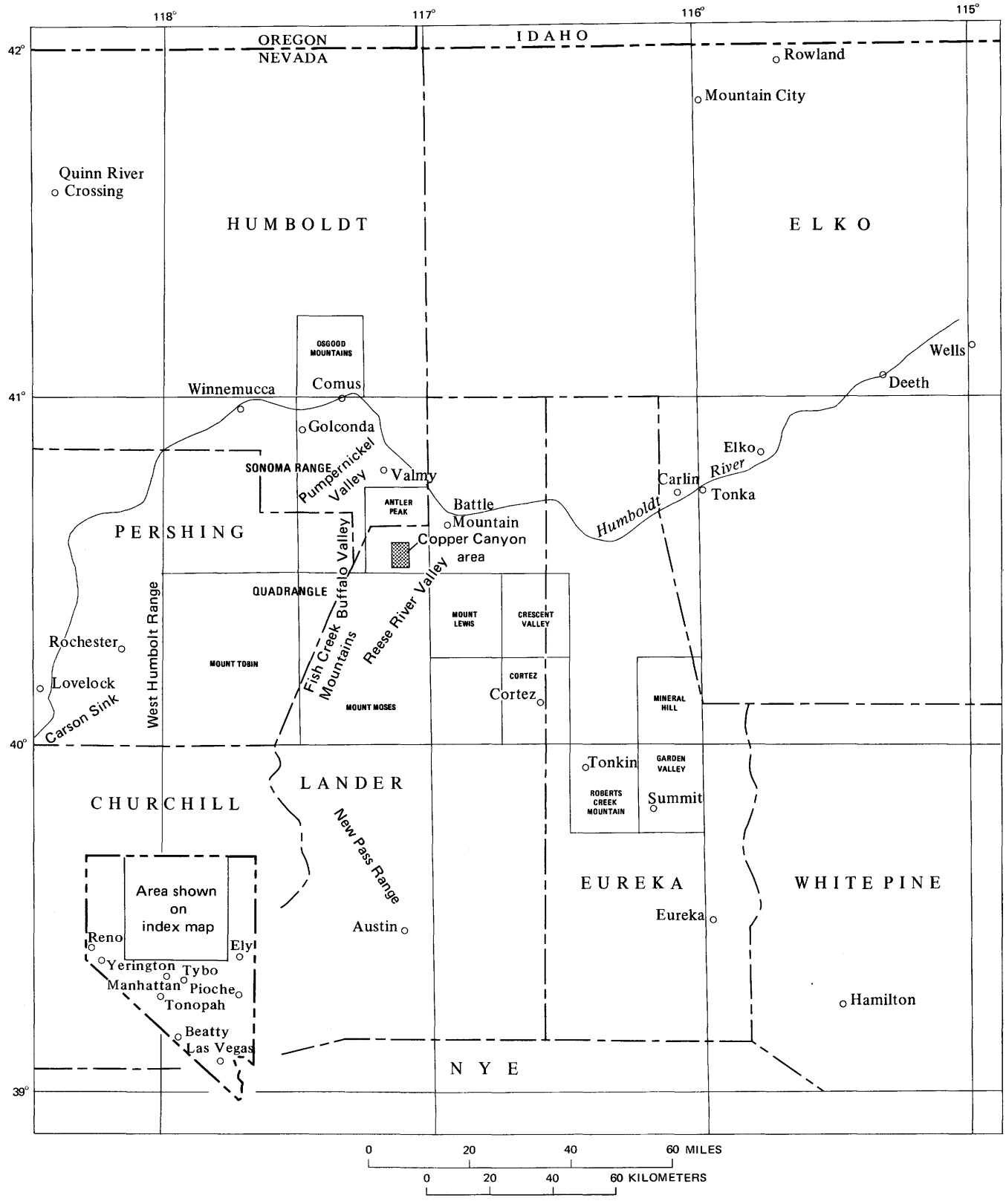


FIGURE 1.—Index map of north-central Nevada.

ously by Duval Corp. (Sayers and others, 1968). Indeed, the operations at Copper Canyon represent the latest exploitations of copper, gold, and silver ore zones, whose copper showings were first located in the 1860's (Roberts and Arnold, 1965, p. B41). Roberts and Arnold described the geology of the ore deposits of the mining district and also summarized the mining history. The history of development of the Copper Canyon underground mine, a former large copper producer that shut down in 1954, was discussed by Trengove (1951).

Up to 1961, the total recorded production from the entire Battle Mountain mining district included 150,282 ounces of gold, 2,130,827 ounces of silver, and 31,826,834 pounds of copper, most of which came from the Copper Canyon area. In 1967, the proved reserves here included 350,000 ounces of gold in about 14 million tons of hypogene copper ore with an average grade of about 0.8 percent copper (Sayers and others, 1968). Production of copper by Duval Corp. from both of its Battle Mountain properties (Copper Canyon and Copper Basin) for the period 1967–70 is shown in table 1. Noble (1970, fig. 3) estimates past production plus unmined reserves of copper in the Battle Mountain mining district to total $300 million. Of this figure, he assigns $250 million to the Copper Canyon area. Among the State's copper deposits, the one at Copper Canyon ranks third in tonnage behind those at Ely and Yerington.

TABLE 1.—*Production of copper by Duval Corp. in 1967–70 from the Battle Mountain mining district*
[From World Mining, July 1971, p. 41]

| Year | Milling operations | | | Leaching operations |
|---|---|---|---|---|
| | Ore (tons) | Copper content (percent) | Copper production (tons) | Copper production (tons) |
| 1967 | 577,000 | 0.81 | 4,670 | 1,145 |
| 1968 | 1,362,000 | .73 | 9,940 | 2,323 |
| 1969 | 1,640,000 | .78 | 12,790 | 3,008 |
| 1970 | 1,636,000 | .73 | 11,940 | 4,181 |

In 1968, the U.S. Geological Survey began a study of the Copper Canyon area in cooperation with Duval Corp. This report, a summary of the results of the joint investigation, describes (1) structure and petrology of the porphyry copper deposit and its surrounding wallrocks, (2) distribution of gold, copper, and silver through a typical ore zone, (3) variations in minor-element concentrations through ore in the deposit, (4) distributions of trace elements in rocks surrounding the deposit, and (5), most importantly, hypotheses of the pressure, temperature, and chemical (P, T, and X) environment of metallization.

*Acknowledgments.*—Those aspects of the study dealing with the porphyry copper deposit would not have been possible without the cooperation of F. H. Howell, J. P. McCarty, and A. E. Shiell, Duval Corp. Stimulating discussions with G. K. Czamanske, J. L. Haas, Jr., J. T. Nash, W. J. Nokleberg, and R. J. Roberts, all of the U.S. Geological Survey, are greatly appreciated. The original computer program, used in preparation of the structural diagrams, was written by C. E. Corbató, Ohio University, and modified by W. J. Nokleberg. Additional computer assistance was provided by J. McMurdie, J. V. Tanida, and G. Van Trump. Many of the geochemical samples were collected by A. H. Barabas and K. Roberts.

## STRUCTURAL AND STRATIGRAPHIC FEATURES OF THE MINING DISTRICT

The locations of many ore deposits in north-central Nevada apparently are structurally controlled; many of them are in or near thrust zones of regionally extensive tectonic plates. One of these zones is along the Roberts Mountains thrust (fig. 2*A*). Much of north-central Nevada is covered by siliceous rocks in the upper plate of the Roberts Mountains thrust. This thrust carried volcanic rocks, chert, shale, and quartzite of early and middle Paleozoic age eastward over lower plate carbonate rocks of an equivalent age during Late Devonian to Early Mississippian thrusting in the Antler orogeny (Roberts and others, 1958; Roberts, 1966). Distribution of siliceous, transitional, and carbonate assemblage rocks in the Cordilleran geosyncline, before the Antler orogeny, was very regular (fig. 2*B*). The Roberts Mountains thrust, however, does not crop out in the Battle Mountain mining district (Roberts, 1964). Deep drill holes into the Roberts Mountains plate indicate that this thrust probably underlies the district at depths greater than 1,300 m (Theodore and Roberts, 1971). In addition, the region subsequently has been overridden by several structurally higher Paleozoic and Mesozoic thrusts. One of these thrusts, the early Mesozoic Golconda thrust, crops out at Copper Canyon, and it may have been genetically important during the formation of the Copper Canyon porphyry copper deposit.

The Battle Mountain mining district also lies at the northwest end of the Eureka–Battle Mountain mineral belt (fig. 2*A*)—a northwest-southeast alinement of metal-mining districts that has been inferred to be closely related to Precambrian basement structural trends (Roberts, 1966). Although it is a major producer of copper, the Battle Mountain mining district also occurs within regionally extensive gold, lead-zinc, mercury, silver, and tungsten metal provinces as outlined by Noble (1970).

Three major thrust plates of regional significance crop out in the Battle Mountain mining district (fig. 3). Two are below an equally important autochthonous block (Roberts, 1964). The lowest plate exposed (fig. 3) is made up of chert, shale, argillite, and greenstone

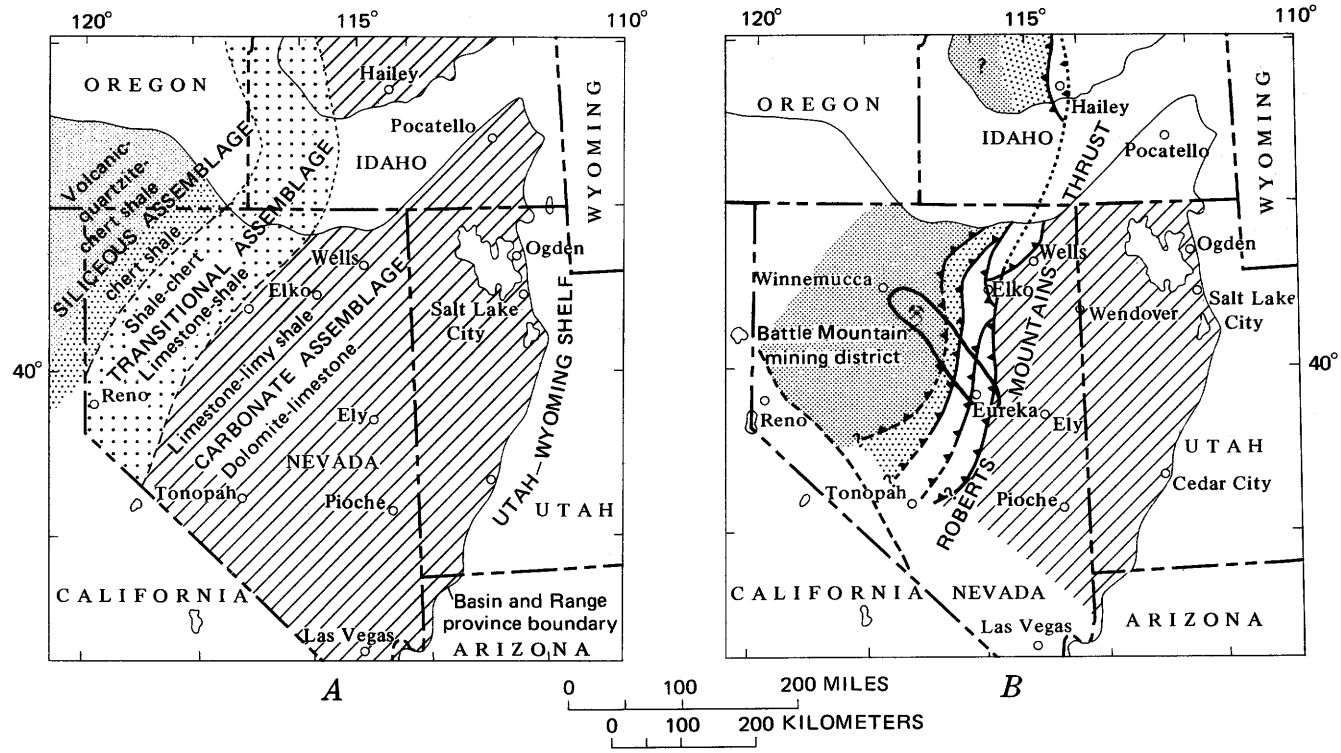


FIGURE 2.—Location of the Battle Mountain mining district, the Eureka–Battle Mountain mineral belt (Roberts, 1966), and and the inferred maximum eastern extent in Mississippian time of the upper plate of the Roberts Mountains thrust (Roberts and others, 1971). *A*, Distribution of facies after Late Devonian to Early Mississippian thrusting. *B*, Distribution of facies in the Cordilleran geosyncline, Cambrian through Devonian time.

of the Lower or Middle Cambrian Scott Canyon Formation; it also includes quartzite and chert of the Ordovician Valmy Formation. Both formations make up the upper plate of the Roberts Mountains thrust (Roberts Mountains plate). These two formations are in fault contact at Galena Canyon (fig. 3) along steeply dipping normal faults and along a shallow-dipping thrust fault. The Scott Canyon and Valmy were both, in turn, overthrust by sandstone and feldspathic sandstone of the Upper Cambrian Harmony Formation along the Dewitt thrust (fig. 3)—a late middle or early late Paleozoic thrust that is about the same age as the Roberts Mountains thrust of the Antler orogeny (Roberts, 1964). The Harmony Formation makes up the middle (the Dewitt plate) of the three thrust plates. These two plates are overlain unconformably by the Antler sequence.

The upper Paleozoic Antler sequence makes up an autochthonous structural block that rests along a major unconformity on the Harmony Formation and the Valmy Formation in the district (fig. 3). The rocks of the Antler sequence belong to the overlap assemblage of post-Antler orogenic time (Roberts, 1964). Three formations compose the Antler sequence: (1) the Middle Pennsylvanian Battle Formation, (2) the Upper Pennsylvanian and Lower Permian Antler Peak Limestone, and (3) the Upper Permian Edna Mountain Formation. Some of the ore zones at the Copper Canyon porphyry copper deposit are in rocks of the Harmony Formation, but most of the ore was localized in rocks of the Battle Formation.

The uppermost of the three thrust plates (the Golconda plate) in the district is made up of chert and argillite belonging to the Pennsylvanian(?) Pumpernickel Formation and sandstone, shale, quartzite, limestone, and chert belonging to the Middle Pennsylvanian and Lower Permian Havallah Formation. The Havallah Formation crops out west of Willow Creek (fig. 3). This plate is in fault contact with the Antler sequence on the Golconda thrust and along steeply dipping Tertiary normal faults. Rocks provisionally assigned to the Pumpernickel Formation include some significant copper plus gold ore bodies at the Copper Canyon porphyry copper deposit.

The style of deformation in the upper plate of the Golconda thrust differs markedly from that in the lower plate. Rocks in the lower plate appear to have been commonly broken by Tertiary fracturing and faulting, whereas in the upper plate, folding at the time of movement along the Golconda thrust is more conspicuous than Tertiary deformation.

These four tectonic blocks, made up of lower to upper Paleozoic rocks, have been intruded by about 50 gabbro to felsic granite stocks and dikes (Roberts, 1964). These may exceed 2.5 sq km in area. The largest body crops out at Trenton Canyon, in the west-central part of the district, about 10 km northwest of Copper Canyon. Although the intrusive rocks vary widely in composition, most were originally emplaced as granodiorites (Theodore and others, 1973). Some of the granodiorites have been altered by postmagmatic hydrothermal fluids to rocks that are now more potassic and chemically equivalent to quartz monzonites.

Plutonism in this part of Nevada occurred during four periods of time from Jurassic to middle Tertiary (McKee and Silberman, 1970; Silberman and McKee, 1971). M. L. Silberman of the U.S. Geological Survey has dated biotites and hornblendes by the K-Ar method from nine of the intrusive bodies across the mining district (Theodore and others, 1973). The plutonic body at Trenton Canyon is Late Cretaceous (87 m.y. (million years)), whereas all other plutonic rocks dated in the district are late Eocene or early Oligocene (41–37 m.y.). Three of these K-Ar dated Tertiary igneous bodies are in the area at Copper Canyon studied for this report (pl. 1). Furthermore, the middle Tertiary plutons at Battle Mountain clearly form part of a regional alinement of middle Tertiary plutons along the Eureka–Battle Mountain mineral belt (Roberts, 1966; McKee and Silberman, 1970). A 1,200-m-wide, 38-m.y.-old intrusion at Copper Canyon, which we will show later in this report to be both spatially and genetically associated with the porphyry copper deposit, is one of these middle Tertiary plutons. After a 5 m.y. gap, during which there was significant uplift and erosion, plutonism in the district was followed by deposition of volcanic rocks.

Two suites of volcanic rocks crop out in the mining district: (1) quartz latites, welded tuffs, and pyroclastics that occur as erosional remnants of the previously much more extensive Oligocene Caetano Tuff (Gilluly and Masursky, 1965; Stewart and McKee, 1970), whose age is 33 m.y. (McKee and Silberman, 1970), and (2) Tertiary or Quaternary basalt (fig. 3), the most conspicuous exposures of which are near the southern edge of the mining district.

## GEOLOGY OF THE COPPER CANYON AREA

The Copper Canyon area includes parts of the Roberts Mountains, Dewitt, Antler, and Golconda tectonic blocks (pl. 1); about one-half of this 16-sq-km area is covered by rocks belonging to the Golconda plate, which forms a prominent ridge west of the ore bodies at Copper Canyon (fig. 4). Stratigraphic assignments, lithologic descriptions, and regional structural implications of the rocks at Copper Canyon have been presented in detail by Roberts (1964). Therefore, in this chapter we will defer to Roberts' lithologic and structural details, except in those instances where our observations and data supplement his earlier work. Our large-scale topographic base allowed us to map in greater detail. Furthermore, we undertook a rigorous statistical evaluation of the outcrop-sized folds in the Golconda plate at Copper Canyon by standard techniques of structural analysis (Turner and Weiss, 1963).

### SILICEOUS AND VOLCANIC ASSEMBLAGE

#### CAMBRIAN SYSTEM

##### SCOTT CANYON FORMATION

The Scott Canyon Formation of the siliceous assemblage is Early or Middle Cambrian (Roberts, 1964, p. A16). It consists predominantly of chert with interbedded carbonaceous shale partings, carbonaceous shales and argillites, and locally abundant greenstones (altered andesites and (or) basalts), with lesser amounts of limestone and quartzite.

The thickness of the formation has not been measured because of a combination of: (1) incomplete sections of rock, (2) postdiagenetic transposition of bedding, (3) numerous local repetitions of section by tight folds, and (4) absence of suitable marker beds. These rocks have been extremely disrupted; chert phacoids, from tens of meters to several millimeters wide, are commonly surrounded by apparently more ductile shaly rock of the same formation. Roberts (1964, p. A14) suggests that the total thickness of the Scott Canyon Formation may be more than 1,500 m. A deep drill hole that was started in the rocks of the Scott Canyon Formation at Iron Canyon about 1.6 km east of the Copper Canyon area bottomed in rock lithologically similar to the Scott Canyon at a depth of about 1,300 m (Theodore and Roberts, 1971).

Only a small part of the Copper Canyon area is underlain by rocks belonging to the Scott Canyon Formation (pl. 1). Black to dark-gray carbonaceous argillite and chert (with minor amounts of greenstone) of this formation crop out east of the Plumas fault near the northeast corner of the area. Slope-forming poorly exposed argillite is the most common rock type here.

Several notable changes occurred in these rocks concomitant with alteration associated with metallization. Where they are hydrothermally altered, especially near the Plumas and Humbug–Lucky Chance mines, the argillite and chert are partly recrystallized and bleached whitish gray. Iron oxides which formed after already-introduced sulfides heavily stain joint, fracture, and bedding surfaces in the most affected areas.

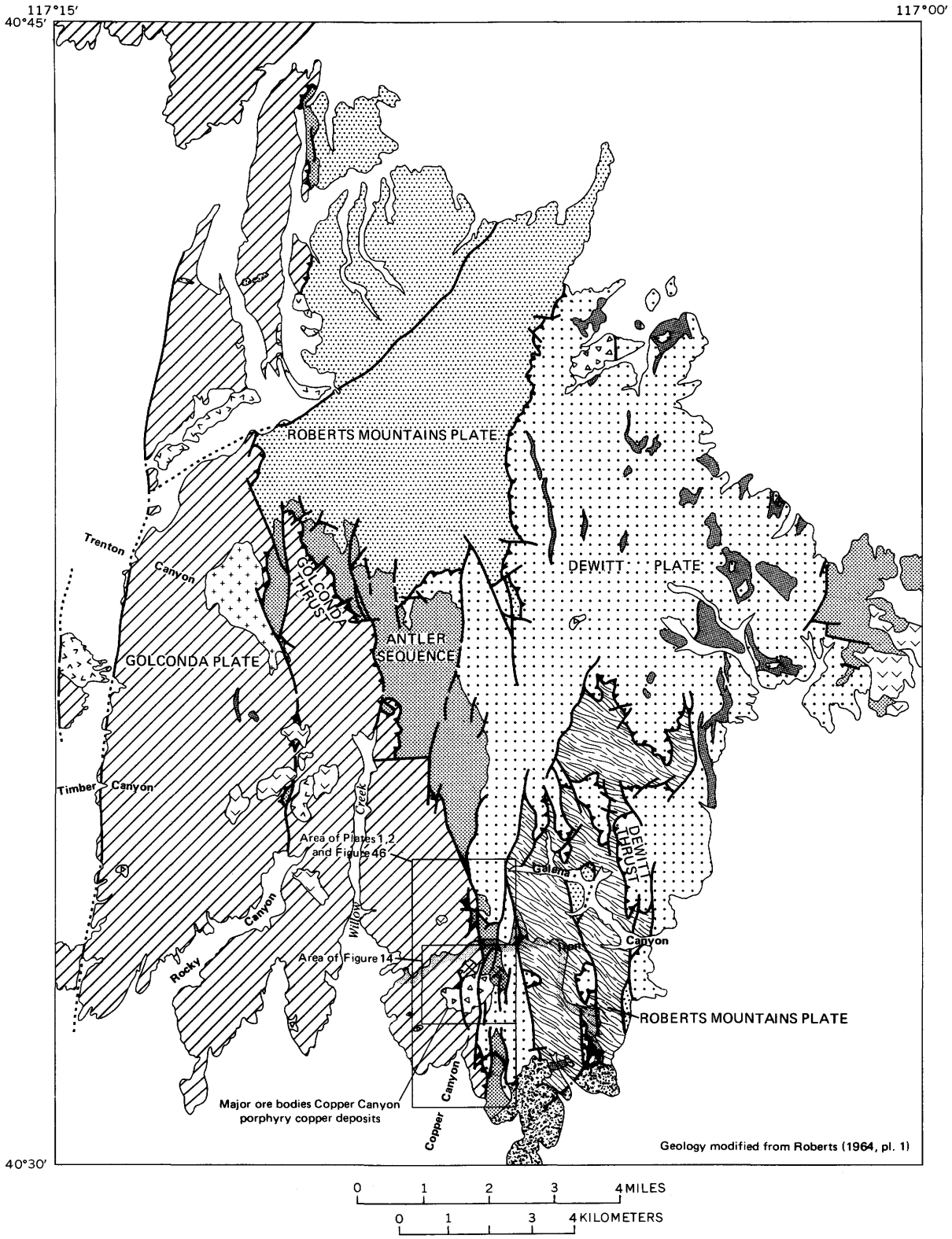


FIGURE 3.—Geologic sketch map of the Antler Peak quadrangle (Battle Mountain mining district), Lander County, Nev.

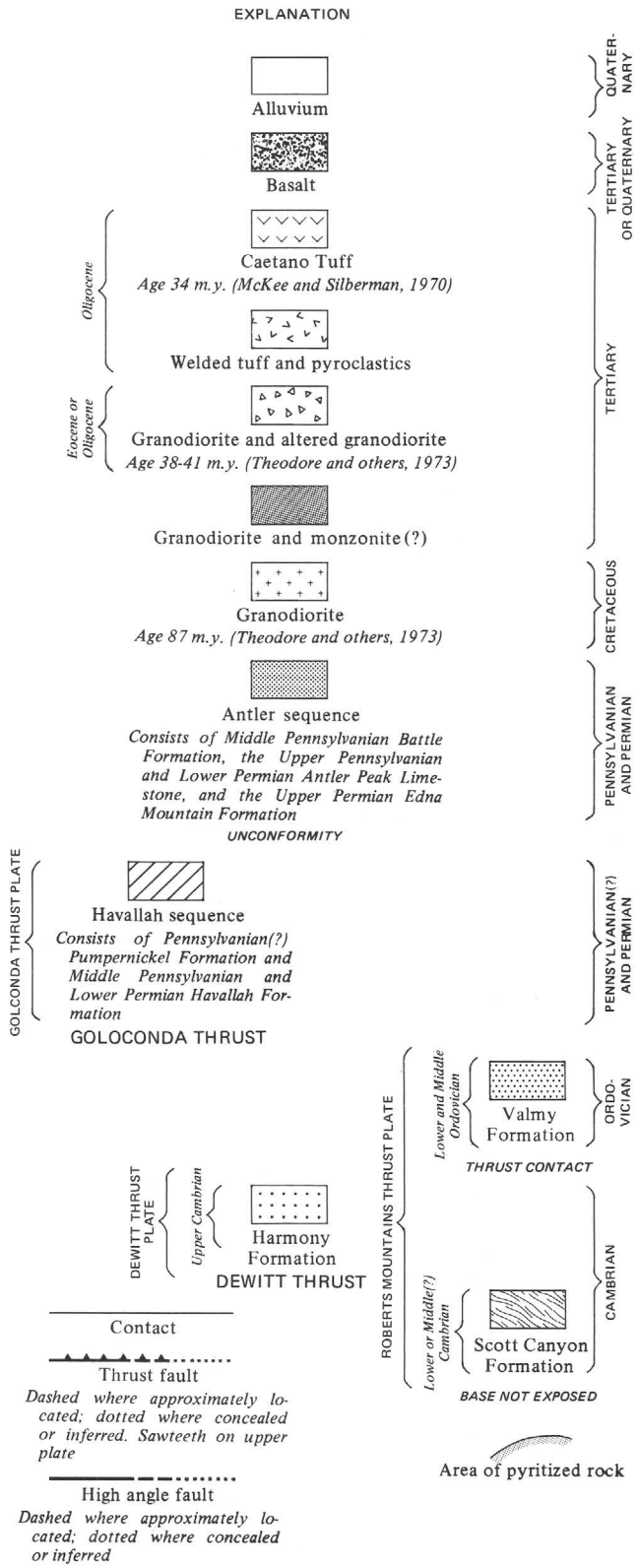


## TRANSITIONAL ASSEMBLAGE

### CAMBRIAN SYSTEM

#### HARMONY FORMATION

The Harmony Formation of the transitional assemblage is Late Cambrian (Roberts, 1964, p. A22). No identifiable fossils have been found in the Harmony in the Antler Peak quadrangle; however, P. E. Hotz of the U.S. Geological Survey collected trilobite fauna of Late Cambrian age in rocks assigned to the Harmony in the Osgood Mountains quadrangle, about 50 km northwest of the Antler Peak quadrangle( fig. 1).

Throughout the Antler Peak quadrangle, the Harmony Formation includes interbedded sandstone, feldspathic sandstone, arkose, granule and pebbly sandstone, shale, and limestone (Roberts, 1964, p. A23). Most of the formation is sandstone. The thickness cannot be measured directly, because the rocks are for the most part poorly exposed, weathering to smooth, gently rounded slopes instead of forming good outcrops. Roberts (1964, p. A23) estimates the total thickness in the Antler Peak quadrangle to be about 900 m.

Greenish-brown sandstone and feldspathic sandstone with minor black shale and red shale of the Harmony crop out irregularly in the northeastern parts of the Copper Canyon area (pl. 1). All rocks of the Harmony are in the upper plate of the Dewitt thrust (Roberts, 1964), which is not exposed at Copper Canyon but crops out in Iron and Galena Canyons (fig. 3).

These unaltered rocks of the Harmony give way to variably altered rocks in the southern part of the Copper Canyon area. Weak alteration consists chiefly of traces of introduced pyrite with partial recrystallization of detrital quartz grains. Sparse amounts of white mica and trace amounts of chlorite have developed in some of these rocks (Roberts and Arnold, 1965, p. B25; Theodore and Blake, 1969). Approaching the areas of conspicuous copper metallization, near the porphyry copper deposit at Copper Canyon, the rocks of the Harmony have been intensely hydrothermally metamorphosed. The rocks here are typically very dense biotite hornfelses that are intricately veined. Mineralogic and chemical changes in the rocks of this formation during metallization are described below in the section on the porphyry copper deposit.

## HAVALLAH SEQUENCE

In the Antler Peak quadrangle, the Havallah sequence is an allochthonous tectonic block of rocks, as are the previously described siliceous and transitional

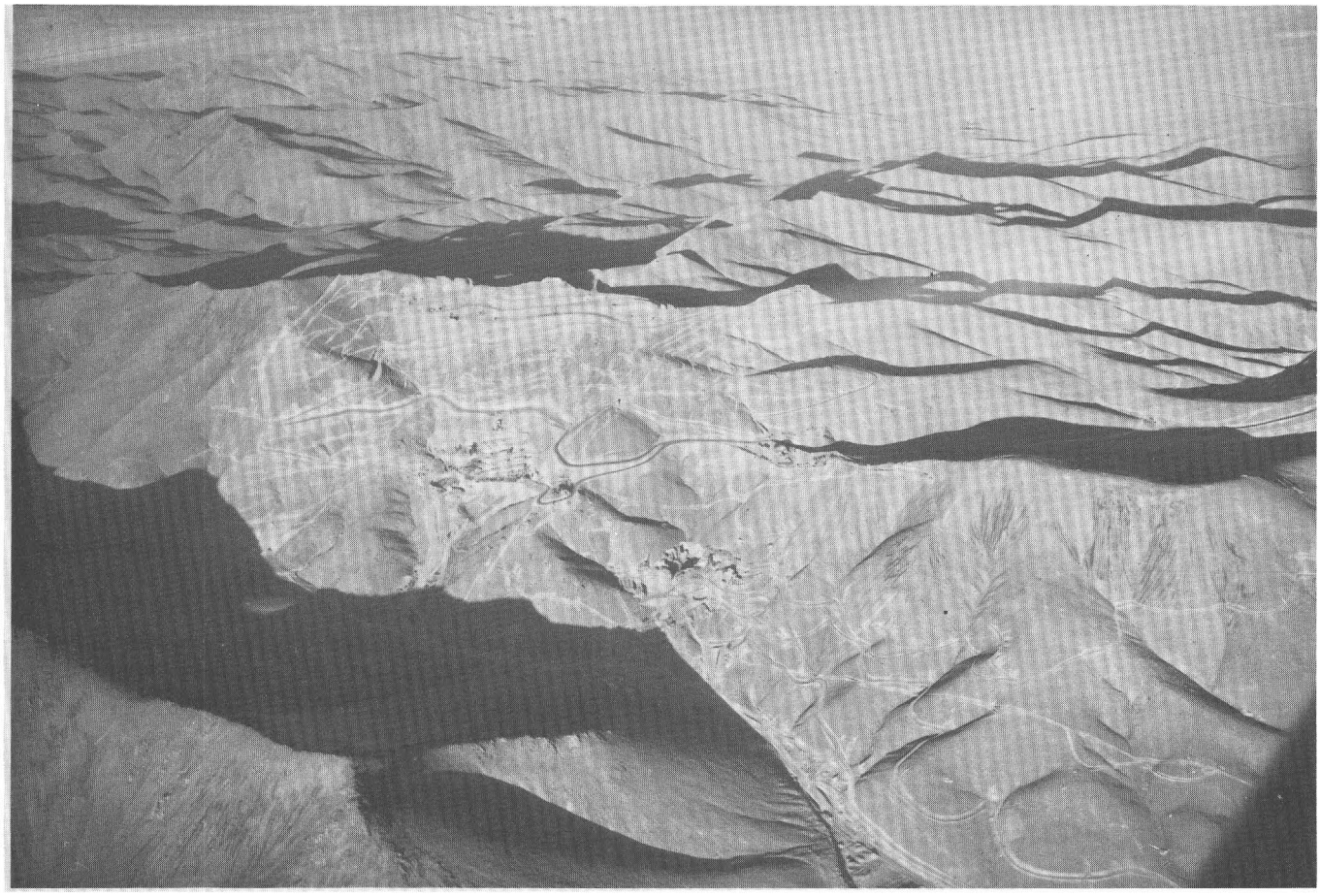

FIGURE 4.—Oblique northwest aerial view of the Copper Canyon mine area. Prominent ridge in the left foreground is composed of rocks in the upper member of the Pennsylvanian(?) Pumpernickel Formation. Photo by R. J. Roberts in 1966.

assemblage ones. Two formations that make up the Havallah sequence are the Pennsylvanian(?) Pumpernickel Formation and the possibly disconformably overlying Middle Pennsylvanian and Lower Permian Havallah Formation (Roberts, 1964, p. A37–A45), which does not crop out at Copper Canyon (pl. 1).

## PENNSYLVANIAN(?) SYSTEM

### PUMPERNICKEL FORMATION

The Pumpernickel Formation is considered to be Pennsylvanian(?). As pointed out by Roberts (1964, p. A44), assignment of a definite age to this formation is still not possible and is contingent upon finding more diagnostic faunal assemblages than have been collected to date.

The Pumpernickel Formation at Copper Canyon is made up chiefly of chert and argillite, with sparse greenstone (altered andesite or basalt), limy shale, siltstone, sandstone, and poorly sorted chert-pebble conglomerate. Although conglomerate makes up only a small fraction of the rocks in the Pumpernickel, individual conglomerate beds, generally less than 1 m thick, serve as local marker horizons for distances up to about 100 m along strike. Two major units have been mapped in the Pumpernickel (pl. 1): an easily eroded basal gray-brown argillite with sparse chert interbeds and a conformably overlying predominantly chert unit. The argillite is the oldest unit of the Pumpernickel described by Roberts (1964, p. A38). The very resistant chert unit underlies the ridge on the west side of Copper Canyon. It is part of the middle unit of the formation previously recognized by Roberts. Roberts' upper unit of the Pumpernickel is predominantly argillite and crops out west of Copper Canyon.

Total thickness of the Pumpernickel cannot be measured directly. Roberts (1964, p. A38) estimated its strata to total at least 1,500 m in thickness, with about 150 m for the basal argillite, about 300 m for the middle unit, and about 1,100 m for the upper unit. At Copper Canyon, complete stratigraphic sections of our lower and upper units are not exposed. The base of the lower unit has been tectonically cut out either by the Golconda thrust or by Tertiary normal faults, and the top

of our upper unit crops out west of the Copper Canyon area. From cross sections at the Nevada mine, we estimate lower unit strata to be 150–300 m thick and upper unit strata to be about 350 m thick. In the vicinity of the Copper Canyon pluton, the lower unit may be about 300 m thick, and the upper unit about 350 m. South of the pluton, the upper unit may be up to about 600 m thick. However, because of structural complications by faulting throughout the Pumpernickel, these are only rough estimates.

The rocks of the Pumpernickel Formation are variously altered by hydrothermal fluids in the Copper Canyon area. Alteration consists primarily of four types: (1) bleaching of argillite around some of the base metal vein deposits, (2) intense to moderate recrystallization of chert to a sugary quartzose hornfels near the Copper Canyon pluton, (3) metamorphism of argillite to biotite hornfels, and (4) metasomatic development of coarse-grained calc-silicate metamorphic minerals in one of the copper ore bodies. The petrologic details of the last type are included in a section of this report on the porphyry copper deposit. Representative chemical changes accompanying the first and second types of alteration are shown in table 2. Our analyses suggest gains in silica and slight losses in most other oxides, if we assume volume for volume replacement during alteration of argillite to a bleached metaargillite. The unaltered argillite sample (1, table 2) was collected about 60 m northeast of the Buena Vista mine. The bleached argillite (sample 2) is from the Buena Vista mine, whose workings are partly along a fault bounding the basal argillite unit and the overlying chert. This mine was chiefly a lead-zinc-silver vein deposit (Roberts and Arnold, 1965). Hydrothermal alteration of chert to quartzose hornfels may have involved slight additions in silica and losses in FeO, MgO, and CaO (samples 3 and 4, table 2). Sample 3 was collected about 8 m from the southern edge of the Copper Canyon pluton, west of the main drainage through the canyon.

TABLE 2.—*Chemical analyses of rocks from the Pumpernickel Formation, Copper Canyon area, Lander County, Nev.*

[Analysts: samples 1–3, L. Artis and P. Elmore, by rapid rock methods (Shapiro, 1967); sample 4, from Roberts (1964, table 4)]

| | 1 | 2 | 3 | 4 |
|---|---|---|---|---|
| $SiO_2$ | 78.6 | 88.1 | 96.2 | 94.6 |
| $Al_2O_3$ | 7.6 | 4.7 | 1.1 | 1.8 |
| $Fe_2O_3$ | .80 | .20 | .54 | .36 |
| FeO | 1.8 | 1.6 | .08 | .28 |
| MgO | 1.7 | .14 | .03 | .64 |
| CaO | 1.8 | .07 | .14 | .49 |
| $Na_2O$ | .86 | .09 | .25 | .15 |
| $K_2O$ | 2.1 | 1.6 | .34 | .37 |
| $H_2O^+$ | 1.8 | 1.3 | .45 | .77 |
| $H_2O^-$ | .35 | .23 | .10 | .09 |
| $TiO_2$ | .55 | .55 | .08 | .07 |
| $P_2O_5$ | .12 | .06 | .01 | .24 |
| MnO | .00 | .00 | .00 | .03 |
| $CO_2$ | 1.3 | .02 | .02 | .60 |
| Total | 99 | 99 | 99 | 100 |
| Specific gravity (lump) | 2.69 | 2.50 | 2.54 | ..... |

1. Argillite (lab. No. M108905W; field No. TT–69–1), lower unit SE¼ sec. 16, T. 31 N., R. 43 E.
2. Bleached metaargillite (lab. No. M108906W; field No. TT–69–2), lower unit, SE¼ sec. 16, T. 31 N., R. 43 E.
3. Metachert (lab. No. M108908W; field No. TT–69–4), upper unit, NE¼ sec. 28, T. 31 N., R. 43 E.
4. Black chert (field No. 53–AP–1) from adit in SE¼ sec. 16, T. 31 N., R. 43 E.

## OVERLAP ASSEMBLAGE

### PENNSYLVANIAN SYSTEM

#### BATTLE FORMATION

The Battle Formation of the overlap assemblage is Middle Pennsylvanian (Atokan) (Roberts, 1964, p. A31). The basal unit of the Antler sequence, it rests on the rocks of the Harmony Formation at Copper Canyon with an angular discordance—an unconformity with paramount regional implications (Roberts and others, 1958). Roberts described three members in the Battle, but he was not able to show them individually on the geologic map of the quadrangle.

The three members (lower, middle, and upper) crop out at Copper Canyon (pl. 1). They are a lower reddish-brown calcareous chert pebble conglomerate, a variously colored middle shale member, and an upper drab quartzite and chert pebble conglomerate, or their pyritically altered equivalents. The three members are conformable with one another, and their contacts are quite recognizable because of contrasting lithologies. Iron-oxide-rich red beds of the lower member of the Battle are locally very conspicuous in unaltered areas at Copper Canyon (pl. 1). Whenever possible, they have been shown as separate map units. In the north-central part of the area, a 10–20-m-thick red bed unit crops out for a 600-m-strike length at the base of the lower member. Farther to the south, sedimentary red bed units have not been recognized in altered rock at Copper Canyon, bcause they are obscured by iron oxides after pyrite associated with alteration. Altered equivalents of the lower member contain most of the ore at the porphyry copper deposit.

The thickness of the Battle is also difficult to measure. As with the previously described Scott Canyon and Harmony Formations, a complete, structurally uncomplicated section of the Battle Formation is not exposed at any one locality in the quadrangle. Roberts (1964, p. A29) measured an aggregate thickness of 222 m for the entire formation in the general vicinity of Antler Peak, about 3.2 km north of the Copper Canyon area. Where strata are best exposed at Copper Canyon, we estimate the lower, middle, and upper members of the Battle to be about 106 m, 46 m, and 24 m thick, respectively. These estimates were made from cross sections. The

top of the upper member is not exposed at Copper Canyon, and the middle member here is a slope-forming unit that is nowhere completely exposed.

#### PENNSYLVANIAN AND PERMIAN SYSTEMS

##### ANTLER PEAK LIMESTONE

The Antler Peak Limestone, middle formation of the overlap assemblage in the quadrangle, is Late Pennsylvanian and Early Permian (Roberts, 1964, p. A34). Its type locality is at Antler Peak, where the unit is about 191 m thick.

At Copper Canyon (pl. 1), the Antler Peak Limestone is a resistant well-bedded dark-gray limestone. Some of the limestone contains well-rounded chert granules. It crops out only in six small areas in the general vicinity of the Nevada mine, and in the largest of these areas, it underlies a $180 \times 60$ m outcrop area. Less than 10 m of the Antler Peak Limestone strata crops out even in this area. The formation at Copper Canyon is everywhere in tectonic contact with surrounding rock—both as lensoid fault slivers along the Golconda thrust and also as a wedge-shaped block, bounded by normal faults.

#### PERMIAN SYSTEM

##### EDNA MOUNTAIN FORMATION

The Edna Mountain Formation, upper unit of the overlap assemblage in the quadrangle, is Late Permian (Roberts, 1964, p. A37). At its type locality in the Golconda quadrangle, the unit is predominantly brown calcareous sandstone at most 120 m thick (Ferguson and others, 1952). The Edna Mountain was deposited after some uplift and erosion of the Antler Peak Limestone.

At Copper Canyon, three interbedded units make up the Edna Mountain Formation: (1) slope-forming brown to buff calcareous sandstone with minor limy shale, (2) resistant white to gray massive limestone, and (3) resistant fairly well sorted, drab chert pebble conglomerate. The few small exposures of this formation in the area are near the townsite of Galena and the Nevada mine. Furthermore, these rocks are everywhere in fault contact with enclosing rocks belonging to other formations, most importantly with rocks of the Pumpernickel Formation thrust over them along the Golconda thrust. Maximum thickness of exposed strata assigned to the Edna Mountain Formation is estimated from cross sections to be about 45 m in the Copper Canyon area.

### SURFICIAL DEPOSITS

#### QUATERNARY SYSTEM

Older alluvium, landslide, talus, hill wash, and younger alluvium make up the surficial Quaternary deposits in the Copper Canyon area. The older alluvium at the mouth of Copper Canyon is part of a broad range-front fan around the Battle Mountain range. In its upper reaches at Copper Canyon, it is a poorly bedded unconsolidated or slightly consolidated sand, gravel, and boulder conglomerate. Lower gravels from this older alluvium at Copper Canyon yielded several million dollars worth of placer gold (Roberts and Arnold, 1965).

### INTRUSIVE ROCKS

#### ALTERED GRANODIORITE OF COPPER CANYON

##### GEOMETRY OF THE INTRUSIVE BODY

A generally equidimensional 1,200-m-wide intrusive body, the largest in the area, lies astride the Dewitt plate, the Antler sequence, and the Golconda plate at Copper Canyon (pl. 1). This body of rock seems to be spatially and genetically associated with many of the surrounding ore deposits in this part of the mining district (Roberts and Arnold, 1965; Nash and Theodore, 1971). Although the geologic map of the pluton suggests a simple cylindrical configuration, several drill holes indicate that the geometry of the intrusion at depth is instead very complex (pl. 1; Blake, 1971). From these data, the pluton in a vertical section is shaped rather like a "doughnut" with a thin center and a thicker rim area. Our mapping also suggests that its emplacement was controlled partly by the Virgin fault and possibly by the Copper Canyon fault and was helped by assimilation of rocks of the Pumpernickel Formation in the Golconda plate. There is no evidence for doming or upheaving in the wallrocks of the pluton. This intrusion may be a cupola of an igneous body that is much more laterally extensive at depth.

##### LITHOLOGY AND CHEMISTRY

Rocks within the granodiorite predominantly have a porphyritic granitic fabric. Tabular oligoclase-andesine (average), primary red-brown biotite, and gray-green hornblende phenocrysts about 1 mm long are all set in a very fine quartz–K-feldspar–white mica–(secondary biotite) matrix (fig. 5). In addition, subhedral quartz bipyramid phenocrysts, as much as about 1.5 cm long, commonly make up about 20 percent of typical hand specimens from the intrusion. Some quartz phenocrysts are partially resorbed, and all have abundant fluid inclusions. Phenocrystic plagioclase makes up 38 percent by volume of drill core through the granodiorite, and it reaches 1 cm in length in some samples. Some complexly and partly resorbed zoned plagioclase phenocrysts have cores as calcic as $An_{65}$. The primary biotites are magnesian (table 3), and their compositions and structural formulas are discussed in Theodore, Silberman, and Blake (1973). Less abundant K-feldspar phenocrysts are cryptoperthitic with an Or content of about

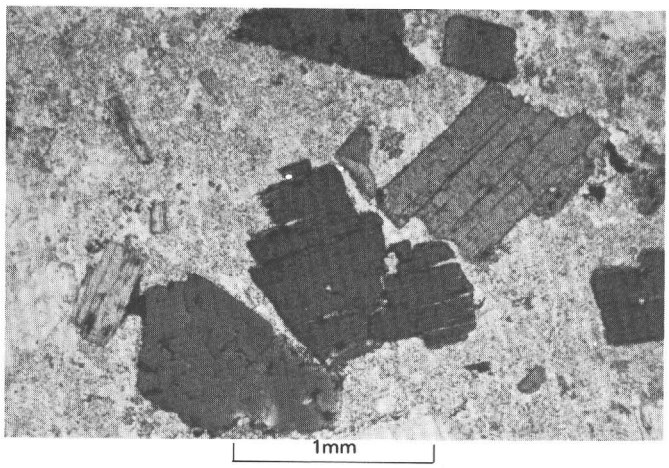


FIGURE 5.—Primary phenocrystic biotite from the altered granodiorite of Copper Canyon, in plane polarized light.

80 mol percent (Clement, 1964), and they show varying degrees of replacement by white mica. Accessory minerals include apatite, sphene, zircon, allanite, rutile, and traces of magnetite. Secondary chlorite is common in a few rock samples both in veinlets and at margins of primary biotite. Supergene copper staining of plagioclase phenocrysts is typical in most exposures of the intrusion (Clement, 1968).

Texturally, the groundmass of the granodiorite represents two different types of fabric. The first type, which is very sparse, consists of an aplitic intergrowth of equant quartz and K-feldspar crystals (about 0.01 mm wide) that are almost everywhere bounded by straight crystal boundaries. The second groundmass type, which is found in the majority of the rocks from the intrusion, consists of quartz and K-feldspar crystals (generally much less than 0.01 mm wide) that have very complexly intergrown and sutured boundaries. In addition, varying amounts of white mica and secondary biotite are sprinkled through the second groundmass type. Our petrographic investigations suggest that the first type is a remnant of original crystallization from a magma and that the second is a hydrothermal alteration phenomenon (Theodore and others, 1973), belonging to Creasey's (1966) potassic type. Rare inclusions of quartz and K-feldspar grains (about 0.01 mm wide, and slightly smaller than those in the enclosing groundmass) along the margins of euhedral, strongly zoned plagioclase phenocrysts also suggest that the first type of groundmass fabric closely reflects the overall initial "quenched" state in the intrusion. In areas of more intense potassic alteration in the intrusion, primary biotites have recrystallized to complexly intergrown clusters of very fine biotite crystals all pseudomorphous after the primary biotites. Hornblende crystals are variously replaced by biotite. The hydrothermal, secondary biotite crystals are red brown (Y=Z), only slightly paler than the primary ones.

TABLE 3.—*Compositions and structural formulas of biotites from the altered granodiorite of Copper Canyon*

[Major elements: analyst, Sarah T. Neil, U.S. Geological Survey, using classical methods, and methods of Ingamells (1962, 1966), Suhr and Ingamells (1966), and Medlin, Suhr, and Bodkin (1969). Minor elements: semiquantitative spectrographic analyses by R. E. Mays, U.S. Geological Survey. Results are reported in percent to the nearest number in the series 1, 0.7, 0.5, 0.3, 0.2, 0.15, 0.1, 0.07, .....; these numbers represent approximate midpoints of group data on a geometric scale. The precision of a reported value is approximately plus or minus one interval about 68 percent of the time or two intervals 95 percent of the time. Elements looked for but not found: As, Au, B, Be, Bi, Cd, Ce, Ge, Hf, Hg, In, La, Li, Mo, Pb, Pd, Pt, Re, Sb, Sn, Ta, Te, Th, Tl, U, W, Y, Yb, Zn. Structural formulas were calculated on the basis of 24 (O, OH, Cl, F) per formula unit. $X_2Y_{4-6}Z_8O_{20}$ (OH, F, Cl)$_4$ is assumed to be the general structural formula]

| | A | B | C |
|---|---|---|---|
| Lab No. | M109678 | M109679 | M109681 |
| Field No. | MB–18 | MB–23 | MB–31 |
| **Major elements (weight percent)** | | | |
| $SiO_2$ | 37.81 | 37.51 | 36.49 |
| $Al_2O_3$ | 15.30 | 14.70 | 15.79 |
| $Fe_2O_3$ | 1.69 | .51 | .35 |
| FeO | 10.97 | 14.49 | 14.49 |
| MgO | 15.72 | 15.12 | 15.91 |
| CaO | .21 | .36 | .16 |
| $Na_2O$ | .10 | .15 | .10 |
| $K_2O$ | 8.73 | 9.12 | 8.48 |
| $H_2O^+$ | 4.05 | 3.59 | 4.11 |
| $H_2O-$ | .32 | .08 | .02 |
| $TiO_2$ | 2.93 | 2.69 | 2.91 |
| $P_2O_5$ | .18 | .32 | .21 |
| MnO | .02 | .09 | .04 |
| Cl | .4 | .5 | .4 |
| F | 1.59 | 1.17 | 1.29 |
| $Cr_2O_3$ | .1 | .1 | .1 |
| BaO | .33 | .37 | .34 |
| $V_2O_5$ | .1 | .1 | .1 |
| Subtotal | 100.6 | 101.0 | 101.3 |
| Less O=F, Cl | .75 | .61 | .63 |
| Total | 99.8 | 100.4 | 100.7 |
| **Minor elements (weight percent)** | | | |
| Ag | 0.0007 | ..... | ..... |
| Co | .002 | 0.005 | 0.003 |
| Cu | .2 | .03 | .01 |
| Mo | .003 | ..... | ..... |
| Nb | .003 | .003 | .003 |
| Ni | .015 | .02 | .015 |
| Sc | .005 | .003 | .003 |
| Sr | .001 | ..... | ..... |
| Zr | .003 | .005 | ..... |
| **Structural formulas** | | | |
| Si } Z | 5.54 } 8.00 | 5.59 } 8.00 | 5.36 } 8.00 |
| $Al^{iv}$ } Z | 2.46 } | 2.41 } | 2.64 } |
| $Al^{vi}$ } Y | .18 } 5.46 | .18 } 5.71 | .10 } 5.74 |
| $Fe^{+3}$ } Y | .19 } | .06 } | .04 } |
| Ti } Y | .32 } | .30 } | .32 } |
| Mg } Y | 3.43 } | 3.36 } | 3.49 } |
| $Fe^{+2}$ } Y | 1.34 } | 1.80 } | 1.78 } |
| Mn } Y | ..... } | .01 } | .01 } |
| Ca } X | .03 } 1.69 | .06 } 1.83 | .03 } 1.65 |
| Na } X | .03 } | .04 } | .03 } |
| K } X | 1.63 } | 1.73 } | 1.59 } |
| OH | 3.96 } 4.80 | 3.57 } 4.25 | 4.03 } 4.73 |
| F | .74 } | .55 } | .60 } |
| Cl | .10 } | .13 } | .10 } |

There is sparse sulfide mineralization in the granodiorite, primarily as chalcopyrite in quartz–K-feldspar veins that cut the igneous fabric of the rocks. Some pyrrhotite is disseminated through the intrusion and generally increases with depth. Because almost all of our samples from the intrusive body reflect some degree of hydrothermal alteration, we cannot rule out the possilibity that some sulfide deposition was contemporaneous with magmatic crystallization.

Because of the pervasive potassic alteration in the general area of the pluton and the nearby ore deposits at Copper Canyon, the unaltered chemical state of the intrusive body cannot be determined directly. Nonetheless, petrographic and chemical studies of many plutons that are both altered and unaltered throughout the Battle Mountain mining district suggest that these altered intrusive bodies were originally intruded as granodiorite (Theodore and others, 1973). The altered bodies, including the Copper Canyon one, are now quartz monzonite, both modally and chemically.

### XENOLITHS

Xenoliths in the granodiorite of Copper Canyon may be classed as two types, largely on the basis of relative size. The larger ones that occur as individual mappable schistose pendants as much as 60 m wide belong to the Pumpernickel Formation. The smaller ones, which also belong to the Pumpernickel, make up an intrusion breccia zone in the central part of the pluton that is several hundred meters wide and about 45 m thick. The zone consists predominantly of subrounded metamorphosed clasts several centimeters across set in a medium- to fine-grained granitic matrix with 1 cm plagioclase laths. These clasts are intensely recrystallized chert fragments of the upper unit of the Pumpernickel Formation. We interpret this intrusion breccia to be a remnant of the intrusive body's "caprock" and conclude that the intrusion at Copper Canyon did not breach the Golconda plate when it was emplaced. Clement (1964) suggested that this zone is fault breccia that developed along the Golconda thrust. However, where the Golconda thrust crops out south of the intrusive body (pl. 1), no breccia of similar lithology and thickness occurs. In addition, examination by Blake of many drill holes through the Golconda thrust reveals that fault breccia and fault gouge at the thrust are generally restricted to zones less than 2 m thick.

Projection of contacts in cross sections through the breccia and into the Pumpernickel in the pluton's wallrock seems to require some central collapse in the intrusion after its emplacement. The breccia in the intrusion at Copper Canyon crops out only between the traces of the Copper Canyon and Virgin faults (pl. 1). Directly to the north of this breccia in the same fault block, the pluton's wallrock is made up of metamorphosed argillite of the lower unit of the Pumpernickel. Because recrystallized fragments of the Pumpernickel in the intrusion breccia most likely belong to the upper chert unit, it is possible that collapse may have been as much as 100 m.

### AGE OF INTRUSIVE BODY

The altered granodiorite of Copper Canyon is late Eocene or early Oligocene in age as indicated by K-Ar age determinations by M. L. Silberman (Theodore and others, 1973). Three primary biotite separates from the pluton yielded ages of 38.0, 38.2, and 38.5 m.y., with about a 2-percent analytical precision in the reported ages. The locations of these three dated samples are shown on plate 1.

### DEPTH OF EMPLACEMENT

Geologic evidence at Copper Canyon suggests that the pluton was emplaced at shallow depths. The Copper Canyon area lies near the inferred eastern limit of the at least 40-km-wide Golconda thrust plate (Silberling and Roberts, 1962). This thrust plate is envisioned by Roberts (1964) to have been originally wedge shaped in section, perhaps even tapering to about 1,500 m thick at its leading edge. A similar wedge-shaped model is proposed for the upper plate of the Roberts Mountains thrust by Carlisle (1965, p. 272–274). The granodiorite of Copper Canyon was emplaced into the upper plate of the Golconda thrust in late Eocene or early Oligocene time but apparently did not breach it. Regional studies by Silberling and Roberts (1962) show that rocks of the Golconda plate were emergent during most of the late Mesozoic and later. But the Copper Canyon area may have been undergoing sedimentation during the early Mesozoic. There may have been a maximum of about 1,000 m of Triassic units deposited on the Golconda plate at Copper Canyon after it was thrust into the area (R. J. Roberts, oral commun., 1971). This volume of rock has since been removed by erosion. The cover over the pluton at the time of its emplacement was thus predominantly the upper plate of the Golconda thrust because the Triassic section presumably was largely eroded by late Eocene or early Oligocene time.

The thickness of the upper plate cannot be determined directly at Copper Canyon. However, we infer that the thrust plate plus the Triassic section were not more than 2,500 m thick at Copper Canyon. If we assume that three-quarters of the Triassic section was removed by the time the intrusive body was emplaced in late Eocene and early Oligocene time, then this body completed its crystallization from a magma under about 1,500 m of cover. The present erosion surface on the

intrusion is probably very close to the uppermost level that this particular body reached in the crust. A corollary of our depth analysis of this one intrusive body is that all intrusive bodies in the mining district that were emplaced into the Golconda plate necessarily must have been emplaced under a fairly shallow cover.

## PETROGENETIC IMPLICATIONS OF PRIMARY BIOTITE COMPOSITIONS

The composition of biotite, chemically buffered by coexisting magnetite and K-feldspar, is related to the biotite's fugacity of water-temperature field (Wones and Eugster, 1965). From this field and experimentally determined minimum melting curves (Luth and others, 1964; Piwinskii, 1968), the maximum temperatures and the minimum depths of crystallization of an igneous rock can be estimated. Determination of P-T (pressure-temperature) conditions during biotite crystallization in igneous bodies spatially associated with hypogene ore deposits helps to define the depth of metallization. Therefore, in an attempt to establish these limiting P-T parameters for the Copper Canyon intrusive body, we selected three biotites from the intrusive body for further investigation.

Experimental studies by Wones and Eugster have established the compositions of synthetic biotites, on the phlogopite-annite join, coexisting with sanidine and magnetite as a function of fugacity of $H_2O$, oxygen fugacity, and temperature. However, there are some limitations to the application of this experimental work to natural systems. If we assume minimal effects on annite stabilities because of substitutions other than $Mg^{+2}$, then the results of Wones and Eugster (1965) may be applied to natural biotites. However, they suggest (p. 1257) that (Na, Ca) $\rightleftarrows$ K and $3Fe^{+2} \rightleftarrows 2Al^{+3} + \square$ substitutions are the only ones that will "tend to decrease the stability of annite," and Rutherford (1969) showed that $Na_2O$ will indeed lower the stability of iron-rich biotites. At Copper Canyon, the biotites (table 3) contain 0.10 and 0.15 weight percent $Na_2O$ and from 0.16 to 0.36 weight percent CaO. $TiO_2$ is probably concentrated in rutile. However, additional experimental data (Munoz and Eugster, 1969; Rosenburg, 1970; Rieder, 1971) indicate that HF gases would also strongly influence the thermal stability of (OH, F)-micas, such as those at Copper Canyon (see table 3). Nevertheless, mica thermal stabilities calculated for a fluorine-free environment and for $P_{H_2O}=P_{total}$ must be considered minimal, because fluorine stabilizes micas to higher temperatures (P. E. Rosenburg, oral commun., 1971).

The two biotites obtained from a drill core in the intrusive body at Copper Canyon (B and C, fig. 6) plot slightly below the trend of the quartz-fayalite-magnetite (QFM) buffer in the ternary system $KFe^{+2}_3AlSi_3O_{12}$ $(OH)_2$ — $KMg^{+2}_3AlSi_3O_{10}$ $(OH)_2$ — $KFe^{+3}_3AlSi_3O_{12}$ $(H_{-1})$. The other biotite analyzed in the altered granodiorite of Copper Canyon (A, fig. 6) plots along the trend of the Ni-NiO buffer. From these relations, we infer that oxygen fugacities during primary crystallization of phenocrystic biotites during plutonism at Copper Canyon were near the trends defined by the Ni-NiO and QFM buffers. These biotites coexisted with K-feldspar and magnetite at hypersolidus conditions. Compared to the oxygen fugacities inferred to have prevailed during batholithic plutonism in the Sierra Nevada (Dodge and others, 1969) oxygen fugacities during plutonism at Battle Mountain seem low.

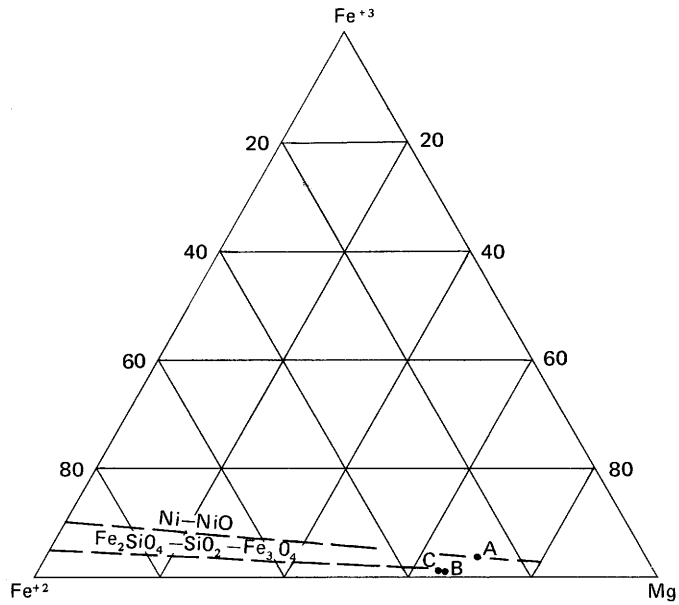


FIGURE 6.—Relation of $Fe^{+3}-Fe^{+2}-Mg$ contents in biotites from table 3. Dashed lines represent compositions of "buffered" biotites in the ternary system $KFe_3^{+2}AlSi_3O_{12}(OH)_2-KMg_3^{+2}AlSi_3O_{10}(OH)_2-KFe_3^{+3}AlSi_3O_{12}(H_{-1})$ from Wones and Eugster (1965, fig. 1). Biotite samples same as table 3.

In figure 7, these calculated univariant biotite breakdown curves (A and B–C) are shown together with a tonalite solidus curve (TO, modified from Piwinskii, 1968) and the granite minimum melting curve (Ab-Or-Q-$H_2O$, modified from Luth and others, 1964). The breakdown curves for biotites B and C (table 3) coincide. These curves are for $P_{H_2O}$ equal to $P_{total}$; for $P_{H_2O}$: $P_{total}$ ratios less than 1.0, the biotites' univariant curves would shift to the left. The granite minimum melting curve and the tonalite melting curve (fig. 7) are for magma saturated with $H_2O$ ($P_{H_2O}=P_{fluid}=$

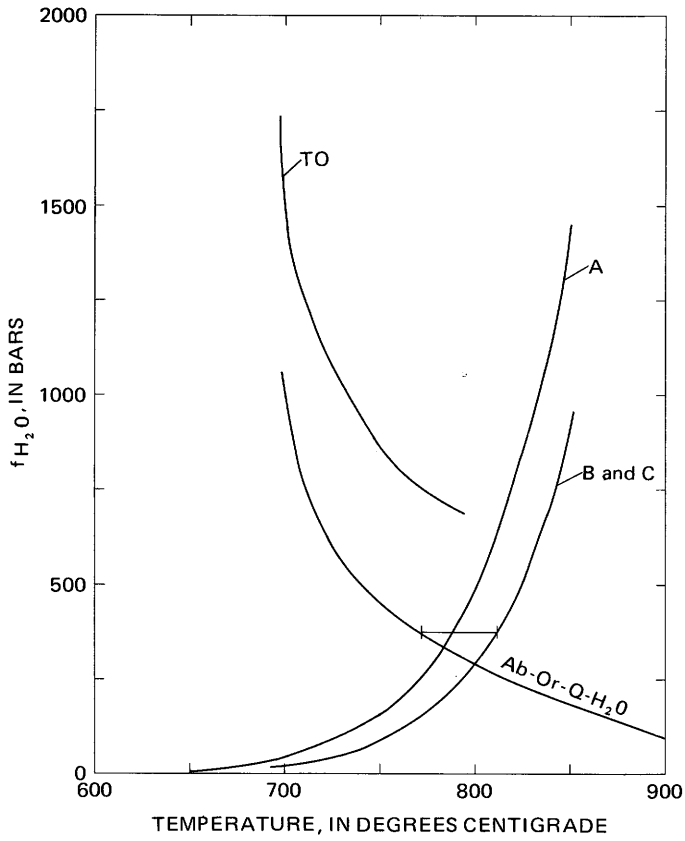


FIGURE 7.—Stability curves for biotites from the altered granodiorite of Copper Canyon relative to both the Ab-Or-Q-$H_2O$ solidus curve and to a Sierran tonalite (TO) solidus curve, The solidus (beginning of melting) curves have been replotted from Luth, Jahns, and Tuttle (1964) and Piwinskii (1968), after converting $P_{H_2O}$ to $f_{H_2O}$ using the fugacity ratios calculated by Anderson (1964). Biotite curves A and B–C from biotites A, B, and C, table 3, respectively.

$P_{total}$). If the rocks were not saturated with $H_2O$ and if all intial $H_2O$ were in hydrous minerals, the solidus curves, where $P_{fluid}=P_{total}$, would shift to the right.

Primary crystallization of the intrusion at Copper Canyon probably occurred in at least two stages involving fractional crystallization: (1) early crystallization of calcic plagioclase, followed by (2) crystallization of phenocrystic biotite, K-feldspar, and finally "quenched" groundmass (Clement, 1964). Stage 2 probably was completed at depths of about 1,500 m, whereas stage 1 began at some unknown but very likely deeper level. Plagioclase is strongly zoned in the intrusion, commonly resorbed, and as calcic as $An_{65}$, suggesting removal of CaO from the magma by its crystallization early in the magmatic cycle. The absence of miarolitic cavities, aplite dikes, and pegmatites in and near the intrusion also suggests that the magma was not $H_2O$-saturated during stage 1. (See Luth, 1969.)

Biotite stability curves were calculated for the three biotites from the altered granodiorite of Copper Canyon using equation 6″ of Wones and Eugster (1965, p. 1249).[2] The fugacityof oxygen in equation 6″ of Wones and Eugster was calculated from

$$\log f_{O_2} = -\frac{A}{T} + B + C\frac{(P-1)}{T} \quad \text{(Eugster and Wones, 1962),}$$

where $T$=temperature (°K),
$A, B, C$=constants (Eugster and Wones, 1962, p. 90),
and $P$=~375 bars (Nash and Theodore, 1971).

An estimate of 375 bars lithostatic pressure is based on a reconstructed thickness of about 1,500 m of sedimentary rock, previously described, overlying the intrusive body at the time of its emplacement. The activity of $KAlSi_3O_8$ in alkali feldspar was assumed to be 0.864 (Clement, 1964, p. 66), and the activity of $Fe_3O_4$ in magnetite was taken to be 1.0. Constants $A$, $B$, and $C$ used for biotite sample A (table 3) are for the Ni-NiO buffer and, for biotite samples B and C, are for the QFM buffer.

Whole-rock chemistry and biotite-granite solidus relations appear to be compatible with the aforementioned history of magmatism at Copper Canyon (fig. 7). The chemistry of rock used by Piwinskii (1968) to determine experimentally curve TO in figure 7 may approximate the magma's early stage 1 solidus at Copper Canyon. We suggest that, through early removal of CaO by fractional crystallization of plagioclase, subsequent magmatic stages became more granitic in the strict sense, and, furthermore, that the minimum of melting of granite curve (fig. 7) may have closely approximated this body's solidus curve during crystallization of the biotites. The body's magma may have persisted to P-T conditions significantly lower than the $H_2O$-saturated tonalite curve (fig. 7) only partly because of its fluorine content (table 3; Koster van Groos and Wyllie, 1968; Burnham, 1967).

From calculated biotite stability fields and from experimentally determined solidus curves (fig. 6), we can estimate the ratio of $P_{H_2O}$: $P_{total}$ during the biotites' primary crystallization at Copper Canyon. It must have been high, about 0.8 or 0.9, because any values much less than these would result in a shift of

[2]Equation 6″ of Wones and Eugster (1965) is:

$$\log f_{H_2O} = \frac{3428-4212(1-x)^2}{T} + \log x + \tfrac{1}{2}\log f_{O_2} + 8{\cdot}23 - \log a_1 - \log a_2 \ (\pm 0{\cdot}20),$$

where $f_{H_2O}$=fugacity of water,
$f_{O_2}$=fugacity of oxygen,
$T$=temperature (°K),
$x$=concentration of $KFe_3^{+2}AlSi_3O_{10}(OH)_2$ in biotite,
$a_1$=activity of $KAlSi_3O_8$ in alkali feldspar,
and $a_2$=activity of $Fe_3O_4$ in magnetite.

the biotites' univariant curves to the left and concomitantly the igneous rocks' solidus curves to the right. Under such conditions, we would have to infer substantially increased minimum depths of hypersolidus biotite crystallization and such depths are geologically unreasonable, as we described above. The magnesian nature of primary biotites in the intrusion at Copper Canyon also may be partly an effect of their shallow crystallization depths. Phlogopite is stable to at least 0.5 kb fluid pressures less than annite at granitic hypersolidus conditions (Wones, 1967).

The compositions of primary biotites in the Copper Canyon pluton thus seem to be compatible with crystallization from $H_2O$-saturated magma at minimum temperatures of about 800°C at these inferred depths of emplacement. At the Ely, Nev., porphyry copper deposit, Fournier (1967, p. 71) suggested formational temperatures of 600°–700°C for primary magnesian biotites.

### ALTERED GRANODIORITE OF THE WILSON-INDEPENDENCE MINE AREA

About 900 m north of the Wilson-Independence mine area (pl. 1), a small intrusive body of altered granodiorite about 100 m wide crops out near the west edge of the Copper Canyon area. This body intrudes the upper unit of the Pumpernickel Formation and is very similar both lithologically and chronologically to the more widely exposed Copper Canyon body. By the K-Ar method, M. L. Silberman (Theodore and others, 1973) dated primary biotite from this intrusion at 38.2 m.y.

### MISCELLANEOUS INTRUSIVE ROCKS

About 30 other small intrusive stocks and dikes crop out in the Copper Canyon area. Their lithologic variations include quartz monzonite, altered granodiorite, chloritized quartz porphyry, quartz diorite, and diorite. Primary biotite from an altered granodiorite sill penetrated by a drill hole, 300 m north of the Copper Canyon body (loc. 12, pl. 1), was dated at 37.6 m.y. by M. L. Silberman (Theodore and others, 1973).

## EXTRUSIVE ROCKS

### CAETANO TUFF

On the basis of its age (33.6 m.y., McKee and Silberman, 1970), lithology, and stratigraphic position, Stewart and McKee (1970) have correlated quartz latite crystal tuff in the district with the Caetano Tuff of Gilluly and Masursky (1965). Quartz latite in the district is a resistant ridge-forming rock that is best exposed at Elephant Head and at the head of Rocky Creek (fig. 3). The unit rests unconformably on the Paleozoic rocks. A small exposure, 150 m long, of the Caetano Tuff crops out about 1.6 km north and 60 m topographically higher than the nearest exposure of the main intrusive body at Copper Canyon. Here the quartz latite rests unconformably on the upper unit of the Pumpernickel Formation.

At Copper Canyon, we can estimate erosion rates from the age of the Caetano Tuff, the age of the pluton at Copper Canyon, their geometric relations, and the thickness of the cover over the pluton when it was emplaced. Our interpretations of the configuration of the pluton's upper surface in cross sections suggest that the pluton at Copper Canyon did not breach the erosion surface upon which the Caetano Tuff was deposited. Between emplacement of the pluton 38 m.y. ago and deposition of the Caetano 34 m.y. ago, erosion at Copper Canyon must have removed rocks totalling about 1,500 m thick, because the Caetano's deposition surface on the Pumpernickel is now about 60 m above the pluton. Earlier in this report we had estimated the cover over the intrusive body at the time of its emplacement to be about 1,500 m. We suggest that plutonism in late Eocene or early Oligocene time, with attendant uplift, substantially increased the average erosion rate at Copper Canyon over the rate prevailing since the mid-Mesozoic. A temperate climate and heavy precipitation in the area (Axelrod, 1966) probably helped to increase middle Tertiary erosion rates.

### BASALT FLOWS

Approximately a 15-m section of a more extensive basalt flow crops out at the southeast corner of the area (pl. 1). This dark-gray to black vesicular olivine basalt is relatively fresh. It rests here unconformably on the Harmony Formation, but to the east, in Philadelphia Canyon, it rests unconformably on the Scott Canyon Formation and also on a quartz monzonite pluton. The age of this flow is Tertiary or Quaternary.

## STRUCTURAL GEOLOGY

### ANTLER OROGENY DEFORMATION

Structures that developed during the thrusting phase of the Antler orogeny are not very well exposed either in the Roberts Mountains plate or in the Dewitt plate at Copper Canyon. However, measurement and analysis of bedding, folds, and axial planes in the Scott Canyon Formation of the Roberts Mountains plate reveal a remarkable structural coherence throughout the Battle Mountain mining district (Theodore, unpub. data). In this plate, outcrop-sized folds strongly trend about N. 20° E., and they commonly plunge about 20° either northward or southward. The folds are not uniformly overturned either to the east or west. These fold trends are almost identical to those in the upper plate of the Roberts Mountains thrust in the Shoshone Range, 25 km southeast of Copper Canyon (Wrucke and Theodore, 1970).

## SONOMA OROGENY DEFORMATION

### REGIONAL CONSIDERATIONS

From earlier regional studies, Silberling and Roberts (1962, p. 35–36) concluded that the Golconda plate, which includes the rocks of the Pennsylvanian(?) Pumpernickel Formation, moved generally eastward from western Nevada in latest Permian time during the Sonoma orogeny. At Copper Canyon, argillite of the Pumpernickel Formation is in thrust contact with sandstone, limestone, and conglomerate of the Upper Permian Edna Mountain Formation at the Nevada mine (pl. 1). Undeformed rocks of the Lower Triassic Koipato Group elsewhere rest unconformably on deformed rocks belonging to the Golconda plate (Ferguson and others, 1952; Burke, 1970; Silberling, 1973).

Recent studies, however, suggest that Golconda thrusting may have occurred during the early Mesozoic, but these are continuing studies, whose results are preliminary and subject to revision. Evidence for the lower age limit of the Golconda thrust apparently occurs in Mineral County, west of Tonapah. There rocks of the early Early Triassic Candelaria Formation have been overthrust by rocks similar to those of the Havallah sequence (Speed, 1971). These relations may be relevant only to southwestern Nevada, and their extrapolation to north-central Nevada is tenuous at this time. Evidence for the upper age limit for at least some movements along this thrust occurs in the area of Mount Lewis, about 25 km southeast of Copper Canyon. There dolomite and clastic rocks resting on rocks of both the Havallah and Antler sequence have been assigned to the upper Middle Triassic Panther Canyon Formation by Nichols (1971). From fission-track age determinations on zircon from a welded tuff in the Koipato Group, McKee and Burke (1972) inferred a minimum age of 225±30 m.y. (Early Triassic) for major movement of the Golconda thrust during the Sonoma orogeny. In a composite pluton at Buffalo Mountain (Neff, 1969) about 30 km northwest of Copper Canyon, rocks ranging in composition from syenite to quartz monzonite were intruded into rocks of the Golconda plate in Middle or Late Jurassic time. K-Ar ages at Buffalo Mountain range from 161 to 146 m.y. (Silberman and McKee, 1971).

### FOLDING IN THE PUMPERNICKEL FORMATION

Outcrop-sized folds are abundant in the rocks of the Pumpernickel Formation at Copper Canyon. The overall style of folding in the Golconda plate is best exemplified by exposures of folded black flinty chert beds in the northwest part of the area (pl. 1). Some of these folds can be traced south through altered (pyritized) rock into intensely recrystallized rock near the margins of the granodiorite at Copper Canyon. Here the metacherts are massive and granoblastic, and their preexisting structures are difficult to recognize. Where unaltered, the cherts of the Pumpernickel Formation are generally well bedded (fig. 8*A*), with individual beds typically averaging approximately 20–30 cm thick. However, some of the cherts are laminated within 5–8-cm beds (fig. 8*B*). Small-scale unconformities and truncation of laminae are common, and the laminae also lap over previously deposited clots of massive chert. There is no apparent cleavage in these rocks.

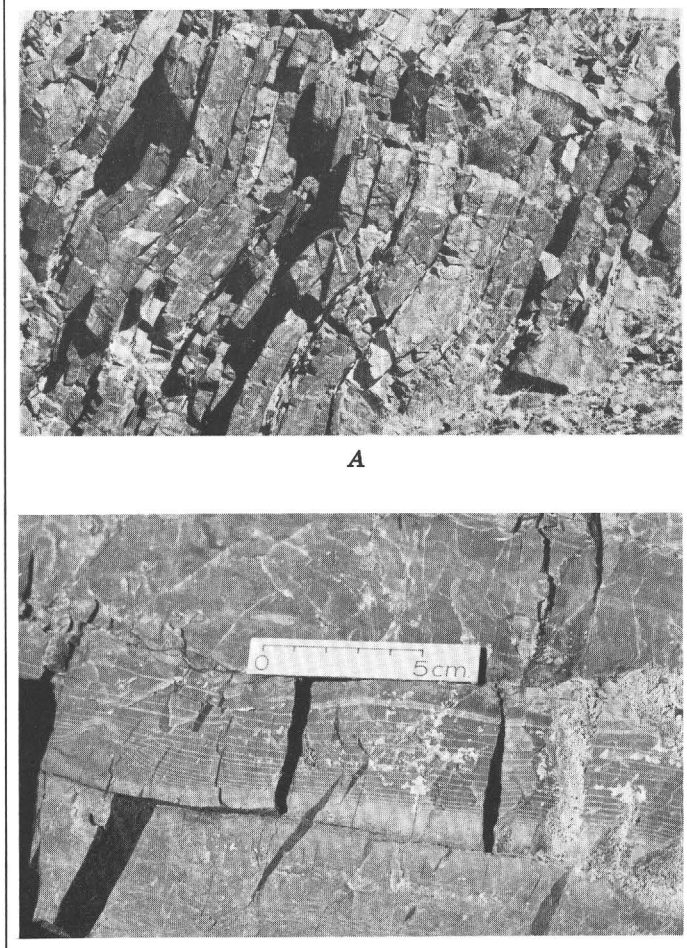


*A*

*B*

FIGURE 8.—The Pumpernickel Formation. *A*, Outcrop of unaltered chert beds. *B*, Laminated chert with small-scale truncation of laminae.

Diagnostic worm trails (fig. 9) that were left at the Pumpernickel's sediment-water interface are very common in the upper chert unit of the Pumpernickel Formation. These trails allow the accurate determination of facing in the rocks and thereby their fold geometry.

Many of the folded chert beds are asymmetrically overturned to the east with their axial plane traces parallel to the inferred trace of the Golconda thrust. The folds have rectilinear axes with tight angular hinges and are generally restricted in areal extent. There is very

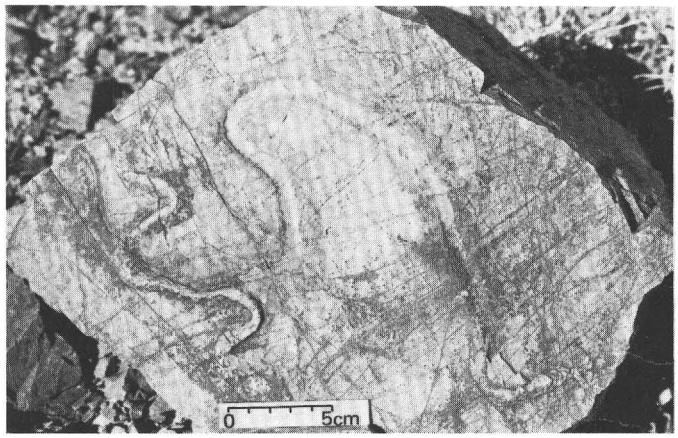


FIGURE 9.—A worm trail in chert of the Pumpernickel Formation at Copper Canyon.

minor flowage toward the hinge region, and the folds locally have curved axial plane traces with striated *ac*-joint surfaces (fig. 10). The folds are characterized by a monoclinic symmetry. Typically, up to about 30 m from the hinge lines, folded chert is intensely lineated by small-amplitude crenulations of the bedding planes (fig. 11*A*) and a more penetrative lineation (fig. 11*B*), which is parallel to the attitudes of nearby outcrop-sized folds.

This type of folding is restricted to rocks both in the Golconda plate and in the Roberts Mountain plate in the quadrangle. It is most likely that these folds in the Golconda plate at Copper Canyon developed during the thrusting phase of the Golconda orogeny, because the folds parallel the trace of the Golconda thrust. Similar folds have not been found near Antler Peak in limestones belonging to the Edna Mountain Formation and Antler Peak Limestone below the thrust. Certainly these carbonate-rich rocks would have recorded an even more ductile type of deformation than that preserved in chert in the overlying Golconda plate, if the Golconda plate and underlying limestones had been folded together. Thus, analysis of folds in the Golconda plate should accurately document the apparent direction of tectonic transport here during Golconda thrusting.

All structural data assembled from the Golconda plate at Copper Canyon were contoured on equal-area, lower hemisphere projections by a modified version of a method originally described by Kamb (1959), whose contouring method uses a variable counting area (fig. 12).[3]

[3]The counting area used in Kamb's method is a function of the total number of structural data points and of the number of times it is considered to be significant that concentrations deviate from a uniform distribution. Because the counting area varies inversely with the number of data points being counted, poles to bedding ($\pi S$) in the Golconda plate were contoured in three groups so that the diameter of the counting area would not be less than the grid spacing used during contouring. All stereograms are contoured with a $2E$ contour interval, where $E$ is the number of data points expected within a counting area for a uniform distribution across the entire stereogram.

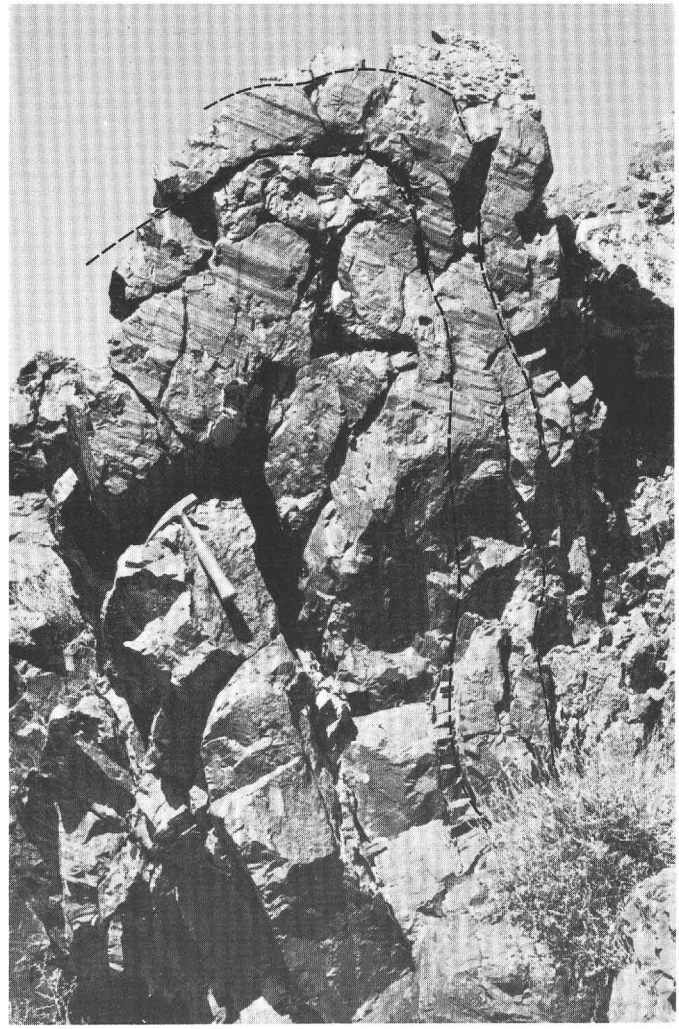

FIGURE 10.—Tightly folded chert beds, in profile, belonging to the upper unit of the Pumpernickel Formation in the northwestern part of the Copper Canyon area. Well-developed striae here developed on the approximately *ac*-joint surface.

The three $\pi S$ diagrams prepared from data gathered in the Golconda plate (fig. 12*A–C*) comprise strong single maxima that plunge moderately towards the east. These data reflect the statistically isoclinal nature of folds mapped here (pl. 1), with most beds dipping toward the west. The $\pi S$ diagrams also define, although admittedly very weakly because of the restricted areal extents of the tight fold hinges, $\pi S$ girdles whose $\beta$ axes (bedding plane intersections) trend slightly east of north and are approximately horizontal. All axial structures measured in the Golconda plate also define a strong single maximum (fig. 12 *D*), with the center of the maximum plunging 5° to N. 5° E. The axial structures, which are minor fold axes and bedding plane crenulations, are statistically parallel to the $\beta$ axes defined by the bedding planes. These axial structures have monoclinic symmetry and define a *B* axis, or axis of rolling. The fold forms indicate shear displacements

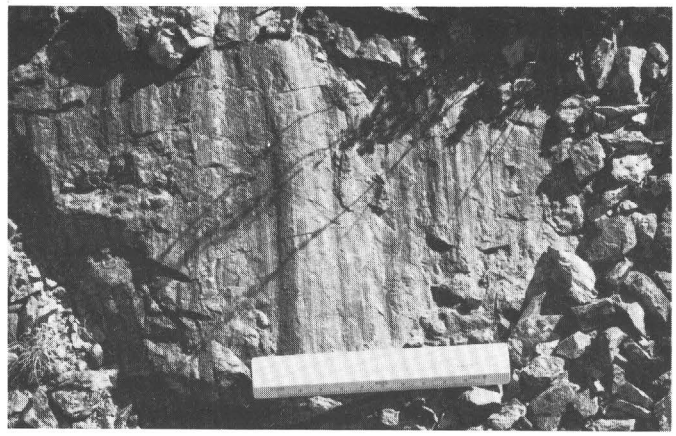

*A*

*B*

FIGURE 11.—The Pumpernickel Formation. *A*, Chert float with small-amplitude crenulations of bedding common in folded areas. *B*, Penetrative lineations in chert.

on the bedding planes, normal to the fold axes, as the dominant type of tectonic transport in the Golconda plate. Therefore, the apparent horizontal component of tectonic transport in the Golconda plate at Copper Canyon has an azimuthal bearing of 95°— that is, towards S. 85° E. Elsewhere in the Battle Mountain mining district, in the upper plate of the Roberts Mountains thrust in rocks belonging to the Scott Canyon Formation, similar structural studies (Theodore, unpub. data) yielded an apparent S. 70° E.—N. 70° W. direction of shortening.

We must emphasize that these structural data yield an apparent movement direction for one small area of the at least 40-km-wide Golconda plate and that this inferred direction of transport should not be extrapolated to other areas. Additional structural investigations, together with detailed regional stratigraphic studies, of many areas of rocks involved in the Golconda thrusting are needed to resolve adequately the entire complex movement history of such a regionally extensive thrust plate.

## TERTIARY FAULTING

Steeply dipping, Tertiary normal faults with many different strikes are very abundant in the Copper Canyon area (pl. 1). The faults that strike north are the most common and the most persistent laterally. Locally, these north-striking faults also have the widest breccia zones (up to about 75 m wide), which suggests a history of repeated displacements (some possibly in a reverse sense), perhaps over a relatively long time. The Virgin fault, which is geologically a significant structure in the area, bounds the Antler sequence on the west. The stratigraphic throw along this fault (down on the west) has been estimated by Roberts (1964, p. A85) to be between 200 and 300 m at the Nevada mine. About 1.6 km farther to the south, just north of the granodiorite, vertical separations across the Virgin and Copper Canyon fault systems measure about 550 m (pl. 1). Along the Copper Canyon fault, vertical separations of both the Golconda thrust and the unconformity between the Harmony and Battle Formations (determined from drill-hole intercepts) are about 180 m down on the west.

Several apophyses from the main body of the granodiorite at Copper Canyon extend into its wallrocks. The largest of these extends about 450 m to the north along the Virgin fault. This relation suggests that initial emplacement of this igneous body was partly controlled by the Virgin fault. Indeed, much of the separation across the Virgin fault probably occurred before the granodiorite was emplaced, because of the present geometry of the granodiorite. However, some movements along the Virgin fault and other north-striking faults must also postdate igneous crystallization because the intrusion has been sheared along their traces.

The north-striking faults have been offset along both northeast- and northwest-striking ones (pl. 1). In the general vicinity of the Copper Canyon underground mine, the Gulch fault, a northeast-striking premetallization fault, offsets the Virgin fault with 360 m of right-lateral separation. Just north of the granodiorite, the north-striking fault through the Sonderman prospects has 120 m of left-lateral separation along a northwest-striking postmetallization fault. Northwest-striking faults may, therefore, be among the youngest structures of the Copper Canyon area.

The north-striking faults are important premetallization structures that localized ore. In the upper levels of the Copper Canyon underground mine, for example (pl. 1), copper ore bodies were mined along the Virgin fault; at the Nevada mine 2.4 km to the north, lead-zinc ore bodies were mined from this same fault (Rob-

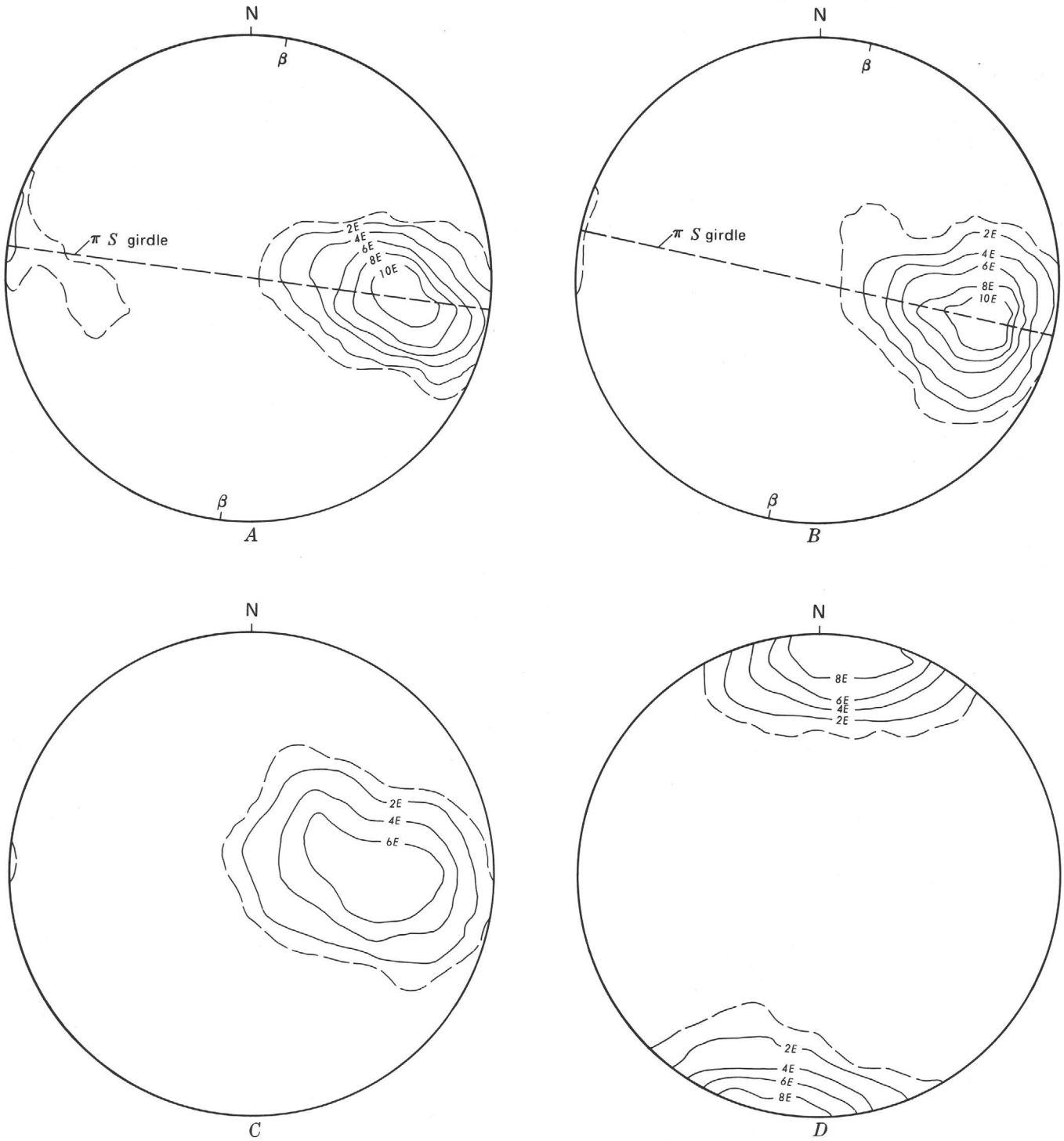


FIGURE 12.—Planar and axial structural data from the upper plate of the Golconda thrust at Copper Canyon. The data are projected from the lower hemisphere and contoured in intervals of $2E$ (see text). The $1E$ contour, the expected density for no preferred orientation, is shown as a broken line. *A*, 269 poles to bedding measured in the northern one-third of the Golconda plate on plate 1. *B*, 267 poles to bedding measured in the central one-third of the Golconda plate on plate 1. *C*, 139 poles to bedding measured in the southern one-third of the Golconda plate on plate 1. *D*, 53 axial structures (minor fold axes, crenulations of bedding) measured across the entire outcrop area of the Golconda plate on plate 1.

erts, 1964, p. A85). The Hayden and the Monitor faults are two subparallel faults that bound much of the ore-bearing rock in the porphyry copper deposit (pl. 1; and see below). These two structures may have been impor-

tant conduits during metallization. More faults were mapped in the pit area than in any other area of equal size (pl. 1), but this may be because excellent artificial exposures along drill roads allowed more faults to be recognized there.

## ORIGIN OF HEMATITE IN RED BEDS OF THE BATTLE FORMATION

The mineralogy and inferred origin of the iron oxides of the Middle Pennsylvanian Battle Formation deserve further discussion because these oxides apparently contributed toward the development of the porphyry-type ore described below. Much of the following introductory discussion is summarized from Roberts (1964).

The abundance of iron oxides in conglomerates belonging to the Battle Formation apparently was first reported by Hague and Emmons (1877), who noted the "fine ferruginous sand[s]" that cement the chert and quartzite pebbles. Later, Lawson (1913) described these rocks in more detail and ascribed the term "fanglomerate" to the formation—the first use of the term. Roberts (1964, p. A31) cited evidence for the deposition of the rocks of the Battle Formation under both marine and terrestrial conditions; regionally, the middle and upper members are made up largely of marine beds. The iron oxide content of the Battle Formation further implied to Roberts (1964, p. A31) that the source rocks of the formation were eroded under conditions typified by seasonal rainfall. McKee (1964) suggests that red beds can originate in arid or semiarid climates.

At Copper Canyon, the red beds are irregularly bedded on a scale of tens of meters. These beds are made up chiefly of poorly sorted, cobble to boulder sandy conglomerates, whose sandstone fractions are fairly well sorted. Typically, the red beds form discoid lenses that are interbedded with, and grade into, drab horizons. The prominent red pigment of the red beds results primarily from abundant hematite both in their clay fraction and also in angular fragile detrital chips (fig. 13). Illite and chlorite are predominant in the clay fraction, an association common to red beds (Van Houten, 1961).

The detrital hematitic clasts generally range from 1 to 2 mm to several centimeters in their longest dimensions, and most are angular with a low sphericity measured according to the roundness scale of Powers (1953). X-ray and microscopic studies of hematitic fragments from the lower member of the Battle indicate that the fragments are made up of hematite–quartz–calcite–amorphous iron oxides (–illite–chlorite–siderite–feldspar?) assemblages in widely varying ratios. They include relatively high concentrations of titanium, with traces of manganese, strontium, and zinc. The delicate nature of these ferruginous fragments suggests short distances to the source area(s), which is consistent with the high-energy transport environment (rugged relief) suggested by large angular poorly sorted boulders in the lower member of the Battle (see Folk, 1968, p. 85). The subrounded sandy quartz and quartzite grains that form the matrix of the clasts are coated by sparse, thin films of ferruginous material, re-

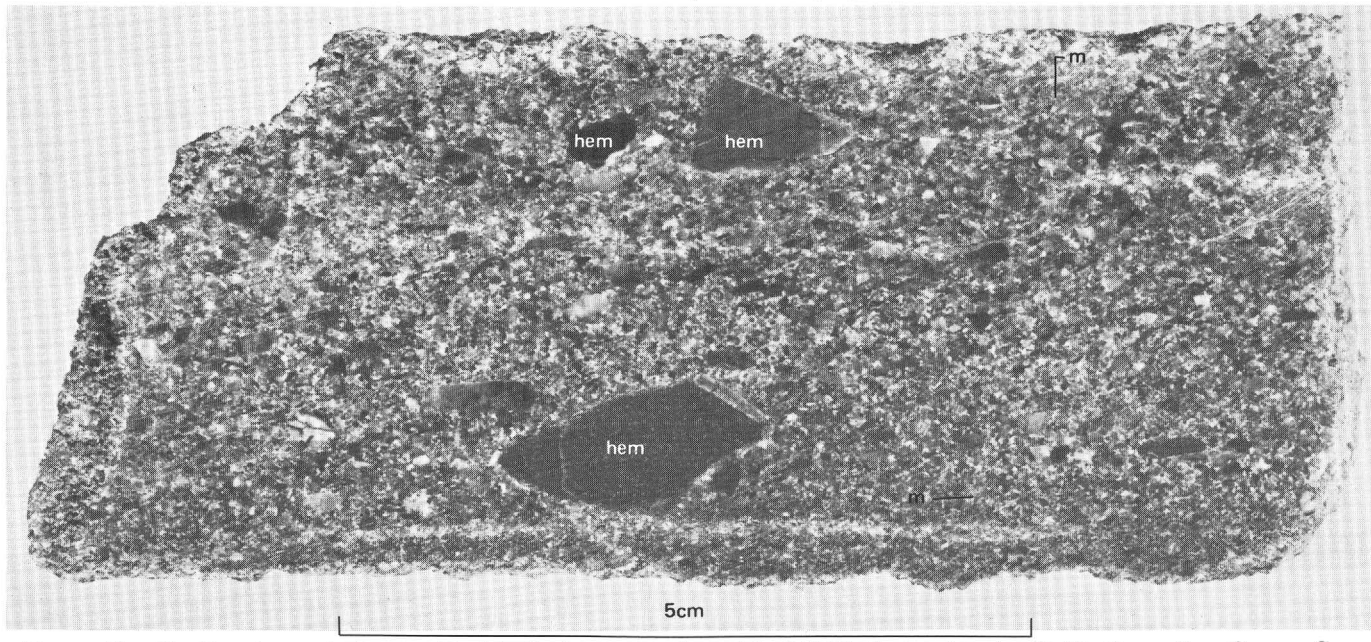


FIGURE 13.—Unaltered sample from red bed in the lower member of the Middle Pennsylvanian Battle Formation, Copper Canyon, Nev. Coarse detrital angular chips (hem) include abundant hematite, as does the fine-grained matrix (m). Collected 1,800 m north of porphyry copper deposit.

mobilized from nearby (in thin section) hematitic fragments. This relation suggests little post-depositional development of iron oxide.

From our petrographic and X-ray studies, we cannot adequately determine the ultimate source of the iron oxide pigment in the red beds of the Battle Formation. Relict magnetite, ilmenite, and leucoxene grains have not been found to date in the hematitic detrital grains at Copper Canyon, as have been reported in red beds elsewhere (Van Houten, 1964). Regardless, the hematitic detrital grains indicate strongly oxidizing conditions in the source area(s) for the Battle. High titanium content suggests that the grains were derived from either titanomagnetite or ilmentite. The iron in the Battle may have been derived from the Lower, Middle, and Upper Ordovician Valmy Formation, where titanomagnetite or ilmentite would be likely constituents of greenstones.

## COPPER CANYON PORPHYRY COPPER DEPOSIT

The Copper Canyon porphyry copper deposit chiefly comprises two spatially separate, and petrologically distinct, contact metasomatic ore bodies near the altered granodiorite of Copper Canyon (fig. 14). The general geologic aspects of both bodies (here termed the east and west ore bodies) have been presented by Sayers, Tippett, and Fields (1968). Common hypogene sulfides in the bodies include pyrite, chalcopyrite, pyrrhotite, and marcasite, with lesser concentrations of arsenopyrite, sphalerite, molybdenite, galena, and native gold. The east ore body was being mined during 1973, while waste rock over the west ore body was being removed. Our report emphasizes a description of that part of the east ore body in the vicinity of the unconformity between the Battle and Harmony Formations along the 6450 bench. This particular bench was selected for

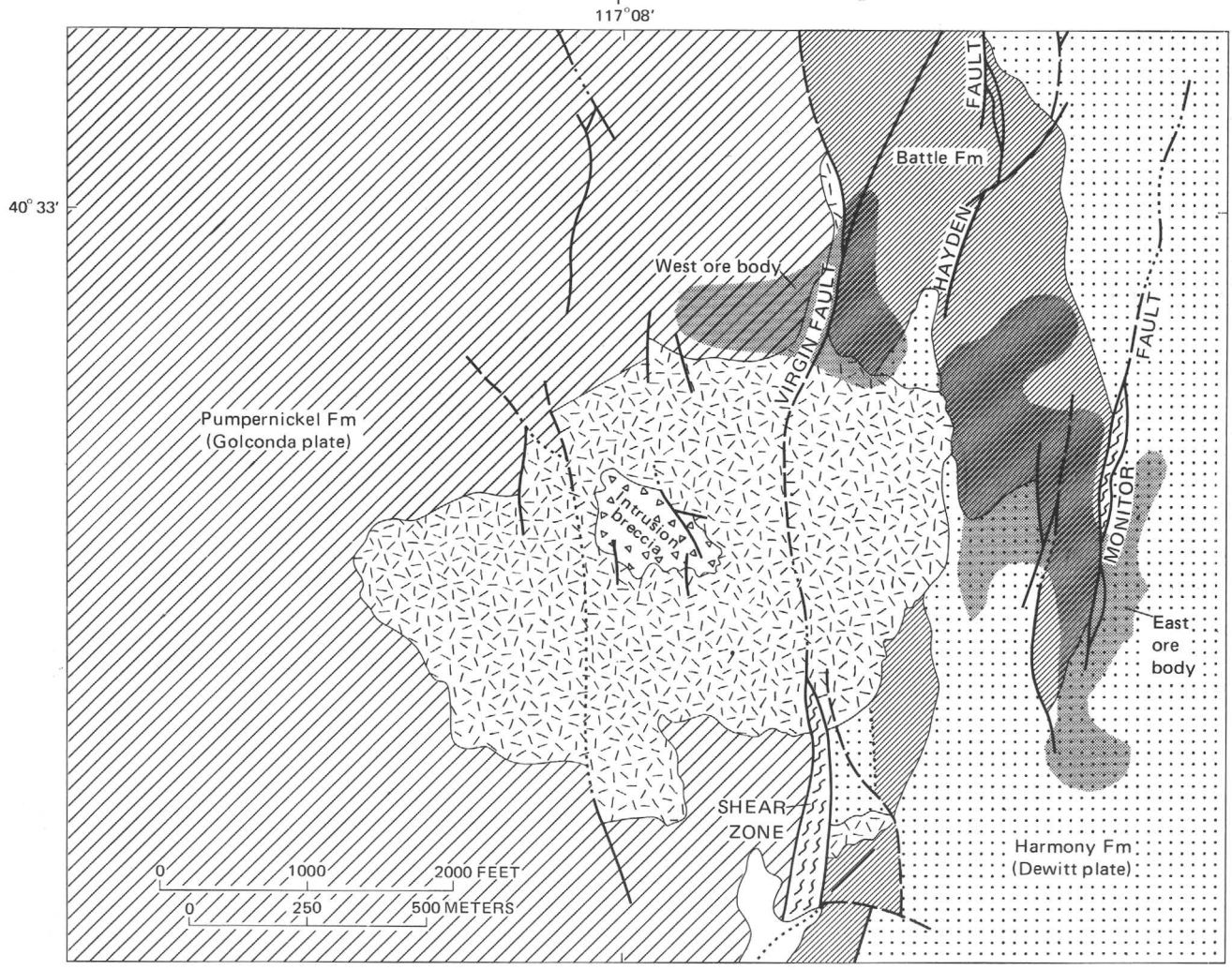


FIGURE 14.—Generalized geology around the intrusive body at Copper Canyon and the location of the west and east hypogene ore bodies. Explanation same as figure 3. Ore body boundaries from Sayers, Tippett, and Fields (1968).

detailed study because of the chemical contrasts among the rock units here, the local high concentrations of hypogene sulfides, and the availability of copper, gold, and silver assays from over 400 blast holes drilled into the bench.

The west ore body straddles the trace of the Virgin fault north of the altered granodiorite of Copper Canyon. Depth to hypogene ore ranges from 15 to 60 m. The body's maximum east-west dimension is about 500 m, and its average north-south dimension is about 150 m. It extends about 220 m further to the north near the Virgin fault (fig. 14). The bulk of the hypogene ore in the body occurs west of the Virgin fault, probably in metamorphosed calcareous argillites, siltstones, and shales of the Pennsylvanian(?) Pumpernickel Formation. Some of it however also is in the upper unit of the Middle Pennsylvanian Battle Formation.

The body consists mainly of several discontinuous, 8–16-m-thick mantoes, or beds of ore. Some ore horizons contain 80–90 percent by volume sulfides. Observations of development drill cores and limited petrographic studies indicate extensive development of coarse-grained calc-silicate metamorphic minerals in the ore horizons. Polymetamorphic assemblages of diopside, diopside-andradite, epidote-diopside, and tremolite with varying lesser amounts of quartz, K-feldspar, sphene, and chlorite are common. Pyrrhotite, the dominant sulfide, selectively replaces andradite (on a volume for volume basis) and has in turn been partly altered to fine-grained marcasite-pyrite assemblages. Late pyrite porphyroblasts(?) may be related to a nearby 5-m-thick sill. Chalcopyrite is one of the last sulfides to be deposited, and it usually occurs along, or near, pyrite-pyrrhotite boundaries. Similar sulfide-silicate textural relations were observed by Titley (1961) at the Linchburg lead-zinc deposit in New Mexico, and by Buseck (1967) at the Tem Piute zinc-tungsten deposit in southeastern Nevada.

This section is chiefly concerned with the east ore body. Sayers, Tippett, and Fields (1968) reported that the bulk of the metallization in this ore body is hypogene and is found in the basal 45 m of the Middle Pennsylvanian Battle Formation, near the unconformity with the underlying Upper Cambrian Harmony Formation. Thickness of ore zones ranges from 8 m to more than 60 m, with depth to ore beneath leached capping and waste rock ranging from 0 to 60 cm. The body is irregularly shaped, and it has an overall north-south dimension of about 1,000 m with about a 400 m maximum east-west dimension. The body lies east of the Virgin fault, the dominant fault in the mine area, and mainly between two other subparallel faults, the Hayden and the Monitor (fig. 13). Supergene mineralization (chalcocite, chrysocolla, copper carbonates, and copper oxides) and clay alteration are primarily restricted to fault zones and nearby shattered rocks and also to rocks of the Harmony Formation, especially in the southeastern part of the ore body. For the most part, we confined our geochemical and petrologic investigations of this ore body to the 6450 bench (figs. 15–18), largely because of the availability of geochemical data and because metallization here is fairly representative of that found throughout the east ore body. About 45 samples were collected from the 6450 bench for minor-element variation studies.

### STRATIGRAPHY AND STRUCTURE ALONG THE 6450 BENCH

Overall geology of the 6450 bench is fairly simple; rocks belonging to the lower member of the Battle Formation are generally in contact with rocks of the Harmony Formation along an unconformity (fig. 15). The unconformity, as it crops out here along the 6450 bench, approximately parallels bedding in both the Harmony Formation and in the overlying Battle Formation. However, about 1.6 km north of the east ore body, the unconformity between these two formations is definitely angular (Roberts, 1964). Bedding in the Harmony Formation on the 6450 bench generally strikes somewhat east of north (about N. 20° E.) and dips on the average 20°–30° to the west. In the Harmony, two distinct lithologic facies have been recognized: a metasandstone or meta-arkose facies and a metashale or metamudstone facies, which underlies about the southern half of the bench. In the Battle, the rocks are predominantly altered calcareous conglomerates and altered siliceous conglomerates. However, the lithology of the Battle is locally quite variable and discontinuous along strike. Chert pebble conglomerates with an original matrix of relatively abundant magnesian calcite or dolomite have been hydrothermally altered to calc-silicate metaconglomerates consisting of at least 25 percent chlorite-tremolite-(epidote).

There are many faults with minor offsets within the ore body that surely facilitated metallization (figs. 19 and 20). Of these, north-striking faults are the most common. Although the unconformity has been faulted along both northwest- and northeast-striking faults, there are also some fractures here with similar strikes that cut the unconformity but apparently do not offset it (fig. 15). Steeply dipping north-northeast- and northwest-striking faults crop out along the northern perimeter of the pit, and have dropped the unconformity (down on the west) to its present trace along the 6450 bench (fig. 19).

Folds are uncommon in the 6450 bench. One lensoid calc-silicate unit, together with the unconformity at the base of the Battle, has been deformed into a broad open fold whose fold axis plunges gently to the northwest.

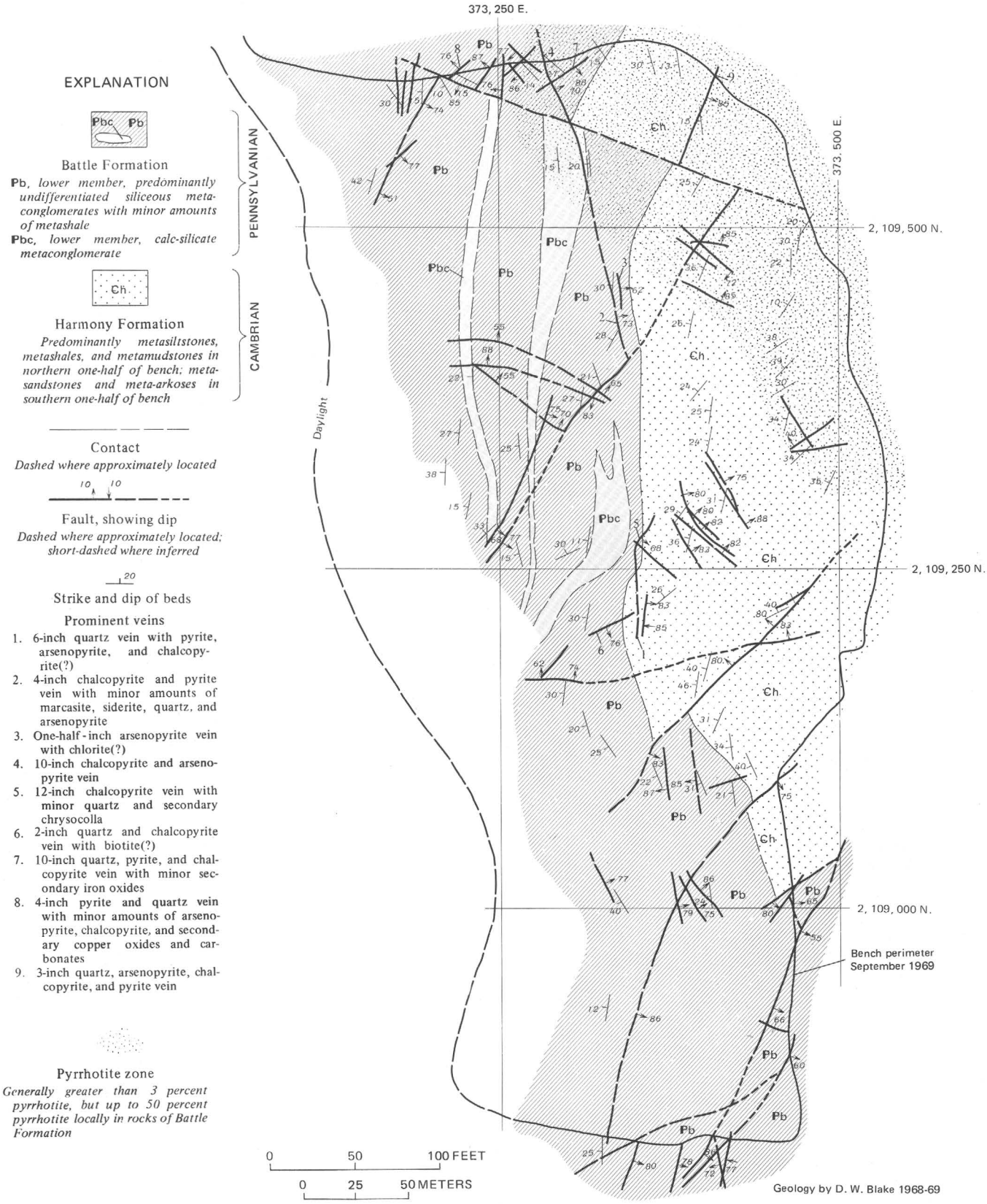


FIGURE 15.—Geologic map of the 6450 bench, east ore body, Copper Canyon porphyry copper deposit.

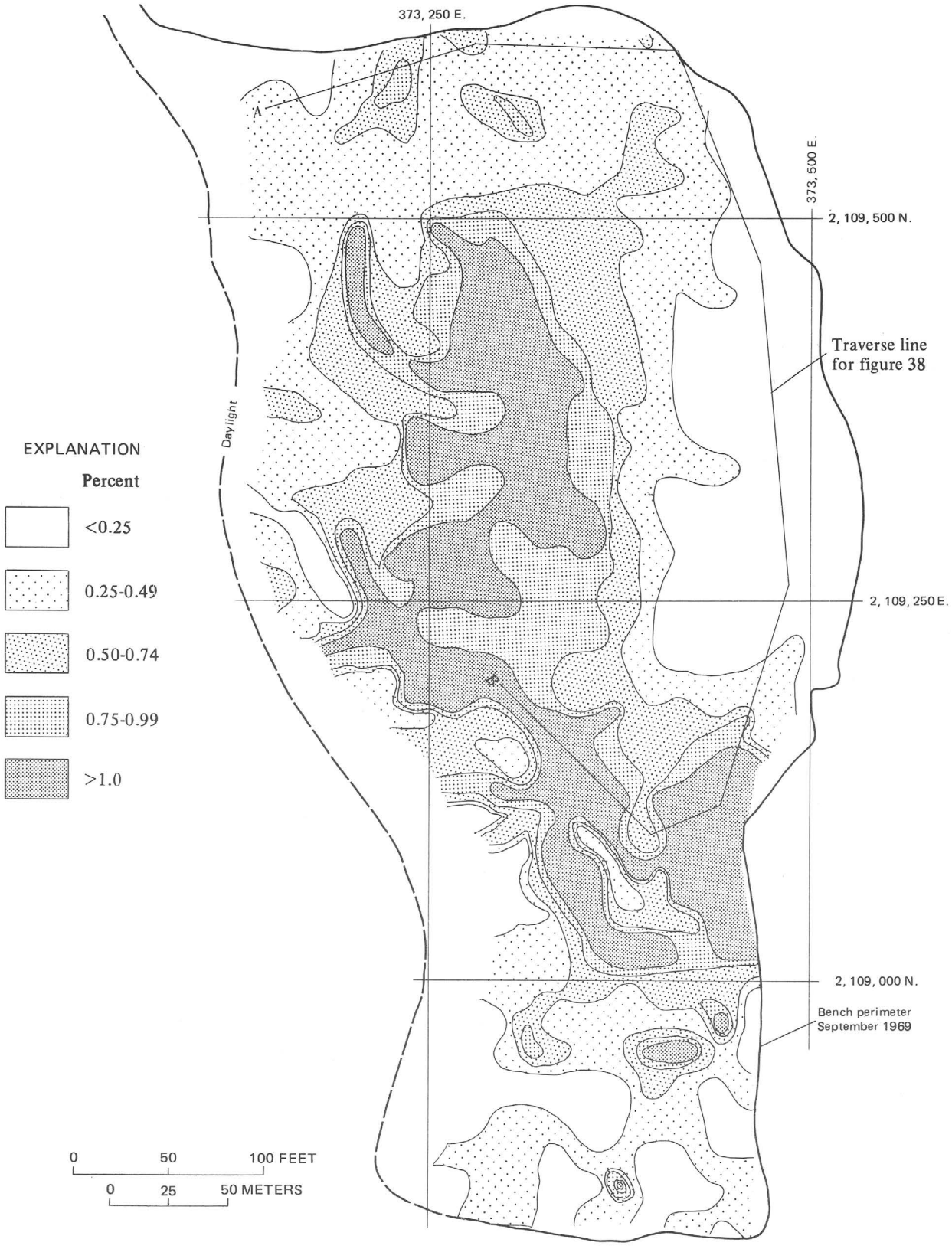


FIGURE 16.—Contoured copper concentrations on the 6450 bench (analyses from blast hole cuttings).

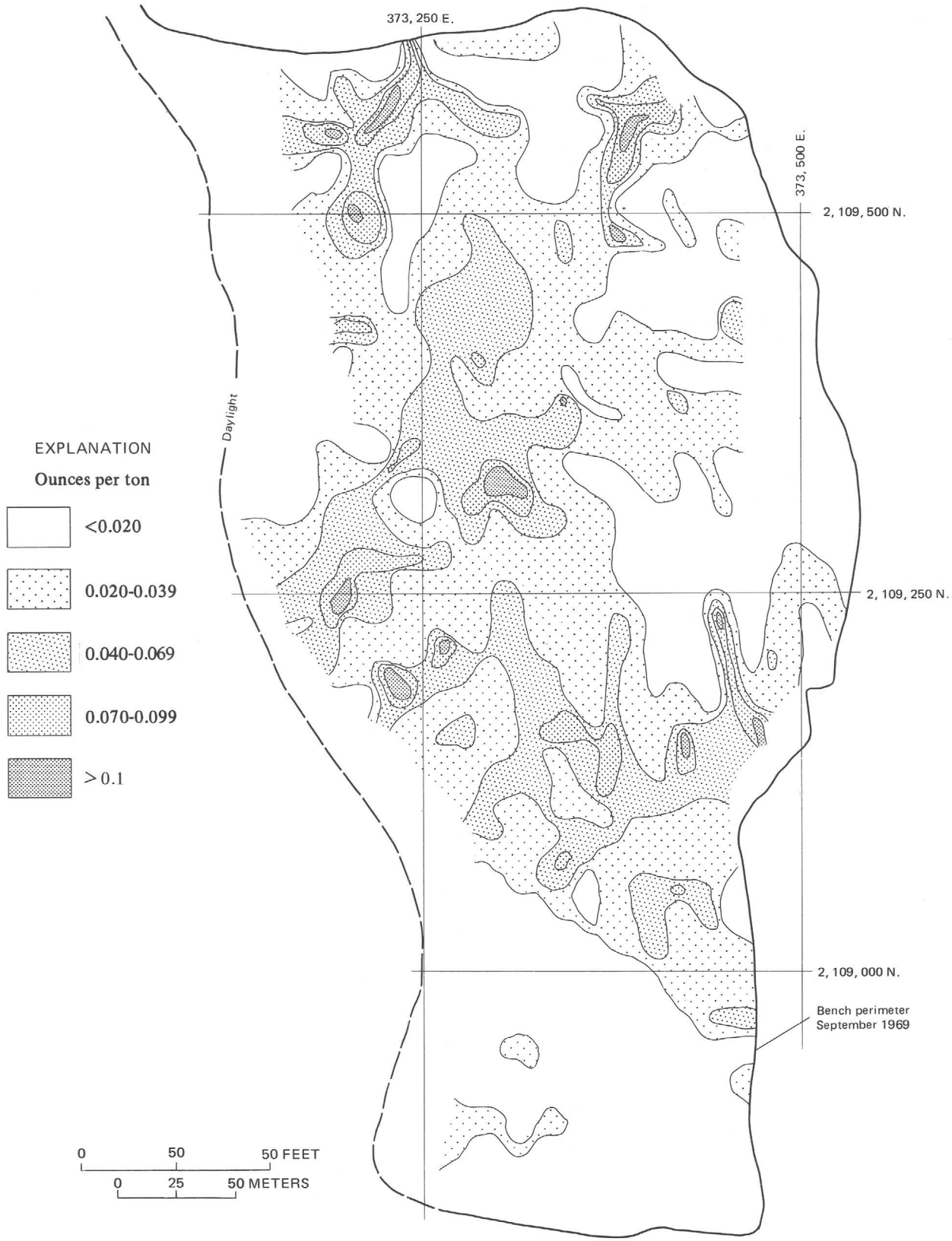


FIGURE 17.—Contoured gold concentrations on the 6450 bench (analyses from blast hole cuttings).

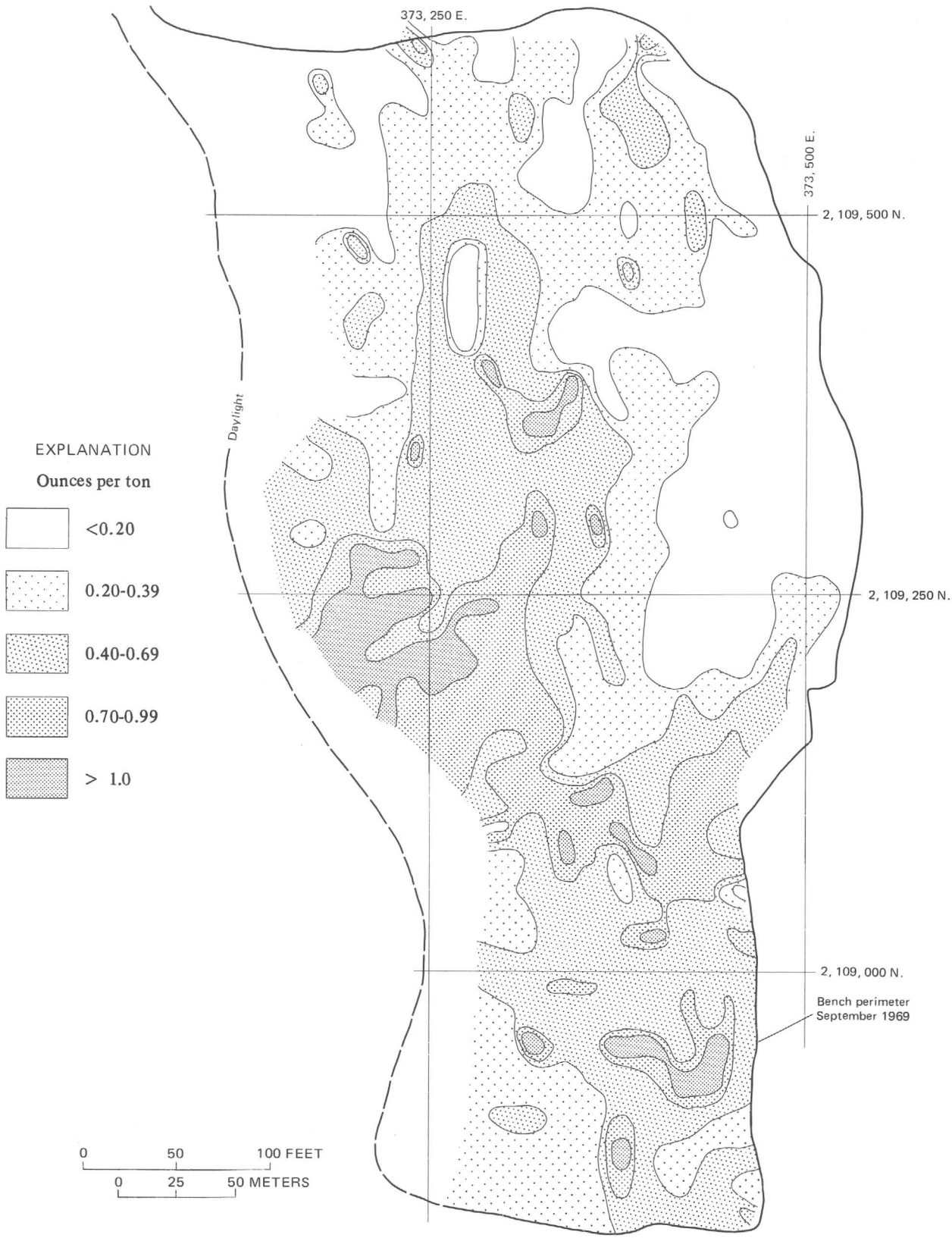


FIGURE 18.—Contoured silver concentrations on the 6450 bench (analyses from blast hole cuttings).

## PETROLOGY OF ROCKS ON THE 6450 BENCH

### HARMONY FORMATION METASHALE AND METASANDSTONE

The composite phase assemblages of 16 rock samples collected on the 6450 bench from the Harmony Formation, determined both under the microscope and by X-ray methods, are indicated in table 4. Total sulfide content in the Harmony Formation seldom exceeds 5 percent, and unless secondarily enriched, the grade of copper generally is less than 0.15 percent. Most sulfides in rocks of this formation occur along fractures or in veins. All but four of these samples (table 4) were collected from a zone of pyrrhotite-rich rock in the northeast quadrant of the bench (fig. 15), where the pyrrhotite content generally ranges between 3 and 10 percent. Smaller amounts of pyrrhotite occur in rocks from the Harmony on this bench to about 55 m south of the outlined pyrrhotite-rich zone and to about 100 m north of the zone.

Samples 613–620 are fine-grained hornfelsic metasedimentary rocks: laminated metashale or massive metamudstone. The groundmass in these rocks, consisting of grains less than 0.01 mm across, is a compact mosaic of quartz–K-feldspar–white mica (biotite-albite), a potassic hydrothermal assemblage typical in many porphyry copper deposits (Creasey, 1966). Albite probably has exsolved from the K-feldspar. The biotite is strongly pleochroic, tan to red brown ($X<Y=Z$), is disseminated ubiquitously in some rocks, and is also preferentially concentrated in clots throughout the groundmass of other rocks. Although some pyrrhotite occurs in the groundmass, most other sulfides are restricted to narrow veinlets that seldom exceed 3 mm in width. Generally poorly crystalline sphene occurs in many domains of these rocks at the thin-section scale and is found either as discrete grains or clots of grains intergrown with hydrothermal biotite and with many of the sulfides, or as partial rims around individual pyrrhotite grains. Obviously, the mineralogy listed in table 4 represents several disequilibrium alteration assemblages. The rocks of the Harmony have not completely recrystallized during the hydrothermal alteration associated with sulfide deposition.

Typical mineralogy of metasandstone and feldspathic metasandstone of the Harmony Formation along the 6450 bench is shown in table 4, samples 621–657. Quartz-rich brown metasandstone is the more common variety along the bench. These fine-grained rocks usually consist of angular to subrounded detrital quartz grains (0.3–0.8 mm across) set in a partially recrystallized quartz–K-feldspar–biotite–white mica matrix that also locally includes traces of sphene, epidote, chlorite, carbonate (siderite?), kaolinite, montmorillonite, and detrital(?) allanite. Detrital quartz grains commonly make up 70–80 percent of the metasand-

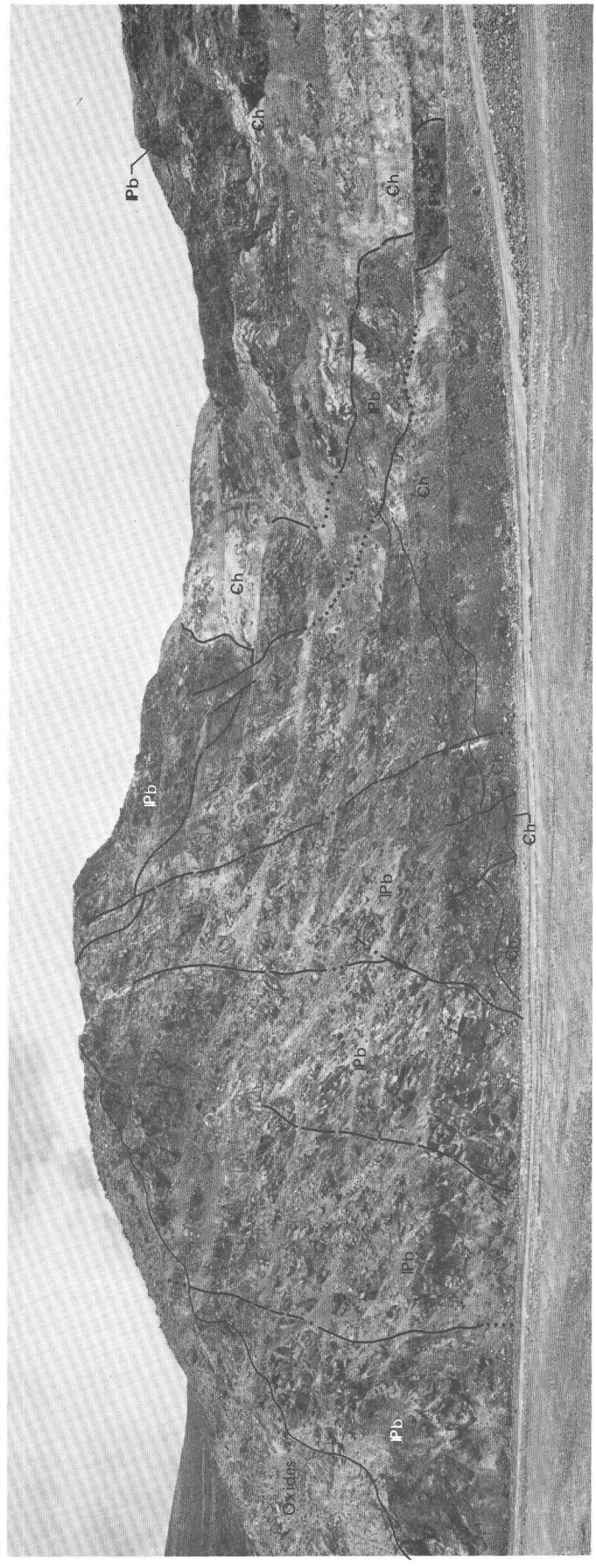


FIGURE 19.—Panoramic view north from 6450 bench, in the east ore body, Copper Canyon. Benches are 7.5 m high. h, Harmony Formation; Pb, Battle Formation.

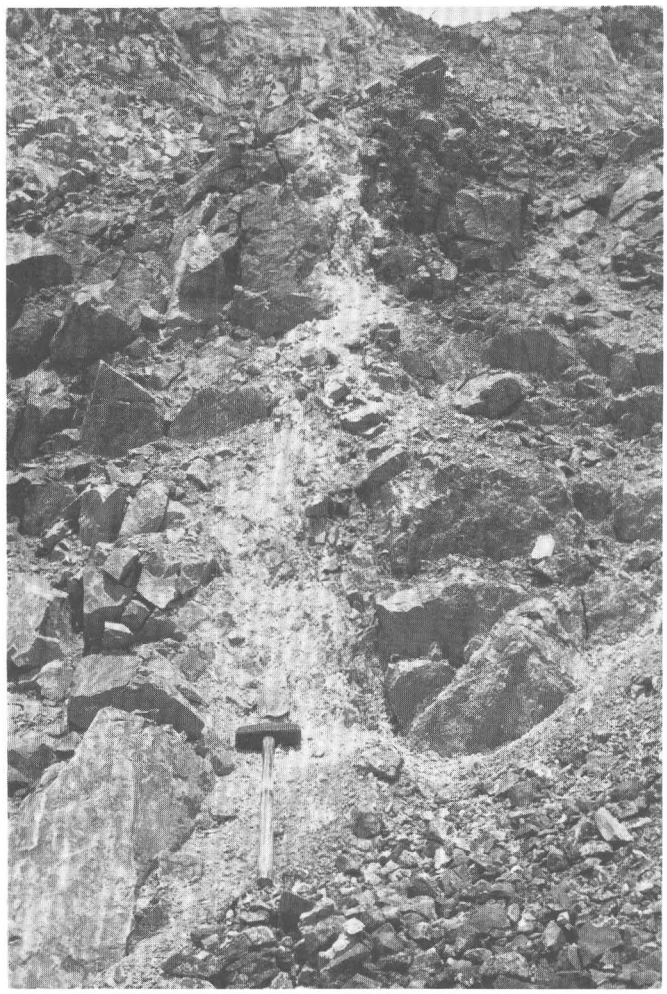

FIGURE 20.—A clay-rich breccia zone along a fault with about a 3-m separation between offset beds (north end of the 6450 bench). Hammer handle about 1 m long.

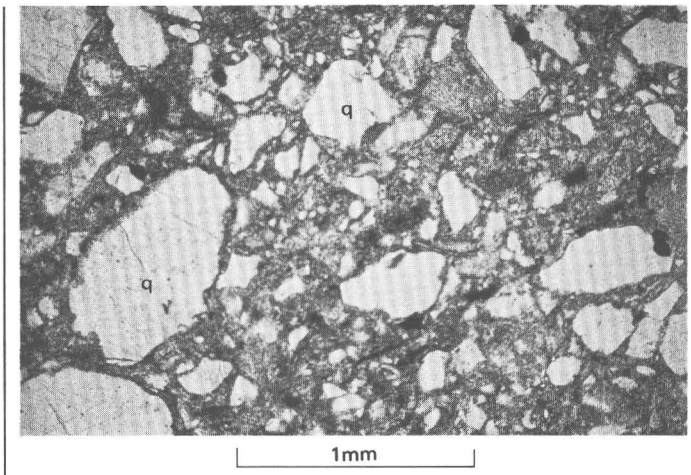


FIGURE 21.—Photomicrograph in plane polarized light of quartz (q) set in partially recrystallized quartz–K-feldspar–mica matrix from metasandstone of the Harmony Formation from the east ore body.

stone (fig. 21), with generally less than 10 percent detrital grains of microcline, perthite, plagioclase and muscovite. Trace amounts of zircon, apatite, and garnet(?) are also present. The detrital minerals in these rocks are not completely recrystallized; nonetheless, detrital quartz grains in a few domains have corroded margins that merge with complex, sutured crystal boundaries into the enclosing matrix. Some of the detrital K-feldspars contain only traces of white mica, while others are thoroughly altered to white mica. Albite, detected here in two of the metasandstone samples, may be either part of the recrystallized matrix or part of their detrital fraction.

Generally, the mineralogy of the metasandstone is very similar to that of the metashale and metamudstone on the bench. As in the metashale and metamudstone of the Harmony Formation, sulfides are both disseminated through the matrix of these metasandstones and concentrated along very narrow veins which generally are less than 0.3 mm thick. Pyrrhotite is the sulfide most commonly found disseminated in the interstitial matrix of the metasandstone.

Veins are prominent through the rocks of the Harmony. The relative abundance of veins in the metasandstone, however, is much less than that noted in metashale or metamudstone. One prominent exception is specimen 656 which has a dense local concentration of veins. Seven separate 1 to 2 mm thick veins cut through a 10 sq cm area of the rock. Petrographic examination of individual veinlets in the Harmony, whose mineralogy is presented in table 5, generally shows that the early phases deposited were either quartz or K-feldspar (or both). This early quartz and K-feldspar locally include pyrrhotite, chalcopyrite, and biotite. These minerals were then followed in places by siderite, with some chalcopyrite and pyrite. Chalcopyrite generally occurs in these rocks in quartz–K-feldspar veins with several other sulfide and silicate phases (table 5). Some of the veins may also contain cubanite after chalcopyrite (see below). Siderite has been found as a reaction rim around pyrrhotite in some veins (fig. 22). Some of the white mica in the veins is a late stage alteration product of earlier K-feldspar grains. Although plagioclase (oligoclase) is very sparse throughout these rocks, it does make up the major fraction of a few discontinuous veinlets through the Harmony. These oligoclase veinlets are partly sericitized and set in white-mica-rich wallrock. Reliable criteria for age relations among all the veins listed above in table 5 have not been observed. The oligoclase veinlets are probably earlier than the others.

Small-scale wallrock contact effects adjacent to the

TABLE 4.—*Mineralogy of rocks from the Upper Cambrian Harmony Formation on the 6450 bench*

[X, mineral present; Tr, trace; ?, questionably present; ....., not found]

| | Metashale and metamudstone | | | | | | | Metasandstone | | | | | | | |
|---|---|---|---|---|---|---|---|---|---|---|---|---|---|---|---|
| Specimen No. | 613 | 614 | 616 | 617 | 618 | 619 | 620 | 652 | 653 | 656 | 657 | 621 | [1]623 | [1]624 | [1]626 | [1]627 |
| Quartz[2 3] | X | X | X | X | X | X | X | X | X | X | X | X | X | X | X | X |
| K-feldspar[2 3] | X | X | X | X | X | X | X | X | X | X | X | X | X | X | X | X |
| Biotite[3] | X | Tr | Tr | X | X | X | X | X | X | Tr | X | X | X | X | X | ..... |
| White mica[2 3] | X | X | X | X | X | X | X | X | X | X | X | X | X | X | X | X |
| Plagioclase[2 3] | Tr | ..... | Tr | ..... | ? | Tr | Tr | X | ..... | ..... | X | Tr | ..... | Tr | X | ..... |
| Epidote[3] | ..... | X | ..... | X | ..... | ..... | X | ..... | ..... | ..... | ..... | ..... | X | ..... | Tr | ..... |
| Chlorite[3] | Tr | X | Tr | ..... | Tr | Tr | Tr | Tr | Tr | Tr | ..... | ..... | ..... | ..... | Tr | Tr |
| Sphene[3] | X | X | Tr | ? | X | X | ? | X | X | Tr | X | X | X | X | X | Tr |
| Siderite[3] | Tr | ..... | Tr | ..... | Tr | ..... | X | ..... | Tr | ..... | ? | ..... | ..... | ..... | Tr | ..... |
| Allanite[4] | ..... | ..... | Tr | ..... | ..... | ..... | ..... | ..... | ..... | ..... | ..... | ..... | X | ..... | Tr | ..... |
| Zircon | ..... | ..... | ..... | Tr | ..... | ..... | ..... | Tr | Tr | Tr | ..... | ..... | Tr | Tr | ..... | ..... |
| Apatite | Tr | Tr | X | Tr | Tr | ..... | Tr | Tr | Tr | Tr | Tr | ..... | Tr | Tr | ..... | ..... |
| Garnet[2] | ..... | ..... | ..... | ..... | ..... | ..... | ..... | ..... | ..... | ..... | ..... | ? | ..... | ..... | ..... | ..... |
| Rutile | ..... | Tr | ..... | ..... | Tr | ..... | ..... | ..... | ..... | ..... | ..... | ..... | ..... | ..... | ..... | ..... |
| Ilmenite | ..... | ..... | ..... | ..... | ..... | ..... | ..... | ..... | ..... | ..... | ..... | Tr | ..... | ..... | ..... | Tr |
| Chalcopyrite | ..... | Tr | Tr | Tr | Tr | Tr | Tr | Tr | Tr | Tr | Tr | Tr | Tr | ..... | Tr | ..... |
| Pyrrhotite | X | Tr | X | X | X | Tr | Tr | Tr | Tr | ? | Tr | X | Tr | Tr | Tr | ..... |
| Pyrite | ..... | ..... | ..... | ..... | ..... | ..... | Tr | ..... | ..... | ..... | ..... | ..... | ..... | ..... | ..... | Tr |
| Arsenopyrite | ..... | ..... | Tr | ..... | ? | ..... | ..... | ..... | ..... | ..... | ..... | ..... | ..... | ..... | ..... | Tr |
| Hematite | Tr | Tr | ..... | ..... | ..... | ..... | X | ..... | ..... | ..... | ..... | ..... | ..... | ..... | ..... | ..... |
| Chalcocite | ..... | Tr | ..... | ..... | ..... | Tr | ..... | ..... | ..... | ..... | ..... | ..... | ..... | ..... | ..... | Tr |
| Montmorillonite | Tr | ..... | ..... | ..... | ..... | ..... | ..... | ..... | ..... | ..... | ..... | ..... | ..... | Tr | ..... | ..... |
| Kaolinite | ..... | ..... | ..... | ..... | ..... | ..... | ..... | ..... | ..... | ..... | ..... | ..... | ..... | Tr | Tr | ..... |

[1]Specimens from outside the mapped pyrrhotite zone.
[2]Detrital.
[3]Metamorphic, hydrothermal.
[4]Questionably detrital.

TABLE 5.—*Mineralogy of typical veins in the Upper Cambrian Harmony Formation on the 6450 bench, Copper Canyon east ore body*

[X, mineral present; ?, questionably present; ....., not found]

| Vein No. | 1 | 2 | 3 | 4 | 5 | 6 | 7 | 8 | 9 | 10 | 11 | 12 | 13 | 14 | 15 | 16 | 17 | 18 | 19 | 20 | 21 | 22 | 23 | 24 | 25 | 26 |
|---|---|---|---|---|---|---|---|---|---|---|---|---|---|---|---|---|---|---|---|---|---|---|---|---|---|---|
| Quartz | X | X | .... | X | X | X | X | X | X | .... | X | X | .... | .... | X | X | X | .... | .... | X | X | X | .... | X | .... | X |
| K-feldspar | X | .... | X | X | X | X | X | X | X | .... | X | .... | X | X | X | X | X | X | .... | .... | .... | X | .... | .... | X | .... |
| Biotite | .... | .... | .... | .... | X | .... | .... | X | .... | .... | X | .... | X | .... | X | .... | X | .... | .... | .... | .... | X | .... | .... | .... | .... |
| Chlorite | .... | .... | .... | X | .... | .... | X | X | X | X | X | X | .... | X | X | X | .... | .... | .... | .... | .... | X | .... | .... | .... | X |
| Plagioclase[1] | .... | X | .... | .... | .... | .... | .... | .... | .... | .... | .... | .... | .... | .... | .... | .... | .... | .... | .... | .... | .... | .... | .... | .... | X | .... |
| White mica | X | .... | .... | .... | .... | .... | X | X | .... | .... | .... | .... | X | X | .... | X | X | X | X | X | X | .... | .... | .... | X | .... |
| Apatite | .... | .... | .... | .... | .... | X | .... | .... | .... | .... | .... | .... | .... | X | X | X | .... | X | .... | .... | .... | .... | .... | .... | .... | .... |
| Rutile | .... | .... | .... | .... | .... | .... | .... | .... | .... | .... | .... | X | .... | .... | .... | .... | .... | .... | .... | .... | .... | .... | .... | .... | .... | .... |
| Epidote | .... | .... | .... | .... | .... | .... | .... | .... | .... | .... | X | X | .... | .... | X | .... | .... | X | .... | .... | .... | .... | .... | .... | .... | .... |
| Zircon | .... | .... | .... | .... | .... | .... | .... | .... | .... | .... | .... | .... | .... | .... | .... | .... | .... | .... | .... | X | .... | .... | .... | .... | .... | .... |
| Allanite | .... | .... | .... | .... | .... | .... | .... | .... | .... | .... | .... | .... | .... | .... | .... | .... | ? | .... | .... | .... | .... | .... | .... | .... | .... | .... |
| Sphene | .... | .... | .... | .... | .... | .... | .... | .... | .... | .... | .... | .... | .... | .... | .... | X | .... | .... | .... | .... | .... | .... | .... | .... | .... | .... |
| Pyrite | .... | .... | .... | .... | ? | .... | .... | X | .... | .... | .... | .... | .... | .... | .... | .... | .... | .... | .... | .... | .... | .... | .... | .... | .... | .... |
| Pyrrhotite | X | X | .... | .... | .... | .... | X | X | ? | .... | X | X | ? | X | X | X | X | X | .... | .... | X | .... | X | X | X | .... |
| Arsenopyrite | .... | .... | .... | .... | .... | .... | .... | .... | .... | .... | .... | .... | .... | .... | .... | .... | X | .... | .... | .... | .... | .... | .... | .... | .... | .... |
| Chalcopyrite | .... | .... | .... | .... | .... | .... | .... | X | .... | .... | X | .... | .... | X | X | X | X | .... | .... | .... | .... | X | X | X | X | .... |
| Siderite | .... | .... | X | .... | .... | X | X | X | X | .... | .... | .... | .... | .... | .... | .... | X | .... | .... | .... | .... | X | .... | .... | .... | .... |
| Chalcocite | .... | .... | .... | .... | .... | .... | .... | .... | .... | .... | .... | X | .... | X | X | .... | .... | .... | .... | .... | .... | .... | .... | .... | X | .... |
| Hematite | .... | .... | X | .... | .... | .... | X | .... | .... | .... | .... | X | .... | X | .... | .... | .... | .... | .... | .... | .... | .... | .... | .... | .... | .... |

[1]Albite-oligoclase.

veins in these rocks commonly measure several millimeters across. These effects consist of either concentrations of biotite or depletion of biotite adjacent to the vein and (or) recrystallization of quartz in the wallrock into a very fine mosaic texture. A particular alteration effect may extend only partly along an individual vein-wallrock contact as observed in thin section.

An unusual composite vein merits detailed description. Although quartz and K-feldspar are the silicate minerals most common in many of the veins through these rocks, there are some notable concentrations of hydrothermal vein biotite in rock specimen 626, a sample somewhat finer grained than the average metasandstone (fig. 23). A composite vein in this rock contains biotite intergrown with pyrrhotite near the vein-wallrock contact. Further into the vein, this biotite-pyrrho-

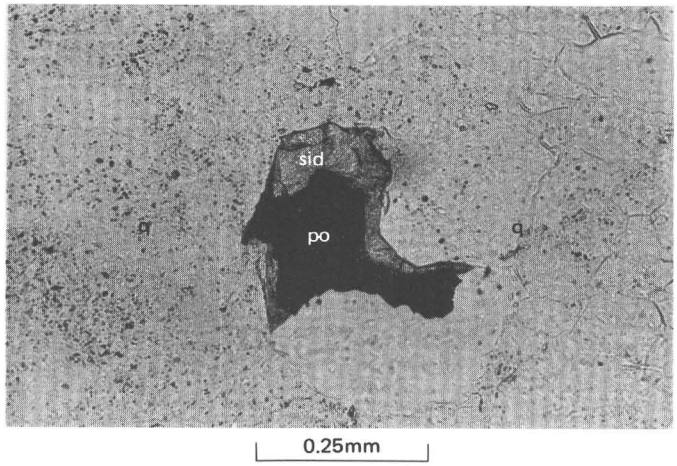


FIGURE 22.—Photomicrograph in plane polarized light of pyrrhotite (po) rimmed by siderite (sid) in a predominantly quartz (q) veinlet in the Harmony Formation.

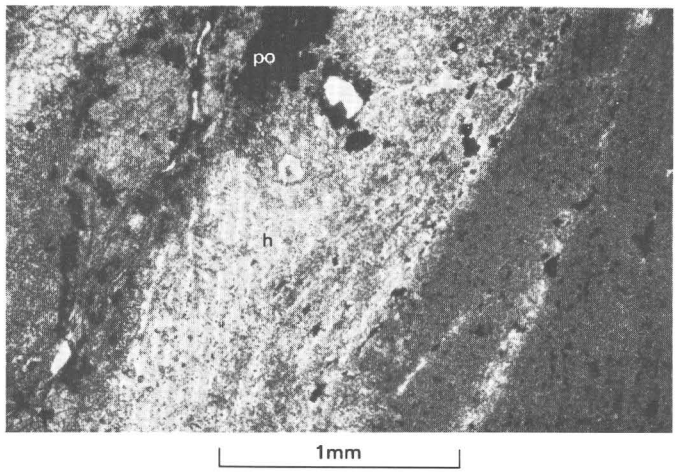


FIGURE 23.—Photomicrograph in plane polarized light of biotite (b) and pyrrhotite (po) in a vein. The vein is mantled by a very fine quartz–K-feldspar–white mica alteration halo (h)—see text. Biotite is also a dominant silicate in the wallrock outside the altered area adjacent to the vein in this rock. Specimen 626.

tite zone is mantled by a K-feldspar zone, which is in turn mantled by a central K-feldspar–quartz intergrowth. Clots of pyrrhotite-chalcopyrite are scattered among the K-feldspar and quartz, and trace amounts of arsenopyrite also occur in the same vein. Although pyrrhotite and biotite are disseminated through wallrock more than 1 mm from the vein, the predominantly quartz–K-feldspar (albite)-biotite wallrock adjacent to the vein has been bleached (biotite altered to white mica), and pyrrhotite does not occur in the bleached zone for 1–3 mm adjacent to the vein. These associations suggest to us that some iron might have been taken up by the vein from the wallrock. Furthermore, chlorite in other parts of this same vein is intergrown locally with chalcopyrite and epidote (fig. 24). There is some epidote mantling very fine grained chalcopyrite. These relations suggest that, for even very small volumes of rock, metallization and alteration were not a single-stage event. Biotite formed in the matrix of the Harmony with sulfides and also developed at some later time in sulfide-bearing veinlets as veinlets continued to open. Although hydrothermal biotite in veins is not altered to chlorite, the hydrothermal vein chlorite appears to have formed a little later than some biotite. However, both hydrothermal chlorite and biotite occur together in the same veinlet.

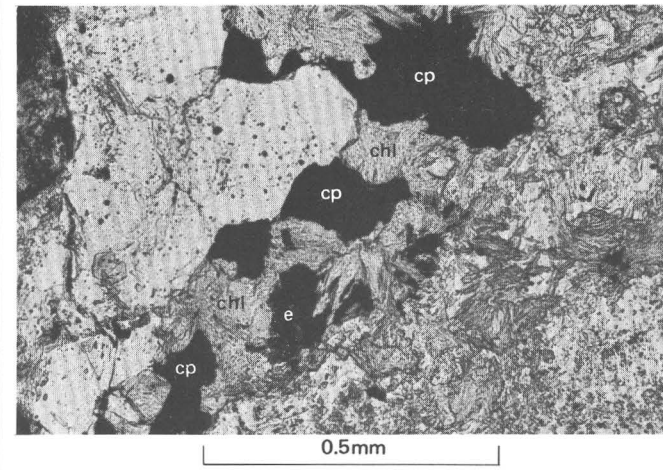


FIGURE 24.—Photomicrograph in plane polarized light of quartz (q), chalcopyrite (cp), chlorite (chl), and epidote (e) from the same vein as in figure 23. From metasandstone of the Harmony Formation.

In addition to the specific mineral associations of chalcopyrite noted above, chalcopyrite also occurs with pyrrhotite coating fractures throughout these rocks of the Harmony.

In summary, we found in even very small metasandstone domains of the Harmony that pyrrhotite deposition was primarily either disseminated or in veins. It appears that, locally in the groundmass of these rocks, disseminated pyrrhotite with silicate potassic assemblages developed before the bulk of the chalcopyrite veins were introduced. However, these chalcopyrite-bearing veins also locally include some pyrrhotite, suggesting a probable second stage of pyrrhotite, also with a potassic assemblage.

The silicate mineralogy of the chalcopyrite-bearing veins differs from that of their wallrocks because some hydrothermal chlorite and epidote occur in the veins. Both chlorite and epidote are closely associated spatially with chalcopyrite. Optically, biotites in the veins and in their wallrocks are identical. Our observations suggest repeated opening and closing of fractures to

fluids possibly with slightly changing $K^+:H^+$, $Mg^{+2}:(2H^+)$, $f_{O_2}$ or $f_{S_2}$ with the time. The later veins seem to be more magnesian.

The occurrence together of thermodynamically incompatible phases in many of the veinlets (table 5) also suggests repeated opening and filling of many individual veinlets as the fluids changed. Many reactions such as pyrrhotite to siderite and pyrrhotite to very late hematite, for example, did not go to completion.

### BATTLE FORMATION CONGLOMERATE

In general, most of these rocks consist of partly recrystallized detrital chert fragments, quartzite fragments, and rounded quartz grains set in a quartz–K-feldspar mica matrix. The mineralogy of representative samples of the Battle Formation from the 6450 bench is shown in table 6. Although hydrothermal alteration and recrystallization obscure the conglomerate texture of a few of these rocks, metachert fragments have been recognized in about 70 percent of the rocks and quartzite fragments in about 20 percent. These detrital fragments are commonly oriented with their short axes perpendicular to the bedding and they measure several centimeters across. Throughout the Battle, sulfide content is extremely variable, ranging from 1 to 2 percent in much of the siliceous metaconglomerate to about 40 percent in calc-silicate specimens. Elsewhere in the east ore body, locally as much as 50 percent of the Battle consists of hypogene sulfides (Sayers and others, 1968).

Most sulfides in the Battle occur in discrete mineral grains, or clusters of different sulfide phases, disseminated in the groundmass of altered conglomerate. Volumetrically smaller amounts of sulfide occur in narrow veins, generally less than 3 mm wide, that cut both cobbles and matrix of the metaconglomerate. Much thicker composite sulfide veins, some up to 30 cm wide, have been emplaced along faults, primarily where the wallrocks are Battle. The mineralogy of these major sulfide veins and their associated breccia zones will be treated separately in the next section.

The rocks of the Battle on the bench span two well-developed iron sulfide zones: a pyrite zone and a pyrrhotite zone (fig. 15). Chalcopyrite is common to both zones. The specimens representative of the pyrite zone (table 6) were collected about 75 m southeast of the pyrrhotite zone. Arsenopyrite was found in two, and possibly three, of these samples from the pyrite zone, and marcasite in one. Very sparse massive arsenopyrite replacement occurs in the matrix of chert pebble metaconglomerate of the Battle from the pyrrhotite zone (fig. 25). Most chalcopyrite was deposited together with pyrrhotite and pyrite. Chalcopyrite-marcasite-pyrite and chalcopyrite-siderite intergrowths, however, suggest continued but diminishing chalcopyrite deposition during later stages of metallization.

Hydrothermal K-feldspar, biotite, sphene, and white mica are very abundant in altered conglomerates of the

TABLE 6.—*Mineralogy of hydrothermally altered rocks belonging to the Middle Pennsylvanian Battle Formation on the 6450 bench*

[X mineral present; ?, questionably present; Tr, trace; ....., not found]

| | Pyrite zone | | | | | | | | | Pyrrhotite zone | | | | | |
|---|---|---|---|---|---|---|---|---|---|---|---|---|---|---|---|
| Specimen No. | 628 | 629 | 630 | 632 | 633 | 636 | 638 | 640 | 642 | 645 | 647 | 648 | 650 | 651 | 655 |
| Quartz | X | X | X | X | X | X | X | X | X | X | X | X | X | X | X |
| K-feldspar[1] | Tr | X | X | X | X | X | X | X | X | X | X | ..... | X | X | X |
| Biotite[1] | Tr | X | X | X | X | Tr | X | X | X | X | X | ..... | X | Tr | X |
| White mica[1] | ..... | ..... | X | X | ..... | Tr | X | ..... | X | X | X | Tr | X | ..... | X |
| Albite | ..... | ..... | ..... | ..... | ..... | ..... | ..... | ..... | ..... | ..... | X | ..... | ..... | ..... | ..... |
| Celsian[1] | ..... | X | ..... | ..... | ..... | ..... | ..... | X | ..... | ..... | Tr | ..... | ..... | X | X |
| Epidote[1] | ..... | ..... | ..... | Tr | ..... | ..... | ..... | ..... | ..... | ..... | ..... | ..... | ..... | X | ..... |
| Chlorite[1] | Tr | X | ..... | X | Tr | ? | X | ..... | X | Tr | ..... | ..... | Tr | Tr | X |
| Tremolite[1] | ..... | ..... | ..... | ..... | ..... | ..... | ..... | ..... | ..... | ..... | ..... | ..... | ..... | X | ..... |
| Sphene [1] | Tr | X | X | X | X | X | ? | X | X | X | X | Tr | X | X | X |
| Siderite[1] | ..... | ..... | ..... | ..... | ..... | ..... | ..... | ..... | ..... | ..... | X | X | X | X | Tr |
| Zircon | ..... | Tr | ..... | Tr | Tr | Tr | ..... | Tr | Tr | Tr | ..... | ..... | Tr | X | Tr |
| Apatite | Tr | Tr | ..... | Tr | ..... | Tr | Tr | ..... | ..... | ..... | Tr | Tr | ..... | Tr | ..... |
| Allanite | ..... | ..... | ..... | ..... | ..... | ..... | ..... | ..... | ..... | ..... | ..... | ..... | ? | ..... | ..... |
| Rutile | ..... | ..... | ..... | ..... | Tr | ..... | ..... | ..... | ..... | Tr | ..... | ? | ..... | ..... | ..... |
| Chalcopyrite[1] | Tr | Tr | ..... | X | X | X | X | X | ..... | ..... | X | X | X | X | X |
| Pyrrhotite[1] | ..... | ..... | ? | ..... | ..... | ..... | ..... | ..... | ..... | X | Tr | ..... | ..... | ..... | X |
| Pyrite[1] | Tr | X | X | X | X | X | ..... | X | X | ..... | X | X | X | X | ..... |
| Arsenopyrite[1] | ..... | ..... | ..... | X | X | ..... | ? | ..... | ..... | ..... | ..... | ..... | ..... | ..... | ..... |
| Marcasite[1] | ..... | ..... | ..... | ..... | ..... | ..... | ..... | X | ..... | ..... | X | X | X | X | ..... |
| Hematite[2] | ..... | ..... | X | ..... | X | Tr | ..... | ..... | ..... | ..... | Tr | Tr | X | Tr | ..... |
| Chalcocite[2] | Tr | X | Tr | Tr | Tr | Tr | ..... | ..... | Tr | ..... | ..... | ..... | ..... | ..... | ..... |
| Montmorillonite[2] | ..... | ..... | Tr | ..... | ..... | ..... | ..... | ..... | ..... | ..... | Tr | ..... | ..... | ..... | ..... |

[1]Hydrothermal, hypogene.
[2]Supergene.

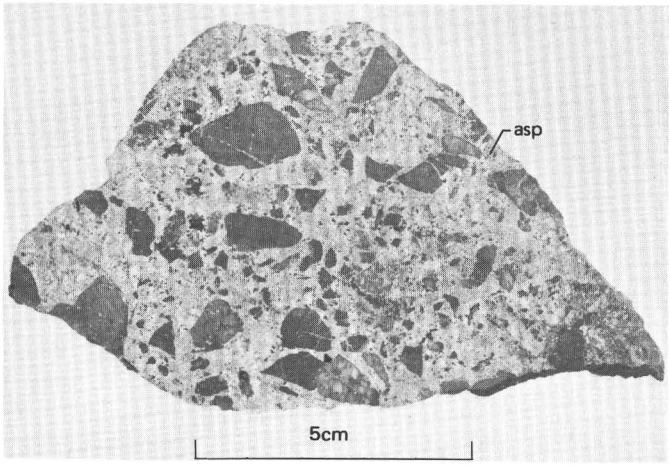


FIGURE 25.—Massive arsenopyrite (asp) matrix replacement in a sample of the lower member of the Battle Formation. Collected from the north end of the 6450 bench.

Battle Formation in the ore zones. They are commonly intergrown with, or spatially associated with, many sulfides both in the pyrite zone and in the pyrrhotite zone rocks and are especially concentrated in the replaced matrix of the conglomerates. Sphene rims many pyrrhotite grains. Confined primarily to the matrix as fine-grained crystals, hydrothermal K-feldspar locally makes up about 35 percent of the conglomerates. In contrast, outlines of large subrounded detrital K-feldspar crystals are barely recognizable in some rocks; this relict K-feldspar commonly has only traces of white mica along cleavage planes. Only trace amounts of biotite are altered to chlorite in the ore zones. In addition, prismatic celsian ($BaAl_2Si_2O_8$) has been found in K-feldspar- and biotite-rich domains of several altered conglomerates of the Battle Formation (fig. 26*A*). Relatively high concentrations of this mineral also occur at Iron Canyon about 3 km northeast of the Copper Canyon deposit (Theodore and Roberts, 1971). Hydrothermal leafy biotite intergrown with chalcopyrite, pyrite, and pyrrhotite (fig. 26*B*) is locally abundant on the 6500 bench. Chemical analyses suggest this biotite is very magnesian (see below).

Calc-silicate conglomerates, more MgO-rich than the rocks just described, occur also in the pyrrhotite zone and in the pyrite zone. They commonly contain tremolite, epidote, and chlorite, together with small amounts of celsian in some rocks. Tremolite[4] here is usually intergrown with pyrite (fig. 27). The original, unaltered matrix of the Battle contained much more MgO than the Harmony. Therefore, the increasing

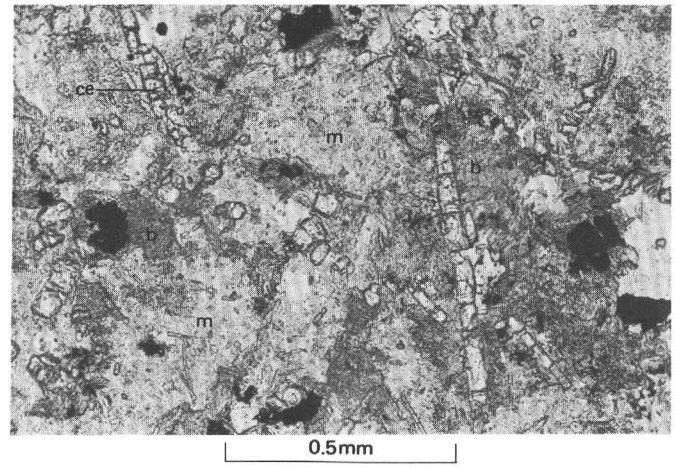


*A*

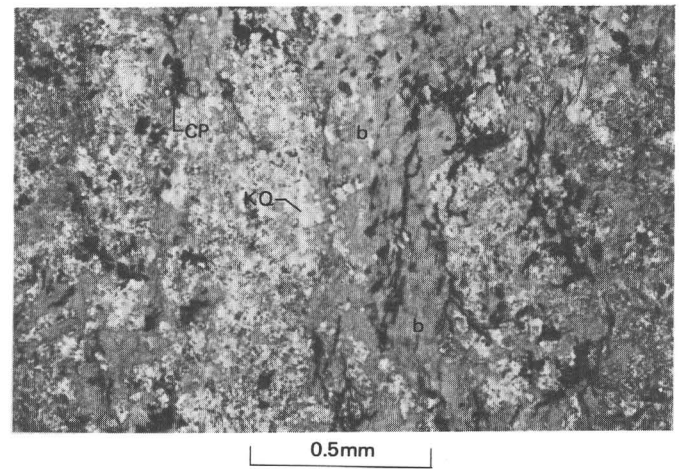


*B*

FIGURE 26.—Textural relations of biotite in the east ore body. Plane polarized light. *A*, Photomicrograph of celsian (ce), biotite (b), and pyrite (py) set in a K-feldspar–quartz matrix (m) from the Battle Formation, 6450 bench. *B*, Photomicrograph of biotite (b), K-feldspar and quartz (KQ), and chalcopyrite and pyrite (CP) from the Battle, 6500 bench.

$Mg^{+2}$:($2H^+$) ratio during metallization that we described for the Harmony probably was masked by relatively high initial Mg-contents in the Battle.

Pyrrhotite and marcasite-pyrite with siderite have an antithetic relationship in many hand specimens. The marcasite-pyrite occurs as very fine-grained granular aggregates. These mineral associations, together with siderite reaction rims mantling pyrrhotite, suggest that local early pyrrhotite reacted with a $CO_2$-rich fluid to produce marcasite-pyrite and siderite at some time after the development of pyrrhotite and its intergrown silicates. Roberts and Arnold (1965, p. B28) also noted this general paragenesis for marcasite. Additional textural evidence is included in a section below dealing specifically with pyrrhotite in

[4]Electron microprobe analyses of hydrothermal tremolite by J. T. Nash indicate that it is almost stoichiometric $Ca_2Mg_5[Si_8O_{22}](OH)_2$.

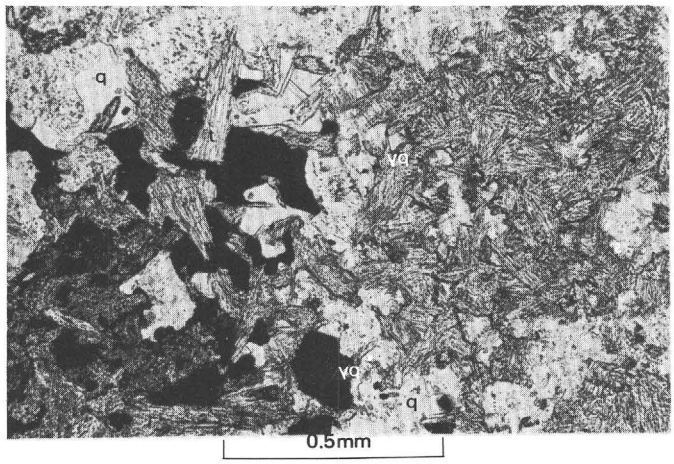


FIGURE 27.—Photomicrograph of tremolite (t), pyrite (py), sphene, and quartz from the Battle Formation, 6450 bench, Copper Canyon porphyry copper deposit. Plane polarized light.

the east ore body. In one specimen from the pyrrhotite zone (648, table 6, a rock with well-developed vein siderite and marcasite-pyrite), deposition of the marcasite-pyrite intergrowths preceded deposition of siderite. The occurrence of these veins within the pyrrhotite zone further suggests local hydrothermal iron migration, with iron derived principally from the alteration of pyrrhotite. Some of this siderite, associated with marcasite-pyrite, filled open cavities previously lined with quartz (fig. 28).

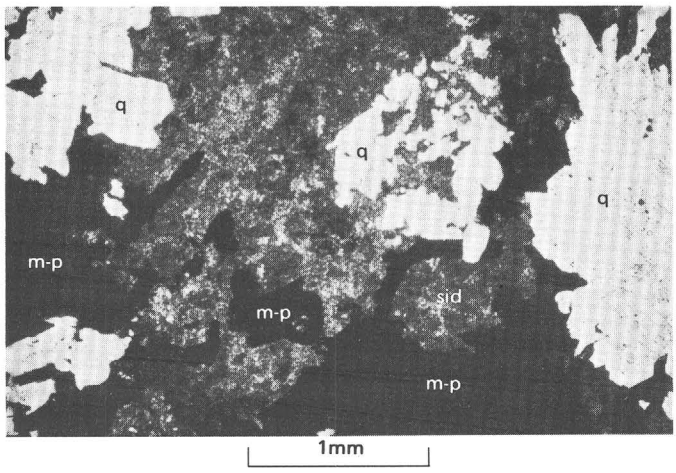


FIGURE 28.—Photomicrograph in plane polarized light of a quartz (q)-lined open cavity filled with siderite (sid) and marcasite-pyrite (m-p). Vein (sample 648) is from the Battle Formation.

Traces of chalcocite overgrowths on pyrite in rocks of the Battle Formation were found in the pyrite zone on this bench (see table 6), suggesting secondary, supergene enrichment of copper in this zone. Copper percentages in drill holes further suggest that this enrichment generally increases toward the south.

## MAJOR SULFIDE VEINS

Three types of major sulfide veins occur in this part of the ore body: (1) arsenopyrite veins, (2) chalcopyrite-pyrite-quartz veins, and (3) pyrrhotite-chalcopyrite veins. These veins range from 2 to 30 cm wide and crop out in many of the fault zones here (fig. 15). They are concentrated mostly in the northern half of the bench and are also generally near the unconformity between the Harmony and the Battle Formations; the majority are found in the Battle. Where traced along strike from the Battle into the Harmony, the veins decrease in width markedly as the wallrock changes from Battle to Harmony.

The mineralogy of many of these veins shows marked contrasts to the mineralogy of the disseminated or replacement type of metallization. As opposed to its very sparse occurrence in the replacement ores, arsenopyrite was found in more than half of the major veins on the bench (fig. 15), and it is the dominant sulfide in several prominent veins (fig. 29).

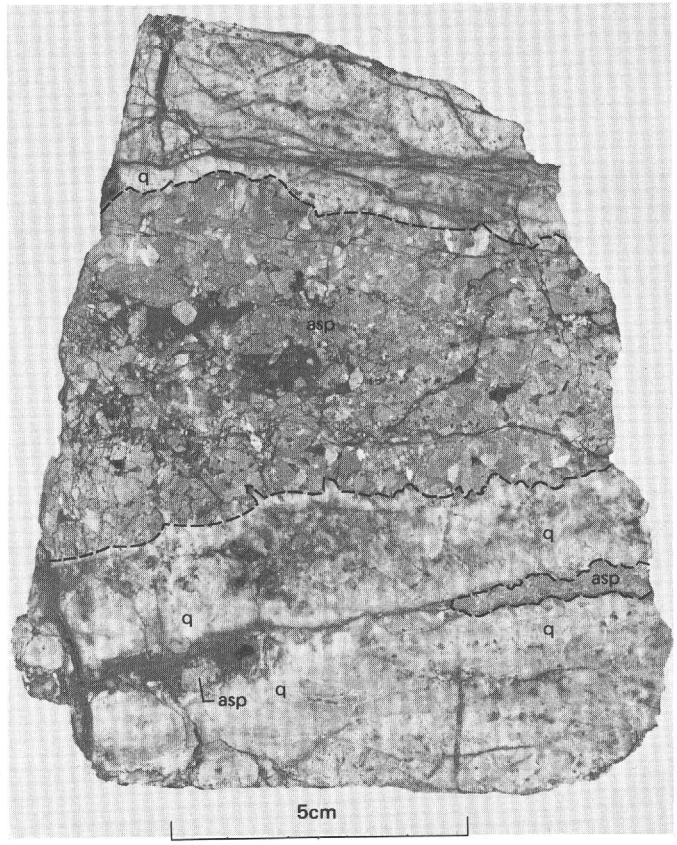


FIGURE 29.—A predominantly arsenopyrite (asp)-quartz (q) vein from the 6500 bench, east ore body.

These arsenopyrite veins cut the replacement ores in the ore body and many of the larger veins show cyclic banding and crustification suggesting repeated open fissure fillings.

Mineral relations in the arsenopyrite veins further document details about the history of metallization in the east ore body. Arsenopyrite in the veins is an early phase occurring together with quartz. These were then followed by pyrite, chalcopyrite, sphalerite, and siderite, generally in that order. Angular fragments of shattered arsenopyrite set in chalcopyrite and filiform chalcopyrite veining irregular fractured arsenopyrite indicate that chalcopyrite was deposited after arsenopyrite was brecciated (fig. 30).

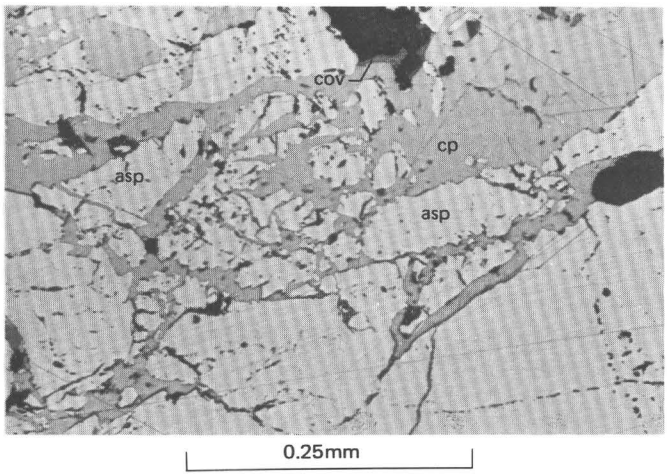


FIGURE 30.—Photomicrograph of arsenopyrite (asp) veined by chalcopyrite (cp) with a trace of covellite (cov). Sample is from an arsenopyrite vein along a north-striking fault in the east ore body. Reflected light.

Brecciation of the arsenopyrite and subsequent filling with chalcopyrite reflect movements along the faults penecontemporaneous with metallization. Deposition of traces of sphalerite, associated with pyrite, locally preceded some chalcopyrite in these veins. Although the bulk of chalcopyrite and arsenopyrite appears texturally to be earlier than siderite, sparse amounts of chalcopyrite are also intergrown with siderite. Thus there appears to have been continued deposition of chalcopyrite during the development of siderite in the deposit. Roberts and Arnold (1965) also found more than one generation of chalcopyrite in the old Copper Canyon underground mine.

Chalcopyrite-pyrite-quartz veins, the second major type of sulfide vein, are another distinct type of mineral association among the more persistent veins on the bench. They include minor amounts of sphalerite, siderite, arsenopyrite, pyrrhotite, and traces of secondary marcasite. Most chalcopyrite in these veins was deposited with pyrite, and about one-half of this pyrite has a mottled aspect that results from abundant very fine silicate(?) inclusions. These mottled domains define irregular zonal growth patterns in some subhedral crystals and are commonly in the core areas of the crystals, while the rims are clear, inclusion-free pyrite (fig. 31). Traces of irregular crystals of arsenopyrite apparently have exsolved from the inclusion-free pyrite and are found locally in some of its rims. Later, after most of the chalcopyrite in these veins was deposited, most veins were reopened, and pyrite filled ruptures among shattered fragments of chalcopyrite. This textural relation suggests continuous opening and closing along the fault zones during metallization. Among the last phases to be deposited in the veins, siderite and quartz fill open cavities previously lined with pyrite cubes. There are traces of arsenopyrite and sphalerite in this quartz also.

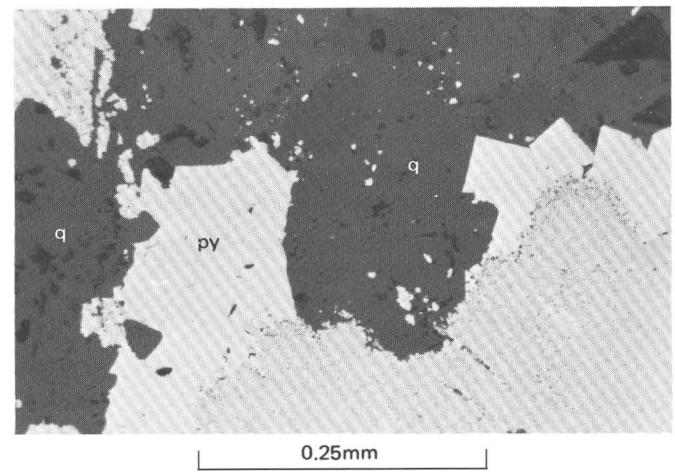


FIGURE 31.—Photomicrograph of pyrite (py) rimming an earlier pyrite, mottled by numerous very fine silicate inclusions. Vein was subsequently filled by quartz (q). Reflected light. Sample is from the 6,450 bench, east ore body.

Native gold is rarely observed but has been noted in some of the chalcopyrite-pyrite-quartz veins, where it occurs as a late phase along microfractures through chalcopyrite (fig. 32*A*). The age of these chalcopyrite-pyrite-quartz veins that carry late gold relative to the arsenopyrite veins could not be determined. Roberts and Arnold (1965) also concluded that gold was deposited late in the metallization of the Copper Canyon underground mine (fig. 32*B*).

Pyrrhotite-chalcopyrite veins with minor quartz and traces of cubanite(?) make up a third major type of vein through the east ore body. These veins are commonly about 10 cm wide. Minor amounts of small, generally anhedral sphalerite grains occur throughout them. As with the preceding two major types of veins, intervein offsets are not available to establish precisely

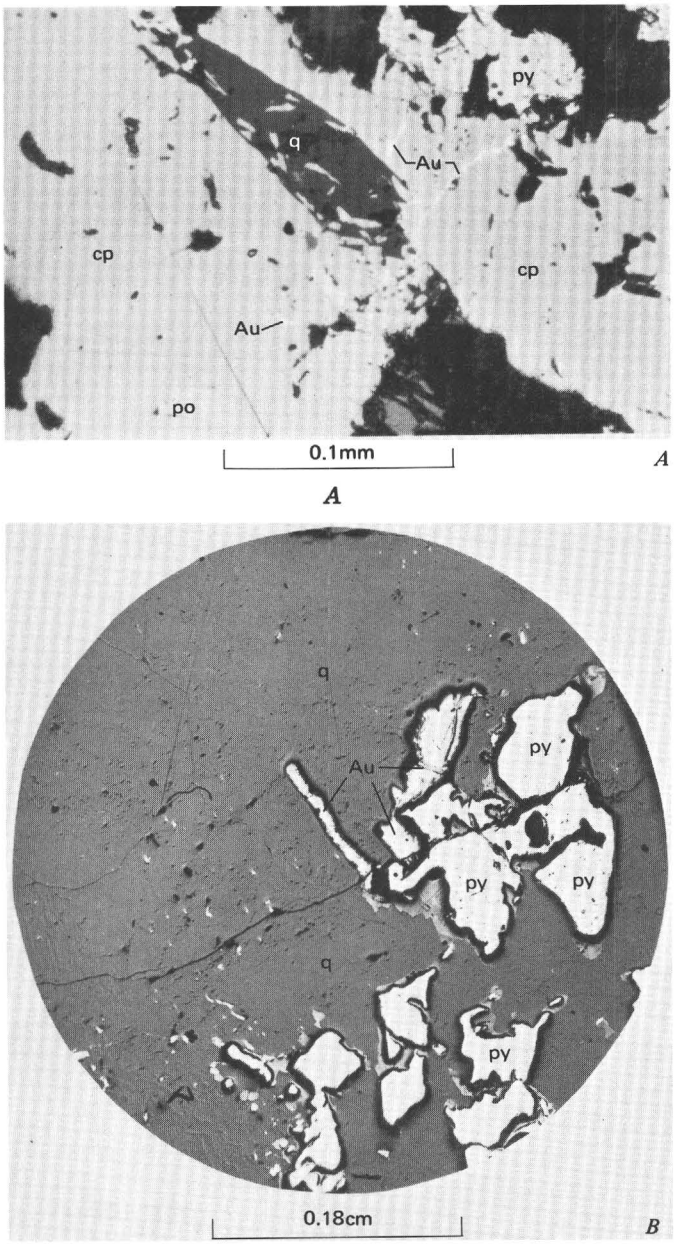


FIGURE 32.—Textural relations of native gold. Photomicrographs in reflected light. *A*, Native gold (Au) along microfracture through chalcopyrite and as irregular "blebs" in chalcopyrite. Some pyrite (py), pyrrhotite (po), and quartz (q) are also in the field of view. From a chalcopyrite-pyrite-quartz vein in the east ore body. Pyrrhotite may be contemporaneous with chalcopyrite; quartz and pyrite are later. *B*, Gold ore from the Copper Canyon underground mine. Amethystine quartz (q) with late pyrite (py) and gold (Au).

the position of the pyrrhotite-chalcopyrite veins in a relative-time framework.

## FAULT ZONES

Iron oxide-rich, 15-cm- to 1-m-wide zones of poorly consolidated breccia and gouge occur along and delimit many of the faults shown in figure 15. The iron oxides have a wide range in color, but different hues of ochre, ochre brown, and dark resinous brown dominate. The general mineralogy in eight samples from seven of these zones (table 7) was determined by X-raying air-dried cell packs in aluminum holders; the layered silicate mineralogy was further refined by X-raying glycolated and heated samples (both oriented and unoriented), as outlined in Warshaw and Roy (1961) and Schultz (1963).

TABLE 7.—*Composite mineral assemblages of fault breccia and fault gouge on the 6450 bench*

[X, mineral present; ?, questionably present; Tr, trace; ....., not found]

| Specimen No. | 615 | 631 | 634 | 635 | 637 | 641 | 646 | 654 |
|---|---|---|---|---|---|---|---|---|
| Quartz | X | X | X | X | X | Tr | X | X |
| K-feldspar | .... | X | X | X | .... | .... | X | .... |
| White mica | Tr | X | .... | .... | Tr | .... | X | .... |
| Iron oxides[1] | X | X | X | X | Tr | X | X | Tr |
| Copper oxides | .... | .... | .... | X | .... | .... | .... | .... |
| Kaolin group[2] | .... | .... | .... | X | .... | .... | X | X |
| Halloysite | X | .... | .... | .... | .... | X | X | .... |
| Chlorite group[2] | .... | .... | .... | .... | X | .... | .... | .... |
| Serpentine group[2] | .... | .... | .... | .... | X | .... | .... | .... |
| Vermiculite | .... | .... | .... | .... | .... | .... | Tr | .... |
| Talc | .... | .... | .... | .... | ? | .... | .... | .... |
| Pyrite | .... | .... | .... | ? | .... | .... | .... | X |
| Chalcopyrite | .... | .... | .... | .... | .... | .... | .... | X |
| Sphalerite | .... | .... | .... | .... | .... | .... | .... | X |

[1]Includes amorphous limonite and also hematite and goethite.
[2]Undifferentiated.

Our study shows that the fault zones consist primarily of iron oxide, quartz, and K-feldspar with lesser, but still significant, amounts of clay minerals. The iron oxides are chiefly amorphous limonite, and hematite and goethite. The K-feldspar d spacings suggest an iron-rich variety. The clay minerals most commonly detected in the zones are the aluminum-rich layered silicates of the kaolin group. Halloysite, a hydrated kaolin group mineral (Deer and others, 1962, p. 194), occurs in rocks from three of the faults (table 7). One fault sample (641) consists almost entirely of halloysite. Chlorite and serpentine were detected along one fault strand through rocks of the Battle Formation. These magnesium clays may have been derived from tremolite-rich conglomerate. White mica (illite or sericite) is generally a minor constituent in these rocks, and vermiculite, detected in only one specimen, is probably an alteration product of biotite.

The clay-rich and iron oxide-rich mineralogy of the fault zones is incompatible with the hypogene assemblages in the replacement ores and also with those in the major sulfide veins. Most of the fault zone minerals are supergene.

## HYDROTHERMAL BIOTITE FROM THE 6500 BENCH

An unusually high concentration of leafy hydrothermal biotite (fig. 26*B*) occurs on the 6500 bench

as hypogene metasomatic replacement of shaly rocks belonging to the lower member of the Battle. This biotite, which makes up 25–40 volume percent in typical hand samples, is much finer grained than primary, "book" biotite in the pluton of Copper Canyon; ragged individual crystals of hydrothermal biotite commonly are 0.1–0.2 mm long. However, the color and pleochroism of the hydrothermal biotite are similar to those of primary phenocrystic biotites in the pluton; under the microscope, the leafy biotite composes a felted aggregate of reddish-brown to pale-reddish-brown (Y=Z) crystals. The leafy biotite, furthermore, is very tightly intergrown with many sulfides; chalcopyrite and pyrite are dominant, and trace amounts of pyrrhotite (made up of both hexagonal and monoclinic varieties, with most of the grains mottled and altered to marcasite-pyrite) are also present. Quartz–K-feldspar—sphene–apatite–chlorite (trace) (epidote-white mica-secondary hematite-zircon-rutile) assemblages make up the remainder of these biotite-rich rocks. Epidote occurs in two textural relations, as (1) lensoid, 0.5- by 2.0-cm clusters of individual epidote grains in silt-sized, quartz-rich, and biotite-free domains, and as (2) sparse single epidote crystals intergrown with biotite and sulfides.

Structural relations of these prominent biotite-bearing assemblages with later quartz-molybdenite veinlets seem to fix the paragenetic position of molybdenite in at least one locality in the east ore body, as postdating the main chalcopyrite–K-silicate alteration stage. The quartz-molybdenite veinlets, about 0.5–1.0 cm wide, are probably a dilation type. Molybdenite occurs in the veinlets as sparse, spathic aggregates near veinlet margins. (Molybdenum has about a 150-ppm concentration in fist-sized samples.) The quartz-molybdenite veinlets are mantled by a diffuse 2–3-cm-wide zone of white mica with relict pyrite and chalcopyrite. The temporal relation of the deposition of molybdenite-bearing veinlets to other major sulfide veins through the ore body has not been established, although molybdenite probably preceded the bulk of the arsenopyrite deposited in the ore body. In the pluton of Copper Canyon, quartz-molybdenite veins both cut and are themselves cut by chalcopyrite-bearing veins, which indicates that most molybdenite deposition occurred sometime after the onset of copper metallization.

## INVESTIGATIONS OF SPECIFIC SULFIDES FROM THE ORE BODY

### CHALCOPYRITE ETCH TESTS

Polished sections of chalcopyrite-rich ore samples of both the replacement and the vein types were studied. The sections were etched with an ammonium dichromate solution (R. A. Yund, written commun., 1969). Petrographic examination then revealed the presence of a mineral that is apparently cubanite after chalcopyrite in two distinct textural habits. The first type, which is less common, forms straight exsolution bands through chalcopyrite. The more common variety was found as sparse small grains, much less than 0.1 mm wide, around quartz inclusions in chalcopyrite and also along fractures through chalcopyrite. Even within 1-sq-mm chalcopyrite domains, this cubanite (?) makes up definitely less than 5 percent of the copper phases and more probably about 1 or 2 percent. These samples also include hexagonal pyrrhotite, which we describe at length below, with the thermal implications of these observations.

### PYRRHOTITE ETCH TESTS AND ANNEALING EXPERIMENTS

Pyrrhotite is rather common at Copper Canyon, and indeed over all the Battle Mountain mining district (Roberts and Arnold, 1965); locally, it is even the dominant iron sulfide material. For this reason, and because its presence has important petrochemical implications, detailed studies of its textures and compositions were undertaken.

Pyrrhotite compositions are partly a function of temperature. However, the pyrrhotite geothermometer (Arnold, 1962) cannot be used unconditionally as an indicator of temperatures during ore formation, because pyrrhotite compositions can adjust as a deposit cools (Yund and Hall, 1969), and initial pyrrhotite compositions are also a function of sulfur fugacity (Toulmin and Barton, 1964; Barton and Skinner, 1967). The thermal history of the deposit must also be established by some means independent of the pyrrhotites (Yund and Hall, 1969). The compositions of selected hexagonal and monoclinic pyrrhotites may be used to establish their respective minimum and maximum temperatures of formation, if certain assumptions are made (Barton and Skinner, 1967).

Pyrrhotite is generally rare in porphyry copper deposits (Creasey, 1966; Lowell and Guilbert, 1970; Ramdohr, 1969; Rose, 1970); pyrite is much more abundant. Furthermore, pyrrhotite is typically not associated with potassic alteration assemblages (Meyer and Hemley, 1967). It is, however, fairly common in contact replacement deposits of limestones (Ramdohr, 1969).

### PYRRHOTITE TYPES AND TEXTURES

Although several crystallographic types of pyrrho-

tite occur naturally (Arnold, 1966; Ramdohr, 1969; Morimoto and others, 1970), the most common appear to be the hexagonal and monoclinic varieties (Clark, 1965; Desborough and Carpenter, 1965; Arnold, 1967; Haynes and Hill, 1970; Vaughan and others, 1971). Under the microscope, the pyrrhotite at Copper Canyon may be texturally classified as either almost entirely monoclinic (associated with retrograde marcasite-pyrite assemblages) or as monoclinic-hexagonal intergrowths, which is the more common variety in the ore body. In the latter type, monoclinic pyrrhotite occurs along cracks and quartz fracture fillings, and it also rims earlier crystallized hexagonal pyrrhotite.

The monoclinic and hexagonal pyrrhotite at Copper Canyon were distinguished by a combination of X-ray (Arnold, 1966), ammonium dichromate, and hydriodic acid etch methods, and treatment of slightly etched polished pyrrhotite sections with a colloidal suspension of magnetite in water (Bitter, 1932; W. C. Kelly, oral commun., 1972) (fig. 33). As Carpenter and Desborough have noted, a typical monoclinic "202-20$\bar{2}$" reflection is made up of four peaks—408, $\bar{4}$08, 228, and $\bar{2}$28—and a "102" natural hexagonal reflection probably is more properly indexed as 20$\bar{2}$·10.

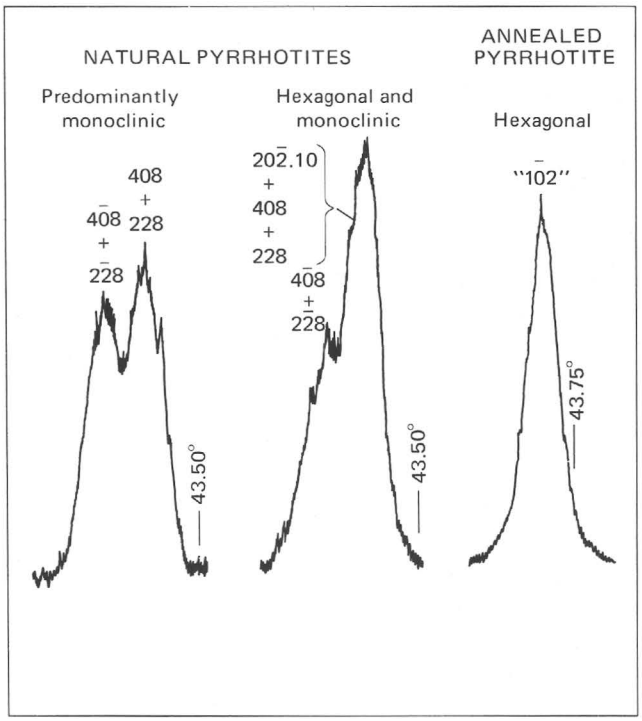


FIGURE 33.—Diffractometer traces of selected monoclinic and hexagonal pyrrhotite peaks and an annealed pyrrhotite, which was converted to hexagonal. Copper K$\alpha$ radiation, 1/8° 2$\theta$/minute scan rate.

Although low 2$\theta$ superlattice reflections were not determined by powder camera studies, the natural hexagonal pyrrhotites at Copper Canyon probably belong to the 2A, 5C hexagonal type of Carpenter and Desborough (1964).

Microscopic examination of etched pyrrhotite is a more sensitive technique for differentiating monoclinic and hexagonal pyrrhotite. Etch tests however must be carefully evaluated. Examination of polished sections of pyrrhotite etched by ammonium dichromate, polished, and then reetched by hydriodic acid solution revealed that similar pyrrhotite domains were sometimes etched (had lower reflectivities) by each solution. The ammonium dichromate etch method (Cowan, 1968) was not reliable applied to Copper Canyon pyrrhotite, as Hayes and Hill (1970) found in attempting to apply the method to material from Renison Bell, Tasmania. Monoclinic pyrrhotite from Copper Canyon remained unetched by ammonium dichromate in some sections, whereas in others it was strongly etched. Hydriodic etch tests yielded consistent results. In addition, the etching characteristics of monoclinic and hexagonal pyrrhotites are extremely variable (compare Arnold, 1966, with Vaughan and others, 1971). In one ore body, monoclinic pyrrhotite may be etched, whereas in another, the hexagonal phase may be etched preferentially. Thus, etch characteristics of pyrrhotites should not be considered diagnostic tests for establishing the type of pyrrhotite in a rock; additional tests are needed. Accordingly, a very fine grained, "colloidlike" suspension of magnetite in water was applied to lightly etched polished sections of pyrrhotite. Magnetite was found to adhere strongly to the brighter unetched pyrrhotite phase, which without exception is later than the darker cores (fig. 34). Monoclinic pyrrhotite is strongly ferrimagnetic at room temperature (Hayase and others, 1963).

Under the microscope, the most common of the hexagonal-monoclinic intergrowths appear to be pyrrhotite grains with a predominantly hexagonal core that is intergrown with lamellar "flames" of the monoclinic phase (fig. 34). These monoclinic "flames" in the grains' core areas commonly merge into monoclinic pyrrhotite at the crystals' rims. Monoclinic pyrrhotite also mantles many cracks and quartz veinlets in these composite grains, and texturally, it seems consistently to postdate crystallization of the hexagonal phase. The relative abundance of the hexagonal phase in the pyrrhotite-chalcopyrite type of veins is somewhat greater than that in the matrix replacement ores, but

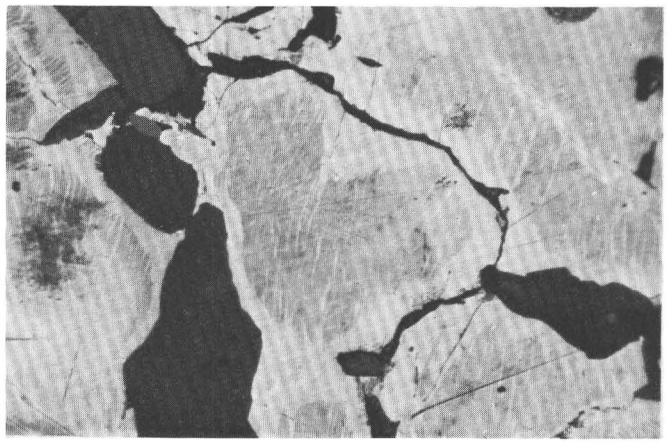


A

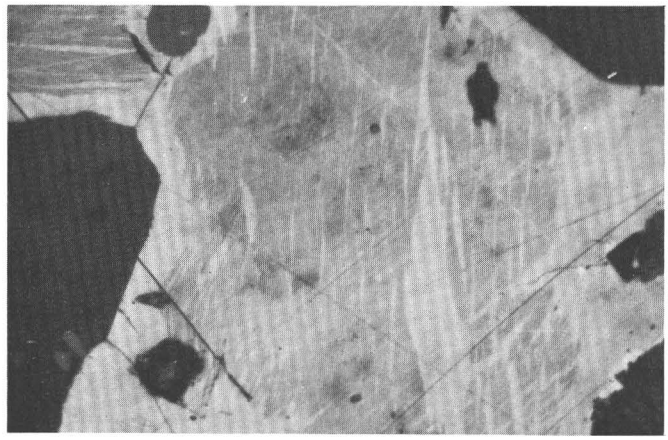


B

FIGURE 34.—Photomicrographs of lamellar "flame" intergrowths of hexagonal and monoclinic pyrrhotite. Etched, in reflected light. *A*, Predominantly hexagonal pyrrhotite (dark) cores with later monoclinic pyrrhotite (light) lamellae and rims. *B*, Hexagonal pyrrhotite (dark) core with central monoclinic pyrrhotite (light) "flames" merging into a fairly uniformly developed monoclinic pyrrhotite rim. See text for interpretation.

similar hexagonal-monoclinic textural relations occur in the veins also. Considering all occurrences at Copper Canyon, the pyrrhotite phase that is judged to be the oldest on a textural basis is invariably hexagonal. The most plausible interpretation of these textural relations is that the monoclinic pyrrhotite rims are a retrograde phenomenon reflecting a temperature decrease. Alternatively, they could also reflect a change in $f_{s2}$ during metallization.

Pyrrhotite at Copper Canyon is commonly altered to a bird's-eye texture of fine-grained marcasite plus pyrite (fig. 35). Such changes are fairly common (Vokes, 1957; Ramdohr, 1969; Kelly and Turneaure,

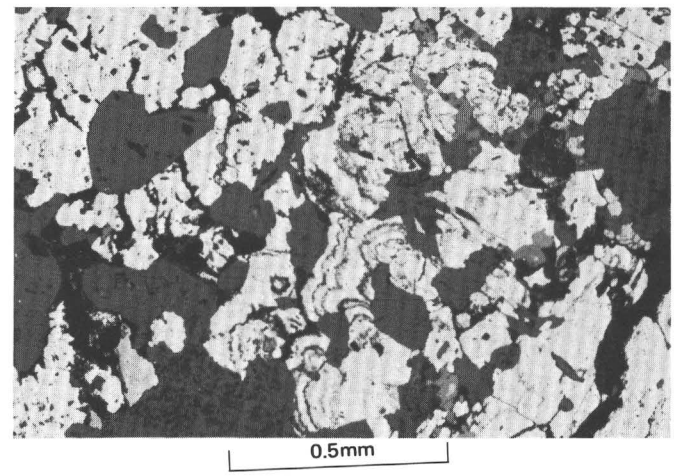


FIGURE 35.—Photomicrograph of bird's-eye texture of fine-grained granular marcasite-pyrite aggregates that replace pyrrhotite. In reflected light. Sample collected from the 6450 bench, east ore body.

1970). The usual close spatial association of these effects at Copper Canyon to siderite veins (Nash and Theodore, 1971) strongly suggests that this alteration predominantly is a result of reaction with intermediate-stage hydrothermal fluids rather than with very late supergene fluids. Furthermore, replacement of pyrrhotite by the pyrite-marcasite assemblage resulted in a net shrinkage of the formerly pyrrhotite domain and an overall accompanying increase in porosity of the rock. As Kelly and Turneaure (1970, p. 630) have pointed out, such increases in porosity during alteration of pyrrhotite to marcasite-pyrite are compatible with removal of iron while sulfur content remains constant. In the ore body, the change from a tight pyrrhotite-bearing rock to porous marcasite-pyrite-rich rock locally occurs along a distinct planar surface that is mappable.

## EXPERIMENTAL TECHNIQUES

Contamination of pyrrhotite separates by other iron-bearing minerals can alter the composition of pyrrhotite when it is annealed. Accordingly we took special care in preparing pyrrhotite separates for analysis. Fine separates ($-60+150$ mesh, Tyler sieve) were each prepared from approximately 5–10 cc of pyrrhotite-rich rocks. All these rocks are from the Middle Pennsylvanian Battle Formation, and most of the rocks are from the north end of the 6450 bench in the east ore body. The samples were initially selected to exclude any marcasite-pyrite-siderite alteration assemblages. Standard mineral-separation techniques were used, employing heavy liquids (methylene iodide) and magnetic methods, to obtain pyrrhotite concentrates. Because of the fine lamellar-type intergrowths

of virtually nonmagnetic hexagonal pyrrhotite and strongly magnetic monoclinic pyrrhotite, most of the final separates consisted chiefly of mixtures of hexagonal and monoclinic pyrrhotite in varying proportions. All separates were carefully examined under a microscope at various stages of the separation procedure to ensure that pyrrhotite eventually made up more than 99 percent of the iron-bearing phases in the samples. Typical contaminants in the final separates prepared included very fine grains of intergrown sphene, quartz, iron oxide, and chalcopyrite.

In a series of trial experiments, dry pyrrhotite charges were annealed in 4- or 5-mm evacuated silica glass tubes for times varying from 5 minutes to 1 hour, at temperatures ranging from 320° to 510°C. The charges were quenched in an ice-water bath immediately upon removal from the furnace. These natural pyrrhotite mixtures failed to invert as rapidly to the hexagonal phase as do synthetic monoclinic pyrrhotites, which Yund and Hall (1969) and Taylor (1970) found usually inverted in about 5 minutes at 325°C. Partial inversion to hexagonal pyrrhotite finally took place in our charges after they had been heated at 510°C for 15 minutes, but about 5 percent of the grains still retained remnant intergrown monoclinic-hexagonal pyrrhotite cores. Accordingly, all other pyrrhotite charges were then annealed dry, in vacuum at 505°C (±2°) for 30 minutes. Etched, polished grain mounts of splits from these charges revealed complete inversion to the hexagonal state. No newly grown pyrite was observed in any polished grain mounts of annealed charges. We are not able to suggest why inversion was relatively sluggish in these samples. However, impurities can affect the exsolution rate of some natural pyrrhotite, although at 425°C the effect of impurities is lessened (Yund and Hall, 1970). X-ray spectroscopic investigations of splits from 18 different final pyrrhotite separates from the ore body typically revealed traces of cobalt, nickel, and selenium(?) that are most likely in the pyrrhotite. Carpenter and Desborough (1964) and Kelly and Turneaure (1970) report that temperatures of 375°C and 600°C were required to convert natural pyrrhotites to the hexagonal state.

### PYRRHOTITE COMPOSITIONS

The compositions of nine unheated hexagonal pyrrhotites and 38 annealed pyrrhotites from the east ore body were determined by the d "102" X-ray determinative technique of Arnold and Reichen (1962). Thirty-three of the 38 were originally mixtures of hexagonal and monoclinic pyrrhotite, and the remaining five were predominantly monoclinic pyrrhotite. All measurements were made on a Picker diffractometer, with Ni-filtered CuK$\alpha$ radiation ($\lambda K\alpha$=1.54178 A) using halite ($a_0$=5.6400 A), annealed 3 days at 500°C, as an internal standard. Acetone smear mounts on glass slides were prepared immediately after the annealed pyrrhotite charges were removed from the evacuated glass tubes. These mounts were then scanned through two cycles at $\frac{1}{8}$° per minute $2\theta$ scan speed between the "102" peak of the annealed pyrrhotite and the 220 peak of the halite. The glass slide was rotated 180° around an axis perpendicular to the slide between cycles. Similar X-ray procedures were followed for determining the composition of the unheated hexagonal pyrrhotite. The compositions were then calculated using an equation derived by Yund and Hall (1969).

The average composition of nine unheated specimens of hexagonal pyrrhotite from Copper Canyon is 47.32 atomic percent Fe, and the average composition of 33 hexagonal-monoclinic pyrrhotite mixtures is about 46.90 atomic percent Fe (table 8). Five of the pyrrhotites are made up almost entirely of monoclinic pyrrhotite, whose Fe contents range from 46.54 to 46.72 atomic percent, with a 46.65 average. The range in composition of all annealed mixtures is 47.41–46.33 atomic percent Fe, coinciding almost exactly with Yund and Hall's (1969) sulfur-rich limit of hexagonal pyrrhotite, 47.45 atomic percent Fe, and their sulfur-poor limit of monoclinic pyrrhotite, about 46.34 atomic percent Fe. However, Arnold's (1969) sulfur-rich limit of hexagonal pyrrhotite below about 300°C is 47.20 atomic percent Fe.

### X-RAY DETERMINATION OF ARSENOPYRITE COMPOSITION

Compositions of 11 arsenopyrites from Copper Canyon also were determined by an X-ray method. Clark (1960) showed that the 313 d-spacing of arsenopyrite is an indicator of arsenic content or of the sulfur:arsenic ratio. In addition, he determined experimentally the T-X stability field of arsenopyrites at 2 kilobars and at $<1$ bar confining pressure. The arsenopyrite veins at Copper Canyon contain pyrite. Using the data of Morimoto and Clark (1961), we found three arsenopyrites to contain 31.9–33.1 atomic percent As. Similar studies of eight other arsenopyrite vein samples from Copper Canyon by J. Thomas Nash (unpub. data) yielded similar compositions.

## PARAGENESIS OF MINERALS IN THE EAST ORE BODY

From mineralogic studies in the east ore body, the paragenesis of the principal hypogene ore and gangue minerals is summarized diagrammatically in figure 36.

TABLE 8.—*X-ray diffraction data and composition of pyrrhotites from the east ore body, Copper Canyon porphyry copper deposit, Lander County, Nev.*

| Spec. No. | Field No. | Predominantly monoclinic | Unheated hexagonal fractions | | Annealed, originally hexagonal and monoclinic mixtures | |
|---|---|---|---|---|---|---|
| | | | d $20\bar{2}\cdot10$ (A) | Atomic percent Fe | d "102" (A) | Atomic percent Fe |
| 1 | 70–181 | | 2.0662 | 47.33 | 2.0633 | 47.08 |
| 2 | 70–186 | | 2.0659 | 47.31 | 2.0622 | 46.98 |
| 3 | 70–179 | | 2.0665 | 47.36 | 2.0632 | 47.07 |
| 4 | 70–184 | | 2.0655 | 47.27 | 2.0634 | 47.09 |
| 5 | AHW–079 | | 2.0658 | 47.30 | 2.0609 | 46.87 |
| 6 | AEH–263A | | 2.0665 | 47.36 | 2.0650 | 47.23 |
| 7 | AEH–263B | | 2.0665 | 47.36 | 2.0649 | 47.22 |
| 8 | 70–185 | | 2.0657 | 47.29 | 2.0619 | 46.96 |
| 9 | 6450–3 | | 2.0665 | 47.36 | N.D. | |
| 10 | 70–180 | | | | 2.0604 | 46.83 |
| 11 | 70–176A | | | | 2.0640 | 47.14 |
| 12 | 70–175B | X | | | 2.0591 | 46.72 |
| 13 | 70–175C | X | | | 2.0570 | 46.54 |
| 14 | 70–175D | X | | | 2.0574 | 46.57 |
| 15 | 6450–5 | | | | 2.0635 | 47.10 |
| 16 | 6450–6 | X | | | 2.0591 | 46.72 |
| 17 | [1]6500–5 | | | | 2.0648 | 47.21 |
| 18 | 70–176 | X | | | 2.0591 | 46.72 |
| 19 | GC–11–69A | | | | 2.0609 | 46.87 |
| 20 | GC–11–69B | | | | 2.0605 | 46.84 |
| 21 | 70–174 | | | | 2.0587 | 46.68 |
| 22 | 70–174–1 | | | | 2.0619 | 46.96 |
| 23 | 70–174–2 | | | | 2.0629 | 47.04 |
| 24 | 70–174–3 | | | | 2.0589 | 46.70 |
| 25 | 70–174–3A | | | | 2.0607 | 46.85 |
| 26 | 70–174–4 | | | | 2.0642 | 47.16 |
| 27 | 70–174–4A | | | | 2.0602 | 46.81 |
| 28 | 70–174–4B | | | | 2.0602 | 46.81 |
| 29 | 70–174–5 | | | | 2.0604 | 46.83 |
| 30 | 70–174–6 | | | | 2.0670 | 47.41 |
| 31 | 70–174–7 | | | | 2.0584 | 46.66 |
| 32 | 70–174–8 | | | | 2.0545 | 46.33 |
| 33 | 70–182 | | | | 2.0582 | 46.64 |
| 34 | 70–187 | | | | 2.0628 | 47.04 |
| 35 | 70–190 | | | | 2.0590 | 46.71 |
| 36 | 70–178 | | | | 2.0576 | 46.59 |
| 37 | 70–188 | | | | 2.0585 | 46.67 |
| 38 | 70–177 | | | | 2.0579 | 46.53 |
| 39 | 70–189 | | | | 2.0613 | 46.91 |

[1]Vein.

The bulk of the minerals in the ore body recrystallized or were introduced during the early stages of metallization. The predominant intermediate-stage minerals are marcasite-pyrite plus siderite. Vug-filling quartz crystallized during the late stage of hypogene metallization. Most gold was also probably introduced at this time, but some of it may occur as lattice substitutions in early stage sulfides. Native gold occurs along microfractures through chalcopyrite, as described above, and therefore must have been deposited during a relatively late stage. Furthermore, gold has been found adhering to clear quartz crystals in jig concentrates; these crystals may belong to the late, dilute fluid phase that Nash and Theodore (1971) described. Electron-microprobe studies by G. K. Czamanske indicate the occurrence of very fine grained inclusions of pyrrhotite in lode gold. This suggests that some gold was also deposited during the early stages of metallization with pyrrhotite.

## CHEMISTRY OF THE ORE AND WALLROCK

### MAJOR-ELEMENT VARIATIONS

Whole-rock chemical analyses of the Harmony and Battle Formations (table 9) reveal systematic changes in major-oxide percentages in the ore zones. A metallized sample of the Harmony Formation (sample 1, table 9) in the east ore body is compared with two samples of unmineralized rock from the same formation (samples 8 and 11). Metallized rocks of the lower member of the Battle are also contrasted with their hematitic, unmetallized apparent equivalents, and finally, analyses of three samples of the middle member of the Battle Formation, one metallized and two unmetallized, are also shown in table 9. Unmetallized samples were obtained at distances of up to 2,500 m from the east ore body.

Changes in major oxide percentages are interpreted as reflecting metasomatic gains and losses. There are, however, four factors that complicate comparison of data: (1) Initial rock chemistry within the ore body can be inferred only to have been similar to that now found in unmetallized rocks outside the body. (2) A wide range in original composition is possible for samples of the Battle, especially the conglomerate. This variation is reflected in the concentration range for some oxides. For example, we found a 23-weight-percent range for $SiO_2$ (table 9). (3) Although we cannot demonstrate that prograde metasomatism occurred on a volume-for-volume basis in the east ore body, such an assumption is probably valid because of volume-for-volume replacements in the west ore body and because of such widespread evidence for this at many other deposits. Changes in major-oxide percentages cannot be accounted for by changes in specific gravity for these samples (table 9). (4) Retrograde breakdown, however, of pyrrhotite to intermediate-stage siderite and marcasite-pyrite assemblages did involve a decrease in volume as we described above. The data of table 9 have not been recalculated in terms of gains and losses per unit volume of rock because of uncertainties of original compositions but are presented schematically as oxide variation diagrams (fig. 37); furthermore, metasomatic composition gradients imposed across different metamorphic facies are not represented. Sulfur percentages (expressed as $SO_3$) in the six samples of the lower member of the Battle from the east ore body (2–7, table 9) suggest total sulfide contents of 4–9 volume percent.

Significant changes in $K_2O$ content occurred at the

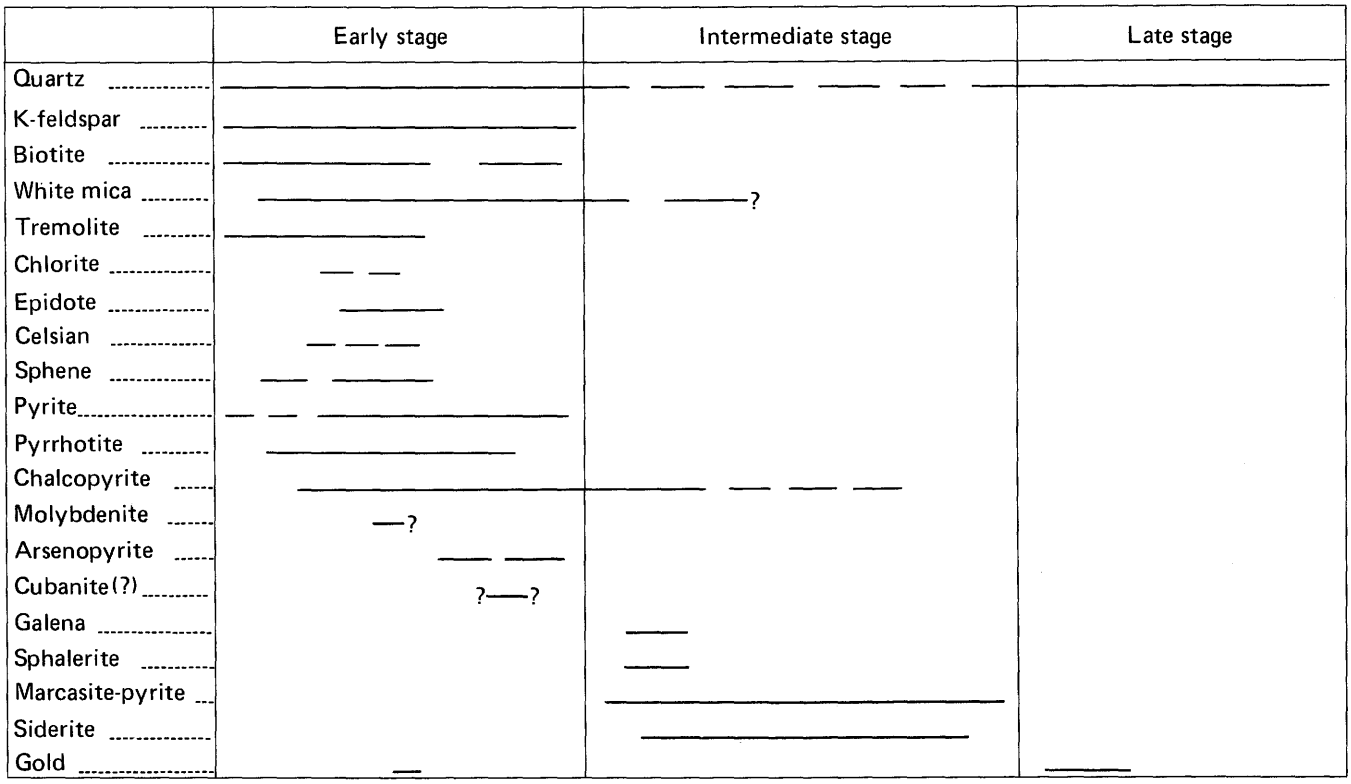


FIGURE 36.—Paragenesis of principal hypogene ore and gangue minerals.

same time as metallization in the east ore body. From the determinations (table 9, fig. 37), we may infer enrichment in $K_2O$ both for the Harmony and for the lower member of the Battle Formations. Much of this gain is in the form of hydrothermal K-feldspar, commonly in the matrix and in veins as described above. From the $H_2O$ values of samples 2–4 from the east ore body, we may also infer that these particular samples are not notably enriched in hydrothermal micas. This conclusion was verified by petrographic examination. The one metallized sample (5, fig. 37) of the middle member of the Battle Formation is not, however, enriched in $K_2O$ but is apparently depleted. This sample was collected about 300 m north of the east ore body, where presumably the effects of $K_2O$ metasomatism are somewhat less. In the granodiorite at Copper Canyon, and in all of the nearby hydrothermally altered plutonic rocks, Theodore, Silberman, and Blake (1973) have shown a progressive addition of $K_2O$ concomitant with increasing intensity of potassic alteration, with the most intensely potassic-altered intrusive rocks found in the east ore body; these are dikes about 5 m thick.

The iron content (shown as $Fe_2O_3$ on fig. 37) of all the metallized samples has also increased, as has the $FeO:Fe_2O_3$ ratio, which reflects reduction of iron upon sulfidation. However, significant amounts of ferric iron were already present in some of the unmetallized rocks, especially the red-bed horizons of the lower member of the Battle Formation. One red-bed sample (7, fig. 37) has almost 6 percent FeO plus $Fe_2O_3$, and almost 90 percent of its Fe as $Fe_2O_3$. $TiO_2$ percentages in these hematitic conglomerates (6, 7, table 9) are 0.55 and 0.82 weight percent; almost all the $TiO_2$ is in detrital hematitic chips as described earlier in the report. Much of the $TiO_2$ in the metallized samples is either in sphene or in hydrothermal biotite.

Metallization of the rocks of the Battle Formation produced significant losses in CaO and $CO_2$ through decarbonation of the carbonate-bearing, premetallization matrix. Progressive losses of CaO from plagioclase during potassic alteration in many of the intrusive rocks around the east ore body have also been documented (Theodore and others, 1973). Comparable losses in CaO and $CO_2$ are reported by Roberts and Arnold (1965, p. B12) for metamorphosed rocks of the Battle Formation in the underground workings of the Copper Canyon mine. $MgCO_3$ in the carbonate matrix in the east ore body was probably fixed in biotite, tremolite, or chlorite upon alteration.

The MgO content of the middle member of the Battle apparently increased as a result of metallization (fig. 37). However, the gains in MgO in the form of hydrothermal tremolite, suggested by this one sample,

TABLE 9.—*Analyses of rocks from the Battle and Harmony Formations in and near the east ore body Copper Canyon porphyry copper deposit*

[Chemical analyses by rapid-rock methods; analysts, P. L. D. Elmore, Lowell Artis, J. L. Glenn, Gillison Chloe, J. Kelsey, and Hezekiah Smith, Methods used are those described in Shapiro and Brannock (1962), supplemented by atomic absorption; and Shapiro (1967). Spectrographic analyses by Chris Heropoulos and H. Bastron. Results are reported to the nearest number in the series 1, 0.7, 0.5, 0.3, 0.2, 0.15, 0.1, 0.07, and so on, which represent approximate midpoints of interval data on a geometric scale. The precision of a reported value is approximately plus or minus one series interval at 68 percent confidence or two intervals at 95 percent confidence. Looked for but not found: As, Au, Pd, Pt, Sb, Te, U, Hf, In, Li, Re, Ta, and Tl. Atomic absorption analyses: Gold was determined by a combined fire-assay atomic absorption technique; copper, lead, and zinc were determined by atomic absorption spectroscopy. Analysts: J. Budinsky, C. L. Burton, J. Marinenko, and M. Pastor]

| | 1 | 2 | 3 | 4 | 5 | 6 | 7 | 8 | 9 | 10 | 11 | 12 | 13 | 14 |
|---|---|---|---|---|---|---|---|---|---|---|---|---|---|---|
| | East ore body | | | | Biotite-rich rock | | | | | | | | | |
| Lab. No. | M106620W | M106621W | M106622W | M106623W | M113888W | M113889W | M113890W | M108907W | M111996W | M111997W | M111998W | M11199W | M112000W | M108909W |
| Field No. | AHW112 | AHW113 | AHW114 | AHW115 | MB6500 | MB6500A | MB6500B | TT–69–3 | AFJ051 | AFJ100 | AFJ158 | AFJ163 | AFJ165 | TT–69–5 |
| **Chemical analyses (weight percent)** | | | | | | | | | | | | | | |
| $SiO_2$ | 75.4 | 73.5 | 77.4 | 58.5 | 59.1 | 55.0 | 60.5 | 51.8 | 61.6 | 72.1 | 78.5 | 48.6 | 63.0 | 82.3 |
| $Al_2O_3$ | 10.8 | 5.9 | 5.7 | 12.2 | 12.5 | 13.2 | 12.5 | 10.0 | 5.2 | 7.7 | 10.4 | 5.9 | 10.5 | 8.5 |
| $Fe_2O_3$ | 1.2 | 5.1 | 4.3 | 2.3 | 4.4 | 5.4 | 3.2 | 1.3 | 2.9 | 4.8 | 1.1 | 1.4 | .90 | 2.2 |
| FeO | 1.4 | 5.4 | 2.5 | 4.0 | 3.9 | 4.8 | 3.8 | 3.9 | .56 | .64 | 1.5 | .60 | 2.3 | .04 |
| MgO | 1.6 | 1.3 | 1.3 | 5.7 | 6.0 | 4.4 | 6.0 | 15.0 | 4.3 | 3.1 | 1.2 | 2.8 | 5.2 | 1.1 |
| CaO | 1.0 | .63 | .81 | 4.4 | .83 | 1.7 | .89 | 11.5 | 11.9 | 3.4 | .45 | 20.1 | 5.2 | .24 |
| $Na_2O$ | .87 | .17 | .15 | .55 | .26 | .59 | .23 | .74 | .09 | .00 | 2.7 | .23 | .09 | 2.6 |
| $K_2O$ | 5.5 | 3.2 | 2.9 | 7.5 | 6.6 | 5.9 | 7.2 | 1.4 | .67 | 1.8 | 1.9 | 2.3 | 4.1 | 1.3 |
| $H_2O-$ | .23 | .19 | .44 | .45 | .53 | .46 | .41 | .50 | .23 | .43 | .22 | .14 | .24 | .16 |
| $H_2O+$ | 1.0 | 1.1 | 1.1 | 1.4 | 2.1 | 2.2 | 2.0 | 1.9 | 2.3 | 2.2 | 1.4 | 1.4 | 2.7 | 1.3 |
| $TiO_2$ | .70 | 1.2 | .49 | .55 | 1.2 | 1.2 | 1.2 | .68 | .55 | .82 | .39 | .30 | .51 | .46 |
| $P_2O_5$ | .08 | .14 | .10 | .27 | .35 | .33 | .38 | .47 | .11 | .37 | .24 | .14 | .40 | .09 |
| MnO | .00 | .00 | .04 | .05 | .01 | .05 | .05 | .18 | .00 | .00 | .00 | .00 | .00 | .00 |
| $CO_2$ | .11 | .20 | .12 | .10 | .02 | .02 | .02 | .02 | 9.5 | 2.3 | .08 | 15.4 | 3.8 | .08 |
| S as $SO_3$ | ..... | 4.7 | 4.1 | 2.4 | 2.8 | 6.5 | 3.3 | ..... | ..... | ..... | ..... | ..... | ..... | ..... |
| F | ..... | ..... | ..... | ..... | .63 | .48 | .66 | ..... | ..... | ..... | ..... | ..... | ..... | ..... |
| Cl | ..... | ..... | ..... | ..... | <.001 | <.001 | <.001 | ..... | ..... | ..... | ..... | ..... | ..... | ..... |
| Subtotal | | 102.7 | 101.5 | 100.4 | 101.2 | 102.2 | 102.3 | | | | | | | |
| Loss O=S, F | | 2.8 | 2.5 | 1.4 | 1.7 | 3.7 | 2.1 | | | | | | | |
| Total | 100 | 100 | 99 | 99 | 100 | 99 | 100 | 99 | 100 | 100 | 100 | 99 | 99 | 100 |
| Specific gravity (lump) | 3.13 | 2.66 | 2.59–2.72 | 2.65–2.76 | ..... | ..... | ..... | 2.92 | 2.66 | 2.42 | 2.64 | 2.70 | 2.69 | 2.64 |
| **Semiquantitative spectrographic analyses (weight percent)** | | | | | | | | | | | | | | |
| Ag | 0.0007 | 0.001 | 0.003 | 0.0005 | 0.001 | 0.003 | 0.001 | 0.0003 | ..... | ..... | ..... | ..... | ..... | ..... |
| B | .001 | ..... | .0007 | ..... | ..... | ..... | ..... | ..... | 0.0015 | 0.002 | 0.0015 | 0.003 | 0.005 | ..... |
| Ba | .15 | .07 | .1 | .15 | .1 | .1 | .1 | .05 | .15 | .3 | .1 | .2 | .3 | ..... |
| Be | ..... | ..... | ..... | ..... | ..... | ..... | ..... | .00015 | ..... | ..... | ..... | ..... | ..... | ..... |
| Bi | .0015 | ..... | ..... | ..... | ..... | ..... | ..... | ..... | ..... | ..... | ..... | ..... | ..... | ..... |
| Cd | ..... | ..... | .007 | ..... | ..... | ..... | ..... | ..... | ..... | ..... | ..... | ..... | ..... | ..... |
| Co | .001 | .007 | .003 | .005 | .005 | .005 | .002 | .001 | .0007 | .001 | .0007 | .0005 | .001 | ..... |
| Cr | .003 | .002 | .0015 | .01 | .015 | .015 | .015 | .02 | .005 | .005 | .003 | .01 | .015 | ..... |
| Cu | .15 | .5 | .7 | .2 | .3 | 1.5 | .3 | .015 | .001 | .001 | .01 | .0003 | .0007 | ..... |
| La | ..... | ..... | ..... | ..... | ..... | .01 | .007 | ..... | ..... | ..... | ..... | ..... | ..... | ..... |
| Mo | ..... | .001 | .0007 | .002 | .015 | ..... | .015 | ..... | ..... | ..... | ..... | ..... | ..... | ..... |
| Nb | .001 | .0015 | .001 | .0015 | .002 | .002 | .002 | .0015 | .001 | .0015 | .0007 | ..... | .0007 | ..... |
| Ni | .002 | .005 | .005 | .01 | .007 | .02 | .003 | .015 | .0015 | .003 | .0015 | .002 | .005 | ..... |
| Pb | .0015 | ..... | ..... | .003 | .001 | .001 | .001 | ..... | .002 | .002 | .001 | .0007 | ..... | ..... |
| Sc | .0005 | .0007 | .0007 | .002 | .002 | .002 | .002 | .002 | .0007 | .0007 | .0007 | .0007 | .0015 | ..... |
| Sn | ..... | .001 | .0015 | .007 | .002 | .002 | .002 | .001 | ..... | ..... | ..... | ..... | ..... | ..... |
| Sr | .007 | .0015 | .002 | .01 | .015 | .02 | .02 | .03 | .01 | .005 | .01 | .1 | .07 | ..... |
| V | .005 | .007 | .01 | .02 | .05 | .05 | .05 | .03 | .005 | .01 | .003 | .01 | .02 | ..... |
| W | ..... | ..... | ..... | ..... | ..... | .02 | ..... | ..... | ..... | ..... | ..... | ..... | ..... | ..... |
| Y | .0015 | .002 | .003 | .003 | .003 | .003 | .003 | .005 | .0015 | .0015 | .002 | .0015 | .002 | ..... |
| Zn | .03 | .015 | .02 | .07 | ..... | ..... | ..... | .03 | ..... | ..... | ..... | ..... | ..... | ..... |
| Zr | .03 | .01 | .007 | .02 | .02 | .02 | .02 | .015 | .005 | .007 | .02 | .007 | .01 | ..... |
| Ga | .001 | .0007 | .0007 | .0015 | .001 | .001 | .001 | .0015 | .0007 | .001 | .0015 | .0007 | .0015 | ..... |
| Yb | .00015 | .0002 | .0002 | .0003 | .0003 | .0005 | .0003 | .0003 | .0001 | .00015 | .00015 | .00015 | .0002 | ..... |
| Ge | ..... | ..... | ..... | .002 | ..... | ..... | ..... | ..... | ..... | ..... | ..... | ..... | ..... | ..... |

Atomic absorption analyses (parts per million)

| | | | | | | | | | | | | | | |
|---|---|---|---|---|---|---|---|---|---|---|---|---|---|---|
| Au | 0.3 | 0.2 | 1.0 | 0.6 | 0.19 | 2.2 | 0.2 | ..... | ..... | ..... | ..... | ..... | ..... | ..... |
| Cu | 1,000 | 3,200 | 5,200 | 1,100 | ..... | ..... | ..... | ..... | ..... | ..... | ..... | ..... | ..... | ..... |
| Pb | 26 | 27 | 28 | 18 | ..... | ..... | ..... | ..... | ..... | ..... | ..... | ..... | ..... | ..... |
| Hg | ..... | ..... | ..... | ..... | .025 | .028 | .015 | ..... | ..... | ..... | ..... | ..... | ..... | ..... |
| Zn | 220 | 95 | 96 | 400 | 125 | 140 | 162 | ..... | ..... | ..... | ..... | ..... | ..... | ..... |

1. Biotite hornfels, Harmony Formation, Copper Canyon east ore body, north end of 6450 bench, SW¼ sec. 22, T. 31 N., R. 43 E.
2. Metaconglomerate, from lower member of Battle Formation, east ore body, north end of 6450 bench, SW¼ sec. 22, T. 31 N., R. 43 E.
3. Metaconglomerate, from lower member of Battle Formation, east ore body, middle of 6550 bench, SW¼ sec. 22, T. 31 N., R. 43 E.
4. Metaconglomerate, from lower member of Battle Formation, east ore body, northeast corner of 6450 bench, SW¼ sec. 22, T. 31 N., R. 43 E.
5. Metashale, from lower member of Battle Formation, east ore body,6600 bench, SW¼ sec. 22, T. 31 N., R. 43 E.
6. Same as 5.
7. Same as 5.
8. Hornfelsic shale, from middle member Battle Formation, 300 m north of east ore body, NW¼ sec. 22, T. 31 N., R. 43 E.
9. Hematitic conglomerate, from lower member of Battle Formation, 1,800 m north of east ore body, SW¼ sec. 15, T. 31 N., R. 43 E.
10. Hematitic conglomerate, from lower member of Battle Formation, 1,500 m north of east ore body, SW¼ sec. 15, T. 31 N., R. 43 E.
11. Arkosic sandstone, from Harmony Formation, 1,200 m north of east ore body, SW¼ sec. 15, T. 31 N., R. 43 E.
12. Calcareous shale, from middle member of Battle Formation, 750 m north of east ore body, NW¼ sec. 22, T. 31 N., R. 43 E.
13. Same as 12.
14. Feldspathic sandstone, from Harmony Formation, 1,200 m north of east ore body, SW¼ sec. 15, T. 31 N., R. 43 E.

may not be statistically representative of the gains in much larger volumes of rock. Regardless, metamorphism of this $MgCO_3$ member yielded magnesium silicates.

## COMPOSITION OF HYDROTHERMAL BIOTITE

Analyses of three rocks (5–7, table 9) with abundant hydrothermal biotite (fig. 26*B*) from the east ore body suggest that the biotite is magnesian. MgO makes up 6.0, 4.4, and 6.0 weight percent of these rocks. Modal estimates of biotite in the rocks range from 25 to 35 percent by volume. The only other probable Mg-bearing minerals in the rock are white mica that may be phengitic (some Mg possibly substituting for octahedral Al (Deer and others, 1962)), and hydrothermal chlorite that occurs in only trace amounts in the rocks. The MgO contents seem to be compatible with our estimates of modal biotite. If we assume about a 2.8 value for the $Mg:Fe^{+2}$ cationic ratio in the biotite, we then calculate Barth's (1962) mesonorm from these analyses to contain 18–23 percent normative biotite. Nevertheless, because of the many uncertainties involved, estimates of the MgO:FeO ratio in the hydrothermal biotites are meaningless from these data. The iron-bearing minerals in the rocks include pyrite, chalcopyrite, biotite, epidote, hematite, marcasite-pyrite, and traces of pyrrhotite. Magnesian biotites in other porphyry-type metal deposits seem to be fairly common (Schwartz, 1953; Anderson and others, 1955; Mauger, 1964; Meyer, 1965; Fournier, 1967; Moore and Czamanske, 1973).

## DISTRIBUTION OF ECONOMIC METALS IN THE 6450 BENCH

### COPPER

Distribution of copper in typical ore zones of the east ore body shows the importance of reactive rock for the development of an ore body (fig. 16). These contours are based on the determination of copper in over 400 blast holes. A broad area of high copper concentrations (greater than 1 percent) occurs in rocks of the Battle Formation in the central part of the bench. Although part of this copper-rich area coincides with the mapped extent of one of the calc-silicate altered conglomerate units (compare figs. 15 and 16), significant amounts of copper here are in siliceous conglomerate. The distribution of copper content reflects structure to a large extent. Lobate extensions of high copper content coincide with prominent northeast- and east-northeast-striking faults. These extensions reflect primary chalcopyrite, secondary chalcocite, chrysocolla, copper oxide, and malachite in and adjacent to faults. The northwest-trending bifurcating zone with copper contents greater than 1 percent in the Battle

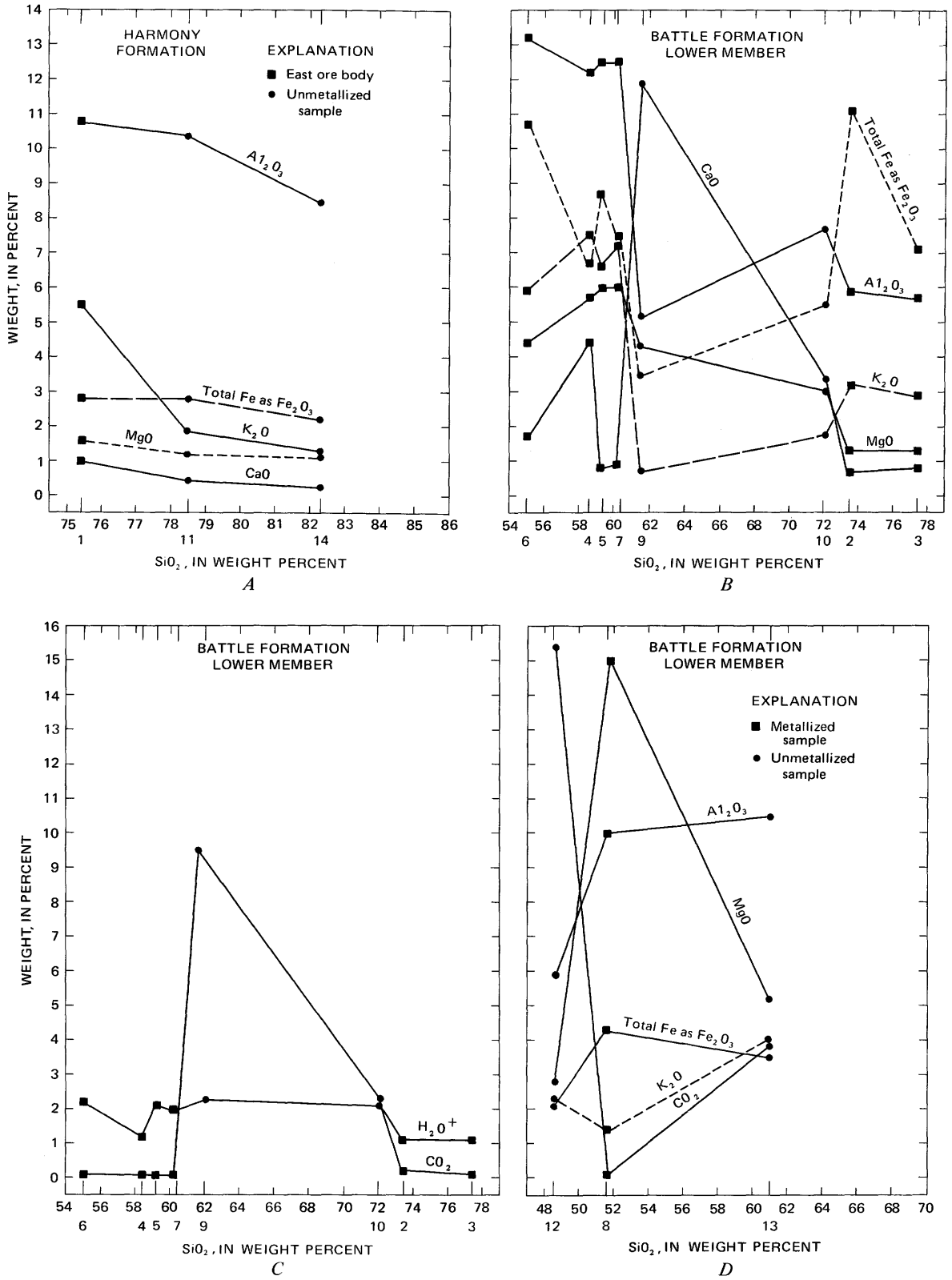


FIGURE 37.—Variation diagrams comparing chemically analyzed altered and unaltered rocks (table 9) from the Battle and Harmony Formations in and near the Copper Canyon east ore body. Sample numbers same as table 9.

Formation across the south-central part of the bench is not directly attributable to northwest-striking structures. Some of this zone, however, reflects copper along northeast-striking faults and fractures. Two other isolated copper highs are on a northerly strike with the termination of this zone, and all three are parallel to, but not coincident with, the uppermost calc-silicate unit shown in the Battle (figs. 15–16). These high copper grades may have resulted either from replacement of a favorable horizon in the Battle or from a local structure that was entirely between mapped faces on the bench.

Another marked change in copper content is noted on crossing the unconformity into the Harmony. In the center of the bench, where the unconformity has not been intensely disturbed by later faults, copper contents decrease sharply from more than 0.75 percent in the Battle Formation to less than 0.25 percent in the Harmony Formation in a distance of about 15 m. Although this is a sharp drop, relatively high quantities of copper persist for about 15 m in rocks of the Harmony Formation. This persistence of copper is generally parallel to the unconformity, which is also approximately parallel to bedding in both formations.

The unconformity may have controlled deposition of some copper. In the northern part of the bench, a lobe of $>0.50$ percent copper extends along the trace of the unconformity. The pyrrhotite zone itself generally has relatively low total copper contents, primarily because much of this zone, as mapped, is underlain by rocks of the Harmony Formation. The lower copper content of the pyrrhotite zone is considered to reflect permeability rather than the different geochemistry of the zone.

Across the entire southern 45 m of the bench, which is made up almost entirely of rocks from the Battle, the copper content is generally less than 0.50 percent, which perhaps reflects chemically less favorable or more impermeable rock. In the southeastern part of the bench, copper contents in a small area of the Harmony are greater than 1 percent, a result of local chalcocite enrichment.

### GOLD

The distribution of gold on the 6450 bench, shown on figure 17, is very similar to that of copper. Again, gold favors the Battle Formation, but within the Battle itself, the distribution of gold is more spotty and discontinuous than the distribution of copper. There are several small areas in the Harmony Formation that have gold concentrations greater than 0.10 ounces per ton (3.5 ppm). Many areas with high gold concentrations are not obviously associated spatially with faults. However, several areas of high gold concentrations coincide with steeply dipping normal faults, and others coincide with the shallow-dipping unconformity (fig. 17). Three of these areas are along mapped minor fault zones that do not have any pronounced lateral extent, but one in the east-central part of the bench is a strong north-south elongate high that does not coincide with any mapped structures; in fact, it is at right angles to faults there. This gold zone in the Harmony is important because it has no copper equivalent. It may reflect concentrations of gold localized along structures in between mapped faces. The broad area of high gold concentrations in the north-central part of the bench is partly coincident with the lowermost calc-silicate conglomerate unit in the Battle, which may reflect some chemical controls on the deposition of gold. Gold contents in the pyrrhotite zone on this bench generally are very low, as they are across approximately the southernmost 35–60 m of the bench where the rocks consist primarily of pyritized Battle.

The strongest associations of gold are noted in individual hand specimens, which show that pyrrhotite, arsenopyrite, and chalcopyrite generally accompany gold. This conclusion is based on analyses of whole-rock grab samples. However, examination of petrographic relations and jig concentrates suggest that gold is chiefly a late mineral in this deposit. Finally, the instances of dissimilar distribution of copper and gold (figs. 16, 17) further suggest that most gold was introduced late and separate from copper.

### SILVER

Silver in the bench may follow copper more closely than does gold (figs. 16–18). Its distribution pattern resembles that of copper more than it does gold, especially in the northern half of the bench. Yet sporadic high silver concentrations occur along a few of the same faults that contain large quantities of both copper and gold. The unique distribution pattern of silver becomes readily apparent in the southern part of the bench. A broad area of relatively high silver concentrations occurs in the southern part of the bench where gold and silver are notably low. Although one 30-m-wide area here spatially coincides with similar high concentrations of copper and gold, this area of high silver concentrations is distinctive by its failure to persist to the north. The concentration may be the result of local secondary silver minerals plus native silver enrichment in oxidized material near a northeast-southwest fault. We have not yet determined the specific sulfide occurrences of silver in the primary ores. In the pyrrhotite zone, silver concentrations are generally low. Preliminary chemical analyses of different

sulfide mineral separates suggest that most sulfides contain small amounts of silver. Roberts and Arnold (1965, p. B18) found sparse concentrations of tetrahedrite (which commonly contains notable amounts of silver) and argentiferous galena in the Copper Canyon underground mine.

## OTHER MINOR-ELEMENT VARIATIONS

Forty-three composite rock samples were collected for minor-element variation studies in the east ore body. The concentrations of As, Mg, Mo, Ni, W, Zn, Ba, Co, and Bi in these 1-kg rock samples, collected along the traverse line A–B (fig. 16), are presented as a variation diagram or geochemical profile (fig. 38). There is probably no uniform gradient in trace element concentration between analyzed samples. The content of Au, Hg, Cd, Cr, Cu, La, Pb, V, and Zr in these 43 samples is shown in table 10.

TABLE 10.—*Analyses of rock samples from the 6450 bench, Copper Canyon east ore body*

[Reported in parts per million. Analysts: Au, R. F. Hansen; Hg, R. J. Smith. Semiquantitative spectrographic analyses by J. Motooka; results are reported to the nearest number in the series 1, 0.7, 0.5, 0.3, 0.2, and 0.15, and so on, which represent approximate midpoints of interval data on a geometric scale. Field numbers here correspond to numbered stations in fig. 38. B, Battle Formation; Bx, fault breccia; H, Harmony Formation]

| Field No. | Rock type | Chemical analyses | | Semiquantitative spectrographic analyses | | | | | | |
|---|---|---|---|---|---|---|---|---|---|---|
| | | Au | Hg | Cd | Cr | Cu | La | Pb | V | Zr |
| AJA-639 | B | 0.08 | 1.2 | <20 | 5 | 150 | <20 | <10 | <10 | 150 |
| 640 | B | .6 | 2.6 | <20 | 50 | 5,000 | <20 | 30 | 50 | 150 |
| 641 | Bx | .04 | 1.4 | <20 | 100 | 1,000 | <20 | <10 | <10 | <10 |
| 642 | B | .2 | .8 | <20 | 15 | 2,000 | <20 | <10 | 50 | 70 |
| 643 | Bx | 2.0 | >10 | 500 | 70 | 3,000 | <20 | 30 | <10 | 10 |
| 644 | Bx | 7.8 | 7 | <20 | 10 | 700 | 20 | 2,000 | <10 | 10 |
| 645 | B | .1 | 1.5 | <20 | 30 | 2,000 | 50 | <10 | 15 | 200 |
| 646 | Bx | .3 | .5 | 200 | 70 | 3,000 | 200 | <10 | 70 | 150 |
| 647 | B | .8 | 1 | <20 | 30 | 5,000 | 100 | 10 | 50 | 100 |
| 648 | B | 4.4 | 1.2 | <20 | 20 | >20,000 | 700 | 50 | 70 | 100 |
| 649 | B | .5 | 1.2 | <20 | 50 | 3,000 | 100 | <10 | 30 | 100 |
| 650 | B | .2 | .3 | <20 | 30 | 3,000 | <20 | <10 | 15 | 100 |
| 652 | H | .1 | .5 | <20 | 70 | 700 | 20 | <10 | 20 | 200 |
| 653 | H | .04 | .28 | <20 | 70 | 200 | 20 | <10 | 15 | 300 |
| 654 | Bx | 1.3 | >10 | 30 | 200 | 5,000 | 70 | 1,500 | 50 | 50 |
| 655 | H | .4 | .55 | <20 | 100 | 5,000 | 50 | <10 | 30 | 200 |
| 656 | H | .2 | .22 | <20 | 30 | 1,000 | 50 | 70 | 20 | 300 |
| 657 | Bx | .1 | .35 | <20 | 50 | 300 | <20 | <10 | 10 | 200 |
| 613 | H | .1 | .4 | <20 | 200 | 500 | 70 | <10 | 300 | 100 |
| 614 | H | .1 | .65 | <20 | 200 | 1,000 | 70 | <10 | 300 | 150 |
| 615 | Bx | .02 | .7 | <20 | 200 | 150 | 150 | <10 | 300 | 20 |
| 616 | H | .2 | .7 | <20 | 100 | 1,000 | 70 | <10 | 300 | 100 |
| 617 | H | .1 | .5 | <20 | 100 | 1,000 | 30 | <10 | 200 | 150 |
| 618 | H | .08 | .4 | <20 | 70 | 1,000 | 50 | <10 | 150 | 200 |
| 619 | H | .08 | .45 | <20 | 70 | 200 | 50 | <10 | 200 | 70 |
| 620 | H | .1 | .3 | <20 | 150 | 1,000 | 100 | <10 | 300 | 150 |
| 621 | H | .1 | .4 | <20 | 70 | 1,000 | 50 | <10 | 150 | 300 |
| 622 | H | .1 | .65 | <20 | 150 | 500 | 30 | <10 | 300 | 100 |
| 623 | H | .3 | .2 | <20 | 50 | 5,000 | 50 | <10 | 100 | 300 |
| 624 | H | .04 | .4 | <20 | 50 | 500 | 50 | 10 | 100 | 500 |
| 625 | H | .2 | >10 | 100 | 150 | 2,000 | 30 | 100 | 300 | 150 |
| 626 | H | .2 | 2.4 | <20 | 200 | 3,000 | 70 | 20 | 300 | 100 |
| 627 | H | .5 | .45 | <20 | 30 | 7,000 | 100 | 10 | 70 | 100 |
| 628 | H | 1.7 | .55 | <20 | 70 | >20,000 | <20 | <10 | 200 | 300 |
| 638 | B | 1.7 | 3 | <20 | 70 | 7,000 | <20 | <10 | 100 | 100 |
| 637 | Bx | 2.3 | 5 | 150 | 500 | >20,000 | 30 | 150 | 300 | 100 |
| 636 | B | .5 | >10 | 300 | 50 | 7,000 | 30 | <10 | 70 | 150 |
| 635 | Bx | .2 | >10 | <20 | 200 | 20,000 | 50 | 100 | 70 | 50 |
| 633 | B | 1.1 | .4 | <20 | 30 | 20,000 | <20 | 50 | 70 | 100 |
| 632 | B | .3 | .4 | <20 | 50 | 5,000 | 30 | <10 | 150 | 150 |
| 631 | Bx | .1 | .35 | <20 | 20 | 7,000 | <20 | <10 | 100 | 70 |
| 630 | B | .5 | .3 | <20 | 50 | 7,000 | <20 | <10 | 100 | 150 |
| 629 | B | 1.3 | .45 | <20 | 50 | 20,000 | 30 | <10 | 150 | 150 |

Minor element variations within the east ore body are not very striking. We found no strong systematic contrast in trace element content between the rocks of the pyrrhotite zone and the adjoining pyrite-rich rocks, although cobalt possibly may have a slightly higher concentration in the pyrite zone (fig. 38). Trace element concentrations generally differ only slightly between the rocks of the Harmony Formation and those of the Battle. Within the Battle, however, trace element concentrations seem to vary more than in the Harmony, which might be anticipated in conglomerate lithologies. Keeping in mind the above discussion, we can still make some generalizations. Manganese appears to be more uniformly distributed and has slightly higher concentrations in the rocks of the Harmony Formation than in the Battle Formation, possibly reflecting original differences in depositional environment. More samples of the Battle Formation contain detectable tungsten than the Harmony, but at very low concentrations. All tungsten analyses indicate concentrations of less than 200 ppm (fig. 38). Sporadic molybdenum concentrations of 20–50 ppm were detected in a few samples from the Battle Formation, whereas its highest concentration detected in the Harmony is 10 ppm. Most of it undoubtedly occurs as molybdenite in quartz veinlets. Copper and gold concentrations along the traverse (table 10) support generalizations deduced from their distributions in the entire bench (figs. 16, 17). Generally, the copper and gold contents of the Battle along the geochemical traverse are higher than that of the Harmony. Mercury concentrations also are high in the Battle (table 10). Chromium and vanadium concentrations are slightly high along the southern two-thirds of the traverse, and quantities of lanthanum and zirconium are fairly uniform in all samples along the traverse (table 10). Chromium in some breccia samples is somewhat higher than others, possibly indicating some concentrations in supergene clays. The high vanadium concentrations, primarily in the Harmony, also may reflect concentrations in supergene clays associated with chalcocite enrichment. The fact that zirconium is low along the fault breccias seems to confirm that most of this element is in detrital zircons and that it is not introduced.

Trace element concentrations in many unconsolidated fault breccias differ markedly from concentrations of the same elements in nearby unshattered rocks. The highest gold content detected, 7.8 ppm, in the rocks sampled along the geochemical traverse occurs in a fault breccia at the north end of the bench (AJA 644, table 10). Mercury in this sample also is high (7 ppm) and five of the 10 fault breccias sampled along the traverse yielded mercury values of 5 ppm or

greater. Arsenic contents are greater than 1,000 ppm in seven of 10 sampled fault breccia zones (fig. 38). Similarly, large quantities of zinc and to a lesser extent cadmium (sphalerite) occur along many of these same fault zones (table 10). There are, however, some zinc concentrations greater than 500 ppm in coherent rocks of the Harmony. Nickel concentrations between 150 and 300 ppm occur along four of the 10 fault breccia zones compared to contents ranging from 20 to 50 ppm in the less fractured rocks. Only two samples from the fault zones have bismuth contents of 200 ppm or greater, possibly reflecting some galena. Cobalt contents seem slightly higher along two faults, while the other fault breccia zones have very low cobalt concentrations. Barium and manganese concentrations in the faults generally are lower than in the surrounding rocks, suggesting that they are original constituents of the sedimentary rocks and not introduced.

These trace element geochemical studies indicate the low concentrations of many economically important metals in the east ore body as contrasted with other porphyry coppers. Molybdenum (molybdenite) is very low; lead-bismuth (galena), zinc-cadmium (sphalerite), and tungsten (scheelite?) are also low when compared with other replacement deposits in a similar geologic environment. Concentrations of many of these elements were large in the Copper Canyon underground mine.

## GEOCHEMISTRY OF GOLD

If gold and copper were introduced together into a deposit, concentrations of certain trace elements in gold should be high, especially copper. To test this, flakes of native lode gold were hand picked from pyrite and pyrrhotite jig concentrates from the Battle Formation in the east ore body. Some of these flakes were attached to clear quartz crystals that are common throughout the east ore body as a very late, vug-filling stage. Custom six-step spectrographic analyses of these gold flakes reveal that their silver contents range from 34,000 to 160,000 ppm (table 11). Copper, at detection levels ranging from about 10 to 100 ppm, was not found in any of the lode gold. These proportions may indicate that gold occupies a discrete late pulse, separate from copper, during the metallogenesis of the deposit, as we concluded from its textural relations and from its distribution in the ore zones. However, the coatings on the gold samples do contain some copper, as well as traces of many other elements (table 11). Mercury was detected at a less than 0.1 percent level of determination in only one of the 15 samples, an anomalously low mercury content for gold compared to similar studies elsewhere (A. L. Sutton, Jr., oral commun., 1970). Bismuth content is high in the gold; up to 2,000 ppm bismuth were found in the samples. The most lead detected is 20 ppm, which suggests that bismuth must occur in the gold in a form other than minor element concentrations in galena. Most of the lead in the gold probably occurs as minute grains of entrapped galena, a relation similar to that found in placer gold at Iron Canyon (Theodore and Roberts, 1971). As a comparison, trace elements in a 10.07 mg fraction of a larger gold nugget, collected from the Dahl Placer at the mouth of Copper Canyon, include Fe, Ag, Bi, Cu, Pb, and Pd (table 11). These elements, with the exception of copper, are compatible with those found in lode gold from the east ore body.

The platinoid element palladium was found at a 10-ppm concentration in one of the 15 lode gold samples analyzed; it was also found in the placer gold, but at a 100-ppm concentration. Palladium, in the lode gold, was detected in a gold flake that contains 36,000 ppm silver, a relatively low silver content for these samples. This flake also contains 30 ppm molybdenum. Elsewhere, platinum metals are a fairly common byproduct from the California gold placers (Mertie, 1969). Gold in the Copper Canyon porphyry copper deposit as described above is apparently a late mineral in the paragenetic sequence. However, platinum metal (Ir, Os, Pd, Pt, Rh, and Ru) deposits are typically associated spatially and genetically with basic or ultrabasic rocks (Goldschmidt, 1937; Wright and Fleischer, 1965; Mertie, 1969); platinum also has been found in quartz-sulfide veins (Knopf, 1915). The palladium-bearing gold flake from the east ore body may have been included in chalcopyrite, pyrrhotite, or arsenopyrite—minerals all known elsewhere as sites of platinum metal deposition (Hawley and others, 1951; Hawley and Rimsaite, 1953; Keays and Crocket, 1970).

Forty-two pyrite, pyrrhotite, and chalcopyrite concentrates from the ore bodies at Copper Canyon were tested for palladium, platinum, and rhodium. Only sparse amounts of palladium, 0.004–0.020 ppm, were found in four of the 42 samples (L. B. Riley, written commun., 1971). Three of the four samples contain greater than 15 ppm gold. We accordingly infer that platinoids in the deposit are most likely restricted to gold and that they are not likely to occur in economically significant amounts elsewhere in the deposit.

## AGE OF METALLIZATION

M. L. Silberman determined by the K-Ar whole-rock method that the age of metallization in the east ore body is $37.2_0 \pm 0.0_6$ m.y., that is, late Eocene or early Oligocene (Theodore and others, 1973). This value is the average of one determination on each of two sepa-

rate metallized samples of the Battle from the 6500 bench that contain abundant hydrothermal K-feldspar, biotite, and quartz together with lesser amounts of disseminated chalcopyrite and pyrite. We recognize a problem, however, in the genetic validity of a comparison between ages from the east ore body and those from primary biotites in the intrusion at Copper Canyon because of differences in grain sizes of the materials dated (Theodore and others, 1973). K-Ar ages indicate a 1-m.y. difference between primary biotites in the altered granodiorite of Copper Canyon ($38.2_2 \pm 0.0_5$) and hydrothermal biotite–K-feldspar assemblages in the east ore body ($37.2_0 \pm 0.0_6$). However, the dated hydrothermal assemblages are much finer grained than the primary biotites and thus may have become closed to statistically significant argon losses at temperatures lower than the pluton's biotites. For the Bingham, Utah, porphyry copper deposit, Moore and Lanphere (1971) determined at least a 3-m.y. duration for the metallization process. Figure 39 is a histogram comparing the age of metallization at Copper Canyon to other porphyry copper deposits in the Great Basin. Metallization at the Yerington deposit, however, may be Early to Middle Jurassic (E. H. McKee, oral commun., 1972).

## ENVIRONMENT OF ORE DEPOSITION

The geologic setting and many physical and chemical parameters jointly contribute to the development of any ore deposit. For an ore body, it is difficult to identify those processes, let alone arrive at a qualitative estimate of the relative contributions of each, and the deposit at Copper Canyon is no exception. As many authors have discussed previously, localization of ore may be considered at several different scales. Primarily because of the limited areal scope of our investigation, we will focus on the major physicochemical processes that we believe contributed to the development of these particular deposits.

Chalcopyrite is the predominant ore mineral, with chalcopyrite-pyrrhotite, chalcopyrite-pyrite-pyrrhotite, chalcopyrite-pyrite, chalcopyrite-pyrite-marcasite, and chalcopyrite-pyrite-arsenopyrite assemblages being most common in the east ore body. At Copper Canyon, hypogene copper metallization is associated with a potassic alteration facies. The silicate gangue minerals in the ore zones include abundant K-feldspar, biotite, and white mica. Copper mineralization associated with potassic alteration assemblages also occurs in most of the Arizona porphyry copper deposits, including the ones at Ajo, Bagdad, Pima, Ray, and San Manuel (Creasey, 1966; Himes, 1972) and many others elsewhere. However, only in a few deposits is hypogene ore found predominantly in intruded altered sedimentary rocks. An intriguing feature of the Copper Canyon deposit is the occurrence of pyrrhotite-bearing copper ores with the potassic facies. Pyrrhotite has not been reported from any of the above five Arizona deposits. Meyer and Hemley (1967) fur-

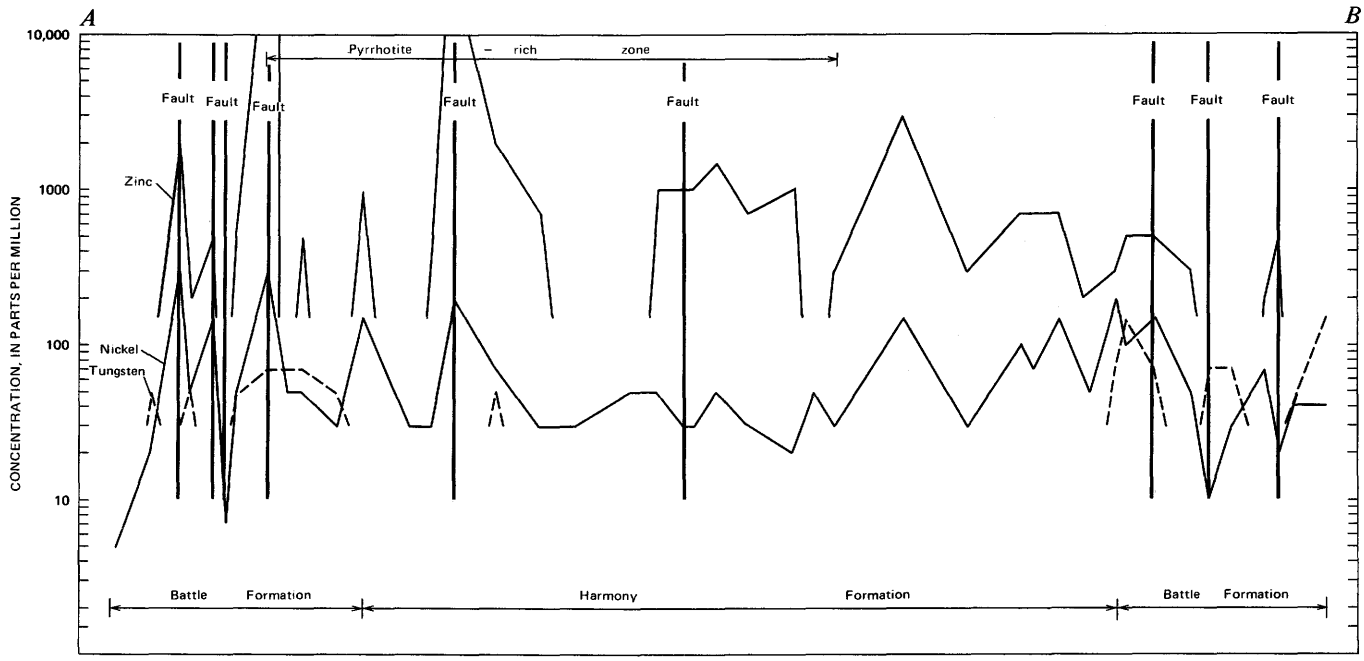


FIGURE 38.—Variations of As, Mn, Mo, Ni, W, Zn, Ba, Co, and Bi concentrations

ther state that potassic assemblages associated with pyrrhotite generally have not been reported in porphyry copper deposits.

Although we need to know more about the fluids to say something definite about their source, we nevertheless do have at Copper Canyon several chemical changes in the rocks that reflect an overall reaction of the general type,

$$\text{Rock}_{\text{initial}} + \text{solution}_{\text{initial}} \rightleftarrows \text{rock}_{\text{final}} + \text{solution}_{\text{final}}.$$

These chemical changes, together with the fluid-inclusion data gathered by Nash (Nash and Theodore, 1971) allow us to set certain limits, both physical and chemical, on the ore-forming fluids as they first arrived and subsequently circulated at the general level of the ore bodies and the granodiorite. This discussion will focus primarily on the east ore body.

## DEPTH OF METALLIZATION

Depth of metallization at Copper Canyon may be determined by (1) geologic reconstruction of the rocks

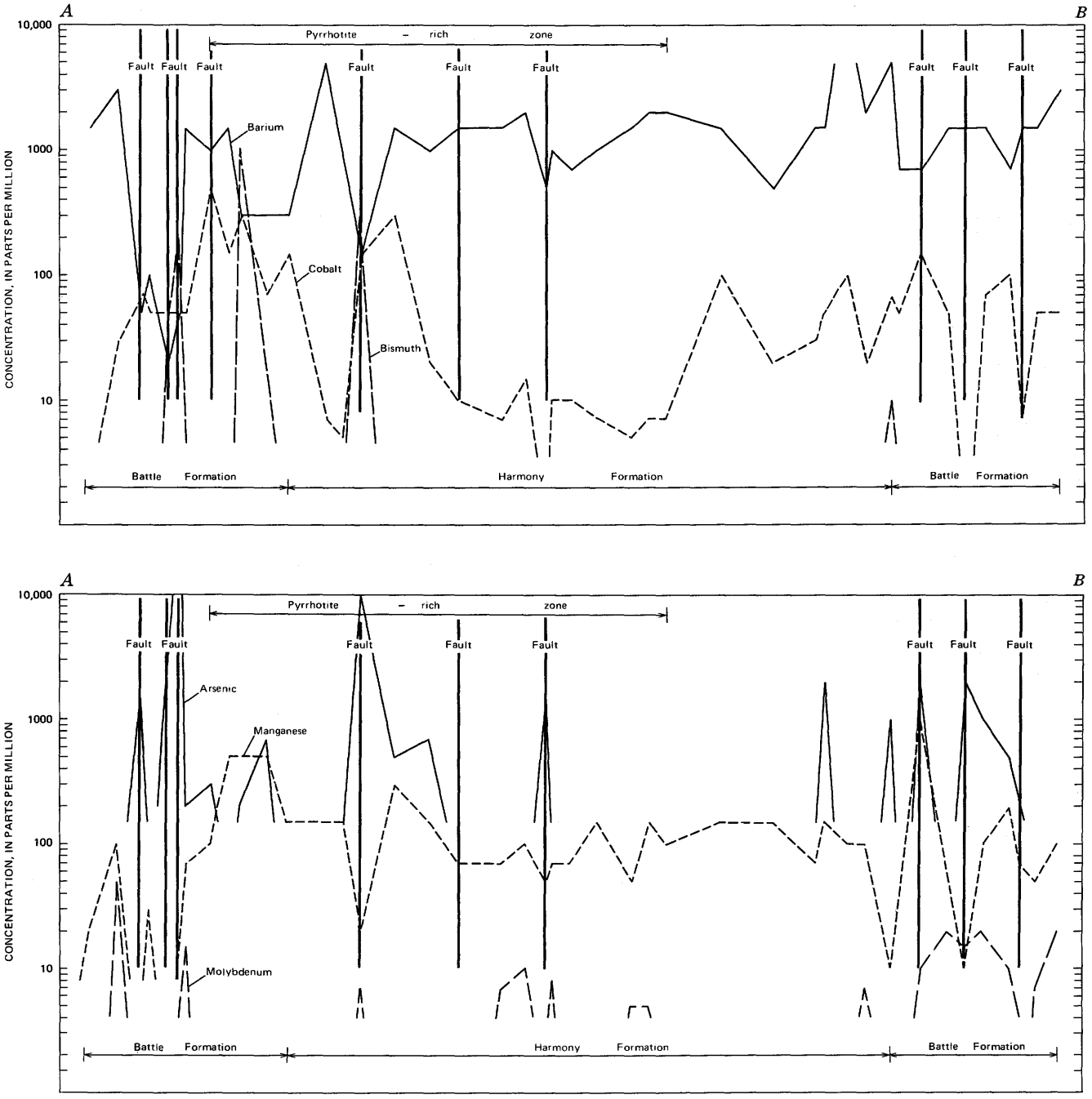


along the traverse line *A–B* (fig. 16) on the 6450 bench, east ore body.

TABLE 11.—*Custom six-step spectrographic analyses of lode and placer gold samples from Copper Canyon and qualitative spectrographic analysis of gold coatings*

[Analyst: A. L. Sutton, Jr.; N, not detected, at limit of detection or at value shown; L, detected but below value shown; G, greater than value shown. Approximate detection limits (0.10 mg samples): Hg, 0.1 percent; As, 0.05 percent; Te, 0.2 percent]

**Lode gold[1]**

| Field No. | Weight (mg) | Percent | | Parts per million | | | | | | | |
|---|---|---|---|---|---|---|---|---|---|---|---|
| | | Fe | Ti | Ag[2] | Ba | Bi | Co | Mo | Pb | Pd | Hg |
| TT–Au–1– 1 | 5.20 | 0.07 | 0.003 | 75,000 | L20 | 700 | N | N | 20 | N | ..... |
| 2 | 3.75 | .03 | N | 94,000 | L30 | 1,000 | N | 10 | N | N | ..... |
| 3 | 4.56 | .03 | .002 | 45,000 | L20 | 2,000 | N | 7 | N | N | ..... |
| 4 | 4.56 | .01 | N | 85,000 | L20 | 300 | N | N | L | N | ..... |
| 5 | 7.07 | .007 | N | 110,000 | L15 | 700 | N | N | 20 | N | ..... |
| TT–Au–2– 1 | 4.08 | L.01 | .002 | 66,000 | L20 | 30 | N | N | N | N | ..... |
| 2 | 4.20 | L.01 | N | 89,000 | L20 | 20 | N | N | N | N | ..... |
| 3 | 2.99 | L.015 | N | 60,000 | L30 | L15 | N | N | N | N | ..... |
| 4 | 4.79 | L.01 | N | 36,000 | L20 | N | N | 30 | N | 10 | ..... |
| 5 | 4.38 | L.01 | N | 34,000 | L20 | N | 30 | N | N | N | ..... |
| TT–Au–3– 1 | .46 | L.1 | N | 160,000 | L200 | N | N | N | N | N | ..... |
| 2 | .96 | L.005 | N | 85,000 | L100 | N | N | N | N | N | ..... |
| 3 | 1.66 | L.03 | N | 89,000 | L70 | 100 | N | N | N | N | ..... |
| 4 | 1.01 | L.05 | N | 83,000 | L100 | N | N | N | N | N | ..... |
| 5 | 1.36 | L.03 | N | 100,000 | L70 | 500 | N | N | N | N | ..... |
| TT–Au–1– 6 | 5.70 | ..... | ..... | ..... | ..... | ..... | ..... | ..... | ..... | ..... | N |
| 7 | 8.48 | ..... | ..... | ..... | ..... | ..... | ..... | ..... | ..... | ..... | N |
| 8 | 12.8 | ..... | ..... | ..... | ..... | ..... | ..... | ..... | ..... | ..... | L |
| 9 | 7.90 | ..... | ..... | ..... | ..... | ..... | ..... | ..... | ..... | ..... | N |
| 10 | 9.49 | ..... | ..... | ..... | ..... | ..... | ..... | ..... | ..... | ..... | N |
| TT–Au–2– 6 | 4.08 | ..... | ..... | ..... | ..... | ..... | ..... | ..... | ..... | ..... | N |
| 7 | 2.78 | ..... | ..... | ..... | ..... | ..... | ..... | ..... | ..... | ..... | N |
| 8 | 2.60 | ..... | ..... | ..... | ..... | ..... | ..... | ..... | ..... | ..... | N |
| 9 | 2.94 | ..... | ..... | ..... | ..... | ..... | ..... | ..... | ..... | ..... | N |
| 10 | 2.02 | ..... | ..... | ..... | ..... | ..... | ..... | ..... | ..... | ..... | N |
| TT–Au–3– 6 | 2.38 | ..... | ..... | ..... | ..... | ..... | ..... | ..... | ..... | ..... | N |
| 7 | 1.43 | ..... | ..... | ..... | ..... | ..... | ..... | ..... | ..... | ..... | N |
| 8 | 1.26 | ..... | ..... | ..... | ..... | ..... | ..... | ..... | ..... | ..... | N |
| 9 | 1.10 | ..... | ..... | ..... | ..... | ..... | ..... | ..... | ..... | ..... | N |
| 10 | 1.38 | ..... | ..... | ..... | ..... | ..... | ..... | ..... | ..... | ..... | N |

**Lode gold coatings[3]**

| Field No. | Percent | | | | Parts per million | | | | | | | | | | |
|---|---|---|---|---|---|---|---|---|---|---|---|---|---|---|---|
| | Fe | Ca | Na | Ti | Mn | Ag | Au | Ba | Bi | Cr | Cu | Ni | Pb | Sn | Yb |
| TT–Au–1 | 0.05 | 0.003 | 0.1 | 0.007 | 2 | 20 | 5,000 | 20 | 300 | 20 | 500 | 20 | 10 | L | N20 |
| 2 | .05 | .01 | .1 | .01 | 30 | 20 | 5,000 | 15 | 10 | 30 | 150 | 20 | 7 | N | N20 |
| 3 | .015 | .002 | .1 | .01 | 1 | 20 | 2,000 | 5 | 15 | 20 | 100 | 20 | N | N | N20 |

**Placer gold[4]**

| Field No. | Weight (mg) | Percent | Parts per million | | | | |
|---|---|---|---|---|---|---|---|
| | | Fe | Ag | Bi | Cu | Pb | Pd |
| AFB–358 | 10.07 | 0.005 | G10,000 | 300 | 200 | 20 | 100 |

[1]The above results are reported to two significant figures and have an overall accuracy of ±15 percent except that they are less accurate near limits of detection, where only one digit is intended. Looked for but not found: Mn, As, B, Be, Cd, Cr, Cu, Ga, Ir, La, Nb, Ni, Os, Pt, Rh, Ru, Sc, Sn, Te, V, Y, Yb, Zn, Zr.

[2]Ag values are quantitative.

[3]The above figures are the results of qualitative spectrographic analyses of the coatings removed from gold nuggets, and are expressed as the relationship of every element found to each of all other elements found. The figures are not to be construed as actual values. The figures of any one sample bear no relationship to those of any other sample. Looked for, but not found: Al, P, Mg, K, As, Be, Cd, Ce, Co, Ga, Hf, In, Ir, La, Li, Mo, Nb, Os, Pd, Pt, Re, Rh, Ru, Sb, Sr, Ta, Th, Tl, U, V, W, Y, Zn, Zr.

[4]Looked for, but not found: Mn, Ba, Be, Cd, Co, Cr, La, Mo, Nb, Ni, Pt, Sb, Sc, V, Y, Zn, Zr, Ga, In, Yb, Ir, Rh, Ru.

overlying the Golconda thrust and granodiorite at the time of metallization, (2) the FeS content of sphalerites, and (3) fluid inclusion barometric considerations. Vertical extent of economic metallization at Copper Canyon from the 700 level of the Copper Canyon underground mine to the east ore body of Duval's porphyry copper deposit is slightly over 300 m. Geologic reconstruction suggests about 1,500 m over the thrust and intrusion when it was emplaced as we described above. This depth is equivalent to about 375 bars lithostatic or 140 bars hydrostatic pressure. Ore horizons in the west ore body are situated within about 100 m of the sole of the Golconda plate, just north of the granodiorite. Metallization in the east ore body belongs structurally below the thrust but presently occurs in general about 250–300 m topographically higher than the thrust's position below the west ore body. The FeS content of sphalerites determined by

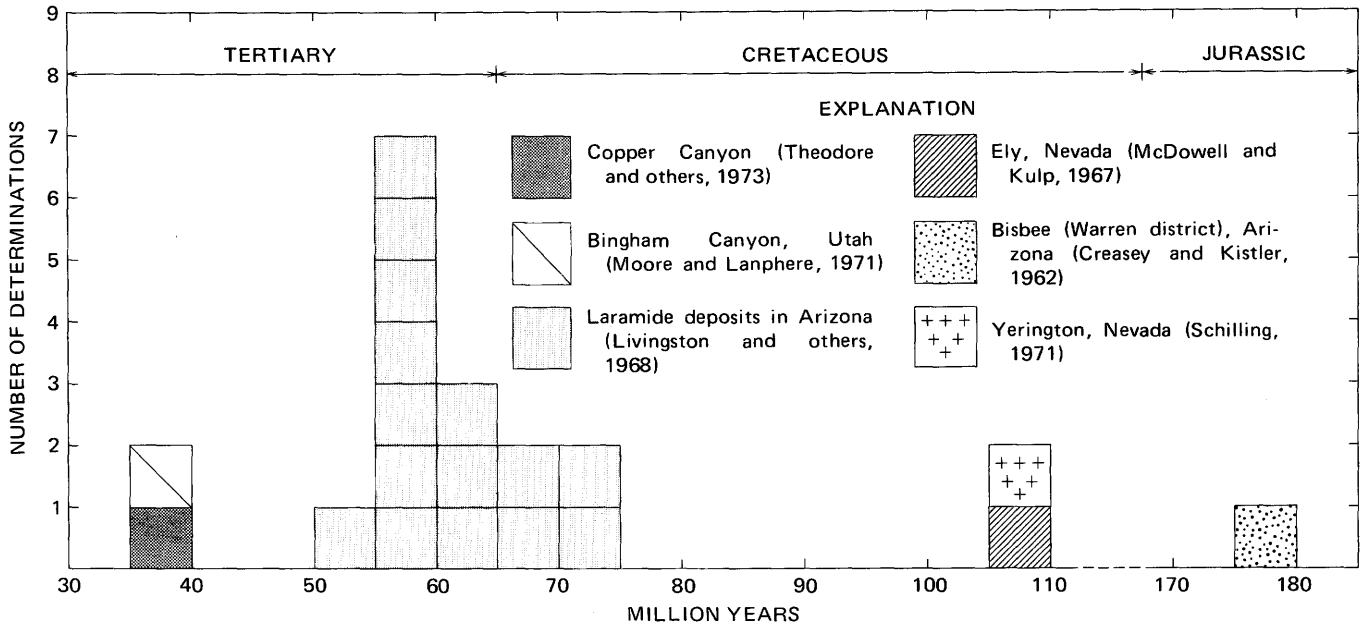


FIGURE 39.—Histogram of radiometrically age-dated porphyry copper deposits or associated plutons in the Great Basin.

electron microprobe by J. Thomas Nash (unpub. data) suggests pressures for the east ore body in the range 250–1,000 bars. (See also Scott and Barnes, 1971.) Fluid inclusion considerations suggest pressures of about 250±100 bars, more than likely reflecting a combined hydrostatic-lithostatic load (Nash and Theodore, 1971). Earlier, the porphyritic texture of the intrusion at Copper Canyon suggested to Clement (1964) that it crystallized at "shallow" depths.

Our depth estimates for the development of the ores at Copper Canyon seem to be consistent with those inferred by others for similar type deposits elsewhere. Gilluly (1946) suggested comparably shallow depths of emplacement, 900–3,000 m, at the Ajo, Ariz., and the Bingham, Utah, porphyry copper deposits. His depth estimates are based on volcanic-stratigraphic evidence and igneous textures. Ishihara (1967) reconstructed a thickness of between 1 and 1.6 km of intrusive and extrusive rocks at the Questa, N. Mex., deposit. Nielsen (1968) suggested that the Santa Rita stock that is associated with the Santa Rita, N. Mex., porphyry copper deposit intruded to within 450 m of the surface; he based this conclusion on overlying sedimentary rock thicknesses. Kesler (1968) suggested that the intrusion associated with the contact metasomatic copper ores at the Memé mine, Haiti, was emplaced at a depth of 1–2 km.

## TEMPERATURE VARIATION IN THE EAST ORE BODY

We estimated temperatures during metallization in the east ore body from experimentally determined thermal stabilities for various sulfides and homogenization temperatures of fluid inclusions in selected veins through the ore body (Nash and Theodore, 1971). A diagrammatic summary of temperature variation with time in the body is shown in figure 40, which includes (1) thermal limits required by the occurrence of critical sulfide assemblages, (2) a schematic summary of fluid inclusion data, and (3) an estimate of the quantity of sulfides deposited relative to thermal changes.

For the east ore body, most replacement ore must have formed within the thermal stability limits indicated by early stage unaltered hexagonal pyrrhotite, which are greater than 290°–308°C (Clark, 1966; Arnold, 1969; Yund and Hall, 1969) (fig. 41). Pyrrhotite-chalcopyrite assemblages in the ore body further suggest maximum depositional temperatures of about 334°C (Yund and Kullerud, 1966) for the bulk of the earliest replacement ores. Elsewhere, Sawkins, Dunham, and Hirst (1964) and Balitskii and Lyubofeyev (1962) have reported hypogene pyrrhotite that developed at relatively low temperatures.

The most sulfur-rich hexagonal pyrrhotite, 47.27 atomic percent Fe (table 8), may approach the composition of the hexagonal pyrrhotites at the time of their initial crystallization. According to the data of Toulmin and Barton (1964) and Barton and Skinner (1967), a hexagonal pyrrhotite of this composition would require a minimum temperature of formation of about 360°C. Therefore, temperatures in the ore body may have increased locally after initial deposition of the bulk of hexagonal pyrrhotite plus chalcopyrite ores in

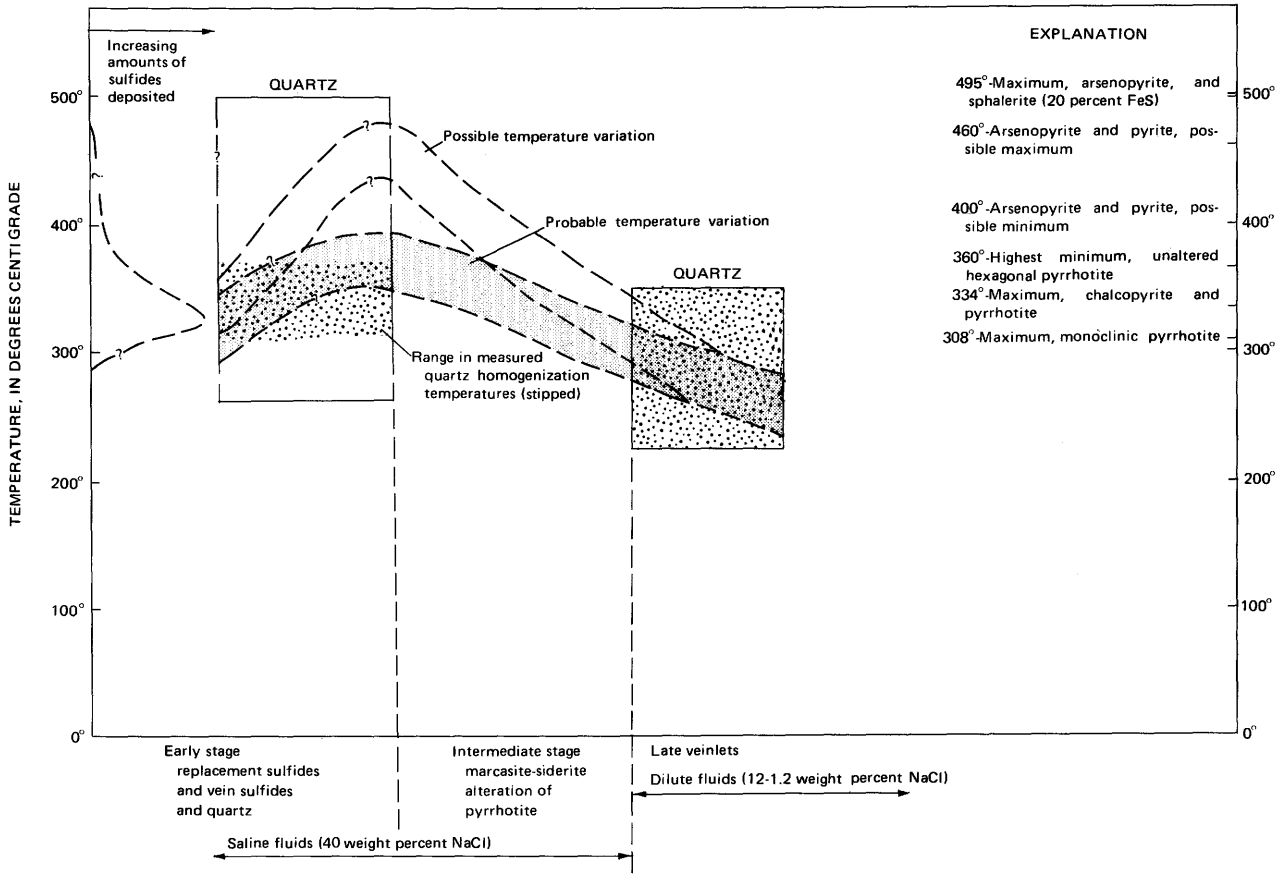


FIGURE 40.—Diagrammatic summary of temperature variation in the east ore body. Fluid salinities and ranges in quartz fluid-inclusion homogenization temperatures from Nash and Theodore (1971).

the 290°–334°C interval (fig. 40), which would account for the fluid-inclusion data. We interpret monoclinic pyrrhotite that rims and postdates hexagonal pyrrhotite to indicate exsolution at sometime subsequent to early stages of metallization.

Thermometric data from fluid inclusions in quartz veins through the ore body show a temperature range that spans the chalcopyrite plus pyrrhotite to cubanite plus pyrite transition. Homogenization temperatures from early fluid inclusions are 310°–360°C in the ore body (Nash and Theodore, 1971). The maximum temperature determined is about 25°C higher than the experimentally determined maximum thermal stability of hexagonal pyrrhotite plus chalcopyrite. These temperature discrepancies may simply reflect inaccuracies of the various methods; the thermal increase inferred during the early stages of metallization (fig. 40) may be only apparent and not real.

The compositions of arsenopyrites in veins that cut the replacement ores also indicate temperatures higher than the experimentally determined maximum thermal stabilities of pyrrhotite plus chalcopyrite-bearing ores. Arsenopyrites here with 31.9–33.1 atomic percent arsenic yield temperatures in the 400° to 460° range, when referred to the low pressure solvus of Clark (1960). However, we maintain a certain skepticism of the highest temperatures determined by this technique because of poorly defined peak heights on diffractograms of several of the arsenopyrites.

Therefore, from these data, some fairly hot sulfide-depositing fluids may have circulated through the east ore body predominantly along veins. These veins may have developed at temperatures higher than those prevailing during the bulk of the deposition of the matrix replacement ore and possibly reflect the thermal culmination in the east ore body. It is possible that the temperature culmination in the ore body may have been as high as 460°C from the arsenopyrite data (fig. 40). A more probable thermal peak, however, would be about 360°C. Nash (oral commun., 1971) subsequently found a 400°C filling temperature for saline fluid inclusions in a quartz vein at the granodiorite's margin. This finding seems to corroborate the hypothesis that the granodiorite acted as a heat source for the hydrother-

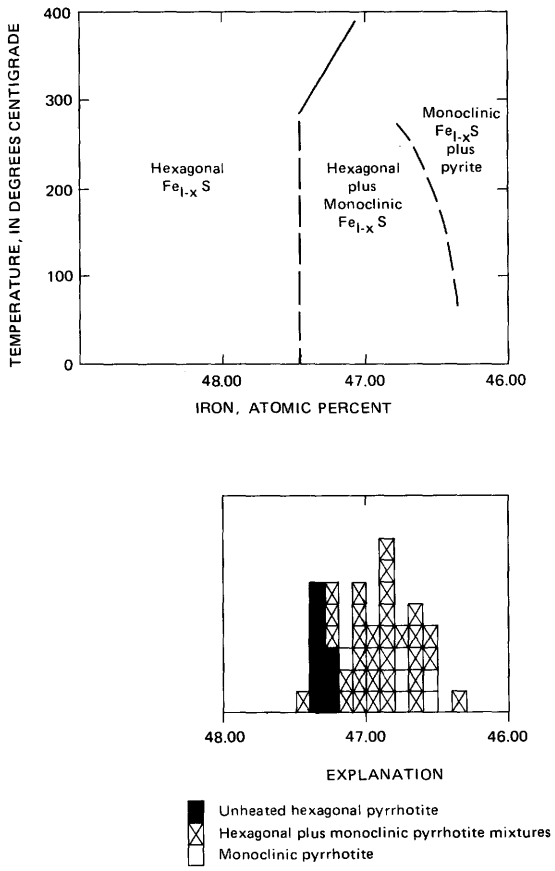


FIGURE 41.—Phase diagram of the Fe-S system from 45.8 to 48.5 atomic percent Fe and between 0° and 400°C, modified from Yund and Hall (1969, fig. 1), with histogram showing variation of pyrrhotite compositions determined at Copper Canyon.

mal fluids associated with metallization. Some of the arsenopyrite vein-structures subsequently opened again during the marcasite-siderite stage of metallization.

Fluid inclusion observations by Nash on sparse quartz veinlets associated with the intermediate stage marcasite-pyrite-siderite alteration of early pyrrhotite suggest that intermediate stage fluids were somewhat cooler, probably 325°±25°C. At these temperatures, the fluids were thermally compatible with much of the preceding early stage metallization. Therefore, in order to alter the pyrrhotites, important changes in fluid chemistry (to be described below) must have occurred between early and intermediate stage metallization. Kelly and Turneaure (1970) found filling temperatures from 203° to 284°C in primary siderite associated with alteration of pyrrhotite in ore deposits of the eastern Andes, Bolivia.

Fluids associated with late, predominantly vug-filling quartz are inferred to have been in the 350°–225°C range (Nash and Theodore, 1971) and much more dilute than either of the two preceding stages of metallization (fig. 40).

Some further generalizations regarding the thermal history of the east ore body are warranted. We believe the temperature increase at the time of metallization and alteration in these ore zones, which are about 300 m from the Copper Canyon intrusion's margin, temporally just preceded the intrusion's emplacement. We find no evidence for a purely thermal event that would have preceded hydrothermal metallization and alteration. Although magmatic temperatures in this relatively small intrusive body may have been about 800°C, calculated heat flow models suggest that maximum imposed temperatures due to conduction would have been about 150°C (Steiger and Hart, 1967) in the 6450 bench (fig. 15). These interpretations seem to be consistent with generally accepted thermal effects due to igneous intrusions (Lovering, 1955; Jaeger, 1964). The temperature history depicted in figure 40 does not reflect a resurgent thermal event in country rock that had been heated by thermal conduction from the intrusion and then cooled. Lastly, the measured and deduced temperatures at Copper Canyon are much lower than those (400°–725°C) inferred from fluid inclusion studies in the Bingham, Utah, porphyry copper deposit (Roedder, 1971). The Bingham deposit, however, is largely in the core area of a 5-sq-km pluton (Lowell and Guilbert, 1970).

## CHEMISTRY OF THE FLUIDS

### TRANSPORT

Recent theoretical and experimental studies provide some insight into the nature of different chemical species in solution, but these solution species are still imperfectly understood. As Helgeson (1964) has shown theoretically from solution equilibria, chloride complexes may provide a likely mechanism by which ore-forming metals were transported to their sites of deposition. Hemley, Meyer, Hodgson, and Thatcher (1967) have shown that significant amounts of sphalerite and galena are soluble in weakly acidic chloride solutions, buffered by K-feldspar–muscovite–quartz, and Mizutani (1970) found that concentrations of Cu and Zn in some fumarolic gases in Japan vary directly with the gases' Cl content and inversely with their $H_2S$ content. On the other hand, Barnes and Czamanske (1967) suggest that metallic sulfides should be soluble as complex ions or molecules in near-neutral solutions in the presence of $Cl^-$ and many other chemical species. Romberger and Barnes (1970) further concluded that complexes between Cu and $Cl^-$ are not significant for ore

transport at temperatures of 20°–200°C. Helz (1971) experimentally found that concentration of NaCl does not affect the solubility of magnetite from which he also concluded that chloride complexes are not predominant. For the present study, the nature of the original complexed copper species in solution at Copper Canyon is unimportant. Nevertheless, the spatial association between dense chloride fluids and copper ores at Copper Canyon and at 14 other porphyry copper deposits (Nash, 1971) strongly suggests the significance of $Cl^-$ in the ore forming process. From calculated solubilities of CuS at 25°C in 3-*m* brine solutions, Nriagu and Anderson (1970) concluded that such solutions can carry enough reduced sulfur to precipitate copper being transported as a chloride complex.

Observations elsewhere bear on the possible nature and the concentration of sulfur in the ore forming fluids at Copper Canyon. Helgeson (1968) and White (1968) note that natural Na-Ca-Cl brines are typically deficient in total sulfur; total sulfur, present as $H_2S$, is about 30 ppm in brines from the Salton Sea geothermal area collected at depths of about 1,500 m. At these depths, temperatures are about 300°C; these P-T (pressure-temperature) conditions are similar to those at Copper Canyon during development of the ores. At the Providencia, Mexico, lead-zinc deposit, Rye and Haffty (1969) also find that sulfur concentrations are low in primary fluid inclusions. Ypma (1968) found $H_2S$ in fluid inclusions from the Mineral Park, Ariz., porphyry copper deposit. Roedder (1971) detected liquid $H_2S$ in fluid inclusions from the U.S. mine in the Bingham district, Utah. Primarily on the basis of the sulfur species in the Salton Sea geothermal area (Helgeson, 1968), it is probable that $H_2S$, or its ionic aqueous equivalents HS or $S^{2-}$, was the predominant sulfur species in the ore-forming fluids at Copper Canyon. Preliminary $\delta S^{34}$ determinations of sulfides from the east ore body cluster about zero per mil (M. L. Jensen, oral commun., 1971). As summarized by Jensen (1971), sulfide sulfur whose $\delta S^{34}$ has a composition of zero per mil has generally been taken to imply a primordial origin, that is, derived from the upper mantle. Ohmoto (1970), however, cautioned that sulfides, whose $\delta S^{34}$ are zero per mil, are not necessarily deposited from solutions with an equivalent $\delta S^{34}$.

## CONDITIONS OF DEPOSITION

### OXYGEN AND SULFUR FUGACITIES

In contrast to the many unknowns still remaining in solution equilibria, oxygen and sulfur stabilities of the common sulfides are well known. Limits to the oxygen and sulfur fugacity in the environment of deposition can be deduced from these stability fields. Initial compositions of solutions that produce a mineral must necessarily lie in the appropriate stability field for that mineral (Raymahashay and Holland, 1969). Figure 42 shows the pyrrhotite, pyrite, magnetite, and hematite stability fields at temperatures close to those apparently prevailing during the early and intermediate stages of metallization.

Near the onset of metallization, perhaps at temperatures in the 308°–334°C range, we infer hexagonal pyrrhotite to have been in equilibrium with pyrite at a maximum $f_{S_2}$ of about $10^{-9}$ atm (atmosphere) and with magnetite at a maximum $f_{O_2}$ of about $10^{-3}$ atm (fig. 42*A*). During deposition of the chalcopyrite-pyrrhotite ores in the east ore body, it is likely that $f_{S_2}$ $f_{O_2}$ did not exceed these values.

The rocks at places in the east ore body may have reached slightly higher temperatures of at least 350°C near the end of the early stage metallization, about the time of the emplacement of the arsenopyrite veins. Pyrite is also now common in the ores, but bornite and magnetite are absent. Therefore, from figure 42*B*, $f_{S_2}$ in the environment ranged between $10^{-6}$ and about $10^{-9}$ atm. There must have been some local geographic variation or temporal fluctuation in $f_{S_2}$ because some pyrrhotite was also deposited at this time. The absence of magnetite from the ore zones suggests that $f_{O_2}$ was less than about $10^{-26}$ to $10^{-30}$ atm at the aforementioned values of $f_{S_2}$.

Temperatures during the intermediate marcasite-pyrite-siderite alteration of pyrrhotite stage of metallization were probably about 325°±25°C. Sulfur and oxygen fugacities in the environment predominantly remained in the pyrite stability field, below the bornite plus pyrite sulfidation curve, or $f_{S_2}$ values from $10^{-7}$ to about $10^{-12}$ atm (fig. 42*C*). The $f_{CO_2}$, however, was much higher than previously as siderite is a common mineral. High-temperature thermodynamic data are not available for siderite to establish accurately its stability field (Robie and Waldbaum, 1968). From available data, Holland (1965) showed that at 400°C and $f_{CO_2}$ of 100 atm, siderite would become stable largely at conditions around the pyrrhotite-magnetite boundary of figure 42.

### DEDUCTIONS FROM ALTERATION REACTIONS

The chemistry of the ore-forming fluids was, of course, continually changing as they moved upwards and circulated through a volume of rock near the granodiorite. Although it is very difficult to deduce what the fluids might have been like at levels far below the exposed granodiorite and the ore bodies, the occurrence of apparently contemporaneous white mica plus K-feldspar as pervasive minerals in potassic alteration assemblages associated with the ores suggests some

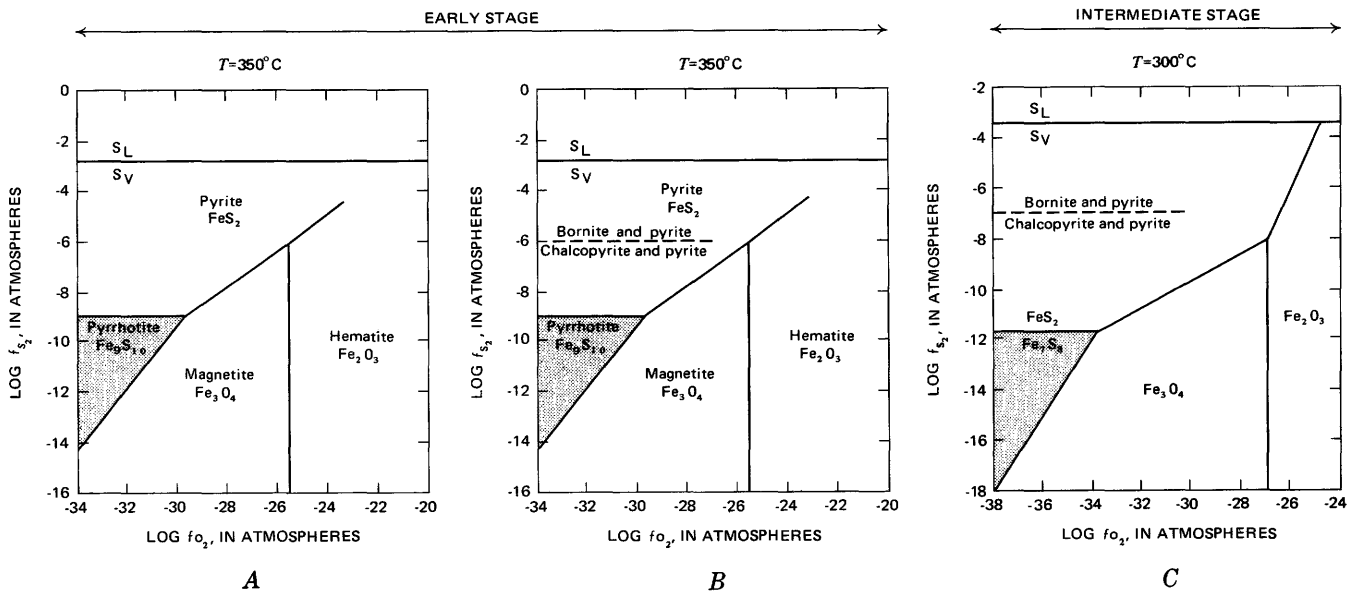


FIGURE 42.—Stability fields of pyrrhotite, pyrite, magnetite, and hematite. *A*, Earliest stage at 350°C, from Raymahashay and Holland (1969). *B*, Later early stage at 350°C, from Raymahashay and Holland (1969). *C*, Intermediate stage at 300°C, modified from Helz (1971) with data from Scott and Barnes (1971). Chalcopyrite plus pyrite to bornite plus pyrite sulfidation curves are from Barton and Skinner (1967). Pertinent parts of the stability diagrams are shaded.

anion metasomatism during their formation (Meyer and Hemley, 1967). This anion metasomatism may reflect in part the increased mobility of $H^+$ relative to $OH^-$ during filtration processes (Korzhinskii, 1957). Such a white mica–K-feldspar association further suggests that slightly acidic conditions prevailed in the environment of ore deposition (Meyer and Hemley, 1967, fig. 6.6). Indeed, decarbonation of the Battle's calcite matrix is most easily accomplished under acidic conditions. Therefore, we infer that the fluids were slightly acidic or near neutral when they first arrived at the east ore body but certainly no more than 2.0 pH units below neutrality (Barnes, 1965).

Our suggestion that the initial fluids at Copper Canyon were slightly acidic conflicts with the pH-$f_{S_2}$-$f_{O_2}$ stability regime of pyrrhotite calculated by Meyer and Hemley (1967, fig. 6.9). They suggest that at 250°C and at total aqueous sulfur of 0.1 *m*, pyrrhotite is stable only under alkaline conditions. Total dissolved sulfur may have been less than 0.1 *m* in the environment of early stage ore deposition at Copper Canyon. From the data of Helgeson (1967) and Meyer and Hemley (1967), Raymahashay and Holland (1969) calculated an approximate log $H^+$ concentration of $-5.0$ in a one molar potassium solution buffered by K-feldspar–muscovite–quartz at 250°C.

Although some hematite immediately adjacent to the granodiorite may have been converted to magnetite during its emplacement, as Roberts found in the Copper Canyon underground mine (Roberts and Arnold, 1965, p. B25), we infer from the presence of rare detrital hematitic chips mantled and microveined by pyrite in the east ore body that hematite did indeed persist there after emplacement of the pluton.

Accordingly, from our petrologic studies and available experimental data, coupled decarbonation and sulfidation reactions involving hematitic and calcitic wallrock with ore fluids during early stage sulfide deposition are inferred to have been:

I
$$CaCO_3(s) + SiO_2(s) + TiO_2(s) \rightleftarrows CaTiSiO_5(s) + CO_2(g) \quad (1)$$
$$4H^+ + 2CaCO_3(s) \rightleftarrows 2Ca^{+2}(aq) + H_2CO_3(aq) + CO_2(g)H_2O \quad (2)$$
$$4H_2(g) + CO_2(g) \rightleftarrows CH_4(aq) + 2H_2O(1) \quad (3)$$
$$H_2(g) + CO_2(g) \rightleftarrows CO(g) + H_2O(1) \quad (4)$$

II
$$4H^+ + Fe_2O_3(s) \rightleftarrows 2Fe^{+2}(aq) + 2H_2O(1) + \tfrac{1}{2}\,O_2(g) \quad (5)$$
$$6H^+ + 10\,H_2S(aq) + 4Fe_2O_3(s) \rightleftarrows 5FeS_2(s) + 3Fe^{+2}(aq) + 12H_2O(1) + H_2(g) \quad (6)$$
$$7.2H_2(g) + 2.3Fe^{+2}(aq) + 7.1\,FeS_2(s) \rightleftarrows 9.3\,Fe_{.9}S(s) + 4.9\,H_2S(aq) + 4.6\,H^+. \quad (7)$$

Schuiling and Vink (1967) experimentally determined the equilibrium curve for reaction 1. As written, 1, the production of 1 mole of sphene from 1 mole each of quartz, calcite, and $TiO_2$ (rutile or anatase) involves about a 35 percent volumetric decrease, assuming complete replacement of the reactants. At 300°C, its

univariant breakdown, 1, (for $P_{CO_2}=P_{total}$) suggests a $P_{CO_2}$ of about 20 bars. However, because $P_{CO_2}$ did not equal $P_{total}$ at Copper Canyon, we cannot use these experimental data as a $CO_2$ estimate, also assuming that $CO_2$ production was entirely controlled by reaction 1. From the relative amounts of $CaCO_3$ and $TiO_2$ in the unaltered rocks of the Battle (table 9), complete dissolution of all $CaCO_3$ by reaction 1 is not probable. Therefore, removal of calcium and carbonate from the rocks may have been accomplished through reaction 2. In addition, $P_{CO_2}$ in the rocks was also probably controlled in part by the production of methane, 3, and carbon monoxide, 4, as intermediate byproducts of the original reactants.

When compared with rocks outside the east ore body, samples inside the body indicate introduction of iron (table 9). Breakdown and sulfidation (II), however, of sedimentary hematite also occurred, a sulfidation coupled to the preceding reactions (I). Constant volume restraints on 6 and 7 impose considerable constraints on the format of these reactions. An interesting feature of reactions 6 and 7 is also the apparent coupling of $H_2(g)$ and $Fe^{+2}(aq)$, products of 6, to 7 as reactants. Furthermore, these three reactions (5–7) suggest a net consumption of 5 moles of $H^+$ and 5 moles of $Fe_2O_3(s)$ for about 9 moles of hexagonal pyrrhotite ($Fe_{0.9}S$) produced during sulfidation. We suggest that the pH of the early stage fluids thus increased (they became more alkaline) during this stage of metallization. Moreover, 7 also suggests the introduction of $H_2(g)$ during early stage metallization at Copper Canyon.

The chemistry of intermediate stage fluids is reflected in the rocks primarily as an alteration of early stage pyrrhotite to marcasite-pyrite-siderite assemblages. As we noted above, this alteration was accompanied by about a 10–20 percent volume decrease in the sulfides, and an overall increase in porosity. Furthermore, fluid inclusion studies by Nash have revealed two fluid types associated with the intermediate stage: (1) an $H_2O$-salt-rich fluid with small amounts of liquid $CO_2$, and (2) a $CO_2$-$H_2O$-rich fluid (Nash and Theodore, 1971). No $CO_2$-bearing fluid inclusions were found associated with early-stage metallization. During the intermediate stage, temperatures were at times about 325°±25°C. Continued dissociation of $H_2(g)$, which apparently was present during early stage metallization, may eventually have lowered the pH of the fluids to a point where early-stage pyrrhotite was no longer stable:

$$1.5\ H^+ + 0.5\ H_2S(aq) + 2Fe_{0.9}S(s) \rightleftharpoons 1.25\ FeS(s) + .75\ Fe^{+2}(aq) + 1.25\ H_2(g). \quad (8)$$

Reaction 8 is written for a 20 percent by volume decrease and is undoubtedly coupled to a reaction similar to

$$Fe^{+2}(aq) + H_2CO_3 \rightleftharpoons FeCO_3(s) + 2H^+, \quad (9)$$

whereby $Fe^{+2}(aq)$ removed by reaction 8 then reacts with $CO_2$-rich intermediate stage fluids (probably as $H_2CO_3(aq)$ (Helgeson, 1969)) to yield siderite.

Late stage fluids that permeated the deposit are evinced primarily by clear vuggy quartz crystals (Nash and Theodore, 1971). Associated pyrite and probable dawsonite ($NaAlCO_3(OH)_2$) (Nash, oral commun., 1972), the latter as a daughter mineral in fluid inclusions, with these quartz crystals, herald several further changes in fluid chemistry during this stage of metallization. (The daughter minerals were previously thought to be chlorite or epidote.) As shown in figure 40, salinities were 12–1.2 percent by weight, and temperatures varied from 350° to 230°C. These fluids may have deposited most of the gold in the ore body.

### Summary of depositional conditions

Figure 43 depicts inferred changes in chemistry for the early and intermediate stage fluids at Copper Canyon referred to stability fields for the Fe-S-O system at 250°C calculated by Barnes and Czamanske (1967, fig. 8.7). The validity of a similar diagram for the apparently higher temperatures associated with ore formation at Copper Canyon would be even more tenuous because of greater uncertainties in thermodynamic functions at these temperatures.

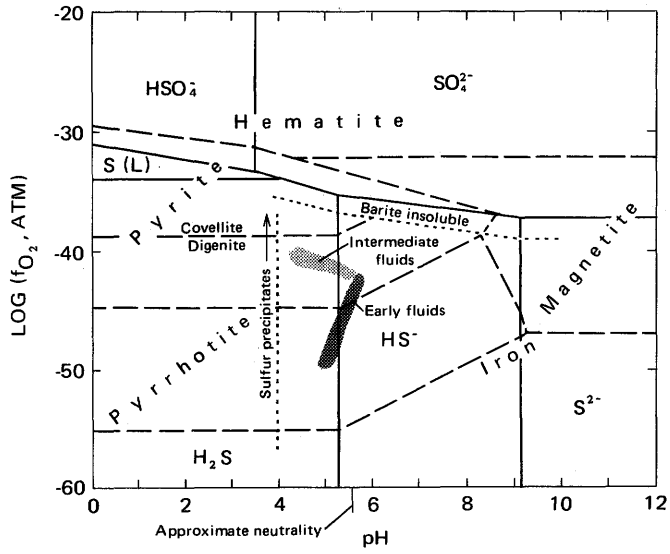


FIGURE 43.—Calculated stability fields for the Fe-S-O system with other aqueous species and minerals at 250°C by Barnes and Czamanske (1967). Dashed lines represent boundaries between stability fields of minerals, and heavy solid lines represent those between aqueous species.

Barnes and Czamanske (1967) describe many possible changes in physicochemical environment that

cause ore deposition from solutions carrying metals:

***cooling in response to movement along a geothermal gradient or mixing with meteoric waters, adiabatic expansion, reaction with wall rocks, or dilution by meteoric waters. In addition any reactions which decrease $a_{H_2S}$, $a_{HS^-}$, or $a_{S^{2-}}$ also decrease the solubility of complexes in which these species are stoichiometric constituents. The most effective reactions chemically but not necessarily geologically, involve oxidation and result from exposure of the ore solution to rocks, solutions, or gases containing oxidized species (p. 374).

At Copper Canyon, a 10–20-m-thick red bed unit at the base of the lower member of the Battle Formation locally contains abundant hematite as detrital clasts and as cement. Such hematite may provide a source of oxygen in an ore fluid-rock system buffered by calcite and hematite to precipitate chemically metal sulfides. In addition, the hematite-calcite reactions influenced pH by making the fluids more alkaline, as did the boiling of the brine.

### ROLE OF CARBON IN THE SCOTT CANYON FORMATION

A possible explanation for the low oxygen fugacities associated with the Copper Canyon fluids may lie in the high organic carbon content of rocks belonging to the Lower or Middle Cambrian Scott Canyon Formation. It appears that the initial ore-forming fluids at Copper Canyon, when they first arrived at the general level of the ore bodies, were characterized by oxygen fugacities much lower than the fluids at most other porphyry copper deposits. Pyrite is the predominant iron sulfide in such deposits elsewhere. This formation is the lowermost and oldest one in the mining district, and it undoubtedly occurs at Copper Canyon but probably at depths greater than 1,500 m. At Iron Canyon, combined geochemical and geophysical studies (Theodore and Roberts, 1971; Zablocki, 1971) have shown that organic-carbon-rich layers with about 3 weight percent organic carbon make up about 30–40 percent of the rocks by volume in a typical section through this formation. Therefore, redox reactions involving this organic carbon could have reduced the oxygen fugacity of fluids which circulated through the Scott Canyon and which eventually formed the porphyry copper ore bodies in tectonic blocks superjacent to the Scott Canyon. Pyritic alteration of the Scott Canyon Formation at Iron Canyon (fig. 3) resulted in bleached chert and argillite that are depleted locally in copper (Theodore and Roberts, 1971).

## SOURCE OF COPPER

An attractive genetic hypothesis is that the copper ore bodies at Copper Canyon formed entirely from volatiles released from an $H_2O$-saturated magma crystallizing under 1,500 m of cover. Porphyritic textures could be explained by pressure quenching (Toulmin and Clark, 1967) caused by rupturing of the magma's upper chamber along the Virgin fault and separation of an $H_2O$-rich phase. Such rupturing could initiate a change from lithostatic to predominantly hydrostatic conditions in and around the intrusion. Two limiting factors, however, are the stability of biotite and the solubility of $H_2O$ in granitic melts. From the primary biotites' calculated stability fields, such losses of $H_2O$ from magma crystallizing at depths of about 1,500 m could have amounted to $P_{H_2O}$ decreases of not much more than 100 bars. Furthermore, from studies of solubilities of $H_2O$ in granitic melts by Burnham and Jahns (1962), we infer magma at such depths to have contained, at most, 3 percent dissolved $H_2O$ by weight of which about one-third must have been taken up by the crystallization of primary biotite, allowing 2 percent to be released to the country rock. Calculations show that such a crystal-magma containing 38 percent by volume phenocrystic plagioclase in a 600-m radius by 370-m-deep chamber (see pl. 1) could contain a maximum of about $5\times10^9$ kg magmatic $H_2O$ available for wallrock alteration and potential metal transport.

An interesting test for magmatic fluid sources of the copper is a calculation of the copper concentration in hydrothermal fluids coming from the intrusion at Copper Canyon. Proved copper reserves included at least $1.7\times10^8$ kg copper (Roberts and Arnold, 1965, p. B42; Sayers and others, 1968), 97 percent of which was in the east and west ore bodies. The Copper Canyon underground mine also contained a minimum of about $5\times10^6$ kg lead and zinc. Accordingly, if all copper metallization at Copper Canyon were assigned to fluids emanating from this body of rock during crystallization at depths of about 1,500 m, this would imply a fantastic copper solubility of about 33 grams per liter ($3.3\times10^4$ ppm) in those fluids. Such a solubility is about three times the maximum metal concentration estimated by Barnes and Czamanske (1967, p. 335) for the development of base-metal ores and about three orders of magnitude greater than minimum copper solubilities allowable by experiment for development of significant ore bodies (Romberger and Barnes, 1970). Such copper concentrations should also be reflected as copper minerals in the fluid inclusions, but such copper minerals are not present. Rose (1970), based on the ZnS solubility data of Hemley, Meyer, Hodgson, and Thatcher (1967), suggested that an ore-forming solution might contain 2,000 ppm copper for the development of a hypothetical porphyry copper deposit. Thus, although we recognize the approximate nature of our calculations from the constraints imposed by them, we reject

the hypothesis that fluids associated with metallization at Copper Canyon were entirely derived from the intrusive body. We must look to $H_2O$ sources other than the intrusion itself, which we will attempt to document better through isotopic studies (O and D) underway.

There are other mechanisms by which the $H_2O$ content of magma may be increased. At deeper levels in the crust, magma can contain increased amounts of dissolved $H_2O$ (Burnham and Jahns, 1962; Burnham, 1967). For the Copper Canyon area, such a relation would imply at some time a deep $H_2O$-saturated magma. Such a magma, as it moved to higher levels in the crust, would increase in temperature and would intrude its own $H_2O$-rich volatiles. As a result, hydrous, sulfide-bearing metamorphic assemblages would be replaced by anhydrous ones. However, we reject this hypothesis because very deep magmas are most likely $H_2O$-undersaturated (Castle, 1964; Bateman, 1968; Luth, 1969). Furthermore, in the west ore body anhydrous contact silicate assemblages are replaced by hydrous ones with sulfides.

Suitable country rock as a source of the metals and gangue in ore deposits is an old concept (Ransome, 1900; Knopf, 1929)which, however, has received considerable attention in the last few years. After a review of the literature, Krauskopf (1967b) concluded that many different crustal rock types fit the source-bed concept. Boyle (1970) believes that crustal country rocks that surround hydrothermal deposits or that lie below them are among the most logical sources of the metals. Jensen (1971) suggested that metalliferous shales should be considered as sources for metals in ore deposits associated with felsic Cordilleran intrusive bodies.

We shall now consider the possibility that the source of some copper in the deposit at Copper Canyon was in unaltered organic-rich shaly horizons of the Scott Canyon Formation, where median copper content is about 100 ppm (Theodore and Roberts, 1971). If we assume that a process by which this copper is put into solution has an efficiency of 50 percent, then about 13 cu km of rock belonging to the Scott Canyon would yield sufficient copper to form the deposits at Copper Canyon. Such a volume of rock (8.7 sq km $\times$ 1,500 m, if we assume a 1,500-m thickness for the Scott Canyon at depth) does not seem too unreasonable. In fact, this calculated area is about equal to the area underlain by pyritized rock around the altered granodiorite of Copper Canyon.

The geology at Copper Canyon and our observations provide an excellent test of the source-bed concept as applied by Jensen (1971) to the Basin and Range geologic province. Appraisal of the Scott Canyon Formation as the source of some of the copper reveals two notable weaknesses to the hypothesis. (1) The Scott Canyon underlies the entire mining district, and there are many intrusive bodies throughout the district that are similar to the Copper Canyon body. All of these intrusive bodies must cut the Scott Canyon at depth. Hence, ore bodies equivalent to those at Copper Canyon might be expected at many places but are not known. (2) The lead-zinc ore bodies in the Copper Canyon underground mine also should have the same source as the copper ore bodies. In the altered parts of the Scott Canyon Formation at Iron Canyon, however, there are notable increases in lead and zinc (and manganese and barium) rather than depletions (Theodore and Roberts, 1971). Therefore, if the source-bed concept were operative with respect to the Scott Canyon Formation, from our data, the ore-forming fluids must extract copper and simultaneously deposit lead and zinc in the altered parts of the formation which does not seem likely.

Therefore, largely through elimination of these two possibilities for the source of the copper, we conclude that the bulk of the copper at Copper Canyon was derived from very deep sources.

## GEOCHEMISTRY OF THE COPPER CANYON AREA

Comprehensive geochemical studies describing the distribution of minor metals in porphyry copper districts are not generally available. We have attempted to fill part of this gap by determining the minor-element content of rocks surrounding the ore deposits at Copper Canyon. We are especially concerned with the primary or hypogene dispersion at the surface in this district in order to aid chemical prospecting in a similar geologic environment elsewhere. Broad areas of Copper Canyon are very suitable for such studies because of the minimal development of secondary or supergene clays, whose presence could otherwise complicate our goal immensely. Nevertheless many factors remain that must be considered in interpretating geochemical data. To depict chemical changes in a complex physical and chemical metallization process, we found analyses of many samples were needed. Metallization and alteration were not a single-stage phenomenon in a chemically simple wallrock system. Multidirectional element migrations occurred during each step of the metallization, from the magmatic stages of the pluton, which may have involved a predominantly diffusional process (Wodzicki, 1971), to flow-type migrations during hydrothermal ore development.

## SAMPLING AND ANALYTICAL PROCEDURES

In the approximately 16-sq-km area of plate 1 outside the open pit, 2,927 rock samples were collected and analyzed for the distribution studies. Chemical and spectrographic analyses were made either in mobile field laboratories or in the permanent analytical facilities of the U.S. Geological Survey at Denver. The material analyzed consisted of approximately 1-kg composite rock-chip samples that commonly were collected over an entire outcrop area of about 10 sq m. Vein, gossan, and mineralized fault gouge material comprises many of the samples. At many localities more than one sample was collected and analyzed. The quantity of 31 elements in each rock sample was determined, and of these, the distribution patterns for 20 elements (Sb, As, Ba, Bi, B, Cd, Cr, Co, Cu, Au, Pb, Mn, Hg, Mo, Ni, Ag, Sr, Sn, V, and Zn) were prepared (Theodore, 1969). However, these 20 element distributions are not discussed in that earlier report. All element concentrations, with the exception of gold and mercury, were analyzed by a six-step spectrograph method (Grimes and Marranzino, 1968), and the results reported to the nearest number in the series 1, 0.7, 0.5, 0.3, 0.2, 0.15, 0.1, and so on. The precision of a reported value is approximately plus 100 percent or minus 50 percent (A. Marranzino, written commun., 1968). Gold here has about a 25-percent relative standard deviation percent[5] calculated from five individual analyses on each of six different samples. The relative standard deviation percent for mercury is about 16 percent, determined from 10 individual analyses on each of 41 different samples.

## FREQUENCY DISTRIBUTIONS AND CONCENTRATION CLASSES

Frequency distributions for many elements around the porphyry copper deposit at Copper Canyon extend beyond their upper and lower detection limits. In the 20 element distribution maps and for all statistical calculations described below, the value at the upper limit of determination was substituted for all analyses reported greater than the detection limit. No value was substituted for those concentrations reported below the detection limit, and, accordingly, these undetected concentrations did not enter into any statistical calculations to be reported below. The number of analyses less than the lower limit and greater than the upper limit of determination for the 29 elements analyzed by emission spectrographic methods have been listed in table 12. As previously described, gold and mercury were analyzed by chemical methods: 838 gold analyses were less than its 0.02 ppm lower detection limit here, and 161 mercury analyses were less than 0.01 ppm, the reported lower detection limit for mercury. Eight mercury analyses were greater than 10 ppm, its upper limit of determination. The total number of mercury analyses (2,609) is less than the total number of samples analyzed for other elements (2,927).

TABLE 12.—*Number of spectrographic results less than the lower detection limit and greater than the upper detection limit in 2,927 analyses around the Copper Canyon porphyry copper deposit*

| Element | Analyses less than lower detection limit | Lower detection limit[1] | Upper detection limit[1] | Analyses greater than upper detection limit |
|---|---|---|---|---|
| Iron | 0 | 500 | 200,000 | 82 |
| Magnesium | 19 | 200 | 50,000 | 0 |
| Calcium | 155 | 500 | 200,000 | 1 |
| Titanium | 3 | 20 | 10,000 | 15 |
| Manganese | 12 | 10 | 5,000 | 7 |
| Silver | 595 | .5 | 5,000 | 0 |
| Arsenic | 1,900 | 200 | 10,000 | 63 |
| Boron | 606 | 10 | 2,000 | 23 |
| Barium | 5 | 20 | 5,000 | 34 |
| Beryllium | 1,910 | 1 | 1,000 | 0 |
| Bismuth | 2,310 | 10 | 1,000 | 6 |
| Cadmium | 2,674 | 20 | 500 | 8 |
| Cobalt | 1,823 | 5 | 2,000 | 1 |
| Chromium | 16 | 5 | 5,000 | 0 |
| Copper | 27 | 5 | 20,000 | 73 |
| Lanthanum | 1,496 | 20 | 1,000 | 2 |
| Molybdenum | 1,995 | 5 | 2,000 | 0 |
| Niobium | 1,796 | 10 | 2,000 | 0 |
| Nickel | 289 | 5 | 5,000 | 0 |
| Lead | 804 | 10 | 20,000 | 32 |
| Antimony | 2,683 | 100 | 10,000 | 1 |
| Scandium | 867 | 5 | 100 | 0 |
| Tin | 2,207 | 10 | 1,000 | 0 |
| Strontium | 2,139 | 100 | 5,000 | 0 |
| Vanadium | 20 | 10 | 10,000 | 0 |
| Tungsten | 2,765 | 50 | 10,000 | 0 |
| Yttrium | 513 | 10 | 200 | 3 |
| Zinc | 2,131 | 200 | 10,000 | 10 |
| Zirconium | 45 | 10 | 1,000 | 7 |

[1]Approximate visual lower and upper limits of determination in parts per million by the six-step spectrographic method (A. Marranzino, written commun., 1968; D. Siems, oral commun., 1970).

The concentration classes shown in the zonation plots (pl. 2; Theodore, 1969) were determined for each element from tests involving 1,025 analyses in the northern one-third of the area, which is generally unaltered. After log transformation of the geochemical data, histograms with appropriate class intervals were prepared. If an element had a frequency distribution such that up to approximately 10 percent of the total observations (1,025) were less than the detection limit, then the detection limit was selected as the upper boundary for the lowest interval. A plus (+) symbol generally represents this range in concentra-

[5]Relative standard deviation percent$=\frac{S(100)}{M}$, where $S$=standard deviation and $M$=mean.

tions. If, on the other hand, an element had a frequency distribution such that very small numbers of samples consisted of concentrations less than the detection limit, then the upper limit of the lowest interval was selected to be as close as possible to the mean of all valid observations for the element. The minimum value of the highest interval, generally indicated by a square (□) in the distribution diagrams (pl. 2; Theodore, 1969), was chosen so that it fell below about 10 percent of the highest concentrations detected for any one element. The number of intervals, and their boundaries were determined from changes in slope in the frequency distribution diagrams for the various elements.

## DISTRIBUTION OF ELEMENTS IN THE COPPER CANYON AREA

### COPPER

Copper was detected in 2,900 of the 2,927 samples analyzed. The median copper content of these 2,900 samples is about 100 ppm. Copper abundances in unmineralized rocks from all formations at Copper Canyon are generally less than 50 ppm. For comparison, Turekian and Wedepohl (1961) cite average copper abundances of 45 and 1–9 ppm for shales and sandstone, respectively. The average abundance of copper in unmineralized granitic rocks ranges from 10 to 30 ppm (Turekian and Wedepohl, 1961; Vinogradov, 1962).

In the areas of unpyritized rock, in about the northern one-third of the Copper Canyon area, the surface pattern of copper concentrations tends toward a bimodal distribution (pl. 2A). Rocks here of all formations generally not close to any major faults have copper contents of less than 50 ppm; in contrast, many breccia and gouge samples at the faults have copper concentrations that range between 200 and 700 ppm. Although many samples with relatively high copper concentrations in the unpyritized areas are spatially associated with fault zones, not all faults in these areas are characterized by high copper contents along their traces. For example, there is no concentration of copper along the traces of three of the more major faults in the area—the Plumas fault, the Hayden fault, and the Buena Vista fault; these three faults have localized lead and zinc ores with minor amounts of gold (Roberts and Arnold, 1965). These results contrast strongly with those obtained closer to the granodiorite where many samples of unfractured rock contain copper at levels greater than 700 ppm.

No systematic increase in dispersed copper was found in rocks at and near the edge of the pyritized zone. However, copper concentrations definitely increase along fault breccias just inside the zone. Indeed, as the east ore body at Copper Canyon is approached from the north along the outcrop area of the Battle Formation, the first surface shows of copper are found about 750 m north of the intrusion on faults just inside the outer margin of pyritized rock. These shows include chrysocolla, malachite, and copper oxides. Generally, such structural controls on the distribution of copper at Copper Canyon (pl. 2*A*) are more apparent than similar geochemical studies revealed at Iron Canyon (Theodore and Roberts, 1971).

We found the distribution of primary dispersed copper at Copper Canyon to be shown best by the rocks belonging to the Pumpernickel Formation that are not so intensely fractured and faulted as those of the Battle. These relatively unfractured rocks eliminated geochemical complications associated with veining along preexisting structures. Dispersed concentrations of copper in the Pumpernickel begin to increase initially to values greater than 50 ppm about 300 m north of the northern contact of the granodiorite. The northern margins of the west ore body are approximately this distance from the intrusive body.

In our geochemical studies, we also attempted to determine the original copper content of the intrusive body toward the end of its magnetic stages. From the granodiorite southeast to the Tomboy mine (pl. 2*A*), a broad area has copper concentrations generally greater than 700 ppm. Indeed, many copper analyses here are greater than 10,000 ppm. In the surface exposures of the granodiorite, there is a strong positive correlation between copper content and the intensity of green coloration in altered plagioclase phenocrysts. Clement (1968) found that plagioclase in the granodiorite has altered to halloysite and that the green color of many of these rocks reflects an adsorption of copper by halloysite. This phenomenon may be fairly common in porphyry-copper-type mining districts because Stephens and Metz (1967) report a similar occurrence at the Ray, Ariz., porphyry copper deposit. Although most copper is in the altered plagioclase phenocrysts, samples from the granodiorite at depth are invariably hydrothermally altered also. Therefore, we were not able to establish the magmatic copper content of the intrusive body at Copper Canyon. However, an unaltered intrusive body at Long Peak (fig. 3), which we infer to be similar to the Copper Canyon one at the end of its magmatic stage in fabric and original chemistry, contains copper in the 8–70 ppm range (Theodore and others, 1973).

Some copper also occurs in primary biotite at Copper Canyon. Coarse primary biotite from the intrusive body contains 100–2,000 ppm copper (Theodore and others, 1973). These values compare favorably with

those of primary biotites reported by Lovering, Cooper, Drewes, and Cone (1970, p. B8) from intrusive rocks genetically associated with porphyry copper deposits in the Pima mining district, Arizona. We suggest, however, that much of the copper at Copper Canyon is not in the biotite lattice, but rather reflects contamination by discrete chalcopyrite grains. As a comparison, biotites from the intrusive bodies at Long Peak and at the Modoc mine, which are not associated with any nearby copper deposits, contain only 5 and 7 ppm copper (Theodore and others, 1973). In an earlier study of the copper concentrations in some biotites from the Basin and Range geologic province, Parry and Nackowski (1963) argued for copper substitution for iron and magnesium in the biotite lattice. From the data available, we cannot assign any value to the copper content of the primary biotites at Copper Canyon as they initially crystallized. Determination of the copper and sulfur contents in biotite by electron microprobe methods commonly reveals chalcopyrite as an intergrown contaminant (N. Banks, oral commun., 1971).

Copper in the granodiorite occurs in two other forms. There are cuprite veins mantled by chrysocolla throughout the granodiorite, and amorphous black copper oxides also coat many fractures throughout it. Both of these copper occurrences contribute significantly to the copper anomaly in this part of the area; these copper enrichments are mainly secondary and are derived principally from the topographically higher east ore body. Distribution of copper in the east ore body also shows structural and stratigraphic controls similar to those determined throughout the Copper Canyon area (pl. 2*A*).

Finally, our geochemical map for copper at Copper Canyon indicates that chemical sampling alone would not have pointed toward either ore body as the primary target for a drilling program. Surface sampling instead focuses on the granodiorite as the most likely host for ore. Therefore, petrogenetic implications of reactive country rock should be considered early in the evaluation of a potential economic target.

The distribution pattern of copper in rocks surrounding the Mineral Park, Ariz., porphyry-type ore bodies also reflects the extreme mobility of copper in the supergene environment (Eidel and others, 1968). At the Ely, Nev., deposits, however, high copper concentrations occupy the central core of the mining district and more closely coincide with the area of hydrothermally altered rock there (Gott and others, 1965) than at Copper Canyon or Mineral Park.

## GOLD

Gold was detected in 2,081 samples, about 70 percent of those analyzed. The highest concentration of gold found was 75 ppm, and the lowest was less than 0.02 ppm. The median gold concentration in these 2,081 samples is between 0.02 and 0.1 ppm. The average abundance of gold in unaltered, unmineralized rocks at Copper Canyon is probably less than 0.02 ppm, its lower detection limit. Turekian and Wedepohl (1961) estimated the average abundance of gold in shales and sandstones to be between 0.001 and 0.009 ppm. Tung and Chi-Lung (1966) give 0.0051 ppm as the average gold content of sedimentary rocks. Various estimates of the abundance of gold in the earth's crust are in the 0.001–0.006 ppm range (Jones, 1968).

The distribution pattern for gold in the Copper Canyon area is shown on plate 2*B*. In the areas of unpyritized rock, the distribution pattern for gold is strongly controlled by faults. This relation is very similar to that found at Iron Canyon (Theodore and Roberts, 1971). At Copper Canyon in the unpyritized rocks, structural controls more strongly affect the distribution of gold than copper (compare pl. 2*A* with pl. 2*B*), primarily because of the strong concentration of gold along the Plumas and Hayden faults.

Like the distribution pattern for copper, there is no marked overall increase in gold content at the northern edge of the pyritized rock surrounding the granodiorite. In the rocks of the Pumpernickel, however, dispersed gold concentrations increase about 450–600 m south of the edge of pyritized rock, or about 300 m north of the granodiorite. Adjacent to the northern edge of the granodiorite is a 300-m-wide zone, with dispersed gold contents generally between 0.10 and 0.99 ppm, which approximately parallels the granodiorite's northern edge. This anomaly is also over the west ore body. Within this zone, gold is especially concentrated along the Copper Canyon fault and along the probable southern extension of the Buena Vista fault at the Sonderman prospects (pl. 2*B*). Gold seems to have been dispersed over a much broader zone to the west of the granodiorite. There is a gold anomaly also in the general vicinity of the Virgin and Hayden fault traces where they cross the pyrite boundary. There are many samples here whose gold contents are as much as 2.9 ppm.

Surface samples of the granodiorite contained no gold concentrations greater than 4.9 ppm, including the xenolith or intrusion breccia zone and heavily iron oxide-stained samples of sheared igneous rock along the many faults cutting the granodiorite. South of the granodiorite, gold appears to be widely dispersed at much higher concentrations than on the north. Throughout the south side of the granodiorite, however, we found no overall strong concentration of gold along faults, perhaps with the exception of a north-

striking fault-vein system at the Wilson-Independence mine and also along part of the Virgin fault just north of the old Copper Canyon underground mine (pl. 2*B*). Both of these mines were notable producers of gold (Roberts and Arnold, 1965).

### SILVER

Silver concentrations comprise detectable amounts in 2,332 of our samples, approximately 80 percent of those analyzed. Over the entire area, the median silver content of these 2,332 samples is about 1.5 ppm, with a 0.5–1,500 ppm range. About 0.065 ppm is the estimated abundance of silver in sedimentary rocks (Tung and Chi-Lung, 1966).

Generally, the distribution pattern for silver (pl. 2*C*) in the Copper Canyon area follows that of gold. Large silver concentrations are found primarily in breccias and gouge along faults, especially in the peripheral vein deposits. However, the distribution pattern for silver at Copper Canyon also differs in many ways from the patterns of gold and copper. For example, whereas both the Hayden and the Plumas faults show comparable concentrations of gold along their traces in the northern part of the area, silver appears to be much more strongly concentrated along the Plumas fault than along the Hayden. Farther to the south, the 300-m-wide zone of increased gold concentrations mantling the northern margin of the granodiorite is not reflected in the distribution pattern of silver. Instead, there seems to be a weak gain from less than 0.5 ppm to 0.5–10.0 ppm in dispersed silver concentrations just outside the pyrite envelope; this gain persists south to the granodiorite. Small zones of high silver contents, both in the granodiorite at Copper Canyon and in the wallrock south of the granodiorite, are more apparent than others for gold.

Silver concentrations in unmineralized, unaltered rocks of the Harmony and Pumpernickel Formations are generally less than 0.5 ppm. Silver concentrations in unmineralized rocks of the Scott Canyon and Battle Formations are higher, in the 0.5–10 ppm range. Dispersed silver concentrations in rocks belonging to the Pumpernickel Formation increase from north to south. The increased abundances begin about 600 m north of the boundary between unpyritized and pyritized rocks and extend to the south edge of the area (pl. 2*C*). Very high concentrations of silver were found at the Sonderman prospects, commonly greater than 50 ppm. Silver abundances generally greater than 15 ppm were detected along the entire trace of the fault-vein system at the Wilson-Independence mine. By way of comparison, the median of 43 silver analyses along the profile in the east ore body is about 3 ppm.

### OTHER ELEMENTS

Additional distribution patterns of other elements in the Copper Canyon area, to be described below in alphabetical order, are not included in this paper. Interested readers are here referred to a previously published report (Theodore, 1969) which contains the distribution patterns for Sb, As, Ba, Bi, B, Cd, Cr, Co, Pb, Mn, Hg, Mo, Ni, Sr, Sn, V, Zn in rock at Copper Canyon.

### ANTIMONY

Only 245 of the 2,927 samples analyzed at Copper Canyon contain antimony concentrations greater than 100 ppm, the lower limit of determination by the spectrographic technique. Most of the samples with detectable antimony are located north of the Copper Canyon pluton, generally very close to faults. Several samples collected at the Buena Vista mine contain antimony at concentrations of more than 1,000 ppm. Another grouping of high antimony concentrations occurs at the Meagher mine, a small lead-silver deposit that had a recorded production of 94 tons of ore between 1904 and 1935 (Roberts and Arnold, 1965, p. B55). A 150-m-wide zone with anomalous antimony concentrations extends about 600 m south from the Meagher mine; 20 rock samples in this zone contain greater than 300 ppm antimony.

The most obvious influence of structural controls on the distribution of antimony occurs at the Sonderman prospects, where anomalous antimony concentrations occur along a 450-m-strike length of a fault that is the inferred southern extension of the Buena Vista fault.

As described above, antimony is low in the east ore body; only five of 43 samples analyzed there contain more than 100 ppm antimony. They range from 200 to 3,000 ppm.

### ARSENIC

Arsenic concentrations greater than 200 ppm, its spectrographic detection limit, were found in 1,026 of the rocks analyzed from the Copper Canyon area. The arithmetic mean of arsenic in these 1,026 samples is about 2,000 ppm although the median of all samples is less than 200 ppm. In rocks several hundred feet laterally away from fault traces, dispersed arsenic concentrations apparently bear no systematic relation to pyritization. There are many reported pyrite analyses elsewhere (Fleischer, 1955; Hawley and Nichol, 1961; Espenshade, 1963) with detectable arsenic, but all of these reports show relatively low levels of arsenic concentration in pyrite. We found no direct relation between pyritization and increased arsenic contents because (1) of the low sensitivity for arsenic by the

spectrographic method employed, and (2) pyrite makes up only about 1 or 2 volume percent of the bulk of the pyritized rock. Because of the high detection limit for arsenic, we have not determined a geochemical background for arsenic.

The arsenic distribution pattern at Copper Canyon reflects a very strong control by the north-striking faults. For example, high concentrations of arsenic occur in gossans, breccia, and gouge along the Hayden, Plumas, and Virgin faults. High arsenic concentrations were found in many of the ore samples of hpyogene sulfides collected from vein deposits peripheral to the granodiorite at Copper Canyon and along these same structures listed above. Most arsenic now occurs as the mineral scorodite ($Fe_2O_3 \cdot As_2O_5 \cdot 4H_2O$), a dark-green to apple-green alteration product of hypogene arsenopyrite that was hydrothermally deposited initially along faults. This strong areal association between north-south faults and high arsenic concentrations is precisely analogous to the relation we found in the east ore body. In the east ore body, as we described above, arsenopyrite veins are restricted to narrow fault zones and veinlets through unshattered rock. The bulk of these veins postdate the matrix replacement ores in the ore body.

### BARIUM

All but five of the 2,927 samples analyzed at Copper Canyon contain barium concentrations greater than 20 ppm, the lower detection limit. Barium concentrations greater than 5,000 ppm, its upper determination limit, were found in only 34 of the rock samples analyzed. The median barium content of the samples from the Copper Canyon area is 700 ppm.

Strong barium concentrations were found in three areas at Copper Canyon: (1) an approximately 600-m-wide east-west belt north of the granodiorite, (2) a 600-m-wide northeast-striking zone between the Wilson-Independence and the old Copper Canyon underground mines, and (3) an equant 300-m-wide area on the Golconda thrust near the south edge of the area (Theodore, 1969, fig. 4).

The first of these three barium concentrations is the strongest. This area's northern edge generally parallels the boundary between pyritized and unpyritized rock north of the granodiorite. This same spatial relation between high barium concentrations and the halo of pyritized rock around the granodiorite at Copper Canyon was also found at Iron Canyon, but it is much more strongly developed there (Theodore and Roberts, 1971). At Iron Canyon, near the Iron Canyon mine, anomalous concentrations of barium result from a widespread introduction of hydrothermal celsian, concomitant with pyritization and sphalerite veining, in chert and argillite of the Scott Canyon Formation. Many samples at Iron Canyon in this zone of anomalous barium contain greater than 7,000 ppm barium.

Although some celsian at Copper Canyon occurs in the east ore body, its occurrence has not been documented in pyritized rocks of the Battle outside the ore body. Possibly, some of the barium in these rocks may be in hydrothermal K-feldspar. Other high barium concentrations along some faults result from barite occurrences. At the Sonderman prospects, barite boxworks consisting of a compact intergrowth of 0.25–0.5-cm-long tabular barite crystals are very abundant.

The elemental associations of barium in the Pumpernickel and Harmony Formations in the east-west belt at Copper Canyon have some bearing on the geochemistry of barium. Barium here has statistically significant positive associations with V, Ni, Zr, Mg, Cr, and Sc and statistically significant negative associations with Ag, As, Au, Bi, Pb, Mo, Cu, Fe, Hg, and Zn. The bulk of the latter group of elements was introduced into the rocks during epigenetic metallization. The Cu, Fe, Hg associations are in the general area of the west ore body. Accordingly, we suggest that most barium in the east-west belt at Copper Canyon is probably syngenetic and reflects the depositional environment of these rocks. The geometry of the belt perhaps fortuitously follows the pyrite envelope, or some barium may have been locally leached from the most intensely metallized areas.

Samples with high barium in the second area at Copper Canyon are distributed randomly through altered rock of the Pumpernickel Formation. These samples do not appear to be closely associated with any individual fault. However, the general outline of the area is approximately on strike with the Gulch fault.

The 1,000-ppm mean barium content of rocks in the east ore body is about the same as that throughout the Copper Canyon area. The overall distribution pattern for barium at Copper Canyon also suggests no strong barium introduction in the general area of the east ore body.

### BISMUTH

Bismuth was found in 617 of the analyzed samples at Copper Canyon; six rock samples contain greater than 1,000 ppm bismuth, the upper limit of determination. The arithmetic mean of these 617 analyses is about 80 ppm; the overall median for the samples is less than 10 ppm.

Detectable bismuth is quite sparse in the samples from the unpyritized rocks except for some collected along the Plumas and Hayden faults (Theodore, 1969,

fig. 5). Bismuth contents along these structures are commonly between 50 and 200 ppm.

In contrast, bismuth values are higher in the pyritized rocks along many faults, especially at the Sonderman prospects and along the Hayden fault just north of the east ore body. Detectable bismuth (at 50–200 ppm concentrations) seems to be dispersed through rocks of the Battle Formation, north of the east ore body. In several rock samples collected over the west ore body, bismuth concentrations are in the 50–200 ppm range. South of the granodiorite, a bismuth anomaly around the Copper Canyon underground mine and also one in the general area of the Tomboy mine result from bismuth concentrations along many of the faults there. In addition, several isolated bismuth concentrations greater than 50 ppm were found in tectonic breccias along the Golconda thrust in the southern part of the area.

From trace element studies of other workers, we can make some inferences as to the hypogene source of the bismuth anomalies at Copper Canyon. Roberts and Arnold (1965) did not find any bismuthinite, $Bi_2S_3$, which is a fairly common primary sulfide, associated with lead ores at Copper Canyon. Much of the bismuth detected in the present study probably originated as a primary trace element constituent of galena, a common association (Goldschmidt, 1954, p. 406; Marshall and Joensuu, 1961; Hall, 1971). However, the absence of even threshold concentrations of bismuth around and in sulfide ores from the Buena Vista, Meagher, and Nevada mines, all of which had important lead (galena)-silver productions, contrasts strongly with bismuth anomalies around former galena-producing mines closer to the granodiorite at Copper Canyon. Significant lead-zinc ores came from the lower levels of the Copper Canyon underground mine (Roberts and Arnold, 1965). Accordingly, much of the bismuth anomaly we find around this deposit probably is derived from these galena-rich ores. It is possible that the absence of bismuth in the galena ores from the peripheral deposits in the unpyritized areas at Copper Canyon may result from the deposition of galena ores at temperatures lower than mineralogically comparable ores in the Copper Canyon underground mine.

Interestingly, the gold-bismuth association detected in free gold from the east ore body may offer some exploration potential, especially when considered in light of the dispersed bismuth anomalies over the west ore body and the unmined extensions of the east ore body northwest of the present (1973) pit. Both of these ore bodies contain economically significant horizons of gold-bearing rock. Some of the bismuth found in rock samples from these two areas may have come from bismuth minerals associated with gold. Native gold in the east ore body contains as much as 2,000 ppm bismuth. Therefore, bismuth anomalies without any accompanying high lead should be tested carefully for gold also. Elsewhere, Fakhri (1965) found that 8–50-m-wide primary dispersion halos, centered over a site of gold deposition in Kazakhstan, were horizontally zoned from bismuth at the center to arsenic at the outer margins.

Bismuth, however, is not everywhere a good pathfinder element for gold at Copper Canyon. Even in the east ore body, only four of the 43 analyzed samples along the geochemical profile have detectable bismuth; mineralized fault breccias make up three of the samples. Of these three samples, two contain greater than 0.1 percent lead. But this profile is not through notably gold-bearing rock. More will be included about the gold-bismuth association below.

### BORON

Boron was detected in 2,321 of the samples analyzed at Copper Canyon (Theodore, 1969, fig. 6); 23 of these have boron contents greater than 2,000 ppm, the upper detection limit. Over the entire area, the median value for boron is about 20 ppm.

The southwest quarter of the Copper Canyon area, made up of altered and pyritized chert and argillite of the Pumpernickel Formation, is underlain by a broad area with anomalously high boron concentrations. Almost all boron analyses here show greater than 70 ppm, with many samples containing boron at 1,000 ppm or greater. Many of these rocks are intensely recrystallized chert that now resembles metaquartzite (Roberts, 1964). As a comparison, the average abundance of boron in this area is about one order of magnitude higher than the mean boron content in unaltered rocks of the Pumpernickel. Boron concentrations in this anomalous area are also about one order of magnitude greater than reported average boron abundances in similar fine-grained siliceous sedimentary rocks elsewhere. (See Barnett, 1961 and Turekian and Wedepohl, 1961.)

The pyritized chert of the Pumpernickel, which contains the high boron concentrations, consists of quartz, feldspar, illitic clay minerals, sparse kaolinite, and sparse hematite. The common boron-bearing mineral tourmaline was not found in these rocks. A tentative hypothesis to explain the specific occurrence of boron may involve its ionic potential. Boron has a high ionic potential (quotient of its positive ionic charge divided by its radius), and it might be precipitated as a hydroxide with illite and kaolinite (Krauskopf, 1967a, p. 593–595). The high concentration of

boron localized in the Pumpernickel may have been derived ultimately from boron-rich fluids coming from the metamorphism of some marine sedimentary beds (Barnes, 1970) much deeper than the exposed rocks at Copper Canyon.

### CADMIUM

In our geochemical studies at Copper Canyon we found only 253 samples whose cadmium contents are greater than the 20-ppm lower detection limit. Isolated high cadmium concentrations occur throughout the area (Theodore, 1969, fig. 7) and generally seem to be spatially associated with north-striking faults and also with some of the peripheral base-metal vein deposits. The greatest cluster of high cadmium concentrations occurs along an approximately 600-m-strike length of the Virgin fault, north of the Nevada mine. Many of these anomalous cadmium concentrations are near workings of the Blossom mine. Roberts and Arnold (1965, p. B58) report that primary sulfide assemblages at this mine included some sphalerite, although much of the ore consisted of secondary oxides, carbonates, and sulfates. Cadmium is a common trace element in sphalerite (Goldschmidt, 1954; Burnham, 1959; Doe, 1962; Rose, 1967). We infer that the cadmium anomaly associated with this deposit reflects the presence of sphalerite. However, there are some other areas at Copper Canyon with strong sphalerite concentrations but with no cadmium.

In the east ore body, only six of 43 samples analyzed contain more than 20 ppm cadmium. The range in these six cadmium analyses is from 30 to 500 ppm. Two of the six samples contain significant concentrations of sphalerite, with zinc contents greater than 1.0 percent. However, in the remaining four samples, there is no strong correlation between zinc and cadmium contents.

### CHROMIUM

The median value for chromium in the samples at Copper Canyon is about 70 ppm. None of the analyzed samples include chromium concentrations greater than 5,000 ppm, the spectrographic upper detection limit. Generally, the distribution pattern for chromium (Theodore, 1969, fig. 8) indicates high chromium contents in two broad, overlapping areas. In the first area, the overall abundance of chromium in unaltered chert of the Pumpernickel Formation, generally in the 70–150 ppm range, appears to be greater than that in rocks both of the Harmony and of the Battle Formations. Elsewhere, unmetallized chert and shale typically contain low concentrations of chromium, in the 1–100 ppm range (Barnett, 1961; Maxwell, 1963).

In the second area, the pyritized rocks seem to be slightly enriched in chromium with respect to the unpyritized ones, but this contrast in chromium contents between pyritized and unpyritized rocks is not so strong as that between rocks of the Pumpernickel Formation and those of the other formations. Throughout the area, there is no consistent, strong, positive spatial association of high chromium concentrations with fault traces. Indeed, many breccia and clay gouge samples along faults have chromium concentrations substantially lower than those in nearby unshattered rocks, suggesting that chromium may have been leached from some fault zones, a relation we also found in the east ore body.

Three primary biotite concentrates from the granodiorite at Copper Canyon each have a concentration of 700 ppm chromium (Theodore and others, 1973). Because most whole-rock chromium analyses in the granodiorite range between 70 and 150 ppm, we suggested that much of the chromium in the granodiorite is in biotite.

In the east ore body at Copper Canyon, chromium was detected in all 43 samples analyzed, with a 5–500 ppm range and with a median of about 70 ppm. There has been a slight overall enrichment of chromium in the mineralized rocks of the Harmony and Battle Formations, but the chromium content in the ore body is about the same as both pyritized and unpyritized rocks of the Pumpernickel Formation.

### COBALT

Cobalt was found in 1,104 of the samples analyzed from the Copper Canyon area. The median value of cobalt determined from all samples is less than 5 ppm. About 10 percent of the samples from the unpyritized rocks have cobalt concentrations greater than 20 ppm, the range of highest concentrations shown on the cobalt distribution map (Theodore, 1969, fig. 9). Cobalt is a common minor element in pyrite (Fleischer, 1955). At Copper Canyon, there is a slight increase in cobalt concentrations in many pyritized rocks of the Pumpernickel Formation near the pyrite halo. The lack of further increases of cobalt in more intensely metallized areas may be a reflection of the fact that pyrrhotite, not pyrite, is a common iron sulfide in these zones. In addition, broad areas of pyritized rock, especially in the Pumpernickel, have cobalt concentrations of less than 5 ppm. Isolated cobalt anomalies occur only along some faults. The only two areas that include widespread anomalous cobalt concentrations are at the Copper Canyon underground mine and at the south end of the east ore body.

In the east ore body, cobalt was found in 40 of 43 samples analyzed; the range is 5–500 ppm, with a

median of about 30 ppm. Much of the cobalt in the ore body undoubtedly resides in pyrite.

### LEAD

Lead was found in about 70 percent of the samples analyzed and spans the entire range of determinable lead concentrations, 10–20,000 ppm. These samples include 32 rocks whose lead contents are greater than the upper limit of determination. Throughout the Copper Canyon area, median value determined for lead is about 20 ppm. However, background lead abundances in unmineralized rocks of all formations are very low, perhaps less than 10 ppm.

In the unpyritized rocks, the distribution pattern for lead (Theodore, 1969, fig. 12) reflects very strong control by north-striking normal faults, especially the Buena Vista, Virgin, Hayden, and Plumas faults. The overall concentration of lead in the unpyritized rocks in the northern parts of the Copper Canyon area is about twice that of pyritized rocks from around the intrusive body.

Anomalous lead concentrations are significant in four areas, generally in the pyritized rocks. These anomalies are not so pronounced nor so laterally extensive as those in the unpyritized rocks. A zone of predominantly more than 700 ppm lead around the Meagher mine extends 1,400 m south to the Sonderman prospects. This zone includes both unpyritized and pyritized rocks of the Pumpernickel Formation. The second one is a broad area of 100 to greater than 700 ppm lead concentrations in pyritized rocks in the vicinity of the Hayden fault, just north of the east ore body. The third one is a strong cluster of greater than 700 ppm lead in rocks around the Copper Canyon underground mine. The fourth one is near the southwest edge of the area, where 700 ppm lead concentrations define the trace of the north-striking fault at the Wilson-Independence mine.

Roberts and Arnold (1965, p. B34) used production figures from metal deposits to establish a district-wide metal zonation. As they have shown by this technique, a lead-zinc-silver zone mantles a gold-silver zone and an inner copper-gold-silver zone near the granodiorite at Copper Canyon. The distribution pattern for lead (Theodore, 1969, fig. 12) corroborates their general location of the lead-zinc-silver boundary. However, the overall distribution of lead abundances determined in the later study (Theodore, 1969) suggests that this boundary should be moved towards the south near the Humbug–Lucky Chance mine. Production figures from the Humbug mine include about 950 ounces of gold and 214 pounds of lead (Roberts and Arnold, 1965, p. B61).

Anomalous lead concentrations contribute significantly to the primary element dispersion pattern in rocks around many of the peripheral vein deposits at Copper Canyon. The strongest anomalies are, of course, associated with those deposits that have recorded mainly lead productions in the past. Similar relations were found by Yellur (1969) around lead-zinc mineralized zones in India. However, at Copper Canyon, 1,000 ppm or greater concentrations of lead are also associated spatially with some quartz-pyrite-arsenopyrite-gold veins, for example, at the Wilson-Independence mine. At this deposit, there are apparently no lead ores.

Galena is generally very sparse in the east ore body, as we described earlier. Lead concentrations greater than 10 ppm were found in only 14 of the 43 analyzed samples along the geochemical profile, with a 10–2,000 ppm range. Two samples have greater than 1,000 ppm lead, and both of these samples are unconsolidated fault breccias with abundant iron oxides.

### MANGANESE

Manganese was found in 2,915 of the 2,927 samples analyzed from the Copper Canyon area. Only seven samples have manganese concentrations greater than the 5,000 ppm upper limit of determination. The median manganese value of these samples is about 100 ppm.

The strongest manganese concentration underlies a wide area of unpyritized rocks of the Harmony and Battle Formations in the northeastern part of the Copper Canyon area (Theodore, 1969, fig. 13), northeast of the Buena Vista and Nevada mines. In this area, manganese contents between 500 and 1,000 ppm are fairly common. Much of this probably results from the occurrence of minor amounts of manganese in the carbonate matrix of unmetamorphosed conglomerates and shales belonging to the Battle Formation and sandstones of the Harmony Formation.

The relative abundance of manganese in this area at Copper Canyon is much greater than the manganese content in other similar quartz-rich detrital rocks. Goldschmidt (1954, p. 637) noted that such rocks have generally low manganese concentrations. Turekian and Wedepohl (1961) estimate the mean abundance of manganese in sandstones to be generally between 10 and 90 ppm. Additional geochemical data suggest that calcite commonly contains abundant manganese. Ronov and Eriskina (in Graf, 1960, p. 25) note that the mean content of manganese in about 300 composite carbonate samples is about 500 ppm. Turekian and Wedepohl (1961) cite 1,100 ppm as the crustal average for manganese in carbonate rocks.

The manganese distribution map (Theodore, 1969, fig. 13) reveals no strong overall increase of manganese in the pyritized rock at Copper Canyon. A compilation of minor element abundances in sulfides by Fleischer (1955) indicates that many manganese analyses of pyrite are in the range of 1,000–5,000 ppm. Manganese is also a common trace element in sphalerite (Rose, 1967). However, where the pyrite envelope crosses Iron Canyon, northeast of Copper Canyon, the overall manganese content of the pyritized rock increases slightly, concomitant with an increase in the relative abundance of barium (celsian) and zinc (sphalerite) (Theodore and Roberts, 1971). At Copper Canyon in the pyritized rocks, a 300-m-wide area of anomalously high manganese concentrations is spatially associated with the Virgin fault. This area is just south of the granodiorite at Copper Canyon, in the general vicinity of the old Copper Canyon underground mine, and the high manganese concentrations here may reflect the sphalerite-bearing ores at the 500–700 levels. In the granodiorite itself, manganese whole-rock abundances are generally less than 300 ppm. The manganese content of primary biotite from the granodiorite is about 500 ppm (Theodore and others, 1973).

In the east ore body, we found manganese in 41 of 43 samples with a median of about 70 ppm, suggesting that manganese is not a significant trace metal in the sulfides there.

### MERCURY

Mercury was found in about 95 percent of the samples analyzed throughout the area. Eight samples have a mercury content greater than 10 ppm, the upper limit of determination. Its median value determined from all samples is about 0.07 ppm.

In the unpyritized rocks, many of the faults that localized anomalous concentrations of other elements also have high mercury concentrations along their traces (Theodore, 1969, fig. 14). These faults are the Buena Vista fault, the Virgin fault (especially north of the Nevada mine), the Plumas fault, and, at a somewhat lower level, the Hayden fault. These anomalous mercury values generally range from 0.21 to 1.0 ppm. Consistently high mercury concentrations occur along a much longer strike length of the Plumas fault than of the Hayden fault. This relation is directly analogous to the silver distribution pattern along these two structures. Background concentrations of mercury are difficult to evaluate in the unpyritized rocks, because of the numerous small metal deposits scattered throughout the area and because of the strong chalcophile nature of mercury (Goldschmidt, 1954, p. 274).

As with many of the previously described elements, no dispersed increase in the mercury content of the rocks was detected at the pyrite envelope. Conspicuous concentrations of mercury found along faults in the unpyritized rocks continue along them south into the pyritized rocks. A broad area of mercury abundances commonly in the 0.21–1.0 ppm range was found north of the east ore body, centered on the Hayden fault. The strongest mercury anomaly in the pyritized rocks occurs at the Sonderman prospects. In this area, seven samples from about 20 analyses along a 450-m-strike length of the southern extension of the Buena Vista fault have mercury contents greater than 5.0 ppm.

Mercury concentrations over most of the grandiorite at Copper Canyon are generally less than 0.21 ppm. However, there are some samples in intrusive rock from near the north margin of the granodiorite and in the adjoining metamorphosed rocks of the Pumpernickel Formation that range between 0.21 and 1.0 ppm mercury. The mercury contents of these samples define fairly well a dispersed mercury halo partly over the west ore body. By way of comparison, Vinogradov (1962) and Turekian and Wedepohl (1961) give average mercury abundances of 0.08 ppm in unmetallized felsic granites, granodiorites, and granites.

South of the granodiorite, mercury appears to be dispersed through most of the pyritized rocks at concentrations generally lower than those north of the granodiorite. Mercury concentrations at greater than 1.0 ppm along most fault traces are not conspicuous south of the granodiorite, although mercury abundances along the trace of the Golconda thrust are somewhat anomalous, commonly between 0.21 and 1.0 ppm.

Wallrock mercury anomalies are spatially associated with many of the vein deposits in both unpyritized and pyritized rock. Peripheral to the granodiorite at Copper Canyon, there are approximately equivalent, strong mercury anomalies about the Buena Vista, Nevada, Copper Canyon, and Meagher mines. Sphalerite, a sulfide that commonly includes mercury as a trace element (Jolly and Heyl, 1968), has been reported from all but the Meagher mine (Roberts and Arnold, 1965). It is likely that much of the mercury associated spatially with these deposits was originally in sphalerite.

Although mercury has been commonly considered as one of the better ore-indicator elements by Hawkes and Webb (1962), Saukov (in Jolly and Heyl, 1968), and Williston (1964), its suitability as an ore-indicator element in certain climatic environments has been questioned (Heiner and others, 1967) primarily because of its mobility. Certainly, elsewhere in Nevada, it has been established that mercury anomalies are

spatially coincident with gold deposits, although mercury anomalies may be temporally unrelated to the economic metals (Erickson and others, 1966; Wells and others, 1967; Wells and others, 1969; Wrucke and others, 1968). However, a striking exception to this common gold-mercury association was found at the Wilson-Independence mine. All samples within 600 m of this gold deposit have mercury concentrations less than its lower detection limit, 0.02 ppm. Iron oxides and the iron arsenate scorodite comprised the bulk of the gangue minerals here (Roberts and Arnold, 1965), and the primary sulfide minerals consisted of pyrite and arsenopyrite.

In the east ore body, mercury was detected in all 43 samples along the profile; five of the samples have mercury concentrations greater than 10 ppm. The median mercury content of the analyses is about 0.5 ppm, a significant contrast with the mercury concentration in rock outside the ore body. No other elements are consistently associated with mercury in those samples with the highest mercury contents in the east ore body. Mercury appears to be strongly associated with zinc and cadmium in some samples but not in others.

### MOLYBDENUM

About 32 percent of the samples analyzed in the Copper Canyon area have molybdenum concentrations greater than the 5 ppm lower detection limit. No molybdenum contents greater than its 2,000 ppm upper limit of determination were found. Over the entire area at Copper Canyon, the median value for molybdenum is less than 5 ppm. However, because of its relatively high limit of spectrographic detection, we have not here determined adequately the background concentrations of molybdenum in the area. Less than 10 percent of about 1,100 analyses in the unpyritized rocks contains molybdenum in amounts greater than 5 ppm. Reported average abundances of molybdenum in unmineralized sedimentary rocks are low. Turekian and Wedepohl (1961) indicate that 0.2 ppm is the average abundance of molybdenum in sandstones. Many reported molybdenum analyses of the Pierre Shale are less than 5 ppm (Rader and Grimaldi, 1961), although its molybdenum content does extend up to several hundred parts per million. Maxwell (1963) in another study found an average of 2.7 ppm molybdenum in 12 unmineralized cherts.

Throughout the area at Copper Canyon (Theodore, 1969, fig. 15), there is no strong, overall spatial association between north-striking normal faults and high concentrations of molybdenum, with one exception. Along a 1-km section of a north-striking fault, east of the trace of the Golconda thrust and west of the Tomboy mine in the southern part of the Copper Canyon area, molybdenum concentrations in the 15–50 ppm range are very common.

We found high molybdenum concentrations to be spatially associated with two potassic altered granodiorites. In the large Copper Canyon body, molybdenum contents greater than 15 ppm compose most of the samples. The high molybdenum abundances abruptly begin at the north edge of the granodiorite and have a maximum extent of about 0.8 km into the granodiorite's wallrock to the south. In addition, many molybdenum concentrations greater than 50 ppm were found at and near several small igneous outcrops that make up the altered granodiorite of the Wilson-Independence mine area near the west edge of the area. This granodiorite undoubtedly represents exposures of satellitic lobes from the same overall body as that exposed at Copper Canyon. Molybdenum at a 30-ppm concentration was found in only one of three primary biotite samples analyzed from the granodiorite at Copper Canyon (Theodore and others, 1973).

Unaltered igneous rocks generally have sparse abundances of molybdenum. Goldschmidt (1937) gives a 1.5 ppm average molybdenum abundance for all igneous rocks, and Rankama (1954) cites a figure of 2.5 ppm. Turekian and Wedepohl (1961) and Vinogradov (1962) give average molybdenum contents of about 1.0 ppm for felsic granites, granodiorites, and granites. The samples of the granodiorite at Copper Canyon are generally porphyritic with varying degrees of K-feldspar–sericite–(biotite) alteration of the groundmass. Samples of unaltered intrusive rock have not been found. The unaltered parts of quartz monzonites and granodiorites associated with many of the Arizona porphyry copper deposits do not appear to be enriched in molybdenum (Peterson and others, 1951; Anderson and others, 1955; Creasey, 1965).

Sparse concentrations of molybdenite ($MoS_2$) in quartz veins have sporadically been exposed in the east ore body. Geochemical data through the ore body indicate 16 of the 43 samples analyzed have determinable concentrations of molybdenum, with a range of 5–50 ppm.

### NICKEL

Nickel was found in about 90 percent of the samples analyzed in the area. The average abundance of nickel in those samples is about 25 ppm. None of the samples have nickel concentrations greater than the upper limit of determination, 5,000 ppm. Nickel is an element that commonly accompanies magnesium, iron, and cobalt because of the similarities in their divalent ionic radii (Goldschmidt, 1954). Accordingly, nickel abundances

in dunites, peridotites, pyroxenites, and norites (Turekian and Wedepohl, 1961; Vinogradov, 1962) typically are about 100 times the abundances of nickel found at Copper Canyon.

Concentrations of nickel greater than 50 ppm, the highest range in nickel contents shown on the distribution map (Theodore, 1969, fig. 16), irregularly occur throughout the unpyritized rocks. However, most nickel concentrations in the unmineralized and unpyritized rocks are generally less than 20 ppm. There is also no strong spatial association between high nickel concentrations and the north-striking faults that localized so many other elements. In addition, we found no strong spatial association between high nickel concentrations and the peripheral lead-zinc vein deposits in the unpyritized zone. However, many samples with nickel concentrations greater than 50 ppm do define a 600-m-wide approximately east-west zone that lies astride the boundary between the unpyritized and pyritized rocks.

The pyritized rocks do not show a general overall increase in nickel concentrations when they are compared to the unpyritized rocks. Approximately 90 percent of about 1,000 pyrite analyses tabulated by Fleischer (1955) include minor amounts of nickel. However, the abundance of pyrite dispersed at Copper Canyon is probably too low to reflect any original nickel sulfide solid solution in the whole rock spectrographic analyses.

We did find a nickel anomaly associated with one base metal deposit in pyritized rock. There are increased nickel abundances in rocks generally within a 300-m radius of the old Copper Canyon underground mine (Theodore, 1969, fig. 16).

In the granodiorite at Copper Canyon, whole-rock nickel abundances are generally less than 50 ppm. Turekian and Wedepohl (1961) and Vinogradov (1962) give average abundances of nickel between 4 and 15 ppm for felsic granites and granodiorites, and granites. Biotite analyses suggest that much of the nickel in the granodiorite at Copper Canyon is in primary phenocrystic biotite (Theodore and others, 1973); nickel contents in all biotite samples range from 150 to 200 ppm. In granitoid rocks elsewhere, seven of 55 biotite analyses tabulated by Lovering (1969) have nickel contents as great as, or greater than, the nickel content of biotites from the granodiorite at Copper Canyon. However, the nickel contents of 34 biotites from granitic and mafic rocks of the Sierra Nevada batholith (Dodge and others, 1969) are all less than the nickel content of biotites from Copper Canyon.

Nickel was found in all 43 samples analyzed along the profile through the east ore body (fig. 40), with a 5–300 ppm range and a median of about 50 ppm, which suggests about a threefold overall increase in nickel concentrations during metallization. The strong positive association between nickel and zinc found along the geochemical profile (fig. 40) also suggests that some nickel may be in sphalerite. Minor amounts of nickel in sphalerite have been found elsewhere (Doe, 1962; Jolly and Heyl, 1968). Nickel is also reported in about one-half of the chalcopyrite analyses tabulated by Fleischer (1955). Although nickel is a common minor element in pyrrhotite (Fleischer, 1955), the geochemical profile (fig. 40) does not reflect any strong increased abundances of nickel in rocks from the pyrrhotite-rich zone, although we found traces of nickel in pyrrhotite grain separates analyzed by X-ray spectroscopic methods.

### STRONTIUM

Strontium, in determinable amounts, was found in 788 of 2,927 samples analyzed from the Copper Canyon area, about 25 percent of the samples. The lower limit of spectrographic detection for strontium is 100 ppm. The arithmetic mean of the strontium concentrations in these 788 samples is about 200 ppm, with a 100–1,500 ppm range. The median value of strontium for all samples in the area is less than 100 ppm. The reported average abundance of strontium in sandstones and shales (Turekian and Wedepohl, 1961) is 20 and 300 ppm, respectively.

In the unpyritized rocks, sporadic strontium concentrations greater than 200 ppm are found along the north-south faults (Theodore, 1969, fig. 18). However, these high strontium values are very local and do not in themselves define the fault traces. In addition, there are no areas of high strontium concentrations associated with the lead-zinc vein deposits in the unpyritized areas.

In the pyritized rocks, strontium also does not commonly outline the normal faults. However, one exception is the north-striking fault at the Wilson-Independence mine which is fairly well defined by strontium generally greater than 200 ppm along its entire length.

We found that the broadest zone of strontium concentrations coincides with the area where the granodiorite at Copper Canyon is exposed. The abundance of strontium in this altered granodiorite is consistent with average strontium abundances in such rocks (Vinogradov, 1962; Turekian and Wedepohl, 1961). Theodore, Silberman, and Blake (1973), however, have shown that strontium in five unaltered granodiorites in the Battle Mountain mining district is in

the 490–640 ppm range. These values are about three times greater than those that we found in the altered granodiorite at Copper Canyon. Therefore, although strontium forms a geochemical high in the granodiorite at Copper Canyon relative to its wallrock, strontium has actually been depleted from its magmatic concentrations during the subsequent potassic alteration. This depletion is not unexpected, because strontium usually follows calcium, which apparently was lost during alteration. Theodore, Silberman, and Blake (1973) have shown increases in Rb:Sr ratios with increasing intensity of potassic alteration for intrusive bodies in the general area of Copper Canyon.

Two other approximately 300-m-wide areas of anomalously high strontium percentages were also found—one centered about 300 m northwest of the northwest corner of the granodiorite and the other about 600 m northeast of the Tomboy mine. These two areas of anomalously high strontium concentrations in rocks of the Pumpernickel and Harmony Formations, respectively, may be indicative of small igneous bodies at depth.

### TIN

Tin values greater than 10 ppm were found in only 740 of the samples analyzed, with a 10–700 ppm range. The distribution of tin is very irregular (Theodore, 1969, fig. 19) and does not suggest that structural controls strongly affected its overall distribution here. Other geochemical studies (Theodore and Roberts, 1971) indicate that at Iron Canyon marked concentrations of tin do occur along certain north-striking faults near the edge of the pyritized rock, where it crosses Iron Canyon. However, at Copper Canyon, we found only slight increases to as much as 70 ppm in tin along the trace of one fault, the Plumas, but many of the other tin values in the 30–70 ppm range are restricted to small areas around the peripheral vein deposits. At the Copper Canyon underground mine, many samples have tin contents in the 30–70 ppm range, and breccias along several faults near the Tomboy mine have tin concentrations greater than 70 ppm. These tin concentrations, however, are not uniformly distributed along the faults there.

There is no general increase in tin in the samples from the altered granodiorite at Copper Canyon. Tin concentrations in this body of rock span the entire range of tin values found in the surrounding wallrocks. By comparison, early estimates of the average abundance of tin in all igneous rocks were about 40 ppm (Goldschmidt, 1937; Rankama, 1954). On the basis of limited geochemical data, Goldschmidt (1954) inferred even higher tin concentrations in granitic rocks. However, later estimates of the average abundance of tin in granitic rocks were revised downward to 1–3 ppm (Turekian and Wedepohl, 1961; Vinogradov, 1962).

In the east ore body, tin was found in ten of the 43 analyzed samples. These ten samples have tin concentrations from 10 to 50 ppm.

### VANADIUM

Vanadium in the range 10–10,000 ppm was found in 2,901 of the samples analyzed at Copper Canyon, with a median value of about 70 ppm. Unpyritized rocks of the Pumpernickel Formation in the northwest part of the area (Theodore, 1969, fig. 20) generally contain vanadium at less than 70 ppm. This part of the Copper Canyon area comprises a broad geochemical vanadium low. Throughout the area, however, the bulk of the samples have vanadium in the 70–150 ppm range. By comparison, the average abundance of vanadium in shales is about 130 ppm, and in sandstone, about 20 ppm (Turekian and Wedepohl, 1961).

Three zones, across which vanadium is dispersed at concentrations commonly greater than 150 ppm, were found at Copper Canyon. One of these near the northeast corner of the area is primarily in rocks belonging to the Scott Canyon Formation, which is in part made up of black carbonaceous shale and argillite. Thin films of carbonaceous material, dominantly amorphous carbon with perhaps some graphite along bedding planes, make up about 3 weight percent of many of these rocks (Theodore and Roberts, 1971). The average abundance of vanadium in rocks of the Scott Canyon Formation is about 200 ppm. Black organic-rich shales commonly have relatively high vanadium contents (Vine and Tourtelot, 1969).

The other two zones of anomalous vanadium at Copper Canyon are in pyritized rock south of the granodiorite. The larger of these two zones is entirely within the Pumpernickel Formation and is made up of numerous samples whose vanadium content is greater than 150 ppm. The zone extends southwest from the granodiorite to the edge of the area. Much of this zone of high vanadium concentrations coincides with the area of high boron contents described above. The smaller of the two zones is about 600 m wide and occurs around the Tomboy mine.

It is possible that some vanadium in these rocks occurs as a minor element in iron sulfides. Many investigators have found that pyrite, arsenopyrite, and pyrrhotite all contain varying amounts of vanadium (Fleischer, 1955). Carstens (in Fleischer, 1955, p. 1007) reported, however, that minor amounts of vanadium in pyrite are found primarily in sedimentary pyrites. Serkies, Oberc, and Idzikowski (1967) found a positive correlation between vanadium and copper concentrations in drill cores through copper deposits at the Lena mine in southwest Poland.

Whole-rock vanadium analyses of the granodiorite at Copper Canyon are generally in the 70–150 ppm range. Semiquantitative spectrographic analyses of biotites from the granodiorite (Theodore and others, 1973) indicate vanadium contents of its primary biotite to be 700 ppm, suggesting that much of the vanadium in these rocks is in biotite. Vanadium of 34 biotites in mafic and granitic rocks from the Sierra Nevada batholith has a 40–500 ppm range in composition (Dodge and others, 1969); this is much less than the biotites at Copper Canyon. In addition, the overall abundance of vanadium in the granodiorite is higher than the 40 ppm average abundance of vanadium in felsic granites and granodiorites (Vinogradov, 1962) and probably higher than the 88 ppm average abundance of vanadium in calcium-rich granites (Turekian and Wedepohl, 1961).

In the east ore body, vanadium was found in 39 of 43 samples; it has a 10–300 ppm range and an arithmetic mean of about 150 ppm. Vanadium contents outside the pyrrhotite zone in the ore body are generally higher than those within the zone.

### ZINC

Zinc has a spectrographic lower detection limit of 200 ppm and accordingly was found in only about 27 percent (795) of the 2,927 samples analyzed throughout the Copper Canyon area. Ten samples have zinc concentrations greater than its 10,000 ppm upper limit of determination. Crustal abundances of zinc in unmineralized rock have been fairly well established. Its abundances in shales and sandstones are 95 and 16 ppm, respectively (Turekian and Wedepohl, 1961). Abundances in felsic granites and granodiorites and high calcium granites are about 60 ppm, and in low calcium granites, about 39 ppm (Turekian and Wedepohl, 1961; Vinogradov, 1962). However, zinc abundances in black shales are somewhat higher than these concentrations (Vine and Tourtelot, 1969).

Zinc anomalies are conspicuous in the unpyritized areas at Copper Canyon. The trace of the Virgin fault in the unpyritized rocks is well defined by high zinc concentrations along it (Theodore, 1969, fig. 21). These high concentrations contrast, however, with generally sparse concentrations of zinc along the nearby Hayden and Plumas faults. This major anomaly along about a 900-m strike length of the Virgin fault in the unpyritized rocks is made up of zinc concentrations greater than 1,000 ppm. It is centered at the Blossom mine workings. In addition, a zinc anomaly of similar intensity, but over a much smaller area, occurs at the Nevada mine about 0.8 km to the south of the Blossom mine. Zinc also forms recognizable anomalies at the Buena Vista and Meagher mines and is widely dispersed about these mines. Many unpyritized rocks collected at varying distances from the mines contain zinc in the 200–700 ppm range.

Dispersed zinc concentrations of similar value were not found to be commonly disseminated in the pyritized rock. Nonetheless, some isolated zinc occurrences greater than 1,000 ppm were found in samples along some faults within the pyritized areas, primarily in the Virgin fault zone, south of the granodiorite, around the Copper Canyon underground mine. All of the above described zinc anomalies, both in the pyritized and unpyritized areas, are spatially associated with deposits that show zinc production or occurrences (Roberts and Arnold, 1965).

Zinc in the granodiorite at Copper Canyon is generally present at levels less than 200 ppm. Whole-rock determinations of the zinc content of 10 samples of the granodiorite by atomic absorption spectroscopy (Theodore and others, 1973) were in the 60–420 ppm range, with an arithmetic mean of 110 ppm. In that same study, no zinc was found at a 200-ppm detection limit in primary biotite grain concentrates from the granodiorite.

In the east ore body, zinc was found in 30 of 43 samples (fig 38). Zinc concentrations here range from less than 200 ppm, to greater than 10,000 ppm, with an average of about 500 ppm in these 30 samples.

## PRIMARY DISPERSED ELEMENT DISTRIBUTIONS

The rocks of the Pumpernickel Formation show fairly well zoned distributions that are related spatially to the granodiorite at Copper Canyon. These zonal distributions must reflect to some degree primary element dispersions about the granodiorite because of the minimal development of supergene clays in these rocks. Figure 44 summarizes the distributions of Ag, Au, Bi, Co, Cu, Hg, Mo, Pb, Sr, and Zn, whose concentrations show a zonal distribution around the granodiorite. This figure is a synoptic geochemical profile from north to south, through the northern part of the granodiorite, the adjoining pyritized rocks of the Pumpernickel, and the bordering unpyritized ones; the profile also passes through the west ore body. The relative strength of the individual element zones in figure 44 was determined by comparing the concentration of each element around the granodiorite and ore bodies with its concentration in unmetallized rocks in the northern part of the area. An attempt has been made on this profile to delete metal concentrations related to the peripheral vein deposits. Furthermore, we should emphasize that the profile is ideal and includes geochemical data projected to it from many tens of meters away.

The geochemical profile (fig. 44) that we have devel-

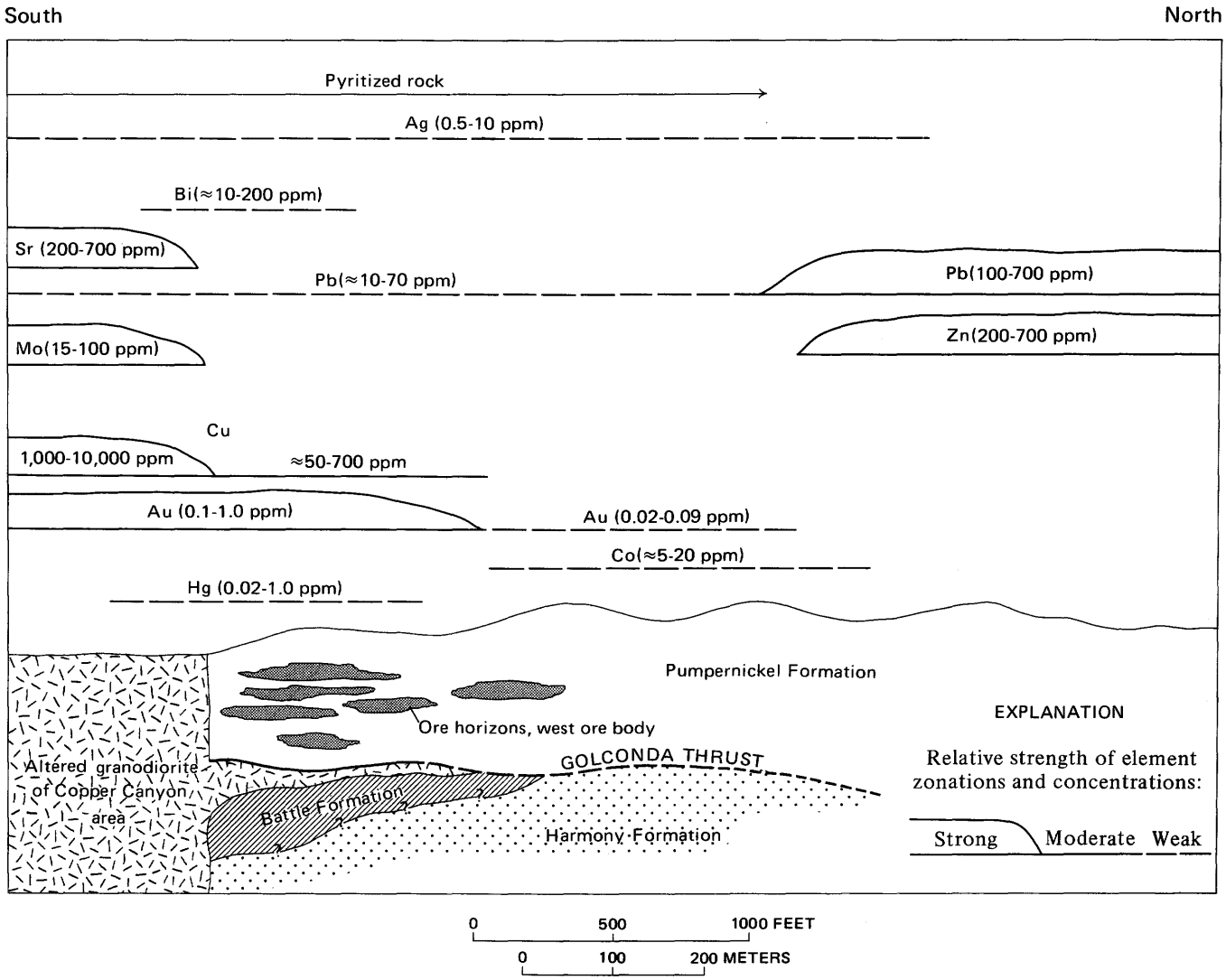


FIGURE 44.—North-south idealized geochemical profiles for dispersed Ag, Bi, Ba, Ni, Pb, Zn, Mo, Sr, Cu, Au, and Co concentrations adjacent to the altered granodiorite of Copper Canyon.

oped at Copper Canyon is not too different from that proposed by Jerome (1966) as occurring over many of the "typical" porphyry copper deposits. The Copper Canyon porphyry copper deposit, however, is a porphyry deposit only in the mining sense. Almost all known ore, as we have described above, is in wallrock, some up to 600 m laterally from the nearest exposure of the intrusion at Copper Canyon. According to Stringham (1966), the ore in 12 of 24 porphyry copper deposits is almost exclusively restricted to the intrusive rocks themselves. Two other porphyry copper deposits at Mission and Pima, Ariz. have altered wallrock as the dominant host for ore. Lowell and Guilbert (1970) also compiled data on 27 porphyry copper deposits and noted that, in their "typical porphyry copper" deposit, 70 percent of the ore body occurs in an igneous host rock. The ore deposits at Mission and Pima comprise sulfide replacements of silicate contact metamorphic minerals (Kinnison, 1966; Himes, 1972), a relation similar to parts of the Copper Canyon deposit. However, their geochemical characteristics are not available for comparison. Huff (1970) concluded from a geochemical study of soils developed on the surficial 60-m-thick conglomerates capping the copper deposits at Pima that sparse copper and molybdenum concentrations were most likely derived from small copper deposits other than the Pima deposit.

We must emphasize again that chemical sampling for copper alone around the Copper Canyon deposits would point toward the granodiorite as the most likely host for ore because of the concentration of secondary copper there. The economic hypogene sulfide zones in these deposits are instead found in the country rock near the granodiorite. Suitable pathfinders for these

zones might be mercury and potassium and increases in the Rb:Sr ratio (Theodore and others, 1973).

## STATISTICAL EVALUATION OF ELEMENT ASSOCIATIONS

One aim of this part of the study is to document changes in element association from environments of lead-zinc-silver vein-type metallization to predominantly dispersed or replacement copper-gold-silver metallization. A secondary objective is to investigate promising pathfinder elements for metals of economic interest.

Strengths of association between variables are usually determined by Pearson, or product moment, correlation, Spearman or Kendall rank correlation, and analysis of variance techniques. The product moment method, which is the most commonly used requires bivariate normal distributions between the variables being compared (Dixon and Massey, 1951; Lovering and others, 1968). After first performing a log transformation for all element concentrations found in the samples at Copper Canyon, we prepared histograms to show diagrammatically the types of element distributions (fig. 45). These histograms include the percent frequency that concentrations were found to be less than their respective lower detection limits for each of the elements. After log transformation, the overall distributions for iron, magnesium, titanium, barium, zirconium, and possibly calcium at Copper Canyon tend toward a normal population distribution. From a visual inspection, of all the transformed element distributions, mercury, chromium, vanadium, and manganese most closely approximate a lognormal distribution. Many of the other elements have very apparent nonnormal frequency distributions that very likely extend well beyond their lower detection limits. Because of the many problems involved in determining abundances from censored data sets (Miesch, 1967), population arithmetic means were estimated by Sichel's (1952) methods for only the ten elements listed above; median values are shown for all elements on figure 45 Although analyses reported as greater than the upper limit of determination make up a small percentage of the total number of analyses for many elements (table 12), they nevertheless should be considered in the calculations. Therefore, the numerical value at the upper limit of determination was substituted for those results in all statistical computations. Ahrens (1954, 1957, 1963) believes that many elements, especially those in igneous rocks, tend toward a lognormal-type distribution. However, others (Chayes, 1954; Aubrey, 1956) question this conclusion.

The aforementioned characteristics of the chemical data at Copper Canyon would weaken or invalidate product moment computations of strengths of association between some elements. Therefore, to test this possibility, the strength of association between gold and all other elements was determined by both product moment and Spearman's nonparametric rank correlation techniques (table 13). Spearman's rank correlation test makes no assumptions about the population distribution (Siegel, 1956, p. 202–213). In all Spearman rank correlation coefficient ($r_s$) tests described below, corrections for tied observations, that is, samples with equal concentrations, have been incorporated into the computer calculations, as suggested by Siegel (1956) and Flanagan (1957). Furthermore, we do not imply that the $r_s$ values should be inferred to be good estimates for total population correlation coefficients. Rank correlation tests may be applied only to the raw data. As an added problem, we were not able to analyze the entire geochemical data matrix from Copper Canyon by the Spearman method, because of computer core limitations (G. Van Trump, oral commun., 1970). Therefore, comparisons between the Spearman and product moment evaluations for the same sets assume additional relevance.

From table 13, the Spearman part of the gold association analysis for all chemical data from Copper

TABLE 13.—*Spearman and product moment correlation coefficients for gold versus all other analyzed elements at Copper Canyon*

| Element | Spearman | | | Product moment |
|---|---|---|---|---|
| | Degrees of freedom | Significance test | Correlation coefficient | Correlation coefficient |
| Iron | 2,079. | 23.420 | 0.4569 | 0.4862 |
| Magnesium | 2,061. | —11.501 | — .2456 | — .2610 |
| Calcium | 1,936. | — 3.865 | — .0875 | — .0670 |
| Titanium | 2,077. | — 6.503 | — .1413 | — .1316 |
| Manganese | 2,067. | — 8.803 | — .1901 | — .1643 |
| Silver | 1,870. | 28.059 | .5443 | .5930 |
| Arsenic | 973. | 21.548 | .5684 | .5726 |
| Boron | 1,563. | — 5.536 | — .1387 | — .0634 |
| Barium | 2,076. | — 9.180 | — .1975 | — .1970 |
| Beryllium | 787. | 1.921 | .0683 | .0708 |
| Bismuth | 591. | 15.534 | .5384 | .5488 |
| Cadmium | 223. | 3.200 | .2096 | .2322 |
| Cobalt | 695. | 1.727 | .0654 | .1128 |
| Chromium | 2,066. | — .001 | .0003 | — .0020 |
| Copper | 2,069. | 15.965 | .3312 | .2735 |
| Lathanum | 938. | 7.557 | .2396 | .2789 |
| Molybdenum | 831. | 3.588 | .1235 | .1368 |
| Niobium | 711. | — .718 | — .0269 | — .0075 |
| Nickel | 1,837. | — 2.254 | — .0525 | — .0365 |
| Lead | 1,575. | 18.614 | .4246 | .4656 |
| Antimony | 234. | 5.799 | .3545 | .3560 |
| Scandium | 1,526. | — 4.073 | — .1037 | — .0761 |
| Tin | 685. | 10.862 | .3833 | .3974 |
| Strontium | 632. | 3.460 | .1363 | .1772 |
| Vanadium | 2,063. | — .069 | — .0151 | — .0052 |
| Tungsten | 154. | 2.600 | .2051 | .1936 |
| Yttrium | 1,687. | 2.396 | .0582 | .1111 |
| Zinc | 631. | 6.581 | .2534 | .2629 |
| Zirconium | 2,045. | — 8.924 | — .1936 | — .1995 |
| Mercury | 1,748. | 12.395 | .2842 | .3909 |

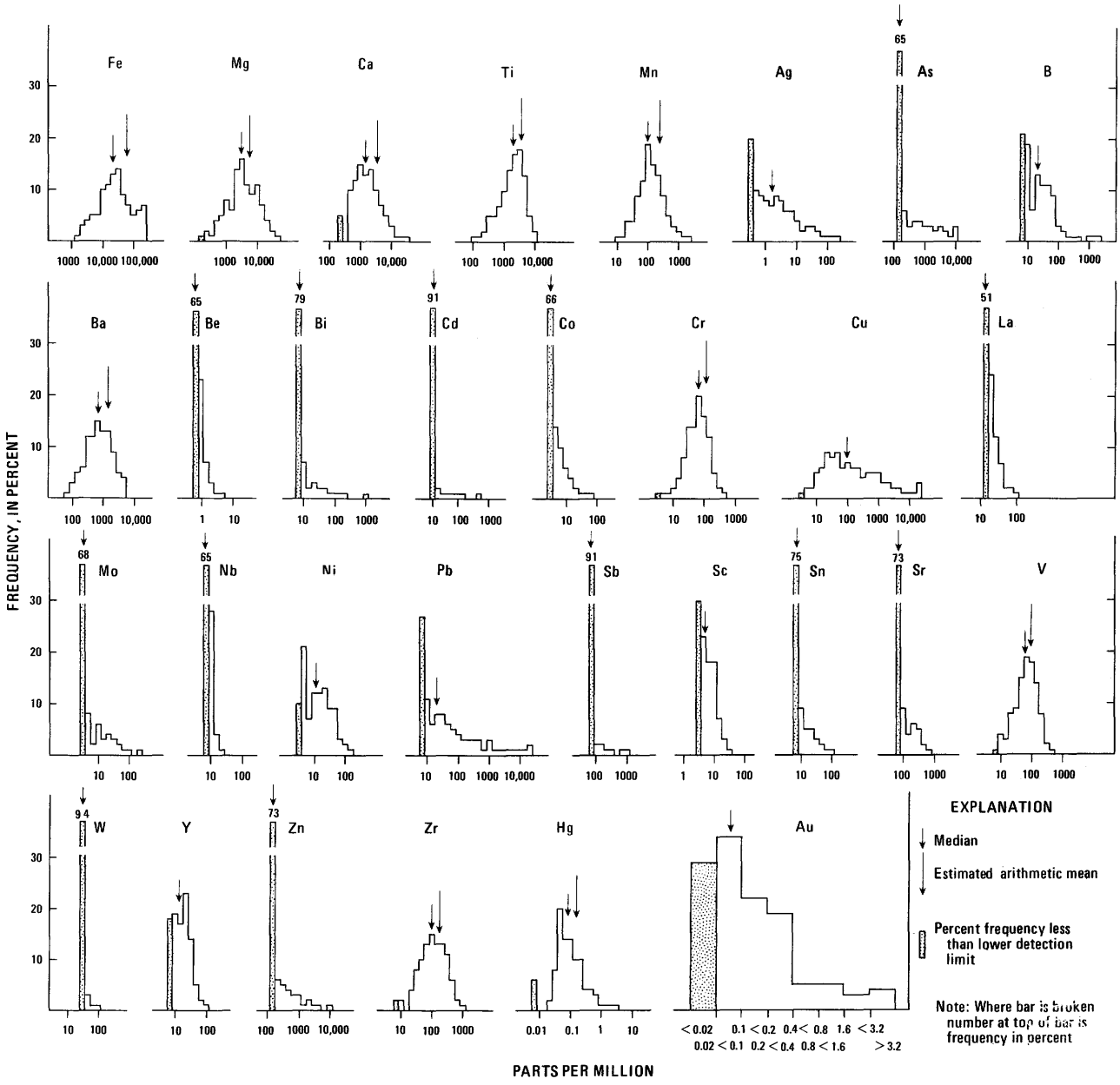


FIGURE 45.—Percent frequency distribution of 31 elements in 2,927 rock samples from the Copper Canyon area.

Canyon indicates that silver, iron, arsenic, lead, copper, bismuth, and mercury (listed in order of decreasing statistical significance) are the elements with the strongest positive associations with gold. Silver, arsenic, and bismuth have positive Spearman coefficients of correlation greater than 0.5000. Magnesium and barium have the strongest negative Spearman coefficients of correlation with gold, whereas chromium shows no association, positive or negative, with gold.

When the strengths of association among all log-transformed chemical data were determined by product moment techniques, we found that silver, arsenic, bismuth, iron, lead, and mercury all have coefficients of correlation for gold greater than 0.3900 (table 13); these are the same elements, minus copper, that Spearman's technique correlated most strongly with gold. The substantial deviation of copper's distribution from a normal population (fig. 46) may account for its absence here. Accordingly, we suggest that the entire chemical data set at Copper Canyon is amenable to at least a qualitative product moment analysis. Therefore, we selected all product moment coefficients of correlation absolutely greater than 0.3700 to estimate the strongest positive element associations within the

entire data matrix at Copper Canyon. These associations, together with all numbers of pairs of elements involved in the calculations, are shown in table 14. Elsewhere, Fenner and Hagner (1967) also used normal distribution correlation statistics to evaluate nonnormal distributions.

The values of the correlation coefficients symbolically represented (table 14) range from a positive 0.74 for zirconium-titanium to a negative 0.38 for antimony-tungsten. However, the latter figure is based on only 25 element pairs, whereas the former involves 2,882 pairs.

From table 14, it is apparent that many economically important metals are strongly associated with one another. The association of gold with other elements has been described above. Copper is strongly associated with iron, silver, and, unexpectedly, lanthanum. Silver has strong affinities for iron, arsenic, gold, bismuth, copper, lead, antimony, tin, and mercury. In addition, the minor element bismuth is strongly associated with iron, silver, and gold, reinforcing our earlier suggestion that bismuth might be a good indicator or pathfinder element for gold and silver. At Iron Canyon, a similar gold-bismuth association was determined by similar statistical methods for pyritized rocks of the Scott Canyon Formation; bismuth-bearing gold was also found in placer gold there (Theodore and Roberts, 1971). However, one of the conclusions of that study is that element associations vary across even relatively small geologically different areas. Accordingly, we then determined the strongest element associations for copper, gold, and silver at Copper Canyon for various areas, partitioned on the basis of geology and metal production (fig. 46).

As shown, figure 46 is made up of 11 rather small areas, within each of which at least 185 rock samples were analyzed as described above. The element associations in each of these areas were determined by Spearman's techniques. Critical values of Spearman's correlation coefficients, above which statistical significance can be inferred, for even 30 observations are numerically fairly low: 0.306 at the 95 percent confidence level and 0.432 at the 99 percent confidence level (Dixon and Massey, 1951, p. 261). Therefore, in order to better approach geologic significance, only those associations that have a minimum $r_s$ value of 0.5049 and that are based on calculations involving at least 50 element pairs are shown. The range of positive $r_s$ values in these 11 areas (fig. 45) is from 0.5049 to 0.9104; the 0.9104 value is for silver-lead in area 3. Those elements associated with copper, gold, and silver in each area are listed on figure 45 in order of decreasing statistical significance, determined by standard Student's $t$ tests. At the 95 percent confidence level, $t$ values for these 75 element pairs range from two to

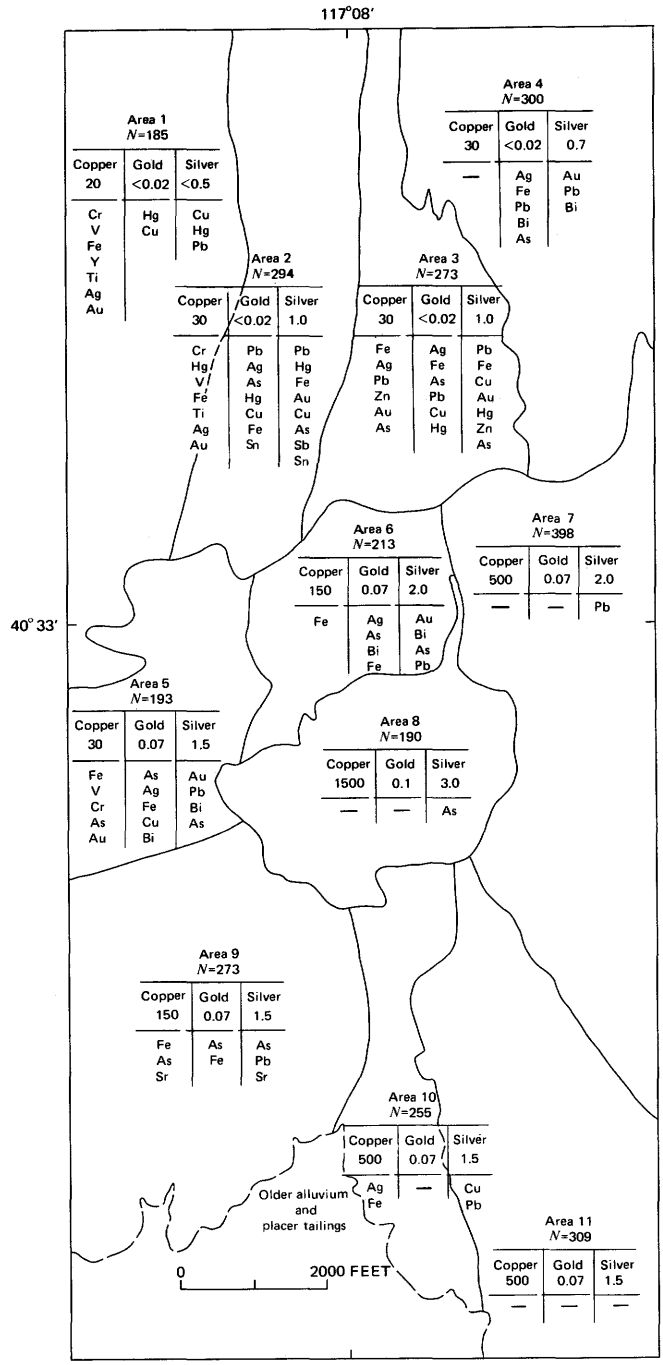


FIGURE 46.—Median values for copper, gold, and silver in parts per million, and elements strongly associated with copper, gold, and silver in 11 partitioned areas at Copper Canyon, Lander County, Nev. Element associations, determined by Spearman techniques (see text), are listed in order of decreasing statistical significance. All element associations have a greater than 0.5049 positive Spearman correlation coefficient, and all correlation calculations are based on at least 50 element pairs. N is the number of samples collected within each area.

TABLE 14.—*Array of numbers of paired-element analyses and product*

[XX, greater than 0.3700; X, between 0.3700 and 0.1000; – less than

| | Log (Fe) | Log (Mg) | Log (Ca) | Log (Ti) | Log (Mn) | Log (Ag) | Log (As) | Log (Au) | Log (B) | Log (Ba) | Log (Be) | Log (Bi) | Log (Cd) | Log (Co) |
|---|---|---|---|---|---|---|---|---|---|---|---|---|---|---|
| LoG (Fe) | 0.0 | – | – | X | – | XX | XX | XX | –X | – | X | XX | – | X |
| LoG (Mg) | 2908. | 0.0 | XX | XX | XX | –X | –X | –X | – | XX | –X | –X | –X | – |
| LoG (Ca) | 2772. | 2762. | 0.0 | – | – | –X | X | – | – | – | – | – | – | – |
| LoG (Ti) | 2924. | 2906. | 2770. | 0.0 | – | – | –X | –X | – | XX | –X | –X | –X | – |
| LoG (Mn) | 2915. | 2901. | 2764. | 2913. | 0.0 | – | – | –X | – | – | – | –X | – | X |
| LoG (Ag) | 2332. | 2317. | 2198. | 2330. | 2321. | 0.0 | XX | XX | –X | –X | – | XX | X | X |
| LoG (As) | 1026. | 1013. | 968. | 1024. | 1017. | 1002. | 0.0 | XX | –X | – | – | – | X | – |
| LoG (Au) | 2081. | 2063. | 1938. | 2079. | 2069. | 1872. | 975. | 0.0 | – | –X | – | XX | X | X |
| LoG (B) | 2321. | 2315. | 2223. | 2319. | 2315. | 1797. | 853. | 1565. | 0.0 | – | – | – | –X | –X |
| LoG (Ba) | 2922. | 2903. | 2767. | 2920. | 2911. | 2327. | 1022. | 2078. | 2318. | 0.0 | –X | – | –X | –X |
| LoG (Be) | 1017. | 1007. | 971. | 1016. | 1015. | 815. | 431. | 789. | 829. | 1015. | 0.0 | – | – | X |
| LoG (Bi) | 617. | 606. | 585. | 615. | 606. | 610. | 443. | 593. | 463. | 615. | 240. | 0.0 | – | X |
| LoG (Cd) | 253. | 251. | 246. | 253. | 253. | 246. | 202. | 225. | 192. | 253. | 117. | 80. | 0.0 | X |
| LoG (Co) | 1104. | 1094. | 1051. | 1103. | 1099. | 772. | 298. | 697. | 849. | 1101. | 542. | 205. | 122. | 0.0 |
| LoG (Cr) | 2911. | 2895. | 2759. | 2910. | 2900. | 2317. | 1018. | 2068. | 2314. | 2908. | 1010. | 613. | 248. | 1097. |
| LoG (Cu) | 2900. | 2881. | 2745. | 2898. | 2888. | 2321. | 1026. | 2071. | 2296. | 2895. | 1015. | 617. | 253. | 1096. |
| LoG (La) | 1431. | 1427. | 1348. | 1431. | 1427. | 1053. | 405. | 940. | 1198. | 1430. | 611. | 266. | 84. | 689. |
| LoG (Mo) | 932. | 926. | 887. | 930. | 927. | 889. | 475. | 833. | 664. | 929. | 424. | 303. | 115. | 345. |
| LoG (Nb) | 1013. | 1011. | 967. | 1013. | 1013. | 789. | 322. | 713. | 851. | 1011. | 489. | 234. | 74. | 463. |
| LoG (Ni) | 2638. | 2626. | 2524. | 2635. | 2633. | 2081. | 903. | 1839. | 2097. | 2633. | 980. | 518. | 243. | 1084. |
| LoG (Pb) | 2123. | 2109. | 2033. | 2121. | 2111. | 1840. | 925. | 1577. | 1703. | 2119. | 800. | 554. | 244. | 652. |
| LoG (Sb) | 245. | 237. | 232. | 244. | 240. | 243. | 239. | 236. | 194. | 245. | 103. | 129. | 89. | 64. |
| LoG (Sc) | 2060. | 2054. | 1942. | 2060. | 2054. | 1647. | 736. | 1528. | 1637. | 2059. | 938. | 462. | 190. | 954. |
| LoG (Sn) | 740. | 732. | 678. | 739. | 734. | 715. | 443. | 687. | 570. | 737. | 312. | 305. | 122. | 244. |
| LoG (Sr) | 788. | 785. | 784. | 788. | 781. | 679. | 332. | 634. | 574. | 788. | 379. | 233. | 98. | 385. |
| LoG (V) | 2901. | 2889. | 2752. | 2899. | 2890. | 2313. | 1017. | 2065. | 2308. | 2896. | 1009. | 610. | 251. | 1098. |
| LoG (W) | 162. | 160. | 146. | 162. | 160. | 156. | 118. | 156. | 129. | 161. | 72. | 88. | 26. | 74. |
| LoG (Y) | 2414. | 2402. | 2300. | 2413. | 2409. | 1913. | 833. | 1689. | 1952. | 2411. | 920. | 490. | 221. | 1009. |
| LoG (Zn) | 795. | 788. | 772. | 793. | 792. | 721. | 439. | 633. | 620. | 790. | 379. | 199. | 218. | 396. |
| LoG (Zr) | 2882. | 2870. | 2732. | 2882. | 2874. | 2299. | 1001. | 2047. | 2290. | 2878. | 1002. | 601. | 244. | 1087. |
| LoG (Hg) | 2448. | 2429. | 2307. | 2445. | 2436. | 1959. | 845. | 1750. | 1914. | 2443. | 839. | 557. | 218. | 921. |

15 times greater than threshold $t$ values for the degrees of freedom involved. Throughout the 11 areas, $t$ values for the 75 pairs average about four times greater than their corresponding thresholds. In addition, the copper:gold:silver ratio may be roughly approximated for the 11 areas, from estimates of median values for copper, gold and silver in each of the 11 areas.

Areas 1 through 4 (fig. 46) are underlain by unpyritized rock, whereas areas 5 through 11 are underlain by pyritized rock. Area 8 is underlain by the altered intrusion at Copper Canyon. Most of the east ore body is in area 7, and the west ore body is predominantly in area 6.

Before discussing in detail the variability of elements associated with copper, gold, and silver across the Copper Canyon area, we should first look at the variation of copper, gold, and silver median values determined for samples from the 11 areas (fig. 46). The values suggest that silver:gold ratios are fairly uniform across seven areas underlain by pyritized rock. The ratios in these seven areas are in the 20–30:1 range. The ratio of silver:gold produced from the entire mining district up to 1961 is about 13:1 (Roberts and Arnold, 1965). By comparison, Jones (1968) estimates crustal silver:gold ratios to be about 20:1. Shcherbina (1960) tabulated silver:gold ratios for ores from many mining districts and suggested that silver:gold ratios may be useful indicators for different chemical and physical environments and for different metallogenic stages and areas.

Median values for copper change significantly among the 11 areas outlined at Copper Canyon (fig. 46). Copper in the four areas (1–4) underlain by unpyritized rock, has median values in the 20–30 ppm range. In the pyritized rock we found that samples from areas 5, 6, and 9 yielded copper medians of 30, 150, and 150 ppm respectively. Areas 5 and 6 are both underlain by rock belonging to the Pumpernickel Formation, and area 6 includes the west ore body. Areas 7 through 11, however, have much higher copper median values—up to about 1,500 ppm in the granodiorite. The copper value in area 7, which includes the east ore body, is also very high—about 500 ppm.

Generally, as the median values for copper increase in the 11 areas examined, it appears that the number of elements strongly associated with copper, gold, and silver decreases (fig. 46). In areas 2 and 3, which include the peripheral Buena Vista and Meagher, and the Nevada lead-zinc-silver vein deposits, respectively, gold and silver are each associated strongly with about seven elements at the levels previously described. However, when the median for copper increases to about 500–1,500 ppm as in areas 7, 8, 10, and 11, no elements were found to be associated with gold in 50 paired analyses or more, at $r_s$ numerical values greater than 0.5049. In samples from any one of these same four areas, silver is, at most, strongly associated statistically with only copper and lead in area 10. Now, this strong silver-lead association in area 10 is undoubtedly a reflection of the lead-zinc ores with silver mined from

*moment correlation coefficients for 2,927 rock analyses at Copper Canyon*
0.1000 and greater than −0.1000; −X, between 0.1000 and −0.3700]

| Log (Cr) | Log (Cu) | Log (La) | Log (Mo) | Log (Nb) | Log (Ni) | Log (Pb) | Log (Sb) | Log (Sc) | Log (Sn) | Log (Sr) | Log (V) | Log (W) | Log (Y) | Log (Zn) | Log (Zr) | Log (Hg) |
|---|---|---|---|---|---|---|---|---|---|---|---|---|---|---|---|---|
| X | XX | X | X | X | X | XX | – | X | XX | X | XX | – | X | X | X | X |
| XX | X | – | – | – | XX | –X | –X | X | –X | – | XX | – | X | –X | XX | –X |
| X | – | – | – | – | X | –X | – | – | – | X | – | – | – | – | – | –X |
| XX | X | – | – | X | XX | –X | –X | XX | –X | –X | XX | –X | X | –X | XX | – |
| X | –X | –X | – | – | XX | – | – | – | – | – | – | – | – | X | – | – |
| – | XX | X | X | – | – | XX | XX | – | XX | X | – | – | X | X | –X | XX |
| – | X | X | X | – | – | XX | X | – | X | X | – | X | X | X | –X | XX |
| – | X | X | X | – | – | XX | X | – | XX | X | – | – | X | X | –X | XX |
| X | –X | – | –X | – | –X | –X | – | X | – | – | XX | – | X | –X | – | – |
| XX | – | – | – | – | X | –X | –X | X | –X | – | – | X | X | –X | XX | –X |
| –X | X | X | X | – | X | X | – | – | – | – | – | X | – | X | –X | – |
| – | X | X | – | – | – | X | X | – | X | X | – | –X | X | – | –X | X |
| – | X | X | – | – | X | X | – | – | X | X | X | – | – | XX | –X | X |
| – | X | X | X | – | XX | X | –X | X | X | – | XX | – | X | X | – | – |
| 0.0 | X | X | – | – | X | – | – | XX | – | – | X | – | XX | –X | X | – |
| 2884. | 0.0 | XX | X | – | X | X | X | – | X | X | X | –X | X | X | – | X |
| 1428. | 1427. | 0.0 | X | – | – | X | – | X | X | X | – | –X | XX | – | –X | X |
| 927. | 932. | 359. | 0.0 | –X | X | X | –X | X | X | X | X | X | – | X | –X | – |
| 1011. | 1012. | 651. | 335. | 0.0 | X | – | –X | –X | – | – | XX | – | X | X | X | – |
| 2632. | 2612. | 1312. | 862. | 931. | 0.0 | –X | –X | X | – | – | | –X | X | X | X | – |
| 2110. | 2110. | 1068. | 759. | 809. | 1929. | 0.0 | X | – | X | X | –X | –XX | X | XX | –X | XX |
| 243. | 245. | 87. | 115. | 63. | 218. | 243. | 0.0 | – | X | – | XX | X | X | – | – | X |
| 2055. | 2056. | 1240. | 718. | 931. | 1906. | 1571. | 183. | 0.0 | – | – | – | X | X | – | X | – |
| 735. | 740. | 332. | 366. | 311. | 638. | 639. | 148. | 642. | 0.0 | – | – | – | X | X | –X | X |
| 783. | 786. | 430. | 370. | 318. | 735. | 684. | 123. | 664. | 236. | 0.0 | – | X | – | – | –X | – |
| 2891. | 2877. | 1424. | 929. | 1010. | 2624. | 2107. | 240. | 2058. | 786. | 784. | 0.0 | X | X | – | XX | – |
| 162. | 162. | 67. | 111. | 60. | 138. | 134. | 25. | 146. | 94. | 51. | 162. | 0.0 | X | –X | – | X |
| 2404. | 2404. | 1372. | 716. | 933. | 2223. | 1794. | 204. | 1863. | 616. | 673. | 2405. | 129. | 0.0 | – | X | – |
| 787. | 794. | 323. | 345. | 264. | 770. | 719. | 139. | 594. | 263. | 259. | 790. | 63. | 674. | 0.0 | –X | X |
| 2871. | 2861. | 1429. | 915. | 1009. | 2596. | 2089. | 236. | 2054. | 733. | 777. | 2862. | 160. | 2397. | 774. | 0.0 | –X |
| 2432. | 2425. | 1191. | 789. | 877. | 2190. | 1815. | 203. | 1716. | 652. | 684. | 2422. | 134. | 2005. | 673. | 2408. | 0.0 |

between the 500 and 700 levels of the Copper Canyon underground mine (Roberts and Arnold, 1965). Similar to the increase in copper, which is primarily a supergene effect, in the southern and southeastern part of the Copper Canyon area, concentrations of some other base metals also increase as we have described above. As the number of individual element analyses with numerically identical copper, gold, and silver (or any other metal) increases substantially, then values of $r_s$ calculated from these analyses would tend to increase, if not corrected for tied observations (Siegel, 1956; Flanagan, 1957).

The failure of our statistical approach to find the copper-gold association in the areas of the ore bodies is puzzling. Almost certainly copper in the area around the east ore body must be associated with gold, at least spatially, if not genetically, as we described above. It may very well be that statistical correlation techniques based on predominantly spectrographic versus more refined analytic methods in areas of widespread metallization are of limited use for adequately detecting geologically significant element associations. These data may reflect also a pronounced disruption of elemental associations during oxidation in the most copper-rich areas. Analyses of individual minerals have been initiated to fix better the location of many of the minor elements. In a study somewhat similar to the one at Copper Canyon, Cornwall and Rose (1957) found no definite association of minor elements with copper ores in the Keweenawan lavas, Michigan. Nevertheless, there are many other statistically significant element associations in these four areas of high copper:gold ratios (table 15).

Although mercury correlations for gold determined from concentrations over the entire Copper Canyon area are fairly strong (table 14), mercury-gold associations are not uniformly distributed (fig. 40). The strongest associations of gold and silver with mercury at Copper Canyon were found in areas 1–3. These areas are underlain mostly by rocks of the Pumpernickel and Battle Formations. Metallization in area 1 is very sparse, if any, whereas areas 2 and 3 have had

TABLE 15.—*Element pairs other than copper, gold, and silver from areas 7, 8, 10, and 11 (fig. 46) that have positive Spearman correlation coefficients greater than 0.5049 and that are based on at least 50 element pair concentration*

| 7 | 8 | 10 | 11 |
|---|---|---|---|
| Fe-As | Fe-Sn | Fe-As | Mg-Sc |
| Fe-Bi | Mg-Ca | Fe-Bi | Mg-V |
| Mg-Ti | Mg-Ni | Fe-Pb | Ti-Cr |
| Mg-Cr | Ti-V | Fe-Sn | Ti-Sc |
| Mg-Sc | As-Pb | Fe-Zn | B-Sc |
| Ti-Cr | Bi-Pb | Mg-Ti | Co-Ni |
| Ti-Sc | Cr-V | Mg-Ba | Cr-V |
| Ti-V | Pb-Sn | Mg-Ni | La-Sc |
| Bi-Pb | | Mg-V | La-Y |
| Co-Ni | | Mg-Zr | Sc-V |
| Cr-Sc | | Ti-Cr | Sc-Y |
| Cr-V | | Ti-V | |
| Cr-V | | Ti-Zr | |
| Sc-V | | Ba-Cr | |
| | | Ba-V | |
| | | Ba-Zr | |
| | | Cr-V | |

significant lead-zinc-silver with some gold production from the Buena Vista, Meagher, Nevada, and Blossom mines (Roberts and Arnold, 1965). There is a very strong mercury-lead correlation in area 2 (0.6719, Spearman correlation coefficient, with a 12.47 Student's $t$ test, and 189 degrees of freedom). The mercury-lead association is not as strong in area 3 (0.4616, Spearman correlation coefficient, with a 7.75 Student's $t$ test, and 222 degrees of freedom). Although the data for zinc in these two areas are markedly censored because of zinc's high lower detection limit, the association data suggest a mercury-zinc association in area 3 stronger than that in area 2. Estimated zinc abundances in samples from area 3 are about three times those of area 2.

The usefulness of mercury as an ore indicator at Copper Canyon thus appears to be best for the vein deposits in unpyritized rock. We have, however, noted the occurrence of a mercury halo (0.21–1.0 ppm) at the north margin of the granodiorite, partly over the west ore body, and the high mercury concentrations along faults in the east ore body. The clay fraction of soil samples over the west ore body also contains anomalous mercury at about 1.0 ppm levels (Theodore, unpub. data).

The strong gold-arsenic association, to which we alluded in descriptions of the spatial distributions of these elements' concentrations, is also reflected in the statistical treatment of the data (fig. 46). Very strong gold-arsenic associations were detected in areas 2–6 and in area 9, which contain significant concentrations of arsenic along north-striking faults. Generally, silver is also associated with arsenic in these same areas.

Over all the 11 areas, silver-lead positive associations were found in nine of the 11 areas (fig. 46). Similar silver-gold associations were found in only five areas. Accordingly, when all analyses at Copper Canyon were considered, the silver-gold association (table 14) is not quite as strong as the silver-lead association: 0.5905 $r_s$, 31.4 Student's $t$ test for 1,838 degrees of freedom.

Although we have pointed out some shortcomings of the strength of association evaluations, especially in areas of intense metallization, the technique seems to have some potential as an aid to exploration in areas of less obvious metallization and in areas of notable vein-metallization. Evaluation of chemical data by correlation methods might yield potential pathfinder elements to limit geochemical target areas. For example, in area 6 (fig. 46), which includes the west ore body, gold has a strong association with silver, arsenic, bismuth, and iron. The strong gold–bismuth association is the interesting one, because free gold in the east ore body commonly contains bismuth. All of the preceding, together with the bismuth anomaly over the west ore body and the significant horizons of gold in the ore body, suggest that bismuth anomalies in the mining district may not be entirely due to bismuth in galena. Bismuth thus may serve as a useful pathfinder element for gold here.

Elements strongly associated with gold can differ widely from mining district to mining district and within a single gold deposit. A similar statistical evaluation of elemental associations around the Dzhamansai deposit, Sultanuizdag, Uzbekistan by Palei, Murovtsev, and Borozenets (1967) revealed that gold there has its strongest positive associations with barium, manganese, arsenic, and beryllium. It also has a strong negative association with lead. Studies of gold deposits in Kazakghstan revealed systematic changes in correlation coefficients between As-Au, Ag-Au, Bi-Au, Zn-Au, Pb-Au, and Cu-Au with depth (Fakhri, 1965).

## SELECTED REFERENCES


Ahrens, L. H., 1954, The lognormal distribution of the elements: Geochim. et Cosmochim. Acta, v. 5, no. 2, p. 49–73.

———1957, Lognormal-type distributions—III: Geochim. et Cosmochim. Acta, v. 11, p. 205–212.

———1963, Lognormal-type distributions in igneous rocks—IV: Geochim. et Cosmochim. Acta, v. 27, p. 333–343.

Anderson, C. A., Scholz, E. A., and Strobell, J. D., Jr., 1955, Geology and ore deposits of the Bagdad area, Yavapai County, Arizona: U.S. Geol. Survey Prof. Paper 278, 103 p.

Anderson, G. M., 1964, The calculated fugacity of water to 1000°C and 10,000 bars: Geochim. et Cosmochim. Acta, v. 28, no. 5, p. 713–715.

Arnold, R. G., 1962, Equilibrium relations between pyrrhotite and pyrite from 325 to 743°C: Econ. Geology, v. 57, p. 72–90.

———1966, Mixtures of hexagonal and monoclinic pyrrhotite and the measurement of the metal content of pyrrhotite by X-ray diffraction: Am. Mineralogist, v. 51, p. 1221–1227.

———1967, Range in composition and structure of 82 natural terrestrial pyrrhotites: Canadian Mineralogist, v. 9, p. 31–50.

———1969, Pyrrhotite phase relations below 304±6°C at <1 Atm total pressure: Econ. Geology, v. 64, p. 405–419.

Arnold, R. G., and Reichen, L. E., 1962, Measurement of the metal content of naturally occurring, metal—deficient, hexagonal pyrrhotite by an X-ray spacing method: Am. Mineralogist, v. 47, p. 105–111.

Aubrey, K. V., 1956, Frequency distributions of elements in igneous rocks: Geochim. et Cosmochim. Acta, v. 9, p. 83–89.

Axelrod, D. I., 1966, The Eocene Copper Basin flora of northeastern Nevada: California Univ. Pubs. Geol. Sci., v. 59, 125 p.

Balitskii, V. S., and Lyubofeyev, V. N., 1962, Physicochemical characteristics of mineralizing solutions as illustrated by polymetallic mineralization in the northwest Caucasus: Geochemistry, v. 9, p. 926.

Barnes, H. L., 1965, Environmental limitations to mechanisms of ore transport: Symposium, Problems of postmagmatic ore deposition, Prague, v. 2, p. 316–326.

Barnes, H. L., and Czamanske, G. K., 1967, Solubilities and transport of ore minerals, *in* Barnes, H. L., ed., Geochemistry of hydrothermal ore deposits: New York, Holt, Rinehart, and Winston, Inc., p. 334–381.

Barnes, Ivan, 1970, Metamorphic waters from the Pacific tectonic belt of the west coast of the United States: Science, v. 168, no. 3934, p. 973–975.

Barnett, P. R., 1961, Spectrographic analysis for selected minor elements in Pierre shale: U.S. Geol. Survey Prof. Paper 391–B, p. B1–B10.

Barth, T. F. W., 1962, Theoretical petrology: New York, John Wiley and Sons, 416 p.

Barton, P. B., Jr., and Skinner, B. J., 1967, Sulfide mineral stabilities, *in* Barnes, H. L., ed., Geochemistry of hydrothermal ore deposits: New York, Holt, Rinehart, and Winston, Inc., p. 236–333.

Bateman, P. C., 1968, Geologic structure and history of the Sierra Nevada: UMR Jour., Univ. Missouri, Rolla, McNutt-Geol. Dept. Colloquium Ser. 1, no. 1, p. 121–132.

Bitter, F., 1932, Experiments on the nature of ferromagnetism: Phys. Rev., v. 41, p. 507–515.

Blake, D. W., 1971, Exploration aspects of the Copper Canyon porphyry copper deposit, Lander County, Nevada—Pt. I, Geology and geometry: Am. Inst. Mining Metall. and Petroleum Engineers, Pacific Southwest Mineral Industry Conf., Reno, Nev., 1971, Program, p. 9.

Boyle, R. W., 1970, The source of metals and gangue elements in hydrothermal deposits, *in* Pouba, Zdenek, and Stemprok, Miroslav, eds., Problems of hydrothermal ore deposition—The origin, evolution, and control of ore-forming fluids: Internat. Union Geol. Sci., ser. A, no. 2, p. 3–6.

Burke, D. B., 1970, Permo-Triassic non-marine deposition and coeval block faulting, west-central Nevada [abs.]: Geol. Soc. America, Abstracts with programs, v. 2, no. 2, p. 77–78.

Burnham, C. W., 1959, Metallogenic provinces of the southwestern United States and northern Mexico: New Mexico Bur. Mines Bull. 65, 76 p.

———1967, Hydrothermal fluids at the magmatic stage, *in* Barnes, H. L., ed., Geochemistry of hydrothermal ore deposits: New York, Holt, Rinehart, and Winston, Inc., p. 34–76.

Burnham, C. W., and Jahns, R. H., 1962, A method for determining the solubility of water in silicate melts: Am. Jour. Sci., v. 260, p. 721–745.

Buseck, P. R., 1967, Contact metasomatism and ore deposition —Tem Piute, Nevada: Econ. Geology, v. 62, p. 331–353.

Carlisle, D., 1965, Sliding friction and overthrust faulting: Jour. Geology, v. 73, p. 271–292.

Carpenter, R. H., and Desborough, G. A., 1964, Range in solid solution and structure of naturally occurring troilite and pyrrhotite: Am. Mineralogist, v. 49, p. 1350–1365.

Castle, R. O., 1964, Geology of the Andover granite and surrounding rocks, Massachusetts: California Univ., Los Angeles, Ph.D. thesis, 627 p.

Chayes, F., 1954, The lognormal distribution of the elements—a discussion: Geochim. et Cosmochim, Acta, v. 6, p. 119–120.

Clark, A. H., 1965, Observations on the applicability of the pyrrhotite geothermometer in the light of the composition and crystal structure of pyrrhotite in differing ore deposits [abs.]: Mineralog. Soc. (London), Mtg. no. 138.

———1966, Stability field of monoclinic pyrrhotite: Inst. Mining Metallurgy Trans., sec. B, v. 75, p. 232–235.

Clark, L. A., 1960, The Fe-As-S system: Carnegie Inst. Washington Year Book 59, p. 127–130.

Clement, S. C., 1964, Mineralogy and petrology of the Copper Canyon quartz monzonite porphyry, Battle Mountain, Nevada: Cornell Univ., Ithaca, N.Y., Ph.D. thesis, 108 p.

———1968, Supergene copper concentration in altered plagioclase feldspar, Copper Canyon, Nevada: Econ. Geology, v. 63, p. 401–408.

Coats, R. R., and Stephens, E. C., 1968, Mountain City copper mine, Elko County, Nevada, *in* Ridge, J. D., ed., Ore deposits of the United States, 1933–1967, The Graton-Sales Volume II: New York, Am. Inst. Mining Metall. and Petroleum Engineers, Inc., p. 1074–1101.

Cornwall, H. R., and Rose, H. J., Jr., 1957, Minor elements in Keweenawan lavas, Michigan: Geochim. et Cosmochim. Acta, v. 12, p. 209–224.

Cowan, J. C., 1968, Geology of the Strathcona ore deposits: Canadian Mining and Metall. Bull., v. 61, p. 38–54.

Creasey, S. C., 1965, Geology of the San Manuel area, Pinal County, Arizona, *with a section on* Ore deposits *by* J. P. Pelletier and S. C. Creasey: U.S. Geol. Survey Prof Paper 471, 64 p.

———1966, Hydrothermal alteration, *in* Titley, S. R., and Hicks, C. L. eds., Geology of the porphyry copper deposits, southwestern North America: Tucson, Ariz., Arizona Univ. Press, p. 51–85.

Creasey, S. C., and Kistler, R. W., 1962, Age of some copper-bearing porphyries and other igneous rocks in southeastern Arizona, *in* Geological Survey Research 1962: U.S. Geol. Survey Prof. Paper 450–D, p. D1–D5.

Deer, W. A., Howie, R. A., and Zussman, J., 1962, Sheet silicates, v. 3 *of* Rock-forming minerals: London, Longmans, Green, and Co., 270 p.

Desborough, G. A., and Carpenter, R. H., 1965, Phase relations of pyrrhotite: Econ. Geology, v. 60, p. 1431–1450.

Dixon, W. J., and Massey, F. J., 1951, Introduction to statistical analysis: New York, McGraw-Hill Book Co., Inc., 370 p.

Dodge, F. C. W., Smith, V. C., and Mays, R. E., 1969, Biotites from granitic rocks of the central Sierra Nevada batholith, California: Jour. Petrology, v. 10, no. 2, p. 250–271.

Doe, B. R., 1962, Distribution and composition of sulfide minerals at Balmat, New York: Geol. Soc. America Bull., v. 73, p. 833–854.

Eidel, J. J., Frost, J. E., and Clippinger, D. M., 1968, Copper-molybdenum mineralization at Mineral Park, Mohave County, Arizona, *in* Ridge, J. D., ed., Ore deposits of the United States, 1933–1967, The Graton-Sales Volume II: New York, Am. Inst. Mining Metall. and Petroleum Engineers, Inc., p. 1258–1281.

Engineering and Mining Journal, 1971, Nevada ["In the news this month" section]: Eng. and Mining Jour., v. 172, no. 6, p. 253.

Erickson, R. L., Van Sickle, G. H., Nakagawa, H.M., McCarthy, J. H., Jr., and Leong, K. W., 1966, Gold geochemical anomaly in the Cortez district, Nevada: U.S. Geol. Survey Circ. 534, 9 p.

Espenshade, G. H., 1963, Geology of some copper deposits in North Carolina, Virginia, and Alabama: U.S. Geol. Survey Bull. 1142–I, p. I1–I48.

Eugster, H. P., and Wones, D. R., 1962, Stability relations of the ferruginous biotite, annite: Jour. Petrology, v. 3, no. 1, p. 82–125.

Fakhri, A., 1965, Zonal'nost pervichnykh oreolov zolotorudnogo mestorozhdeniya i migratsionnaya sposobnost' elementov [Zoning of primary dispersion halos over a gold deposit and the migration capacity of the elements]: Moskov. Univ. Vestnik, Ser. 4, Geologiya, no. 5, p. 31–43.

Fenner, P., and Hagner, A. F., 1967, Correlation of variations in trace elements and mineralogy of the Esopus Formation, Kingston, New York: Geochim. et Cosmochim. Acta, v. 31, p. 237–262.

Ferguson, H. G., Roberts, R. J., and Muller, S. W., 1952, Geology of the Golconda quadrangle, Nevada: U.S. Geol. Survey Geol. Quad. Map GQ–15.

Flanagan, F. J., 1957, Semi-quantitative spectrographic analysis and rank correlation in geochemistry: Geochim. et Cosmochim. Acta, v. 12, p. 315–322.

Fleischer, Michael, 1955, Minor elements in some sulfide minerals: Econ. Geology, Fiftieth Anniv. Volume, pt. 2, p. 970–1024.

Folk, R. L., 1968, Petrology of sedimentary rocks: Austin, Tex., Hemphill's, 170 p.

Fournier, R. O., 1967, The porphyry copper deposit exposed in the Liberty open-pit mine near Ely, Nevada—Part I. Syngenetic formation: Econ. Geology, v. 62, p. 57–81.

Gilluly, James, 1946, The Ajo mining district, Arizona: U.S. Geol. Survey Prof. Paper 209, 112 p.

Gilluly, James, and Masursky, Harold, 1965, Geology of the Cortez quadrangle, Nevada, *with a section on* Gravity and aeromagnetic surveys, *by* D. R. Mabey: U.S. Geol. Survey Bull. 1175, 117 p.

Goldschmidt, V. M., 1937, Geochemische Verteilungsgesetze der Elemente—9. Die Mengenverhältnisse der Elemente und der Atom-Arten: Norske Vidensk.-Akad., Oslo, Mat.-Naturv. Kl., no. 4, p. 1–148.

———1954, Geochemistry: London, Oxford Univ. Press, 730 p.

Gott, G. B., McCarthy, J. H., Jr., Oda, Uteana, Lakin, H. W., and Thompson, C. E., 1965, Preliminary report comparing geochemical halos around an exposed and a concealed copper deposit: CENTO Seminar Field Techniques Mineral Inv., 6th Mineral Conf., Isfahan, Iran, 1965, p. 133–145.

Graf, D. L., 1960, Geochemistry of carbonate sediments and sedimentary carbonate rocks, pt. 3—Minor element distribution: Illinois Geol. Survey Circ. 301, 71 p.

Grimes, D. J., and Marranzino, A. P., 1968, Direct-current arc and alternation-current spark emission spectrographic field methods for the semiquantitative analysis of geologic materials: U.S. Geol. Survey Circ. 591, 6 p.

Hague, Arnold, and Emmons, S. F., 1877, Descriptive geology: U.S. Geol. Explor. 40th Parallel (King), v. 2, 890 p.

Hall, W. E., 1971, Minor-element contents of the sulfide minerals, Darwin lead-silver-zinc mine, Inyo County, California: Soc. Mining Geol. Japan, Spec. Issue 2, p. 119–126.

Hawley, J. E., Lewis, C. L., and Wark, W. J., 1951, Spectrographic study of platinum and palladium in common sulphides and arsenides of the Sudbury district, Ontario: Econ. Geology, v. 46, p. 149–162.

Hawley, J. E., and Nichol, Ian, 1961, Trace elements in pyrite, pyrrhotite and chalcopyrite of different ores: Econ. Geology, v. 56, p. 467–487.

Hawley, J. E., and Rimsaite, Y., 1953, Platinum metals in some Canadian uranium and sulphide ores: Am. Mineralogist, v. 38, p. 463–475.

Hawkes, H. E., and Webb, J. S., 1962, Geochemistry in mineral exploration: New York, Harper and Row, 415 p.

Hayase, Kitaro, Otsuka, Ryohei, and Mariko, Tadashi, 1963, On the magnetic properties of natural pyrrhotites: Mineralog. Jour., v. 4, no. 1, p. 41–56.

Haynes, S. J., and Hill, P. A., 1970, Pyrrhotite phases and pyrrhotite-pyrite relationships—Renison Bell, Tasmania: Econ. Geology, v. 65, p. 838–848.

Heiner, L. E., Beistline, E. H., Moody, D. W., Thomas, B. I., Wallis, J. E., Loperfido, J. C., Peterson, R. J., and Wolff, E. N., 1967, Geochemical-geophysical investigations, Fairbanks district, Alaska: Alaska Univ. Mineral Industry Research Lab., rept. 12, 133 p.

Helgeson, H. C., 1964, Complexing and hydrothermal ore deposition: New York, Macmillan Co., 128 p.

———1967, Thermodynamics of complex dissociation in aqueous solution at elevated temperatures: Jour. Phys. Chemistry, v. 71, p. 3121–3126.

———1968, Geologic and thermodynamic characteristics of the Salton Sea geothermal system: Am. Jour. Sci., v. 266, p. 129–166.

———1969, Thermodynamics of hydrothermal systems at elevated temperatures and pressures: Am. Jour. Sci., v. 267, p. 729–804.

Helz, G. R., 1971, Hydrothermal solubility of magnetite: Pennsylvania State Univ., University Park, Pa., Ph.D. thesis, 110 p.

Hemley, J. J., Meyer, C., Hodgson, C. J., and Thatcher, A. B., 1967, Sulfide solubilities in alteration-controlled systems: Science, v. 158, p. 1580–1582.

Himes, M. D., 1972, Mineralization and alteration at the Pima mine, a complex porphyry copper deposit, Pima County, Arizona: New York, Soc. Mining Engineers of AIME (presented at AIME Ann. Mtg., San Francisco, Calif., 1972), Preprint 72–I–57, 47 p.

Huff, L. C., 1970, A geochemical study of alluvium-covered copper deposits in Pima County, Arizona, *with a section on* Analytical methods, *by* A. P. Marranzino and H. M. Nakagawa: U.S. Geol. Survey Bull. 1312–C, p. C1–C31.

Ingamells, C. O., 1962, The application of an improved steam distillation apparatus to the determination of fluoride in rocks and minerals: Talanta, v. 9, p. 507–516.

———1966, Absorptometric methods in rapid silicate analysis: Anal. Chemistry, v. 38, p. 1228–1234.

Ishihara, S., 1967, Molybdenum mineralization at Questa mine, New Mexico, U.S.A.: Japan Geol. Survey, rept. 218, 64 p.

Jaeger, J. C., 1964, Thermal effects of intrusions: Reviews of Geophysics, v. 2, no. 3, p. 443–466.

Jensen, M. L., 1971, Provenance of Cordilleran intrusives and associated metals: Econ. Geology, v. 66, p. 34–42.

Jerome, S. E., 1966, Some features pertinent in exploration of porphyry copper deposits, *in* Titley, S. R., and Hicks, C. L., eds., Geology of the porphyry copper deposits, southwestern North America: Tucson, Ariz., Arizona Univ. Press, p. 75–86.

Jolly, J. L., and Heyl, A. V., 1968, Mercury and other trace elements in sphalerite and wallrocks from central Kentucky, Tennessee, and Appalachian zinc districts: U.S. Geol. Survey Bull. 1252–F, p. F1–F29.

Jones, R. S., 1968, Gold in meteorites and in the earth's crust: U.S. Geol. Survey Circ. 603, 4 p.

Kamb, W. B., 1959, Ice petrofabric observations from Blue Glacier, Washington, in relation to theory and experiment: Jour. Geophys. Research, v. 64, p. 1891–1909.

Keays, R. R., and Crocket, J. H., 1970, A study of precious metals in the Sudbury nickel irruptive ores: Econ. Geology, v. 65, p. 438–450.

Kelly, W. C., and Turneaure, F. S., 1970, Mineralogy, paragenesis and geothermometry of the tin and tungsten deposits of the eastern Andes, Bolivia: Econ. Geology, v. 65, p. 609–680.

Kesler, S. E., 1968, Contact-localized ore formation at the Memé mine, Haiti: Econ. Geology, v. 63, p. 541–552.

Kinnison, J. E., 1966, The Mission copper deposit, Arizona, *in* Titley, S. R., and Hicks, C. L., eds., Geology of the porphyry copper deposits, southwestern North America: Tucson, Ariz., Arizona Univ. Press, p. 281–287.

Knopf, Adolph, 1915, A gold-platinum-palladium lode in southern Nevada: U.S. Geol. Survey Bull. 620, p. 1–18.

———1929, The Mother Lode system of California: U.S. Geol. Survey Prof. Paper 157, 88 p.

Korzhinskii, D. S., 1957, Acidity regimen of postmagmatic solutions: Akad. Nauk SSSR Izv., Ser. Geol., no. 12, p. 3–12. [In Russian. Translation by Ivan Mittin, 1963]

Koster van Groos, A. F., and Wyllie, P. J., 1969, Melting relations in the system $NaAlSi_3O_8$-NaCl-$H_2O$ at 1 kilobar pressure, with petrological applications: Jour. Geology, v. 77, no. 5, p. 581–605.

Krauskopf, K. B., 1967a, Introduction to geochemistry: New York, McGraw-Hill Book Co., 721 p.

———1967b, Source rocks for metal-bearing fluids, *in* Barnes, H. L., ed., Geochemistry of hydrothermal ore deposits: New York, Holt, Rinehart, and Winston, Inc., p. 1–33.

Lawson, A. C., 1913, The petrographic designation of alluvial-fan formations: California Univ., Dept. Geology Bull., v. 7, no. 15, p. 325-334.

Livingston, D. E., Mauger, R. L., and Damon, P. E., 1968, Geochronology of the emplacement, enrichment, and preservation of Arizona porphyry copper deposits: Econ. Geology, v. 63, p. 30–36.

Lovering, T. G., 1969, Distribution of minor elements in samples of biotite from igneous rocks—basic data: U.S. Geol. Survey open-file report, 2 tab. sheets.

Lovering, T. G., Cooper, J. R., Drewes, Harald, and Cone, G. C., 1970, Copper in biotite from igneous rocks in southern Arizona as an ore indicator, *in* Geological Survey research, 1970: U.S. Geol. Survey Prof. Paper 700–B, p. B1–B8.

Lovering, T. G., Lakin, H. W., and Hubert, A. E., 1968, Concentration and minor element association of gold in ore-related jasperoid samples, *in* Geological Survey research, 1968: U.S. Geol. Survey Prof. Paper 600–B, p. B112–B114.

Lovering, T. S., 1955, Temperatures in and near intrusions, *in* pt. 1 *of* Bateman, A. M., ed., Econ. Geology Fiftieth Ann. Vol., p. 249–281.

Lowell, J. D., and Guilbert, J. M., 1970, Lateral and vertical alteration-mineralization zoning in porphyry ore deposits: Econ. Geology, v. 65, p. 373–408.

Luth, W. C., 1969, The systems $NaAlSi_3O_8$-$SiO_2$ and $KAlSi_3O_8$-$SiO_2$ to 20kb and the relationship between $H_2O$ content, $P_{H_2O}$ and $P_{total}$ in granitic magmas: Am. Jour. Sci., v. 267–A (Schairer Volume), p. 325–341.

Luth, W. C., Jahns, R. H., and Tuttle, O. F., 1964, The granite system at pressure of 4 to 10 kilobars: Jour. Geophys. Research, v. 69, p. 759–773.

Marshall, R. R., and Joensuu, Oiva, 1961, Crystal habit and trace element content of some galenas: Econ. Geology, v. 56, p. 759–771.

Mauger, R. L., 1964, Geochemical and petrologic investigations of the Silver Bell and Esperanza quartz monzonite porphyries, *in* Damon, P. E., Correlation and chronology of ore deposits and volcanic rocks: U.S. Atomic Energy Comm., Research Div., Ann. Progress Rept. C00–689–4, Contract AT (11–1)–689, p. AIII–1 to AAIII–18.

Maxwell, J. A., 1963, Geochemical study of some chert and related deposits: Canada Geol. Survey Bull. 104, 31 p.

McDowell, F. W., and Kulp, J. L., 1967, Age of intrusion and ore deposition in the Robinson mining district of Nevada: Econ. Geology, v. 62, no. 7, p. 905–909.

McKee, E. D., 1964, Problems on the recognition of arid and of hot climates of the past, *in* Nairn, A. E. M., ed., Problems in paleoclimatology: NATO Paleoclimates Conf. Proc., Newcastle-upon-Tyne and Durham, England, 1963: New York, Interscience, p. 367–377.

McKee, E. H., and Burke, D. B., 1972, Fission track age bearing on the Permian-Triassic boundary and time of the Sonoma orogeny in north-central Nevada: Geol. Soc. America Bull. v. 83, p. 1949–1952.

McKee, E. H., and Silberman, M. L., 1970, Geochronology of Tertiary igneous rocks in central Nevada: Geol. Soc. America Bull., v. 81, no. 8, p. 2317–2328.

Medlin, J. H., Suhr, N. H., and Bodkin, J. B., 1969, Atomic absorption analysis of silicates employing $LiBO_2$ fusion: Atomic Absorption Newsletter 8, p. 25–29.

Mertie, J. B., Jr., 1969, Economic geology of the platinum metals: U.S. Geol. Survey Prof. Paper 630, 120 p.

Meyer, Charles, 1965, An early potassic type of wall-rock alteration of Butte, Montana: Am. Mineralogist, v. 50, p. 1717–1722.

Meyer, C., and Hemley, J. J., 1967, Wall rock alteration, *in* Barnes, H. L., ed., Geochemistry of hydrothermal ore deposits: New York, Holt, Rinehart, and Winston, Inc., p. 166–235.

Miesch, A. T., 1967, Methods of computation for estimating geochemical abundance: U.S. Geol. Survey Prof. Paper 574–B, p. B1–B15.

Mizutani, Y., 1970, Copper and zinc in fumarolic gases of Showashinzan volcano, Hokkaido, Japan: Geochem. Jour., v. 4, no. 2, p. 87–91.

Moore, W. J., and Czamanske, G. K., 1973, Compositions of biotites from unaltered and altered monzonite rocks in the Bingham mining district, Utah: Econ. Geology, v. 68, p. 269–274.

Moore, W. J., and Lanphere, M. A., 1971, The age of porphyry-type copper mineralization in the Bingham mining district, Utah—a refined estimate: Econ. Geology, v. 66, p. 331–334.

Morimoto, N., and Clark, L. A., 1961, Arsenopyrite crystal-chemical relations: Am. Mineralogist, v. 46, p. 1448–1469.

Morimoto, N., Nakazawa, H., Nishiguchi, K., Tokonami, M., 1970, pyrrhotites—stoichiometric compounds with composition $Fe_{n-1}Sn$ ($n \geqslant 8$): Science, v. 168, p. 964–966.

Munoz, J. L., and Eugster, H. P., 1969, Experimental control of fluorine reactions in hydrothermal systems: Am. Mineralogist, v. 54, p. 943–959.

Nash, J. T., 1971, Fluid inclusions in exploration for porphyry-type mineralization [abs.]: Econ. Geology, v. 66, p. 1268.

Nash, J. T., and Theodore, T. G., 1971, Ore fluids in the porphyry copper deposit at Copper Canyon, Nevada: Econ. Geology, v. 66, p. 385–399.

Neff, T. R., 1969, Petrology and structure of the Buffalo Mountain pluton, Humboldt County, Nevada: Stanford Univ., Stanford, Calif., Ph.D. thesis.

Nichols, K. M., 1971, Overlap of the Golconda thrust by Triassic strata, north-central Nevada [abs.]: Geol. Soc. America, Abstracts with programs, v. 3, no. 2, p. 171.

Nielsen, R. L., 1968, Hypogene texture and mineral zoning in a copper-bearing granodiorite porphyry stock, Santa Rita, New Mexico: Econ. Geology, v. 68, p. 37–50.

Noble, J. A., 1970, Metal provinces of the western United States: Geol. Soc. America Bull., v. 71, no. 6, p. 1607–1624.

Nriagu, J. O., and Anderson, G. M., 1970, Calculated solubilities of some base-metal sulphides in brine solutions: London, Inst. Mining Metallurgy Trans., v. 79, Bull. 768, p. B208–B212.

Ohmoto, H., 1970, Influence of pH and $f_{O_2}$ of hydrothermal fluids on the isotopic composition of sulfur species: Geol. Soc. America, Abstract with programs, v. 2, no. 7, p. 640.

Palei, L. Z., Murovtsev, A. V., and Borozenets, N. I., 1967, The geochemistry of gold in Sultanuizdag: Uzbek, Geol. Zhurnal, no. 6, p. 50–55. [Translation by Michael Fleischer, 1968.]

Parry, W. T., and Nackowski, M. P., 1963, Copper, lead, and zinc in biotites from Basin and Range quartz monzonites: Econ. Geology, v. 58, p. 1126–1144.

Peterson, N. P., Gilbert, C. M., and Quick, G. L., 1951, Geology and ore deposits of the Castle Dome area, Gila County, Arizona: U.S. Geol. Survey Bull. 971, 134 p.

Piwinskii, A. J., 1968, Experimental studies of igneous rocks series, central Sierra Nevada batholith, California: Jour. Geology, v. 76, p. 548–570.

Powers, M. C., 1953, A new roundness scale for sedimentary particles: Jour. Sed. Petrology, v. 23, no. 2, p. 117–119.

Rader, L. F., and Grimaldi, F. S., 1961, Chemical analyses for selected minor elements in Pierre Shale: U.S. Geol. Survey Prof. Paper 391–A, p. A1–A45.

Ramdohr, Paul, 1969, The ore minerals and their intergrowths: Oxford, Pergamon Press, 1174 p.

Rankama, Kalervo, 1954, Isotope geology: New York, Pergamon Press, 535 p.

Ransome, F. L., 1900, Mother Lode district, California: U. S. Geol. Survey Geol. Atlas, Folio 63, 11 p.

Raymahashay, B. C., and Holland, H. D., 1969, Redox reactions accompanying hydrothermal wall rock alteration: Econ. Geology, v. 64, p. 291–305.

Rieder, Milan, 1971, Stability and physical properties of synthetic lithium-iron micas: Am. Mineralogist, v. 56, p. 256–280.

Roberts, R. J., 1964, Stratigraphy and structure of the Antler Peak quadrangle, Humboldt and Lander Counties, Nevada: U.S. Geol. Survey Prof. Paper 459–A, p. A1–A93.

———1966, Metallogenic provinces and mineral belts in Nevada: Nevada Bur. Mines Rept. 13, pt. A, p. 47–72.

Roberts, R. J., and Arnold, D. C., 1965, Ore deposits of the Antler Peak quadrangle, Humboldt and Lander Counties, Nevada: U.S. Geol. Survey Prof. Paper 459–B, p. B1–B94.

Roberts, R. J., Hotz, P. E., Gilluly, James, and Ferguson, H. G., 1958, Paleozoic rocks in north-central Nevada: Am. Assoc. Petroleum Geologists Bull., v. 42, no. 12, p. 2813–2857.

Roberts, R. J., Radtke, A. S., and Coats, R. R., 1971, Gold-bearing deposits in north-central Nevada and southwestern Idaho, *with a section on* Periods of plutonism in north-central Nevada, *by* M. L. Silberman and E. H. McKee: Econ. Geology, v. 66, no. 1, p. 14–33.

Robie, R. A., and Waldbaum, D. R., 1968, Thermodynamic properties of minerals and related substances at 298.15°K (25.0°C) and one atmosphere (1.013 bars) pressure and at higher temperatures: U.S. Geol. Survey Bull. 1259, 256 p.

Roedder, Edwin, 1971, Fluid inclusion studies on the porphyry-type ore deposits at Bingham, Utah; Butte, Montana, and Climax, Colorado: Econ. Geology, v. 66, p. 98–120.

Romberger, S. B., and Barnes, H. L., 1970, Ore solution chemistry III—Solubility of CuS in sulfide solutions: Econ. Geology, v. 65, p. 901–919.

Rose, A. W., 1967, Trace elements in sulfide minerals from the Central district, New Mexico and the Bingham district, Utah: Geochim. et Cosmochim. Acta, v. 31, p. 547–585.

———1970, Zonal relations of wallrock alteration and sulfide distribution at porphyry copper deposits: Econ. Geology, v. 65, p. 920–936.

Rosenburg, P. E., 1970, Fluorine substitution in muscovite and pyrophyllite [abs.]: Geol. Soc. America Ann. Mtg., Program, v. 2, no. 7, p. 668–669.

Rutherford, M. J., 1969, An experimental determination of iron biotite-alkali feldspar equilibria: Jour. Petrology, v. 10, no. 3, p. 381–408.

Rye, R. O., and Haffty, Joseph, 1969, Chemical composition of the hydrothermal fluids responsible for the lead-zinc deposits at Providencia, Zacatecas, Mexico: Econ. Geology, v. 64, p. 629–643.

Sawkins, F. J., Dunham, A. C., and Hirst, D. M., 1964, Iron-deficient low-temperature pyrrhotite: Nature, v. 204, no. 4954, p. 175–176.

Sayers, R. W., Tippett, M. C., and Fields, E. D., 1968, Duval's new copper mines show complex geologic history: Mining Eng., p. 55–62.

Schilling, J. H., 1971, Miscellaneous K-Ar ages of Nevada intrusive rocks: Isochron/West, no. 2, p. 46.

Schuiling, R. D., and Vink, B. W., 1967, Stability relations of some titanium minerals (sphene, perovskite, rutile, anatase): Geochim. et Cosmochim. Acta, v. 31, p. 2399–2412.

Schultz, L. G., 1963, Quantitative interpretation of mineralogical composition from X-ray and chemical data for the Pierre Shale: U.S. Geol. Survey Prof. Paper 391–C, p. C1–C31.

Schwartz, G. M., 1953, Geology of the San Manuel copper deposit, Arizona: U.S. Geol. Survey Prof. Paper 256, 65 p.

Scott, S. D., and Barnes, H. L., 1971, Sphalerite geothermometry and geobarometry: Econ. Geology, v. 66, p. 653–669.

Serkies, J., Oberc, J., and Idzikowski, A., 1967, The geochemical bearings of the genesis of Zechstein copper deposits in southwest Poland as exemplified by the studies on the Zechstein of the Leszczyna syncline: Chem. Geol., v. 2, p. 217–232.

Shapiro, Leonard, 1967, Rapid analysis of rocks and minerals by a single-solution method: U.S. Geol. Survey Prof. Paper 575–B, p. B187–B191.

Shapiro, Leonard, and Brannock, W. W., 1962, Rapid analysis of silicate, carbonate, and phosphate rocks: U.S. Geol. Survey Bull. 1144–A, p. A1–A44.

Shcherbina, V. V., 1960, Geochemical significance of quantitative Ag/Au ratios: Geochemistry, no. 3, p. 301–311.

Sichel, H. S., 1952, New methods in the statistical evaluation of mine sampling data: London, Inst. Mining Metallurgy Trans., v. 61, p. 261–288.

Siegel, Sidney, 1956, Nonparametric statistics — for the behavioral sciences: New York, McGraw-Hill Book Co., Inc., 312 p.

Silberling, N. J., 1973, Geologic events during Permo-Triassic time along the Pacific margin of the United States *in* Hills, L. V. ed., Permian and Triassic Systems and their mutual boundary: Canadian Soc. Petroleum Geologists, Mem. 2 [in press].

Silberling, N. J., and Roberts, R. J., 1962, Pre-Tertiary stratigraphy and structure of northwestern Nevada: Geol. Soc. America Spec. Paper 72, 58 p.

Silberman, M. L., and McKee, E. H., 1971, Periods of plutonism in north-central Nevada, *in* Roberts, R. J., Radtke, A. S., and Coats, R. R., Gold-bearing deposits in north-central Nevada and southwestern Idaho: Econ. Geology, v. 66, p. 14–33.

Speed, R. C., 1971, Golconda thrust, western Nevada — Regional extent [abs.]: Geol. Soc. America, Abstracts with programs, v. 3, no. 2, p. 199–200.

Steiger, R. H., and Hart, S. R., 1967, The microcline-orthoclase transition within a contact aureole: Am. Mineralogist, v. 52, p. 87–116.

Stephens, J. D., and Metz, R. A., 1967, Copper-bearing clay minerals in oxidized portions of the disseminated copper deposit at Ray, Arizona [abs.]: Geol. Soc. America Spec. Paper 115, p. 208.

Stewart, J. H., and McKee, E. H., 1970, Geologic map of Lander County, Nevada: U.S. Geol. Survey open-file map, scale 1:250,000.

Stringham, Bronson, 1966, Igneous rock types and host rocks associated with prophyry copper deposits, *in* Titley, S. R., and Hicks, C. L., eds., Geology of the porphyry copper deposits, southwestern North America: Tucson, Ariz., Arizona Univ. Press, p. 35–40.

Suhr, N. H., and Ingamells, C. O., 1966, Solution techniques for analysis of silicates: Anal. Chemistry, v. 38, p. 730–734.

Taylor, L. A., 1970, Smythite, $Fe_{3+x}S_4$, and associated minerals from the Silverfields mine, Cobalt, Ontario: Am. Mineralogist, v. 55, p. 1650–1658.

Theodore, T. G., 1969, Surface distribution of selected elements around the Copper Canyon copper-gold-silver open-pit mine, Lander County, Nevada: U.S. Geol. Survey open-file report, 21 sheets.

Theodore, T. G., and Blake, D. W., 1969, Geochemistry and geometry of the pyritic halo around the Copper Canyon stock at Iron Canyon, Lander County, Nevada [abs.]: Geol. Soc. America, Cordilleran Sec.–Paleont. Soc., Pacific Coast Sec., 65th Ann. Mtg., Eugene, Oreg., 1969, Program, pt. 3, p. 69.

Theodore, T. G., and Roberts, R. J., 1971, Geochemistry and geology of deep drill holes at Iron Canyon, Lander County, Nevada, *with a section on* Geophysical logs of drill hole DDH–2 *by* Charles J. Zablocki: U.S. Geol. Survey Bull. 1318, 32 p.

Theodore, T. G., Silberman, M. L., and Blake, D. W., 1973, Geochemistry and K-Ar ages of plutonic rocks in the Battle Mountain mining district, Lander County, Nevada: U.S. Geol. Survey Prof. Paper 798–A, 24 p.

Titley, S. R., 1961, Genesis and control of the Linchburg orebody Socorro County, New Mexico: Econ. Geology, v. 56, p. 695–722.

Toulmin, P., 3d, and Barton, P. B., Jr., 1964, A thermodynamic study of pyrite and pyrrhotite: Geochim. et Cosmochim. Acta, v. 28, p. 641–672.

Toulmin, P., 3d, and Clark, S. P., Jr., 1967, Thermal aspects of ore formation, *in* Barnes, H. L., ed. Geochemistry of hydrothermal ore deposits: New York, Holt, Rinehart, and Winston, Inc., p. 437–464.

Trengove, R. R., 1951, Investigation of Copper Canyon lead-zinc deposit, Lander County, Nevada: U.S. Bur. Mines Rept. Inv. 4774, 61 p.

Tung, Li, and Chi-Lung, Yio, 1966, The abundance of chemical elements in the earth's crust and its major tectonic units: Scientia Sinica, v. 15, no. 2, p. 258–272.

Turekian, K. K., and Wedepohl, K. H., 1961, Distribution of the elements in some major units of the earth's crust: Geol. Soc. America Bull., v. 72, p. 175–192.

Turner, F. J., and Weiss, L. E., 1963, Structural and analysis of metamorphic tectonites: New York, McGraw-Hill Book Co., 694 p.

U.S. Geological Survey, 1971, Geological Survey research, 1971: U.S. Geol. Survey Prof. Paper 750–A, 418 p.

Van Houten, F. B., 1961, Clay minerals, red beds, zeolites in sedimentation: Transcripcion de conferencias dictadas, Caracas 1961; Venezuela, Direccion de Geologia, 59 p.

———1964, Origin of red beds–some unsolved problems, *in* Nairn, A. E. M., ed., Problems in paleoclimatology: NATO Paleoclimates Conf. Proc., Newcastle-upon-Tyne and Durham, England, 1963: New York, Interscience, p. 647–659.

Vaughan, D. J., Schwarz, E. J., and Owens, D. R., 1971, Pyrrhotites from the Strathcona mine, Sudbury, Canada—a thermomagnetic and mineralogical study: Econ. Geology, v. 66, no. 8, p. 1131–1144.

Vine, J. D., and Tourtelot, E. B., 1969, Geochemical investigations of some black shales and associated rocks: U.S. Geol. Survey Bull. 1314–A, p. A1–A43.

Vinogradov, A. P., 1962, Average content of chemical elements in the principal types of igneous rocks of the earth's crust: Geochemistry, no. 7, p. 641–664.

Vokes, F. M., 1957, The copper deposits of the Birtavarre district, Troms northern Norway: Norges Geologiske Undersokelse no. 199, Oslo, H. Aschehoug Co., 239 p.

Warshaw, C. M., and Roy, Rustom, 1961, Classification and a scheme for the identification of layer silicates: Geol. Soc. America Bull., v. 72, p. 1455–1472.

Wells, J. D., Erickson, Ralph, and Stoiser, L. R., 1967, Geology and mineralogy of the Cortez gold deposits, Nevada [abs.]: Mining Eng., v. 19, no. 12, p. 40.

Wells, J. D., Stoiser, L. R., and Eliott, J. E., 1969, Geology and geochemistry of the Cortez gold deposits, Nevada: Econ. Geology, v. 64, p. 526–537.

White, D. E., 1968, Environments of generation of some base-metal ore deposits: Econ. Geology, v. 63, p. 301–335.

Williston, S. H., 1964, The mercury halo method of exploration: Eng. and Mining Jour., v. 165, no. 5, p. 98–101. .

Wodzicki, A., 1971, Migration of trace elements during contact metamorphism in the Santa Rosa Range, Nevada, and its bearing on the origin of ore deposits associated with granitic intrusions: Mineralium Deposita, v. 6, p. 49–64.

Wones, D. R., 1967, A low pressure investigation of the stability of phylogopite: Geochim. et Cosmochim. Acta, v. 31, p. 2248–2253.

Wones, D. R., and Eugster, H. P., 1965, Stability of biotite—experiment, theory, and application: Am. Mineralogist, v. 50, p. 1228–1272.

World Mining, 1971, United States, Duval Corporation Battle Mountain production and costs, *in* What's going on in world mining: World Mining, July 1971, p. 41.

Wright, T. L., and Fleischer, Michael, 1965, Geochemistry of the platinum metals: U.S. Geol. Survey Bull. 1214–A, p. A1–A24.

Wrucke, C. T., Armbrustmacher, T. J., and Hessin, T. D., 1968, Distribution of gold, silver, and other metals near Gold Acres and Tenabo, Lander County, Nevada: U.S. Geol. Survey Circ. 589, 19 p.

Wrucke, C. T., and Theodore, T. G., 1970, Direction of movement of the Roberts Mountains thrust determined from folds, northern Shoshone Range and Battle Mountain, Nevada [abs.]: Geol. Soc. America, Abstracts with programs, v. 2, no. 5, p. 356.

Yellur, D. D., 1969, Lead-zinc mineralization in the Champaner rocks of Khandia, Boroda district, Gujarat, India: Econ. Geology, v. 64, p. 677–682.

Ypma, P. J. M., 1968, A fluid inclusions study of the role of volatiles in the formation of porphyry copper deposits [abs.], *in* Fluid inclusion research — Proceedings of COFFI: Washington, D.C., privately published, p. 10.

Yund, R. A., and Hall, H. T., 1969, Hexagonal and monoclinic pyrrhotites: Econ. Geology, v. 64, p. 420–423.

———1970, Kinetics and mechanism of pyrite exsolution from pyrrhotite: Jour. Petrology, v. 11, pt. 2, p. 381–404.

Yund, R. A., and Kullerud, G., 1966, Thermal stability of assemblages in the Cu-Fe-S system: Jour. Petrology, v. 7, p. 458–488.

Zablocki, C. J., 1971, Geophysical logs of DDH–2, *in* Theodore, T. G., and Roberts, R. J., Geochemistry and geology of deep drill holes at Iron Canyon, Lander County, Nevada: U.S. Geol. Survey Bull. 1318, p. 26–30.

# INDEX

[Italic page numbers indicate major references]


A

Page

Abstract ..... B1
Acknowledgments ..... 3
Alluvium ..... 10
Alteration reactions ..... 54
Altered granodiorite of Copper Canyon ..... 10
  age ..... 12
  alteration to quartz monzonite ..... 12
  analyses
  assimilation ..... 10
  biotite composition ..... 13
  biotite stability curves ..... 13
  crystallization stages ..... 14
  depth of emplacement ..... 12
  doming ..... 10
  emplacement control ..... 10
  geometry ..... 10
  intrusion breccia ..... 12
  lithology and chemical analyses ..... 10
  original emplacement ..... 5, 12
  petrogenesis ..... 13
  pressure-temperature conditions ..... 13
  temperature of emplacement ..... 15
  texture ..... 11
  xenoliths ..... 12
Altered granodiorite of the Wilson–Independence mine area ..... 15
Anion metasomatism ..... 55
Antimony distribution ..... 62
Antler orogeny ..... 15
Antler Peak ..... 9
Antler Peak Limestone ..... 10
  age ..... 10
  lithology ..... 10
Antler sequence ..... 4
Arsenic distribution ..... 62
Arsenopyrite replacement ..... 31
Arsenopyrite veins ..... 33, 34

B

Barium distribution ..... 63
Basalt ..... 5
Basalt flows ..... 15
Battle Formation ..... 9, 20
  age ..... 9
  contact relations ..... 9
  hematite source ..... 21
  lithology ..... 9
  members ..... 9
  mineralogy of iron oxides ..... 20
  ore zone ..... 4
  red beds ..... 20
  thickness ..... 9
Bismuth distribution ..... 63
Blossom mine ..... 71
Boron distribution ..... 64
Buena Vista fault ..... 62, 67
Buena Vista mine ..... 9, 62, 64, 66, 71
Buffalo Mountain ..... 16

C

Cadmium distribution ..... 65
Carbon in the Scott Canyon Formation ..... 57
Caetano Tuff ..... 5, 15
Cambrian system ..... *5, 7*
Candelaria Formation ..... 16
Censored data sets ..... 73
Chromium distribution ..... 65

Page

Cobalt distribution ..... B65
Copper Canyon faults ..... 12, 18
Copper Canyon underground mine ..... 62, 64, 66, 67, 70, 77
Copper-gold association ..... 77
Copper:gold:silver ratio ..... 76
Copper in fluids ..... 57
Copper, primary target ..... 61
Copper solubility ..... 57
Copper source, seep ..... 58
Critical values ..... 75

D, E, F

Dawsonite ..... 56
Depositional environment ..... *48*
Dewitt thrust ..... 4
Distribution of elements ..... 60
Edna Mountain Formation ..... 10
  age ..... 10
  lithology ..... 10
  thickness ..... 10
  units ..... 10
Element associations ..... 73
Elephant Head ..... 15
Erosion rate, Eocene or Oligocene ..... 15
Eureka–Battle Mountain mineral belt ..... 3, 5
Extrusive rocks ..... 15
Faulting ..... *18*
Faults, north-striking ..... 18
  northwest-striking ..... 18
Fluid inclusive data ..... 52, 53
Fluids, intermediate stage ..... 56
  late stage ..... 56

G

Galena ..... 10
Galena Canyon ..... 4, 7
Geochemical profile ..... 71
Geochemistry, Copper Canyon ..... *53*
  analytical ..... 59
  frequency ..... 59
  precision ..... 59
  sample size ..... 59
  sampling procedures ..... 59
Golconda orogeny ..... 17
Golconda plate, direction of transport ..... 17
Golconda thrust ..... 3, 16
  thickness ..... 12
Gold ..... 10, 34, 40, 45, 47
  distribution ..... 61
  elements strongly associated with ..... 73
Gold and copper ..... 62
Gold-arsenic association ..... 78
Gold-bismuth ..... 64

H

Harmony Formation ..... 7
  age ..... 7
  hydrothermal alteration ..... 7
  in Dewitt thrust plate ..... 4
  lithology ..... 7
  ore zones ..... 4
  supergene mineralization ..... 22
  thickness ..... 7
Havillah Formation ..... 4, 8
Havillah sequence ..... 7
Hayden fault ..... 22, 62, 63, 66, 67

Page

Hematite, origin ..... B20
Histograms of elements ..... 73
Humbug-Lucky Chance mine ..... 5, 66
Hydrothermal biotite ..... 30, 32, 43
Hypogene dispersion ..... 58

I, K, L

Intrusive rocks ..... 5, *10*
  age ..... 5
  alteration to quartz monzonite ..... 5, 12
  miscellaneous ..... 15
Iron Canyon ..... 7, 32
Kendall rank correlation ..... 73
Koipato Group ..... 16
Lead distribution ..... 66
Lognormal distribution ..... 73
Long Peak ..... 61

M

Manganese distribution ..... 66
Meagher mine ..... 62, 64, 66, 71
Medians for elements ..... 73
Mercury content, soils over west ore body ..... 78
Mercury-gold associations ..... 77
Mercury-lead association ..... 78
Mercury, ore indicator ..... 78
Metal source, country rock ..... 58
  magma ..... 57
Mineral belt, Eureka–Battle Mountain ..... 3, 5
Modoc mine ..... 61
Molybdenum distribution ..... 68
Monitor fault ..... 22
Mount Lewis ..... 16

N, O

Nevada mine ..... 9, 10, 16, 18, 64, 66
Nickel distribution ..... 68
Oxygen and sulfur fugacities ..... 54
Oxygen, source ..... 57

P

Panther Canyon Formation ..... 16
Pathfinder elements ..... 73
Pennsylvanian System ..... *8, 9*
Pennsylvanian and Permian Systems ..... *10*
Permian System ..... *10*
Philadelphia Canyon ..... 15
Plumas fault ..... 5, 62, 63, 67
Plumas mine ..... 5
Population arithmetic means ..... 73
Population distribution ..... 73
Porphyry copper deposit ..... *21*
  arsenopyrite composition ..... 39
  chalcopyrite etch tests ..... 36
  east ore body, age of metallization ..... 47
    chemical analyses ..... 40
    depth of metallization ..... 49
    hypogene metallization ..... 22
    major oxide percentages ..... 40
    ore minerals ..... 48
    paragenesis ..... 39
    6450 bench. *See* 6450 bench.
    sulfur isotopes ..... 54
    temperature during metallization ..... 51
    temperature variations ..... 52
    thickness ..... 22
  gold geochemistry ..... 47

Porphyry copper deposit—Continued Page

minor elements in gold B47
pyrrhotite compositions 39
pyrrhotite etch tests 36
pyrrhotite types 37
west ore body 22
Potassic assemblage 27
Pressure quenching 57
Primary dispersed copper 60
Primary element distributions 71
Production 3
Product moment correlation 73
Pumpernickel Formation 4, 8
age 8
chemical analyses 9
folding 16
fold trends 17
hydrothermal alteration 9
in thrust plate 4
lithology 8
thickness 8
units 7
worm trails 16
Pyritized rocks, gold content 61
silver content 62

Q, R

Quaternary System *10*
Reserves 3
Roberts Mountains thrust 3
depth 3
Rocky Creek 15

S Page

Scorodite B63
Scott Canyon Formation 4, 5
age 5
contact relations 15
hydrothermal alteration 5
in thrust plate 4
lithology 5
thickness 5
Shoshone Range 15
Silver distribution 62
Silver:gold ratios 76
6500 bench, hydrothermal biotite 35
6450 bench, Battle Formation
conglomerate, mineralogy 31
bedding 22
contact effects near veins 29
copper content 43
copper distribution 43
faults 22
fault zone mineralogy 35
folds 22
gold associations 45
gold content 45, 46
gold distribution 45
lithology 22
mineralogy of Harmony Formation 27
mineralogy of veins 28, 33
minor element concentrations 46
minor element variations 46
silver content 45
silver distribution 45
sulfide content of Harmony Formation 27

6450 bench—Continued Page

sulfide vein types B33
sulfides in Battle Formation 31
vein abundance 28
Solution species 53
Sonderman prospects 62, 67
Sonoma orogeny 16
Source-bed concept 58
Source of copper *57*
Spearman rank correlation 73
Stratigraphic features 3
Strontium distribution 69
Structural data, contouring method 17
Structural features 3
Structural geology, analysis of folding 16
Student's *t* tests 75
Surficial deposits 10

T, V, W, Z

Tin distribution 70
Tomboy mine 70
Tonopah 16
Trenton Canyon 5
Valmy Formation 4
Vanadium distribution 70
Virgin fault 12, 18, 22, 63, 67
Volcanic rock suites 5
Water content of magma 57
Willow Creek 4
Wilson-Independence mine 62, 66
Wilson-Independence mine area 15
Zinc distribution 71


* U.S. GOVERNMENT PRINTING OFFICE: 1975 O—585—474/57